NEURAL NETWORK ADAPTIVE FORCE AND MOTION CONTROL OF ROBOT MANIPULATORS IN THE OPERATIONAL SPACE FORMULATION

DANDY BARATA SOEWANDITO
(MSME, New Jersey Inst. of Technology)

A THESIS SUBMITTED
FOR THE DEGREE OF DOCTOR OF PHILOSOPHY
DEPARTMENT OF MECHANICAL ENGINEERING
NATIONAL UNIVERSITY OF SINGAPORE
2009

ACKNOWLEDGMENTS

I would like to express my gratitude to my supervisor, Assoc. Prof. Marcelo H. Ang Jr., for the opportunity to have worked with during my research at National University of Singapore. Also to the following professors for their inspiring works: Prof. Oussama Khatib of Stanford Univ. USA and Prof. Frank L. Lewis of Univ. of Texas Arlington, USA. Special thanks to Denny Oetomo Ph.D. of The Univ. of Melbourne, Australia, for his help so far.

My gratitude also to my college professor Prof. I Nyoman Sutantra, who made me find an article on adaptive control application, which instilled my curiosity for years to come. Also to Assoc. Prof. Zhiming ”Jimmy” Ji and Prof. Ian S. Fischer of New Jersey Inst. of Tech. (NJIT), who taught me robotics and dual-number kinematics, respectively. And also to my former college lecturers: Joni Dewanto and Frans Soetomo (Petra Christian University), who taught me the thinking style.

I am also thankful for having such a great parents, Jimmy Soewandito and Ina Christanti, a loving wife and son, Irene Sagita and Gallant Lovinggod Soewandito, for all support, love and encouragement during my Ph.D. years. Finally, my gratitude to one man who made this thesis possible, Jesus Christ; who endowed me all formulations and programmings I have derived so far.

TABLE OF CONTENTS

SUMMARY

It is well-established that dynamically compensated (model-based) force / motion controller strategy provides better performance than the standard Proportional - Integral - Derivative (PID) controller. However, the dynamic model and parameter values, especially for a real robot, are very difficult to identify precisely. Therefore a fast and cost-effective adaptive method is highly desired.

The main objective in this thesis deals ultimately with the Neural Network (NN) adaptive control for parallel force and motion in the operational space formulation. The operational space formulation, capable of providing unified force motion control and tracing contoured surface without the need for the knowledge of the surface geometry, is selected as the working platform. In this thesis, all the proposed neuro-adaptive control strategies were constructed in operational space formulation.

The development of this thesis is presented in incremental manner: (1) motion only neuro-adaptive control, (2) motion only neuro-adaptive control with velocity observer (since our physical robot does not have a joint velocity feedback), (3) force and motion neuro-adaptive control which, and accompanied by (4) neuro-adaptive impact force control.

All the proposed strategies assume no prior knowledge of the robot dynamics where the NN weights were initialized with zero. Lyapunov stabilities showing bounded stability of the tracking errors and NN weight errors were also

provided for all the proposed strategies. The proposed strategies were not only shown to be stable in real-time implementation on PUMA 560, but also produced comparable performances to those of the well-tuned inverse dynamics control strategies.

NOMENCLATURE

The main notations used in this thesis are compiled below:

$\boldsymbol{\eta}$	the uncertainties in the robot dynamic model, ($m \times 1$), in operational space.
$\boldsymbol{\Gamma}$	generalized joint space force vector, ($n \times 1$).
$\boldsymbol{\Lambda}_1, \boldsymbol{\Lambda}_2, \boldsymbol{\Lambda}_i$	($m \times m$) positive diagonal matrices in operational space, used as control gains.
$\boldsymbol{\Omega}, \bar{\boldsymbol{\Omega}}$	($m \times m$) selection matrices, to properly select the axes assigned for translation/rotation (motion control) and those for force/moment (force control).
$\boldsymbol{\pi}$	a ($13n \times 1$) vector of actual dynamic parameters.
$\boldsymbol{\sigma}(\cdot)$	a vector where each element is differentiable function, such as sigmoid and hyperbolic functions.
$\boldsymbol{\tau}_{\text{fric}}$	the joint space joint friction vector, ($n \times 1$).
$\boldsymbol{\tau}_{vis}, \boldsymbol{\tau}_{cou}, \boldsymbol{\tau}_{sti}, \boldsymbol{\tau}_{dec}$	components of $\boldsymbol{\tau}_{\text{fric}}$: the viscous friction, coulomb friction, stiction, and Stribeck effect, respectively, ($n \times 1$).

$\tau_{vis,M}$	a positive scalar upper bound of $\|\boldsymbol{\tau}_{vis}\|$.
$\tau_{cou,M}$	a positive scalar upper bound of $\|\boldsymbol{\tau}_{cou}\|$.
$\tau_{sti,M}$	a positive scalar upper bound of $\|\boldsymbol{\tau}_{sti}\exp^{(-\boldsymbol{\tau}_{dec}\dot{\mathbf{q}}^2)}\|$.
$\boldsymbol{\tau}_{\mathbf{x}}$	the operational space joint friction vector, ($m \times 1$).
a	scalar variable a (lower case, regular font).
$\mathbf{a}$	a vector $\mathbf{a}$ (lower case, bold font).
$\mathbf{a}(\mathbf{q}, \dot{\mathbf{q}})$	a vector $\mathbf{a}$ where each element is a function of vector $\mathbf{q}$ and vector $\dot{\mathbf{q}}$.
$\mathbf{A}$	a matrix $\mathbf{A}$ (upper case, bold font).
A_m, A_M	minimum and maximum eigenvalues of any positive definite general matrix $\mathbf{A}$, respectively.
$\mathbf{B}(\mathbf{q}, \dot{\mathbf{q}})$	the joint space Coriolis and Centrifugal matrix, ($n \times n$).
$\mathbf{B}_{\mathbf{x}}(\mathbf{q}, \dot{\mathbf{q}})$	the operational space Coriolis and Centrifugal matrix, ($m \times m$).
$B_{x,M}$	a positive scalar upper bound of $\|\mathbf{B}_{\mathbf{x}}(\mathbf{q}, \dot{\mathbf{q}})\|$.
$\mathbf{f}_{\text{contact}}$	contact forces/moments exerted by the effector onto environment, ($m \times 1$).
$\mathbf{f}_{\text{sensor}}$	force sensor reading of $\mathbf{f}_{\text{contact}}$ by force/torque sensor, ($m \times 1$).
$\mathbf{F}$	the generalized operational space force vector, ($m \times 1$).

$\mathbf{g}(\mathbf{q})$	the joint space gravity vector in joint space, ($n \times 1$).
$\mathbf{g_x}(\mathbf{q})$	the operational space gravity vector, ($m \times 1$).
g_M	a positive scalar upper bound of $\|\mathbf{g_x}(\mathbf{q})\|$.
$\mathbf{h}$	The sliding friction vector, ($m \times 1$).
$\mathbf{h}_{vis}, \mathbf{h}_{cou}, \mathbf{h}_{sti}, \mathbf{h}_{dec}$	components of $\mathbf{h}$: the viscous friction, coulomb friction, stiction, and Stribeck effect, respectively, ($m \times 1$).
$h_{vis,M}$	a positive scalar upper bound of $\|\mathbf{h}_{vis}\|$.
$h_{cou,M}$	a positive scalar upper bound of $\|\mathbf{h}_{cou}\|$.
$h_{sti,M}$	a positive scalar upper bound of $\|\mathbf{h}_{sti}\exp^{(-\mathbf{h}_{dec}\dot{\mathbf{q}}^2)}\|$.
$\mathbf{J}$	the geometric Jacobian matrix, ($m \times n$).
$\mathbf{K}_e$	a ($m \times m$) linear (hence diagonal) spring matrix relating the operational space coordinates and the contact forces; it is positive definite.
$\mathbf{K_v}, \mathbf{K_p}, \mathbf{K_I}$	($m \times m$) positive diagonal matrices, used as control gains.
$\mathbf{L}_D, \mathbf{L}_P$	($m \times m$) positive diagonal matrices, used as control gains.
m	the number of degree-of-freedom of the operational space coordinates, ($m \leq 6$).
$\mathbf{M}(\mathbf{q})$	the joint space inertia (or kinetic energy) matrix, ($n \times n$).
$\mathbf{M_x}(\mathbf{q})$	the operational space inertia (or kinetic energy) matrix, ($m \times m$).

$M_{x,m}, M_{x,M}$	the positive lower and upper bounds of $\|\mathbf{M_x(q)}\|$, respectively.
n	the number of joints.
N_1, N_2 and N_3	the number of neurons in layers 1, 2 and 3, respectively, for an NN output vector.
N_1, N_2 and $N_3 \times N_4$	the number of neurons in layers 1, 2 and 3, respectively, for an NN output matrix.
$\mathbf{p}_j^i$	a (3×1) position vector describing the position of frame$\{$j$\}$ expressed in frame$\{$i$\}$.
$\mathbf{q}, \dot{\mathbf{q}}, \ddot{\mathbf{q}}$	joint space coordinates, with its first and second derivatives, respectively, $(n \times 1)$.
$\mathbf{R}_j^i$	a (3×3) rotation matrix describing the orientation of frame$\{$j$\}$ expressed in frame$\{$i$\}$.
$\mathbf{s}_1$, $\mathbf{s}_2$, $\mathbf{s}_3$	the 1^{st}, 2^{nd}, and 3^{rd} (3×1) column vectors of a rotation matrix $\mathbf{R}_j^i$.
V	a scalar, denotes a Lyapunov function.
$\mathbf{V}$	the optimum first-to-second layer node weights, $(N_2 \times N_1)$.
$\hat{\mathbf{V}}, \tilde{\mathbf{V}}$	the estimate of $\mathbf{V}$ and the error between $\mathbf{V}$ and $\hat{\mathbf{V}}$, respectively.
$V_M, \hat{V}_M, \tilde{V}_M$	positive scalar upper bounds of $\mathbf{V}, \hat{\mathbf{V}}, \tilde{\mathbf{V}}$, respectively.
$\mathbf{W}$	the optimum second-to-third layer node weights, the size can be $(N_3 \times N_2)$, to accommodate an $(N_3 \times 1)$ NN output vector, or $(N_3 \times N_4 \times N_2)$, to accommodate an $(N_3 \times N_4)$ NN output matrix.

$\hat{\mathbf{W}}, \tilde{\mathbf{W}}$	the estimate of $\mathbf{W}$ and the error between $\mathbf{W}$ and $\hat{\mathbf{W}}$, respectively.
$W_M, \hat{W}_M, \tilde{W}_M$	positive scalar upper bounds of $\mathbf{W}, \hat{\mathbf{W}}, \tilde{\mathbf{W}}$, respectively.
$\mathbf{x}, \dot{\mathbf{x}}, \ddot{\mathbf{x}}$	the operational space coordinates, with its first and second derivatives, respectively, ($m \times 1$).
$\mathbf{x}_d, \dot{\mathbf{x}}_d, \ddot{\mathbf{x}}_d$	the desired operational space coordinates, with its first and second derivatives, respectively, ($m \times 1$).
$\mathbf{Y}(\mathbf{q}, \dot{\mathbf{q}}, \ddot{\mathbf{q}})$	the joint space $n \times 13n$ regression matrix of dynamic parameters.
$\bar{\mathbf{Y}}(\mathbf{q}, \dot{\mathbf{q}}, \ddot{\mathbf{q}})$	the operational space $m \times 13n$ regression matrix of dynamic parameters.
$\mathbf{Z}$	the definition of $\mathbf{Z} = \text{diag}[\mathbf{W}, \mathbf{V}]$.
$\hat{\mathbf{Z}}, \tilde{\mathbf{Z}}$	the estimate of $\mathbf{Z}$ and the error between $\mathbf{Z}$ and $\hat{\mathbf{Z}}$, respectively.

LIST OF TABLES

LIST OF FIGURES

CHAPTER 1

INTRODUCTION

1.1 Background and Problem Definition

Robotic manipulators have been used for industrial automation. The classical example is the assembly line in the automotive industry where cars in the production are placed and positioned at exact locations on a conveyor belt for manipulators to operate on the cars for operations such as welding and pick-and-place as shown in Fig. 1.1(a) and 1.1(b).

Up to present, however, in practice many robotics tasks including those in the

(a) Six-axis robots used for welding.

(b) An industrial robot operating in a foundry.

Figure 1.1: Industrial manipulators (http://en.wikipedia.org/wiki/Industrial_robot).

industrial automation, utilize simple independent joint space strategy using Proportional - Integral - Derivative (PID) control method. Other applications described in task space, in general, cannot be easily accommodated by joint space control. The task space motion control, done at end-effector of the robot, is a significant topic in the study of robotics as it can relate the natural spatial frames of human-related tasks, as shown in [1]. Task space also accommodates the interactive control (*compliant motion* or *force-motion* control), which enables the effector to provide an interaction capability of the effector with its environment, such as: to apply static force needed for a manufacturing process (e.g. grinding, polishing), part-mating, or dealing with geometric uncertainty of the workpiece by establishing controlled contact forces [2].

Compliant motion control strategies basically can be grouped into two major mainstreams: the stiffness/impedance control [3, 4] and the parallel (or, simultaneous), force and motion control [5, 6, 7, 8, 9].

The impedance control is basically position control which is manipulated to exert the force produced onto the working surface. This is achieved if an accurate stiffness of the environment (serial stiffness of the end-effector and the surface) is known and an accurate desired trajectory can be designed based upon known surface's geometry of which deflection can be computed. And therefore the force produced equals to deflection times the stiffness. However, in practice the accuracy of the stiffness and the desired trajectory according to surface geometry, is hard to be achieved. And therefore it cannot provide reliable performance.

The parallel force-motion control uses the contact force feedback from the force / torque sensor mounted in the robot. It was shown in [10], that the parallel

force-motion strategy produces superior performance than that of the impedance control strategy. Note that the force/torque sensor can be used in impedance strategy, however, it serves as a reading only, not a feedback.

The parallel force and motion strategies can then be further distinguished into two categories: (1) the coupled motion and force subsystems [5, 6], and (2) the decoupled motion and force subsystems [7, 8, 11, 9], where the latter is expected, theoretically, to give better performance since the motion and force subsystems are separated.

The first strategy is the operational space formulation for unified motion/force control [8]. The operational space formulation does not require the knowledge of the exact contact surface geometry and it was shown to perform successfully in many real-time experimentations such as an industrial polishing task of an unknown surface [12]. It is also established that the operational space formulation provides an elegant handling of highly redundant and branching mechanisms [13].

The second strategy is the reduced state position/force control of constrained robot [9]. The reduced state position/force control requires the contact surface geometry of a particular surface. However, this geometric constraint poses a difficult problem for implementation, because: the surface geometry is required *a priori*, afterwards some mathematical transformations are to follow, consequently a different surface would require a different set of transformations. Therefore, so far works based upon this framework are mostly done in simulation studies using up to 3 DOF manipulators or real-time experiments on simple planar surfaces. In operational space framework, surface geometry is not

needed and all mathematical transformations are consistent. Note that, manual inspection to determine the normal direction of the surface is still required for the operational space framework. However, precise or analytical surface geometric is not required. For example, the surface $F(x, y, z) = c$ has its normal vector equals to $\nabla F = (\frac{\partial F}{\partial x}, \frac{\partial F}{\partial y}, \frac{\partial F}{\partial z})$. In the application, robot operator will determine whether the orientation of the end-effector is within acceptable range of ∇F or not.

To achieve each own performance, both frameworks do not use PID control strategy, but rather model-based (*computed torque* or *inverse dynamics*) control. It is well known that PID control limits the task flexibility because it is only tuned for a particular set of the robotic task dynamics (which is configuration dependent). If the perfect model of the robot dynamics exists and is employed, then the inverse dynamics control strategy would perfectly cancel the robot dynamics, leading to the perfect tracking performance in robot motion control.

The manipulator model refers to the closed-form Lagrange formulation (or the recursive Newton-Euler formulation; however, in this thesis we mainly use and focus on the Lagrange formulation) and joint friction dynamics. The Lagrange dynamics correlates with the robot inertial parameters (11 for each link) which are: one element of the link mass, three elements of the first moments (by product of the link mass times the coordinates of the center-of-mass), six elements of the inertia tensor and one element of the motor inertia. The joint friction dynamics correlates with the joint friction parameters.

The Lagrangian derivation dynamics model basically involves two basic steps:

1. First is the symbolic derivation of the kinetic/ inertia matrix, Coriolis/ centrifugal matrix and gravity vector through the closed-form Lagrange energy formula. Several approaches to derive the robot dynamic model symbolically were presented in [14, 15, 16, 17, 18, 19, 20, 21]. Inclusive in this derivation is the simplification procedure, which is needed to meet the requirement of the real-time deterministic sampling time for real-time implementation.

   The simplification procedure includes:

   - Common sub-expression elimination: by eliminating intermediate expressions, the total arithmetic operations can be further reduced [22, 23, 19, 24], however, so far these proposed procedures are still heuristic and manual;
   - Reducing the number of standard inertial parameters ($13n \times 1$, where n is the number of joints) into a minimum set of parameters [25, 26, 27, 28, 29, 30], however, so far these proposed procedures are not yet full automatic

   It is well established that for a real robot with more than three degrees of freedom, the expressions of robot dynamic model are extremely complex, therefore, it makes the simplification procedure is not an easy task.

2. Secondly, the parameters of the model have to be estimated.

   The most basic method is by physical experiments. By dismantling the robot and isolating each link, the link's inertial parameters could be obtained by physical experiments [19]. However, this physical experiment

procedure, is tedious and error prone; and it is practical only when performed before the robot assembly by the manufacturer.

A more practical procedure is by the off-line system identification. By exploiting the *linearity-in-parameter* (LIP) property of robot dynamic model, regression analysis of the collected input/output data (the robot is moved into certain trajectories) can be performed by using the *least-square-estimation* procedure to identify the robot dynamic parameters [31, 32, 33, 24, 34].

Furthermore, joint friction identification depends on ambient condition. Therefore, ideally, to produce accurate result it must be performed every time prior to the operation of the robot. Several joint friction identification by physical experiments has been reported such as [24, 35, 36].

By-and-large, robot dynamics derivation and identification have been the major obstacle for real robotic manipulator implementation (or any other mechanisms). It is therefore desirable to obtain an adaptive strategy.

1.2 Main Objective

The focus task is compliant motion when a desired force is exerted to the surface while the end-effector moves according to the desired motion tangent to the surface.

The following specifications are desired:

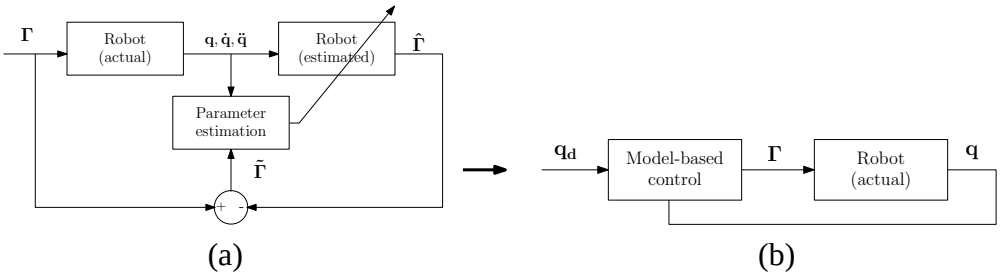

Figure 1.2: Indirect adaptive control: (a) off-line system Identification (b) model-based control.

1. All adaptive control strategies do not require *a priori* knowledge of the manipulator dynamics.

2. The knowledge of surface geometry is not needed.

3. All control strategies are expected to provide equivalent performance of that of dynamics compensated strategy.

4. All control strategies should be able to be implemented on the real robotic manipulator. The test bed would be the PUMA 560 industrial robotic arm.

In this thesis, all strategies are limited for non-redundant manipulator only.

1.3 Summary of Related Works

We review briefly some literature. Earlier works [37, 38, 39, 40, 41] exploit the linearity-in-parameter (LIP) property of robot dynamic model and use the least-square-estimation method to identify the robot parameters, where the model-based control can then be implemented afterward. Hence this method is often referred as *off-line* identification method or *indirect* LIP adaptive control.

The architecture of the indirect method can be shown as a two-step process (Fig. 1.2). The linear-in-parameter model of robot dynamics can be shown as follows

$$\boldsymbol{\Gamma} = \mathbf{Y}(\mathbf{q}, \dot{\mathbf{q}}, \ddot{\mathbf{q}})\, \boldsymbol{\pi} \tag{1.1}$$

where $\boldsymbol{\Gamma} \in \Re^n$ is the actual joint torque vector and $\mathbf{Y}(\mathbf{q}, \dot{\mathbf{q}}, \ddot{\mathbf{q}}) \in \Re^{n \times 13n}$ is the measured regression matrix (computed from joint positions, velocities and accelerations) and $\boldsymbol{\pi} \in \Re^{13n}$ is the vector of the actual dynamic parameters. Note that, the thirteen dynamic parameters, with respect to Joint i, are comprised of the standard inertial parameters and the joint friction parameters, as follows:

- The (11×1) standard inertial parameters are defined as follows: the mass of Link i (scalar), three components of the first moment of inertia of Link i, six components of the inertia tensor of Link i and the moment inertia of the motor (scalar).
- The (2×1) joint friction parameters are comprised with the viscous and Coulomb friction terms. Only viscous and Coulomb terms are included, in order to preserve the linearity-in-parameter property.

Now, let's consider the most general off-line identification method based upon the least-square-estimation procedure as in [31, 32, 34], that is: if we move the robot through certain trajectories at N time instants $t_1, t_2, \ldots, t_N$, then the over-determined actual system can be written as

$$\boldsymbol{\Gamma}_N = \begin{bmatrix} \boldsymbol{\Gamma}(t_1) \\ \boldsymbol{\Gamma}(t_2) \\ \vdots \\ \boldsymbol{\Gamma}(t_N) \end{bmatrix} = \begin{bmatrix} \mathbf{Y}(\mathbf{q}(t_1), \dot{\mathbf{q}}(t_1), \ddot{\mathbf{q}}(t_1)) \\ \mathbf{Y}(\mathbf{q}(t_2), \dot{\mathbf{q}}(t_2), \ddot{\mathbf{q}}(t_2)) \\ \vdots \\ \mathbf{Y}(\mathbf{q}(t_N), \dot{\mathbf{q}}(t_N), \ddot{\mathbf{q}}(t_N)) \end{bmatrix} \boldsymbol{\pi} = \mathbf{Y}_N\, \boldsymbol{\pi}. \tag{1.2}$$

And the over-determined estimated system can be written as

$$\hat{\boldsymbol{\Gamma}}_N = \begin{bmatrix} \hat{\boldsymbol{\Gamma}}(t_1) \\ \hat{\boldsymbol{\Gamma}}(t_2) \\ \vdots \\ \hat{\boldsymbol{\Gamma}}(t_N) \end{bmatrix} = \begin{bmatrix} \mathbf{Y}(\mathbf{q}(t_1), \dot{\mathbf{q}}(t_1), \ddot{\mathbf{q}}(t_1)) \\ \mathbf{Y}(\mathbf{q}(t_2), \dot{\mathbf{q}}(t_2), \ddot{\mathbf{q}}(t_2)) \\ \vdots \\ \mathbf{Y}(\mathbf{q}(t_N), \dot{\mathbf{q}}(t_N), \ddot{\mathbf{q}}(t_N)) \end{bmatrix} \hat{\boldsymbol{\pi}} = \mathbf{Y}_N \, \hat{\boldsymbol{\pi}}. \qquad (1.3)$$

Therefore, by evaluating the cost function

$$\|\tilde{\boldsymbol{\Gamma}}_N\|^{\mathrm{T}} = \tilde{\boldsymbol{\Gamma}}_N^{\mathrm{T}} \, \tilde{\boldsymbol{\Gamma}}_N = 0, \qquad (1.4)$$

where $\tilde{\boldsymbol{\Gamma}} = \boldsymbol{\Gamma} - \hat{\boldsymbol{\Gamma}}$ is the error between the actual and estimated joint torque vectors, $\boldsymbol{\Gamma}, \hat{\boldsymbol{\Gamma}}$, respectively, therefore the estimated dynamic parameters, $\hat{\boldsymbol{\pi}}$, can be obtained as follows

$$\hat{\boldsymbol{\pi}} = (\mathbf{Y}_N^{\mathrm{T}} \, \mathbf{Y}_N)^{-1} \, \mathbf{Y}_N^{\mathrm{T}} \, \boldsymbol{\Gamma}_N. \qquad (1.5)$$

A similar procedure by measuring the lumped inertias, instead of the joint torques, was presented in [33, 24]; however, essentially, it also use the regression analysis method.

Subsequently, it is then clear that off-line identification is not practical. The cycle time of robotic usage is relatively not short i.e. clearly if there are changes in the dynamics, then one must redo the identification procedure. Therefore, some researchers preferred to have an *on-line* identification method to directly adapt the control, as shown in Fig. 1.3. This method is often referred as *direct* LIP adaptive control.

Earlier works on direct LIP adaptive control initially can only achieve the adaptive control without parameter estimation [42, 43, 44, 45], where only the trajectory tracking errors are guaranteed to converge (asymptotic stability) while

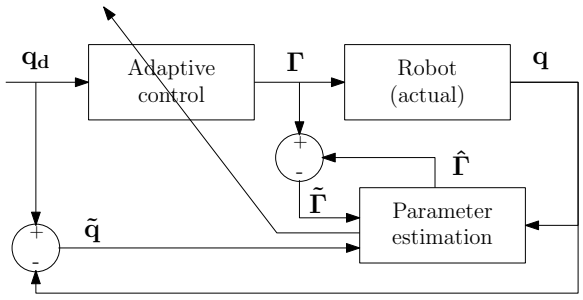

Figure 1.3: Direct adaptive control.

the parameter errors can be only ensured to be bounded (bounded stability) i.e. the estimated parameters cannot be guaranteed to converge to their true values, regardless whether optimal trajectories are given or not.

Finally, [46] proposed the adaptive control with parameter estimation (in Fig. 1.3). It can be shown that the trajectory tracking errors are guaranteed to converge and the parameter errors can be guaranteed to converge if exciting trajectories are given. In the case the exciting trajectories are not given, then the parameter errors can only be guaranteed to be bounded.

Some challenges in implementing LIP direct adaptive strategy are:

1. The first is similar to the previous classical model (with kinetic, Coriolis / centrifugal matrices and gravity vector), which is about the LIP model symbolic derivation involving two factors: (i) the LIP model formulation and (ii) the simplification procedure.

   A relatively complete treatment on the LIP model formulation based upon Lagrangian formalism, including motor inertia parameter, can be found in [47]. However, the motor i is restricted to be located on Link $i-1$. Hence, the whole LIP formulation must be reformulated.

Therefore, the present challenge is the availability of a systematic LIP model formulation and its simplification. This problem is presently the main bottleneck in this methodology.

2. Secondly, the regression matrix $\mathbf{Y}(\mathbf{q}, \dot{\mathbf{q}}, \ddot{\mathbf{q}})$ used in direct adaptive control with identification [46] requires the availability of joint velocities and accelerations, which are often not available in industrial robots. Obtaining these variables through filtering often produces noisy signals. Several algorithms were proposed to provide the needed matrix without the need of the joint accelerations, as in [48, 49, 50, 51, 52].

3. Thirdly, the need for optimal (*exciting*) trajectories in order to make the parameters converge rapidly. The optimal trajectories are those that excite all possible dynamics of the manipulator. It is also often described as *dynamically rich* trajectories. Derivation of optimal trajectories generator algorithm were proposed by [53, 54, 55, 56], however, these proposed trajectory generator algorithms are still relatively a complex process. (From practical side, if exciting trajectories cannot be determined, then any working trajectories can be used directly, where the performance of the tracking errors can be verified afterward.)

4. Additionally, extension to operational space in direct method can be shown to be more complex as further transformations are required to obtain the operational space matrices and vectors [8, 47] from the joint space dynamics. One must derive a separate linear dynamic model in operational space, should one use the direct approach. Note that this extension can still be done indirectly by performing parameter estimation in joint space

(either using on-line or off-line method), then employing model-based control in operational space. However, since the operational space control is non-adaptive, one needs to redo the joint space parameter identification procedure whenever necessary.

Recent experimental indirect methods on higher ($>= 6$) DOF robots were shown in [57, 58, 59]. However, albeit numerous theoretical and fundamental works have been proposed, experimental works in both indirect or direct methods on higher ($>= 6$) DOF robots are still relatively far and few.

By-and-large, the expressions of robot dynamic model are extremely complex, especially for higher ($>= 6$) DOF robots. It makes the derivation and simplification procedure are not an easy task. A recent work even assumed the robot dynamic model to be a linear system model; where for ease of parameter identification, it includes only joint friction model [60].

Therefore, cheaper alternative than direct or indirect LIP adaptive controls, if any, is desirable.

Neural-network (NN) strategies then were explored as means of nonlinear system identification [61] and robot control strategy [62, 63, 64, 65, 66, 67]. The NN theorem dictates that given unlimited number of hidden layer nodes, three-layer NN with ideal weights can approximate any function given the neural nets were properly trained without the need for an exact model. As summarized by [68], similar with the LIP adaptive control strategies, NN adaptive control strategies can be categorized as: indirect NN adaptive control where system identification must be performed a priori, and direct NN adaptive control.

Despite promising results early studies lacked the mathematical proof of stability for the proposed control algorithms. This posed a problem in ensuring the reliability of the approach as arbitrary learning rules of the NN weights could lead into instability of the closed-loop system as observed by [69]. Therefore the main challenge in designing a neural-network, whether it is used as a controller, classifier or identifier, is to define a learning rule which is easy-to-use and can guarantee stability of the overall system with no strong constraints.

Subsequently, linear-in-parameter Neural Networks strategy (LPNN or two-layer NN) with Lyapunov stability, analysis was proposed for nonlinear system identification in [70, 71] and for robotic control in [72, 73]. However, LPNN strategy requires that suitable basis functions must be first selected (e.g. radial basis function (RBF)), which in practice this constraint is hard to satisfy.

To confront this deficiency, a three-layer joint space NN adaptive robot motion control was proposed by Lewis *et. al.* [74, 75]. It has several interesting characteristics:

1. The proposed strategy does not have strong constraints and was also shown to have a satisfactory performance,
2. The formulation was developed based upon well known joint space LIP adaptive robotic controller proposed by Slotine and Li's [45, 76, 46],
3. Off-line learning is not needed and the NN weights are initialized with zero,
4. A Lyapunov analysis is provided to show bounded stability for both the

tracking errors and NN weight errors.

These characteristics made this strategy very attractive for practical implementation. However, the work [74, 75] was only validated through a simulated study of a 2 DOF robot in joint space. Therefore, it is interesting to develop this strategy into operational space formulation with real-time implementation.

Several works of neuro-adaptive compliant motion, based-upon [9], then followed such as [77, 78, 79], however, all these works required the contact surface geometry to be known. Hu [80], based upon model-based equivalent in [81], proposed a full NN based adaptive control to overcome the requirement of the contact surface geometry. However, this strategy required a 2 dimensional virtual constraint plane to be known, which in practice would be limiting the dexterity of the effector movement within 2D constraint plane. More recent neuro-adaptive control works attempted to adaptively accommodate the contact surface geometry through impedance control [82, 83] and compliant motion based approach [84, 85], however, all these works required the contact surface normal direction to be known. Some recent works were proposed for compliant motion law [86, 87]; however, they are not an adaptive strategy, but based upon model-based Lagrangian strategy.

An NN adaptive algorithm designed for the compliant motion control on an unknown contact geometry was presented in [88], where an additional vision system was required to extract the surface geometry information. However, it was done in simulation where the extracted geometry information was already obtained. In reality, this extraction might not be easily obtained. Furthermore,

the real time setup could be more complicated with an additional vision system.

All previously mentioned NN algorithms were mainly validated through simulated robots of up to 3 DOFs, where only [77, 80] were validated by real-time experiments of a real 2 DOF robot.

1.4 Main Methodology

It is previously shown that the recent works on neuro-adaptive control failed to overcome the problem of the knowledge of the contact surface geometry. However, it is established that:

- The operational space formulation provides a natural framework, not only the free-motion control, but also for the parallel force and motion control (compliant motion) as well, without requiring the knowledge of the contact surface geometry.

  The drawback of this framework, however, is that it requires *a priori* knowledge of the manipulator dynamics, which is difficult to obtain.

- The neuro-adaptive control in [74, 75] was shown to have a satisfactory performance, without prior knowledge of the robot dynamics..

Therefore, our main methodology is to combine the joint space neuro-adaptive strategy by [74, 75] with the unified force/motion formulation in the operational space.

1.5 Summary of Contributions

The contributions of this Ph.D work are the development of the following control algorithms that do not rely on knowledge of robot dynamics and environment geometry:

- **The Operational Space Neuro-Adaptive Motion Control:**

  In the first formulation, the original approach [74, 75] was extended into operational space motion only framework. It was shown in simulation study that a comparable performance, with that of the Lagrangian dynamics.

  However, it was shown that its performance on real-time experimentation was found to be inferior to the simulation equivalents.

  A separate Lyapunov analysis was presented to show that the estimated velocity signals, obtained by approximation through the filtered backward difference of the displacement feedback, are not suitable replacements to the non-existing actual velocity signals for the proposed adaptive motion strategy in real-time implementation.

- **The Operational Space Neuro-Adaptive Motion Control with Velocity Observer:**

  In the second formulation, an improved formulation of NN motion control with velocity observer, to overcome the absence of an actual velocity signal in the real robot, was introduced.

It can be shown in real-time implementation that the performance of the NN motion controller with velocity observer strategy is better than that of the NN motion control (where filtered velocity is used to fill the absence of the actual velocity). Also, the improved NN formulation yielded a comparable performance to that of the Lagrangian dynamics strategy.

- **The Operational Space Neuro-Adaptive Force and Motion Control with Velocity Observer, coupled with The Operational Space Neuro-Adaptive Impact Force Control:**

  In the third formulation, the NN force/ motion formulation with velocity observer, for compliant motion, was proposed. An NN adaptive impact strategy is also proposed to complement the main strategy.

  It can be shown that the proposed neuro-adaptive compliant control yielded comparable performance with that of Lagrangian dynamics strategy.

Lyapunov stability proofs for all algorithms are also provided, together with experimental verification.

1.6 Organization of Thesis

The development of this thesis was presented in incremental manner starting from the neuro-adaptive task space free motion up to the neuro-adaptive compliant motion control:

- Chapter two presents background on robot kinematics, dynamics and the operational space formulation.

- Chapter three presents the review of the existing adaptive control works as follows: the joint space direct LIP adaptive control, the operational space direct LIP motion control and the original joint space NN based adaptive control.

- Chapter four presents a neuro-adaptive motion controller in the operational space by extending and improving the original three-layer NN adaptive joint space motion control by [74, 75] into operational space framework [8]. Several useful end-effector properties to develop the proposed formulation were also introduced.

  The stability analysis of the proposed strategy was presented. Simulated and real time comparison to the performance of the Lagrangian dynamics and the PD-plus-gravity motion control strategies were also presented. It was shown in simulation that a comparable performance, with that of the Lagrangian dynamics, was achieved, but has the advantage of no a priori knowledge of dynamics is required.

  However, it was shown that its performance on real-time experimentation was found to be inferior to the simulation equivalents. A separate Lyapunov analysis reveals that, the filtered velocity signals, obtained by approximation through the filtered backward difference of the displacement feedback, are not suitable replacements to the non-existing actual velocity signals for the proposed adaptive motion strategy in real-time implementation (physically PUMA 560 does not have joint velocity sensor).

- Chapter five presents a neuro-adaptive motion control strategy with velocity observer. This work was extended from previous formulation in

Chapter three, to overcome the absence of the actual velocity signal in the real-time experimentation. The stability analysis of the proposed strategy was also presented.

It can be shown in real-time implementation that the performance of the NN motion controller with velocity observer strategy, where it takes only position feedback, is better than that of the NN motion control (where filtered velocity is used to replace the actual velocity).

It also yielded, in real-time, a comparable performance to that of the Lagrangian dynamics strategy, but has the advantage of no a priori knowledge of dynamics is required.

- Chapter six presents a neuro-adaptive force and motion control strategy with velocity observer, which was extended from Chapter four. The stability analysis of the proposed strategy was presented in this chapter. An adaptive impact strategy and its stability analysis to complement the main strategy were also given.

  It is shown that the proposed neuro-adaptive compliant control yielded comparable performance with that of Lagrangian dynamics strategy, but has the advantage of no a priori knowledge of dynamics is required.

- Chapter seven presents a consolidated view on how to combine overall algorithms for a multi-task operation.

  A case study is presented where two main tasks are: (i) a circular compliant motion, followed by (ii) a circular free motion.

- Chapter eight presents summary of contributions and suggestions for future works.

CHAPTER 2

MANIPULATOR KINEMATICS AND THE OPERATIONAL SPACE FORMULATION

2.1 Chapter Overview

This chapter covers the necessary background on robot kinematics, dynamics [89, 90, 47] and the operational space formulation [8, 91] as our working platform.

2.2 Direct Kinematics

A manipulator is treated as a structure of an open kinematic chain of n+1 links, articulated through n rotational (revolute) and/or linear (prismatic) joints having one degree of freedom. Let's define as illustrated in Fig. 2.1, Frame $\{i\}$ $(\mathcal{O}_i, \mathbf{x}_i, \mathbf{y}_i, \mathbf{z}_i)$, attached to Joint i, be such a frame with the origin at $\mathcal{O}_i$ and $\mathbf{x}_i, \mathbf{y}_i, \mathbf{z}_i$ are its unit vectors, and let the $\mathbf{z}_i$ is along the axis of Joint i. The kinematic relationship (the position and orientation) between two coordinate frames

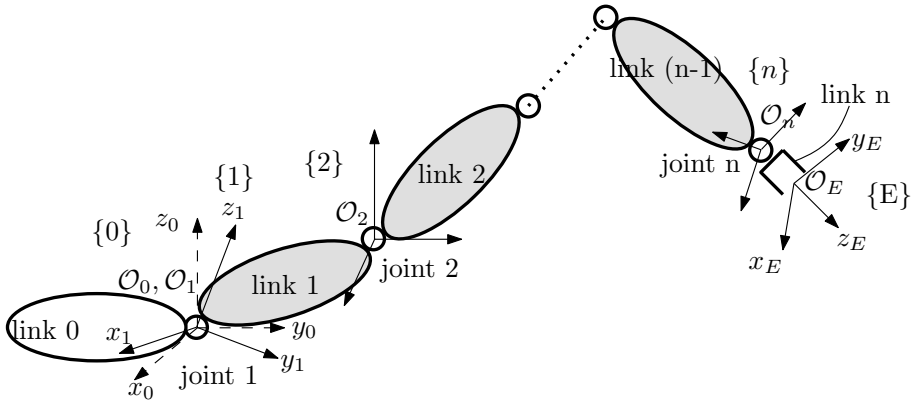

Figure 2.1: An open kinematic chain.

attached to two adjacent joints, $i-1$ and i, can then be described by the homogenous matrix transformation between Frame $\{i-1\}$ and Frame $\{i\}$ is

$$\mathbf{T}_i^{i-1}(q_i) = \begin{pmatrix} \cos\theta_i & -\sin\theta_i & 0 & a_{i-1} \\ \sin\theta_i \cos\alpha_{i-1} & \cos\theta_i \cos\alpha_{i-1} & -\sin\alpha_{i-1} & -d_i \sin\alpha_{i-1} \\ \sin\theta_i \sin\alpha_{i-1} & \cos\theta_i \sin\alpha_{i-1} & \cos\alpha_{i-1} & d_i \cos\alpha_{i-1} \\ 0 & 0 & 0 & 1 \end{pmatrix} \tag{2.1}$$

where $\alpha_{i-1}, a_{i-1}, \theta_i, d_i$ are Denavit-Hartenberg (DH) parameters according to [89]. The dependent variable q_i equals to θ_i, or d_i, depending on rotational or linear joint, respectively.

In this thesis, our test bed is PUMA 560 and the DH parameters of PUMA 560 are provided in Appendix A.1. Note, the homogenous matrix transformation (2.1) can also be written as

$$\mathbf{T}_i^{i-1}(q_i) = \begin{pmatrix} \mathbf{R}_i^{i-1}(q_i) & \mathbf{p}_i^{i-1}(q_i) \\ \mathbf{0} & 1 \end{pmatrix} \tag{2.2}$$

where $\mathbf{R}_i^{i-1}$ is a (3×3) rotational matrix and $\mathbf{p}_i^{i-1}$ is a (3×1) positional vector of Frame $\{i\}$ expressed in Frame $\{i-1\}$.

2.2.1 End-effector Representation

As shown in Fig. 2.1, for task application, it is more convenient to place the end-effector frame at Frame $\{\mathrm{E}\}$ at different location with Frame $\{n\}$. Therefore, by exploiting (2.2) and the open kinematic chain concept, then the orientation and position in Cartesian space of the Frame $\{\mathrm{E}\}$ expressed with respect to the base frame, Frame $\{0\}$, can be obtained as

$$\mathbf{T}_E(\mathbf{q}) = \mathbf{T}_1(q_1)\,\mathbf{T}_2^1(q_2)\,\ldots\mathbf{T}_E^n(q_n) = \begin{pmatrix} \mathbf{R}_E(\mathbf{q}) & \mathbf{p}_E(\mathbf{q}) \\ \mathbf{0} & 1 \end{pmatrix} \tag{2.3}$$

where $\mathbf{p}_E$ is a (3×1) position vector of Frame $\{\mathrm{E}\}$ in the Frame $\{0\}$

$$\mathbf{p}_E(\mathbf{q}) = \begin{pmatrix} p_x(\mathbf{q}) & p_y(\mathbf{q}) & p_z(\mathbf{q}) \end{pmatrix}^{\mathrm{T}} \tag{2.4}$$

And $\mathbf{R}_E$ is a (3×3) rotational matrix of Frame $\{\mathrm{E}\}$ in the Frame $\{0\}$

$$\mathbf{R}_E(\mathbf{q}) = \begin{pmatrix} \mathbf{s}_1(\mathbf{q}) & \mathbf{s}_2(\mathbf{q}) & \mathbf{s}_3(\mathbf{q}) \end{pmatrix} \tag{2.5}$$

where $\mathbf{s}_1, \mathbf{s}_2, \mathbf{s}_3 \in \Re^3$ are the orientation of the unit vectors $\mathbf{x}_E, \mathbf{y}_E, \mathbf{z}_E$, respectively, as shown in Fig. 2.1. The vector $\mathbf{q} \in \Re^n$ is defined as a *joint space* coordinate vector, with n as the number of degree-of-freedom of the joint space coordinates.

We can then define the *end-effector configuration parameters*, $\mathbf{x}_{\text{rep}} \in \Re^{m_{\text{rep}}}$, as

$$\mathbf{x}_{\text{rep}} = \begin{pmatrix} \mathbf{x}_p \\ \mathbf{x}_r \end{pmatrix} \tag{2.6}$$

where the positional representation $\mathbf{x}_p$ to describe $\mathbf{p}_E$ and the orientational representation $\mathbf{x}_r$ to describe $\mathbf{R}_E$. Among various possible selections for the positional representation $\mathbf{x}_p$ and the orientational representation $\mathbf{x}_r$, the most straightforward representations are based on the direct use of the elements of (4×4) homogenous transformation matrix, such as:

- **Cartesian coordinates:** where $\mathbf{x}_p$ exactly equals to $\mathbf{p}_E$:

$$\mathbf{x}_p = \mathbf{p}_E = \begin{pmatrix} p_x(\mathbf{q}) & p_y(\mathbf{q}) & p_z(\mathbf{q}) \end{pmatrix}^{\mathrm{T}} \in \Re^3 \tag{2.7}$$

- **Direction Cosines:** where $\mathbf{x}_r$ is obtained by stacking up $\mathbf{s}_1, \mathbf{s}_2, \mathbf{s}_3$ into one (9×1) vector

$$\mathbf{x}_r = \begin{pmatrix} \mathbf{s}_1^{\mathrm{T}}(\mathbf{q}) & \mathbf{s}_2^{\mathrm{T}}(\mathbf{q}) & \mathbf{s}_3^{\mathrm{T}}(\mathbf{q}) \end{pmatrix}^{\mathrm{T}} \in \Re^9. \tag{2.8}$$

  Note that physically, in 3D space, there are, at most, three positions in x, y, z direction and, at most, three orientations in x, y, z direction. Therefore, a (3×1) vector $\mathbf{x}_p$ representation by Cartesian coordinates in (2.7) can be seen as a minimal representation of the position of the end-effector. While, a (9×1) vector $\mathbf{x}_r$ representation by direction cosines in (2.8) can be seen as a non-minimal representation of the orientation of the end-effector. Therefore $m_{\text{rep}} = 12$.

2.3 Differential Kinematics

In this section, differential kinematics is presented to describe the the relationship between the joint velocities and the end-effector velocities. We present first the differential kinematics model of the end-effector representation.

Let direct kinematics is described by $\mathbf{x}_{\text{rep}} = \mathbf{k}(\mathbf{q})$. Therefore, by differentiating the direct kinematics function with respect to joint variables, it can be obtained

$$\frac{\partial \mathbf{x}_{\text{rep}}}{\partial \mathbf{q}} = \mathbf{J}_{\text{rep}}(\mathbf{q}) \tag{2.9}$$

where $\mathbf{J}_{\text{rep}}(\mathbf{q})$ denotes a $(m_{\text{rep}} \times n)$ *analytical* Jacobian matrix whose elements are defined as:

$$J_{\text{rep}_{ij}}(\mathbf{q}) = \frac{\partial k_i(\mathbf{q})}{\partial q_j}, \quad i = 1, \ldots, m_{\text{rep}},\ j = 1, \ldots, n. \tag{2.10}$$

Differentiating the left and right side of (2.9) with time t, it can be obtained the *representation differential kinematic model*, as

$$\dot{\mathbf{x}}_{\text{rep}} = \begin{pmatrix} \dot{\mathbf{x}}_p \\ \dot{\mathbf{x}}_r \end{pmatrix} = \mathbf{J}_{\text{rep}}(\mathbf{q})\ \dot{\mathbf{q}}. \tag{2.11}$$

Note, however, the representation differential kinematic model (2.11) is non-minimal (the orientational representation velocity is a (9×1) vector). It is therefore desirable to obtain a differential kinematic model with minimal representation.

It can be shown, by using *geometric technique* [47], that each joint velocity contributes to the end-effector linear and angular velocity. This leads to establishing the *basic differential kinematic model*, with minimal representation, describing the relationship between the joint velocities and the end-effector linear and angular velocities, expressed in Frame $\{0\}$ in Fig. 2.2, as

$$\dot{\mathbf{x}} = \begin{pmatrix} \mathbf{v} \\ \boldsymbol{\omega} \end{pmatrix} = \mathbf{J}(\mathbf{q})\ \dot{\mathbf{q}} \tag{2.12}$$

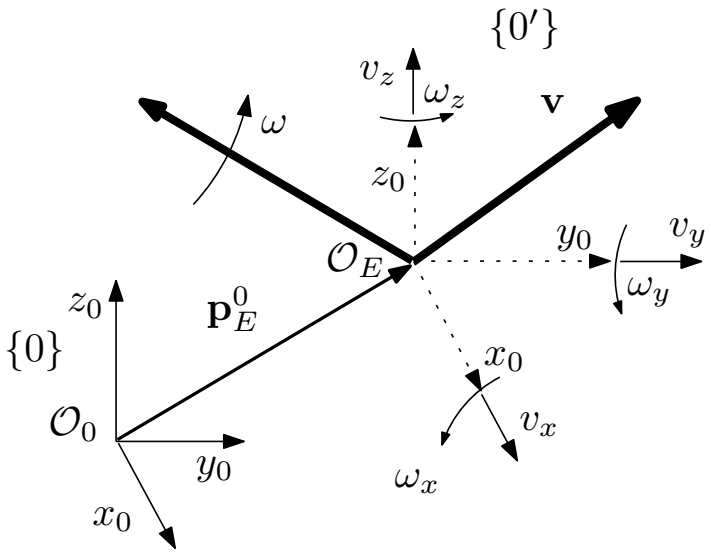

Figure 2.2: End-effector velocities.

where the matrix $\mathbf{J}(\mathbf{q}) \in \Re^{m \times n}$ denotes the *geometric* Jacobian.

The effector velocity, $\dot{\mathbf{x}}$ consists of a vector $\mathbf{v}$ to denote a $\max(3 \times 1)$ linear (translational) velocity vector as

$$\mathbf{v} = \begin{pmatrix} v_x(\mathbf{q}) & v_y(\mathbf{q}) & v_z(\mathbf{q}) \end{pmatrix}^{\mathrm{T}} \tag{2.13}$$

and a vector $\boldsymbol{\omega}$ to denote a $\max(3 \times 1)$ angular (rotational) velocity vector as

$$\boldsymbol{\omega} = \begin{pmatrix} \omega_x(\mathbf{q}) & \omega_y(\mathbf{q}) & \omega_z(\mathbf{q}) \end{pmatrix}^{\mathrm{T}}. \tag{2.14}$$

The vector $\dot{\mathbf{x}} \in \Re^m$, with $(m \leq 6)$, is then defined as the *operational space* coordinate vector, with m as the number of degree-of-freedom of the operational space coordinates and it is also independent of end-effector configuration parameters.

Note, for a manipulator, whose the number of degree-of-freedom of the operational space coordinates is less than the number of its joints i.e. $m < n$, is

defined as a redundant manipulator. And for a manipulator with the same number of joints and the operational space coordinates, is defined as non-redundant manipulator i.e. $m = n$. Throughout this thesis, our test bed is the PUMA 560, where $m = n = 6$ is non-redundant. The basic Jacobian $\mathbf{J}(\mathbf{q})$ is computed as

$$\mathbf{J}(\mathbf{q}) = \begin{pmatrix} \mathbf{J}_{P_1} & \dots & \mathbf{J}_{P_n} \\ \mathbf{J}_{O_1} & \dots & \mathbf{J}_{O_n} \end{pmatrix} \tag{2.15}$$

and $\mathbf{J}_{P_i} \in \Re^{m_P \times 1}$ and $\mathbf{J}_{O_i} \in \Re^{m_O \times 1}$, with $m_P, m_O \leq 3$, are defined as

$$\mathbf{J}_{P_i} = \begin{cases} \mathbf{s}_{3_i} & \text{for a prismatic joint} \\ [\mathbf{s}_3\times]\ (\mathbf{p}_E - \mathbf{p}_i) & \text{for a revolute joint} \end{cases} \tag{2.16}$$

$$\mathbf{J}_{O_i} = \begin{cases} \mathbf{0} & \text{for a prismatic joint} \\ \mathbf{s}_{3_i} & \text{for a revolute joint} \end{cases} \tag{2.17}$$

where the 3×3 skew-symmetric matrix operator $[\mathbf{s}\times]$ is defined as

$$\begin{pmatrix} 0 & -s_z & s_y \\ s_z & 0 & -s_x \\ -s_y & s_x & 0 \end{pmatrix}. \tag{2.18}$$

Note that, it is possible to express $\mathbf{J}(\mathbf{q})$ in frame $\{\mathrm{E}\}$ using the following transformation

$$\mathbf{J}^E(\mathbf{q}) = \begin{pmatrix} \mathbf{R}^E & \mathbf{0} \\ \mathbf{0} & \mathbf{R}^E \end{pmatrix} \mathbf{J}, \tag{2.19}$$

therefore, by using $\mathbf{J}^E(\mathbf{q})$ (2.19), the end-effector linear and angular velocity can be expressed in Frame $\{\mathrm{E}\}$ as

$$\dot{\mathbf{x}}^E = \begin{pmatrix} \mathbf{v}^E \\ \boldsymbol{\omega}^E \end{pmatrix} = \mathbf{J}^E(\mathbf{q})\ \dot{\mathbf{q}}. \tag{2.20}$$

2.3.1 $\mathbf{E}_p$ and $\mathbf{E}_r$ Jacobian

It can be shown in [91] that it is possible to relate the end-effector operational space velocity with the representation velocity as follows

$$\dot{\mathbf{x}}_{\text{rep}} = \mathbf{E}\,\dot{\mathbf{x}} \tag{2.21}$$

or,

$$\begin{pmatrix} \dot{\mathbf{x}}_p \\ \dot{\mathbf{x}}_r \end{pmatrix} = \begin{pmatrix} \mathbf{E}_p & 0 \\ 0 & \mathbf{E}_r \end{pmatrix} \begin{pmatrix} \mathbf{v} \\ \boldsymbol{\omega} \end{pmatrix}. \tag{2.22}$$

The matrix $\mathbf{E}_p \in \Re^{m_P \times m_P}$ relates the operational space linear velocity, $\mathbf{v}$, with the end-effector translational velocity $\dot{\mathbf{x}}_p$. In general $m_P \leq 3$, however for a full 3D space translational motion, $m_P = 3$. Therefore, if $\mathbf{x}_p$ is chosen as the Cartesian coordinates representation (2.7), we have

$$\dot{\mathbf{x}}_p = \mathbf{v} = \begin{pmatrix} \dot{p}_x(\mathbf{q}) & \dot{p}_y(\mathbf{q}) & \dot{p}_z(\mathbf{q}) \end{pmatrix}^{\mathrm{T}}, \tag{2.23}$$

then, $\mathbf{E}_p$ is simply an identity matrix of size (3×3). The matrix $\mathbf{E}_r \in \Re^{9 \times m_O}$ relates the operational space linear velocity, $\boldsymbol{\omega}$, with the end-effector angular velocity, $\dot{\mathbf{x}}_r$. In general $m_O \leq 3$, however for a full 3D space rotational motion, $m_O = 3$. Therefore, if $\mathbf{x}_r$ is chosen as the direction cosines representation (2.8), then $\mathbf{E}_r$ can be determined as follows [91]

$$\mathbf{E}_r(\mathbf{x}_r) = \begin{pmatrix} -[\mathbf{s}_1\times] \\ -[\mathbf{s}_2\times] \\ -[\mathbf{s}_3\times] \end{pmatrix}. \tag{2.24}$$

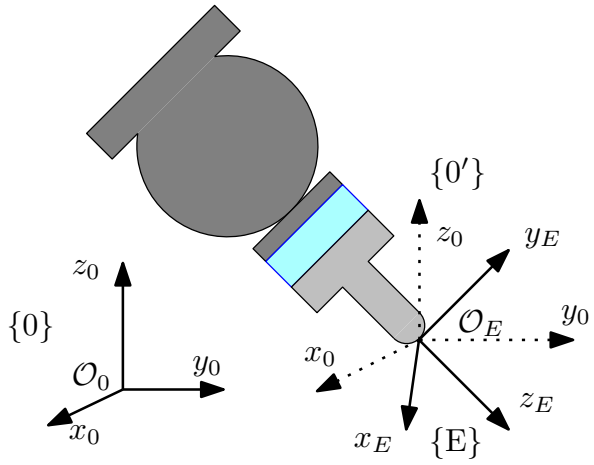

Figure 2.3: Operational frames assignment

2.4 The Operational Space Formulation

The operational framework perceives the operation of a manipulator at some point attached to the end-effector, where the task is specified. This point is called the *operational point*, and for convenience the origin of Frame $\{\mathrm{E}\}$, $\mathcal{O}_{\mathrm{E}}$, can be selected as the operational point as illustrated in Figure 2.3. At point $\mathcal{O}_{\mathrm{E}}$ is also attached Frame $\{0'\}(\mathcal{O}_{\mathrm{E}}, x_0, y_0, z_0)$, which is parallel with the base frame $\{0\}(\mathcal{O}_0, x_0, y_0, z_0)$. This shows that the operational space parameters, depending on implementation, can be expressed in to base Frame $\{0\}$ or Frame $\{\mathrm{E}\}$.

Note that, the operational space dynamics of the end-effector can be derived from both the *representation differential kinematic model* (2.11) or the *basic differential kinematic model* (2.12), or (2.20).

It can be shown in [47] that, the operational space dynamics based upon the

representation differential kinematic model can provide only the motion formulation. However, the operational space dynamic based upon the basic differential kinematic model can be shown to provide a unified framework for the the free-motion (motion only) formulation and the parallel force-motion formulation [8, 91].

Let us now explain what the operational space formulation is, starting with the free-motion formulation.

2.4.1 Unconstrained Motion Formulation

Before we discuss the end-effector unconstrained motion dynamics, let us present the joint space dynamics of the manipulator; this describes completely the dynamics of the system. The joint space dynamics for any manipulator, where no interaction exists with the environment, can be described as follows [89, 47, 90, 91]

$$\mathbf{M}(\mathbf{q})\ddot{\mathbf{q}} + \mathbf{B}(\mathbf{q},\dot{\mathbf{q}})\dot{\mathbf{q}} + \mathbf{g}(\mathbf{q}) + \boldsymbol{\tau}_{\text{fric}}(\dot{\mathbf{q}}) = \boldsymbol{\Gamma} \tag{2.25}$$

where $\mathbf{q} \in \Re^n$ denotes the vector of joint space coordinates and $\boldsymbol{\Gamma} \in \Re^n$ denotes the vector of generalized joint space force. The Lagrangian joint space matrices and vectors: $\mathbf{M}(\mathbf{q}) \in \Re^{n\times n}$, $\mathbf{B}(\mathbf{q},\dot{\mathbf{q}}) \in \Re^{n\times n}$, $\mathbf{g}(\mathbf{q}) \in \Re^n$, and $\boldsymbol{\tau}_{\text{fric}}(\dot{\mathbf{q}}) \in \Re^n$ denote the inertia matrix, Coriolis/centrifugal matrix, gravity vector and joint friction vector, respectively. Joint friction vector $\boldsymbol{\tau}_{\text{fric}}(\dot{\mathbf{q}})$ can be defined as in [92]

$$\boldsymbol{\tau}_{\text{fric}}(\dot{\mathbf{q}}) = \boldsymbol{\tau}_{vis}\dot{\mathbf{q}} + \left[\boldsymbol{\tau}_{cou} + \boldsymbol{\tau}_{sti}\text{exp}^{(-\boldsymbol{\tau}_{dec}\dot{\mathbf{q}}^2)}\right]\text{sgn}(\dot{\mathbf{q}}) \tag{2.26}$$

where $\text{sgn}(\dot{q}) = +1, -1, 0$ if $\dot{q} =$ positive, negative and zero, respectively and

$\boldsymbol{\tau}_{vis}$, $\boldsymbol{\tau}_{cou}$, $\boldsymbol{\tau}_{sti}$, and $\boldsymbol{\tau}_{dec} \in \Re^n$ are the viscous friction, coulomb friction, static friction (stiction) and Stribeck effect, respectively.

By using the basic differential kinematic model (2.12) and its derivative, it is possible to transform the joint space dynamics (2.25) into the unconstrained motion (free-motion, or simply, motion) of the effector dynamics of a non-redundant manipulator in the operational space defined as

$$\mathbf{M}_{\mathbf{x}}(\mathbf{q})\ddot{\mathbf{x}} + \mathbf{B}_{\mathbf{x}}(\mathbf{q}, \dot{\mathbf{q}})\dot{\mathbf{x}} + \mathbf{g}_{\mathbf{x}}(\mathbf{q}) + \boldsymbol{\tau}_{\mathbf{x}}(\mathbf{q}, \dot{\mathbf{q}}) = \mathbf{F} \tag{2.27}$$

where the vector $\mathbf{F} \in \Re^m$ denotes the generalized forces in the operational space. The operational space matrices and vectors $\mathbf{M}_{\mathbf{x}}(\mathbf{q}) \in \Re^{m\times m}$, $\mathbf{B}_{\mathbf{x}}(\mathbf{q}, \dot{\mathbf{q}}) \in \Re^{m\times m}$, $\mathbf{g}_{\mathbf{x}}(\mathbf{q}) \in \Re^m$ and $\boldsymbol{\tau}_{\mathbf{x}}(\mathbf{q}, \dot{\mathbf{q}}) \in \Re^m$ denote the inertia, Coriolis/centrifugal, gravity and joint friction dynamical terms expressed in operational space, respectively, for a non-redundant manipulator in non-singular configuration. These operational space dynamic terms can be obtained from the joint space equivalents as [47]:

$$\mathbf{M}_{\mathbf{x}}(\mathbf{q}) = \mathbf{J}^{-\mathrm{T}}(\mathbf{q})\mathbf{M}(\mathbf{q})\mathbf{J}^{-1}(\mathbf{q}) \tag{2.28}$$

$$\mathbf{B}_{\mathbf{x}}(\mathbf{q}, \dot{\mathbf{q}}) = [\mathbf{J}^{-\mathrm{T}}(\mathbf{q})\mathbf{B}(\mathbf{q}, \dot{\mathbf{q}}) - \mathbf{M}_{\mathbf{x}}(\mathbf{q})\dot{\mathbf{J}}(\mathbf{q}, \dot{\mathbf{q}})]\mathbf{J}^{-1}(\mathbf{q}) \tag{2.29}$$

$$\mathbf{g}_{\mathbf{x}}(\mathbf{q}) = \mathbf{J}^{-\mathrm{T}}(\mathbf{q})\mathbf{g}(\mathbf{q}) \tag{2.30}$$

$$\boldsymbol{\tau}_{\mathbf{x}}(\mathbf{q}, \dot{\mathbf{q}}) = \mathbf{J}^{-\mathrm{T}}(\mathbf{q})\boldsymbol{\tau}_{\text{fric}}(\dot{\mathbf{q}}) \tag{2.31}$$

When all the dynamic terms are known a priori, the inverse dynamics motion control can be designed for (2.27) as in [8]

$$\mathbf{F} = \mathbf{M}_{\mathbf{x}}(\mathbf{q})\mathbf{F}^*_{\text{motion}} + \mathbf{B}_{\mathbf{x}}(\mathbf{q}, \dot{\mathbf{q}})\dot{\mathbf{x}} + \mathbf{g}_{\mathbf{x}}(\mathbf{q}) + \boldsymbol{\tau}_{\mathbf{x}}(\mathbf{q}, \dot{\mathbf{q}}) \tag{2.32}$$

where

$$\mathbf{F}^*_{\text{motion}} = \ \ddot{\mathbf{x}}_d + \mathbf{K_v}\dot{\mathbf{e}}_\mathbf{x} + \mathbf{K_p}\mathbf{e}_\mathbf{x} \tag{2.33}$$

where $\mathbf{e_x} = \mathbf{x}_d - \mathbf{x}$ and $\dot{\mathbf{e}}_\mathbf{x} = \dot{\mathbf{x}}_d - \dot{\mathbf{x}}$ denote the operational space position and velocity tracking errors, respectively; and $\mathbf{x}_d$, $\dot{\mathbf{x}}_d$ and $\ddot{\mathbf{x}}_d$ are the desired operational space trajectories. Details on the operational signals making up $\mathbf{F}^*_{\text{motion}}$ is provided in Appendix B.1.

Note that the controller (2.32) is similar to the well known the joint space *computed-torque control*, except it is now done in operational space. Thus, to show the stability is quite straightforward. Combining (2.27) and (2.32), yields the following second-order closed-loop equation

$$\ddot{\mathbf{e}}_\mathbf{x} + \mathbf{K_v}\dot{\mathbf{e}}_\mathbf{x} + \mathbf{K_p}\mathbf{e}_\mathbf{x} = 0 \tag{2.34}$$

Hence with proper choice of $\mathbf{K_p}, \mathbf{K_v}$, as $t \to \infty$, $\dot{\mathbf{e}}_\mathbf{x}, \mathbf{e}_\mathbf{x} \to 0$.

2.4.2 Constrained Motion Formulation

The effector dynamics of a non-redundant manipulator interacting with the environment (constrained motion or compliant motion dynamics) in operational space can be written as

$$\mathbf{M_x}(\mathbf{q})\ddot{\mathbf{x}} + \mathbf{B_x}(\mathbf{q},\dot{\mathbf{q}})\dot{\mathbf{x}} + \mathbf{g_x}(\mathbf{q}) + \boldsymbol{\tau}_\mathbf{x}(\mathbf{q},\dot{\mathbf{q}}) + \boldsymbol{\Omega}\mathbf{h}(\dot{\mathbf{x}}) + \bar{\boldsymbol{\Omega}}\mathbf{f}_{\text{contact}} = \mathbf{F} \tag{2.35}$$

where the operational space matrices and vectors $\mathbf{M_x}(\mathbf{q}) \in \Re^{m\times m}$, $\mathbf{B_x}(\mathbf{q},\dot{\mathbf{q}}) \in \Re^{m\times m}$, $\mathbf{g_x}(\mathbf{q}) \in \Re^m$ and $\boldsymbol{\tau}_\mathbf{x}(\mathbf{q},\dot{\mathbf{q}}) \in \Re^m$ are similar with (2.28) – (2.31), with now there is an additional term: the vector $\mathbf{f} \in \Re^m$ represents the contact

force vector exerted by the effector onto the contact surface. The relationship between the operational space coordinates and the contact forces can be safely assumed to be represented by a simple linear spring model

$$\mathbf{f}_{\text{contact}} = \mathbf{K}_e \, \delta\mathbf{x} = \mathbf{K}_e(\mathbf{x} - \mathbf{x}_{\text{init}}) \tag{2.36}$$

where $\mathbf{x}_{\text{init}}$ is the end-effector position when in contact with the surface with zero contact force, and $\mathbf{K}_e$ is defined as the linear spring matrix. This linear spring model is applied to both translational and rotational degrees of freedom of the manipulator. Therefore, the first and second derivatives of (2.36) can be obtained as

$$\dot{\mathbf{x}} = \mathbf{K}_e^{-1} \, \dot{\mathbf{f}}_{\text{contact}} \tag{2.37}$$

$$\ddot{\mathbf{x}} = \mathbf{K}_e^{-1} \, \ddot{\mathbf{f}}_{\text{contact}}. \tag{2.38}$$

For ease of explanation, let's assume that we have a full 3D space translational and rotational motion i.e. $m_P, m_O = 3$, which can be achieved by a non-redundant manipulator with six DOF, therefore we have $m = m_P + m_O \equiv n = 6$.

In the operational space formulation, compliant motion can be achieved by decoupling between the axes assigned for translation/rotation (motion control) and to those for force/moment (force control). This is achieved by using selection matrices, $\mathbf{\Omega}$ and $\bar{\mathbf{\Omega}}$, constructed as 6×6 matrices as in the original formulation

in [8]:

$$\mathbf{\Omega} = \begin{bmatrix} (\mathbf{R}_{\mathrm{E}})^{\mathrm{T}}\, \mathbf{\Sigma}_F\, \mathbf{R}_{\mathrm{E}} & 0 \\ 0 & (\mathbf{R}_{\mathrm{E}})^{\mathrm{T}}\, \mathbf{\Sigma}_M\, \mathbf{R}_{\mathrm{E}} \end{bmatrix}$$
$$\bar{\mathbf{\Omega}} = \begin{bmatrix} (\mathbf{R}_{\mathrm{E}})^{\mathrm{T}}\, \bar{\mathbf{\Sigma}}_F\, \mathbf{R}_{\mathrm{E}} & 0 \\ 0 & (\mathbf{R}_{\mathrm{E}})^{\mathrm{T}}\, \bar{\mathbf{\Sigma}}_M\, \mathbf{R}_{\mathrm{E}} \end{bmatrix} \tag{2.39}$$

where $\mathbf{R}_{\mathrm{E}}$ is the appropriate rotational matrix to transform the reference frame in the base frame, $\{0\}$, to the end-effector frame, $\{\mathrm{E}\}$. Furthermore

$$\mathbf{\Sigma}_F = \begin{bmatrix} \sigma_{f_x} & 0 & 0 \\ 0 & \sigma_{f_y} & 0 \\ 0 & 0 & \sigma_{f_z} \end{bmatrix}, \bar{\mathbf{\Sigma}}_F = \mathbf{I}_{3\times 3} - \mathbf{\Sigma}_F$$
$$\mathbf{\Sigma}_M = \begin{bmatrix} \sigma_{m_x} & 0 & 0 \\ 0 & \sigma_{m_y} & 0 \\ 0 & 0 & \sigma_{m_z} \end{bmatrix}, \bar{\mathbf{\Sigma}}_M = \mathbf{I}_{3\times 3} - \mathbf{\Sigma}_M \tag{2.40}$$

in which $\sigma_{f_x}, \sigma_{f_y}, \sigma_{f_z}$ are given the value 1 for free-motion and 0 for constrained motion i.e. translational motion control and force control, respectively. Similarly, $\sigma_{m_x}, \sigma_{m_y}, \sigma_{m_z}$ are given the value 1 and 0 to represent free and constrained rotation i.e. rotational motion control and moment control, respectively.

Note that, (2.39) is true when the operational space coordinates are expressed in to Frame $\{0\}$. However, it is possible to express all operational space variables in Frame $\{\mathrm{E}\}$ i.e. $\mathbf{R}_{\mathrm{E}} = \mathbf{I}$, therefore, in this thesis, $\mathbf{\Omega}$ and $\bar{\mathbf{\Omega}}$ can be simplified as follows

$$\mathbf{\Omega} = \begin{bmatrix} 1 & 0 & 0 & 0 & 0 & 0 \\ 0 & 1 & 0 & 0 & 0 & 0 \\ 0 & 0 & 0 & 0 & 0 & 0 \\ 0 & 0 & 0 & 0 & 0 & 0 \\ 0 & 0 & 0 & 0 & 0 & 0 \\ 0 & 0 & 0 & 0 & 0 & 1 \end{bmatrix}, \quad \bar{\mathbf{\Omega}} = \begin{bmatrix} 0 & 0 & 0 & 0 & 0 & 0 \\ 0 & 0 & 0 & 0 & 0 & 0 \\ 0 & 0 & 1 & 0 & 0 & 0 \\ 0 & 0 & 0 & 1 & 0 & 0 \\ 0 & 0 & 0 & 0 & 1 & 0 \\ 0 & 0 & 0 & 0 & 0 & 0 \end{bmatrix}. \tag{2.41}$$

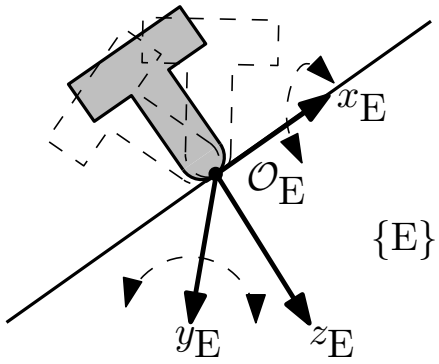

Figure 2.4: Compliant motion at the effector frame $\{\mathrm{E}\}(\mathcal{O}_{\mathrm{E}}, x_{\mathrm{E}}, y_{\mathrm{E}}, z_{\mathrm{E}})$.

Therefore, specifically in our implementation, all operational space dynamics and coordinates are expressed in Frame $\{\mathrm{E}\}$ and for convenience the superscript 'E' is dropped.

Compliant motion in the operational space can then be shown as follows: as shown in Fig. 2.4, using selection matrices $\mathbf{\Omega}$ and $\bar{\mathbf{\Omega}}$ (2.41), we can have force control along z_{E} axis (F_z), and the moment controls along $x_{\mathrm{E}}, y_{\mathrm{E}}$ axes (M_x, M_y), respectively. By controlling M_x, M_y to zeroes, then the effector axis z_E can be controlled to be always normal to the surface and it can move on the surface's curvature accordingly by translational motion control along x_E, y_E axes. Therefore the surface's geometry is not needed.

As in motion control equivalent, similarly, when all the dynamic terms are known a priori, the inverse dynamics parallel force-motion control can be designed for (2.35) as in

$$\mathbf{M_x}(\mathbf{q})(\mathbf{\Omega F}^*_{\mathrm{motion}} + \bar{\mathbf{\Omega}}\mathbf{F}^*_{\mathrm{force}}) + \mathbf{B_x}(\mathbf{q}, \dot{\mathbf{q}})\dot{\mathbf{x}} + \mathbf{g_x}(\mathbf{q}) + \boldsymbol{\tau}_{\mathbf{x}}(\mathbf{q}, \dot{\mathbf{q}}) + \mathbf{f}_{\text{sensor}} = \mathbf{F} \tag{2.42}$$

with the $\mathbf{F}^*_{\text{motion}}$ is the same as in (2.33), while $\mathbf{F}^*_{\text{force}}$ is defined as

$$\begin{aligned}\mathbf{F}^*_{\text{force}} &= -\dot{\mathbf{x}} + \mathbf{K_p}\,\mathbf{e_f} + \mathbf{K_I}\int_{\text{t}}\mathbf{e_f}\;\text{dt} \\ &= \mathbf{K}_e^{-1}\,\dot{\mathbf{e}}_\mathbf{f} + \mathbf{K_p}\,\mathbf{e_f} + \mathbf{K_I}\int_{\text{t}}\mathbf{e_f}\;\text{dt}\end{aligned} \tag{2.43}$$

where $\mathbf{e_f} = \mathbf{f}_d - \mathbf{f}$ and $\dot{\mathbf{e}}_\mathbf{f} = -\dot{\mathbf{f}} = -\mathbf{K}_e\,\dot{\mathbf{x}}$ are the force tracking errors, where $\mathbf{f}_d$ is a constant desired active-force. The vector $\mathbf{f}_{\text{sensor}} \in \Re^m$ denotes the force/moment readings at the tip of the end-effector, expressed in Frame $\{\text{E}\}$, where it can be assumed that $\mathbf{f}_{\text{sensor}}$ equals to $\mathbf{f}_{\text{contact}}$.

Therefore, by combining (2.35) and (2.42), taking into account selection matrices $\mathbf{\Omega}$ and $\bar{\mathbf{\Omega}}$ in (2.41), the motion and force closed-loop subsystems can be obtained as

$$\mathbf{\Omega}(\ddot{\mathbf{e}}_\mathbf{x} + \mathbf{K_v}\dot{\mathbf{e}}_\mathbf{x} + \mathbf{K_p}\mathbf{e_x}) = 0 \tag{2.44}$$

$$\bar{\mathbf{\Omega}}(-\mathbf{K}_e^{-1}\,\ddot{\mathbf{f}} + \mathbf{K}_e^{-1}\dot{\mathbf{e}}_\mathbf{f} + \mathbf{K_p}\mathbf{e_f} + \mathbf{K_I}\int_{\text{t}}\mathbf{e_f}\;\text{dt}) = 0 \tag{2.45}$$

The stability analysis for the closed-loop motion subsystem has been discussed in Section 2.4.1. For the closed-loop force subsystem, using (2.36)–(2.38), it can be shown as

$$\ddot{\mathbf{e}}_\mathbf{f} + \dot{\mathbf{e}}_\mathbf{f} + \mathbf{K}_e\,\mathbf{K_p}\mathbf{e_f} + \mathbf{K}_e\,\mathbf{K_I}\int_{\text{t}}\mathbf{e_f}\;\text{dt} = 0 \tag{2.46}$$

Hence with proper and tunable gains $\mathbf{K_p}, \mathbf{K_I}$, then as $t \to \infty$, $\mathbf{e_f} \to 0$.

2.5 Torque/Force Relationship

In the real time implementation, the actuators of the robot only take the generalized joint forces $\mathbf{\Gamma}$. Therefore, the generalized operational space control

signal $\mathbf{F}$ must be converted into the generalized joint space equivalent. For a non-redundant manipulator, the generalized joint forces $\boldsymbol{\Gamma}$ is given by the relationship [8, 47]

$$\boldsymbol{\Gamma} = \mathbf{J}^{\mathrm{T}}(\mathbf{q})\,\mathbf{F} \tag{2.47}$$

where it is then sent into the actuators of the robot.

CHAPTER 3

ADAPTIVE CONTROL REVIEW

3.1 Chapter Overview

In this chapter we present a critical review of the existing adaptive control of robot manipulators of the following works: (i) the joint space direct LIP adaptive control, (ii) the operational space direct LIP motion control, and (iii) the original joint space NN based adaptive control.

3.2 Joint Space Direct LIP Adaptive Control

In this section, we present the concept and stability analysis of the LIP direct adaptive control in joint space [46]. We first introduce some useful properties of the joint space dynamic to be used later for control development and the stability analysis.

Note, unless otherwise specified, in this thesis all vector/matrix norms are defined as Frobenius norm $\|\cdot\|_F$, which is: the square-root of the sums of the square of individual element of a matrix / vector.

The Frobenius norm of vector $\mathbf{a} \in \Re^m$ is defined as

$$\|\mathbf{a}\| = \sqrt{\sum_i^m a_i^2} \tag{3.1}$$

The Frobenius norm of matrix $\mathbf{A} \in \Re^{m \times n}$ is defined as

$$\|\mathbf{A}\| = \text{trace}(\mathbf{A}^{\mathrm{T}}\mathbf{A}) = \sqrt{\sum_{j}^{n}\sum_{i}^{m} a_{ij}^2} \tag{3.2}$$

Also the Frobenius inner product of two matrices $\mathbf{A}, \mathbf{B} \in \Re^{m \times n}$ can be defined as

$$\langle \mathbf{A}, \mathbf{B} \rangle = \text{trace}(\mathbf{A}^{\mathrm{T}}\mathbf{B}) = \sum_{j}^{n}\sum_{i}^{m} a_{ij} b_{ij} \tag{3.3}$$

3.2.1 Properties of Joint Space Dynamics

Property 3.2.1 *The joint space kinetic energy matrix $\mathbf{M}(\mathbf{q}) \in \Re^{n \times n}$ is symmetric and positive definite matrix, and therefore all its eigenvalues are positive. It follows from Rayleigh-Ritz theorem [93] that: any positive definite matrix $\mathbf{A}$ satisfies $A_m \leq \|\mathbf{A}\| \leq A_M$, where $A_m, A_M > 0$ denote the minimum and maximum eigenvalues of $\mathbf{A}$, respectively. Therefore $\mathbf{M}(\mathbf{q}(t))$ is lower and upper-bounded by its global minimum and maximum eigenvalues along $t \geq 0$, respectively, as:*

$$M_m \leq \|\mathbf{M}(\mathbf{q}(t))\| \leq M_M, \quad t \geq 0 \tag{3.4}$$

where $M_m = min(\lambda_{min}(\mathbf{M}(\mathbf{q}(t)))) > 0$ and $M_M = max(\lambda_{max}(\mathbf{M}(\mathbf{q}(t)))) > 0$, where $\lambda_{min}(\cdot)$ and $\lambda_{max}(\cdot)$ denote the minimum and maximum eigenvalue operators, respectively.

Property 3.2.2 *The joint space Coriolis / centrifugal matrix $\mathbf{B}(\mathbf{q}, \dot{\mathbf{q}})$ is upper-bounded [47]*

$$\|\mathbf{B}(\mathbf{q}, \dot{\mathbf{q}})\| \leq B_M \, \dot{q}_M \tag{3.5}$$

where B_M is a positive scalar constant. Note $\dot{\mathbf{q}}$ can be assumed to bounded since in reality saturation occurs on the maximum velocity of the motor [47].

Property 3.2.3 *The joint space gravity vector $\mathbf{g}(\mathbf{q})$ is upper-bounded [47]*

$$\|\mathbf{g}(\mathbf{q})\| \leq g_M < \infty \tag{3.6}$$

Property 3.2.4 *As shown in [90], the joint friction forces, $\boldsymbol{\tau}_{fric}(\dot{\mathbf{q}})$ (2.31), are bounded in magnitude*

$$\|\boldsymbol{\tau}_{vis}\dot{\mathbf{q}}\| \leq \tau_{vis_M}\ \dot{q}_M \tag{3.7}$$

$$\|\boldsymbol{\tau}_{cou} sgn(\dot{\mathbf{q}})\| \leq \tau_{cou_M} \tag{3.8}$$

$$\|\boldsymbol{\tau}_{sti} exp^{(-\boldsymbol{\tau}_{dec}\dot{\mathbf{q}}^2)} sgn(\dot{\mathbf{q}})\| \leq \tau_{sti_M} \tag{3.9}$$

Property 3.2.5 *The matrix $\dot{\mathbf{M}}(\mathbf{q}) - 2\mathbf{B}(\mathbf{q}, \dot{\mathbf{q}})$ is a skew-symmetric matrix [90], hence given any joint space vector $\mathbf{z} \in \Re^n$, it satisfies*

$$\mathbf{z}^{\mathrm{T}} \left(\dot{\mathbf{M}}(\mathbf{q}) - 2\mathbf{B}(\mathbf{q}, \dot{\mathbf{q}}) \right) \mathbf{z} = 0. \tag{3.10}$$

3.2.2 LIP Model and Direct LIP Adaptive Control

In this section, we first review the linearity property of robot dynamics, the direct LIP adaptive control, and then the closed-loop error dynamics. And finally, we will present the stability analysis. The joint space dynamics (2.25), considering only joint viscous and coulomb friction vectors, can be written as

$$\boldsymbol{\Gamma} = \mathbf{M}(\mathbf{q})\ddot{\mathbf{q}} + \mathbf{B}(\mathbf{q}, \dot{\mathbf{q}}) + \mathbf{g}(\mathbf{q}) + \boldsymbol{\tau}_{vis}\dot{\mathbf{q}} + \boldsymbol{\tau}_{cou}\ \mathrm{sgn}(\dot{\mathbf{q}}) \tag{3.11}$$

Note that, (3.11) was obtained by considering only joint viscous and coulomb friction vectors in order to achieve the linearity property, therefore (3.11) can be shown in linear-in-parameter model as follows [94, 47]

$$\mathbf{\Gamma} = \mathbf{Y}(\mathbf{q}, \dot{\mathbf{q}}, \ddot{\mathbf{q}})\, \boldsymbol{\pi} \tag{3.12}$$

where $\mathbf{Y}(\mathbf{q}, \dot{\mathbf{q}}, \ddot{\mathbf{q}}) \in \Re^{n \times 13n}$ is the calculable regression matrix and $\boldsymbol{\pi} \in \Re^{13n}$ is the vector of actual dynamic parameters. Note that (3.12) can be expanded as follows

$$\begin{bmatrix} \Gamma_1 \\ \Gamma_2 \\ \vdots \\ \Gamma_n \end{bmatrix} = \begin{bmatrix} \mathbf{y}_{11}^{\mathrm{T}} & \mathbf{y}_{12}^{\mathrm{T}} & \cdots & \mathbf{y}_{1n}^{\mathrm{T}} \\ \mathbf{y}_{21}^{\mathrm{T}} & \mathbf{y}_{22}^{\mathrm{T}} & \cdots & \mathbf{y}_{2n}^{\mathrm{T}} \\ \vdots & \vdots & \ddots & \vdots \\ \mathbf{y}_{n1}^{\mathrm{T}} & \mathbf{y}_{n2}^{\mathrm{T}} & \cdots & \mathbf{y}_{nn}^{\mathrm{T}} \end{bmatrix} \begin{bmatrix} \boldsymbol{\pi}_1 \\ \boldsymbol{\pi}_2 \\ \vdots \\ \boldsymbol{\pi}_n \end{bmatrix} \tag{3.13}$$

where $\boldsymbol{\pi}_i$ is a (13×1) vector of actual inertial parameters defined as follows

$$\begin{aligned} \boldsymbol{\pi}_i = [&m_{l_i}\ m_{l_i} l_{C_i x}\ m_{l_i} l_{C_i y}\ m_{l_i} l_{C_i z}\ \bar{I}^i_{l_i xx}\ \bar{I}^i_{l_i yy}\ \bar{I}^i_{l_i zz}\ \bar{I}^i_{l_i xy}\ \bar{I}^i_{l_i yz}\ \bar{I}^i_{l_i xz}\ I_{m_i}\ \tau_{vis_i}\ \tau_{cou_i}]^{\mathrm{T}} \\ &\text{for } i = 1, \ldots, n \end{aligned} \tag{3.14}$$

In details, the inertial parameters are defined as follows:

- m_{l_i} is the mass of Link i (scalar).
- $m_{l_i} l_{C_i x}\ m_{l_i} l_{C_i y}\ m_{l_i} l_{C_i z}$ are the components of the first moment of inertia of Link i, which are obtained by multiplying the link mass with the 3×1 position vector

$$\mathbf{r}^i_{i,C_i} = \begin{pmatrix} l_{C_i x} & l_{C_i y} & l_{C_i z} \end{pmatrix}^{\mathrm{T}} \tag{3.15}$$

  which is defined as the center-of-mass of link i with respect to frame i.

- The variables $\bar{I}^i_{l_ixx}, \bar{I}^i_{l_iyy}, \bar{I}^i_{l_izz}, \bar{I}^i_{l_ixy}, \bar{I}^i_{l_iyz}, \bar{I}^i_{l_ixz}$ are defined as

$$\bar{I}^i_{l_ixx} = I^i_{l_ixx} + m_{l_i}(l^2_{C_iy} + l^2_{C_iz}) \tag{3.16}$$

$$\bar{I}^i_{l_iyy} = I^i_{l_iyy} + m_{l_i}(l^2_{C_ix} + l^2_{C_iy}) \tag{3.17}$$

$$\bar{I}^i_{l_izz} = I^i_{l_izz} + m_{l_i}(l^2_{C_ix} + l^2_{C_iy}) \tag{3.18}$$

$$\bar{I}^i_{l_ixy} = I^i_{l_ixz} + m_{l_i}(l_{C_ix} + l_{C_iy}) \tag{3.19}$$

$$\bar{I}^i_{l_iyz} = I^i_{l_iyz} + m_{l_i}(l_{C_iy} + l_{C_iz}) \tag{3.20}$$

$$\bar{I}^i_{l_ixz} = I^i_{l_ixz} + m_{l_i}(l_{C_ix} + l_{C_iz}) \tag{3.21}$$

which is obtained from the following computation

$$\bar{\mathbf{I}}^i_{l_i} = \mathbf{I}^i_{l_i} + m_{l_i}\mathbf{S}(\mathbf{r}^i_{i,C_i})^{\mathrm{T}}\mathbf{S}(\mathbf{r}^i_{i,C_i}) \tag{3.22}$$

where

$$\mathbf{I}^i_{l_i} = \begin{bmatrix} I^i_{l_ixx} & -I^i_{l_ixy} & -I^i_{l_ixz} \\ -I^i_{l_ixy} & I^i_{l_iyy} & -I^i_{l_iyz} \\ -I^i_{l_ixz} & -I^i_{l_iyz} & I^i_{l_izz} \end{bmatrix} \tag{3.23}$$

is the inertia tensor of the center-of-mass of Link i, expressed in frame i.

And $\mathbf{S}(\mathbf{r}^i_{i,C_i})$ is a 3×3 skew-symmetric operator matrix defined as

$$\mathbf{S}(\mathbf{r}^i_{i,C_i}) = \begin{pmatrix} 0 & -l_{C_iz} & l_{C_iy} \\ l_{C_iz} & 0 & -l_{C_ix} \\ -l_{C_iy} & l_{C_ix} & 0 \end{pmatrix} \tag{3.24}$$

given a 3×1 vector $\mathbf{r}^i_{i,C_i} = \begin{pmatrix} l_{C_ix} & l_{C_iy} & l_{C_iz} \end{pmatrix}^{\mathrm{T}}$.

- I_{m_i} is a scalar motor inertia about its axis of rotation z_{m_i}. It is taken from the $(3,3)$ element of the motor inertia tensor $\mathbf{I}^{m_i}_{m_i}$ as follows:

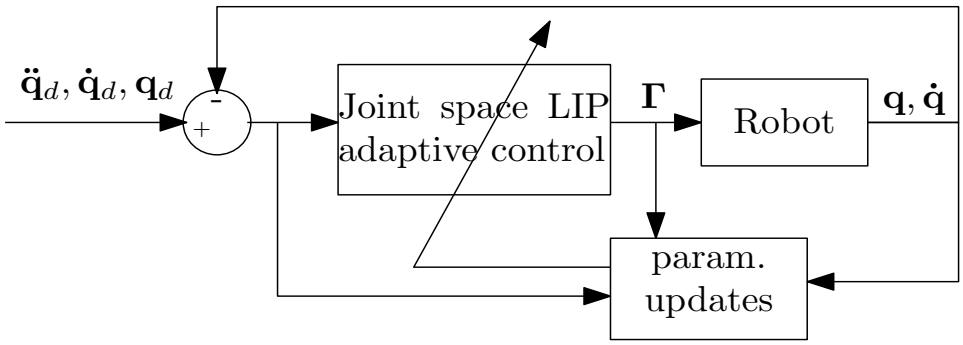

Figure 3.1: The joint space direct LIP adaptive control structure.

Assuming the rotor has symmetric mass distribution about its axis of rotation and selecting a proper frame, the motor inertia tensor $\mathbf{I}_{m_i}^{m_i}$, expressed in its own frame m_i, can be written as

$$\mathbf{I}_{m_i}^{m_i} = \begin{bmatrix} I_{m_i xx}^{m_i} & 0 & 0 \\ 0 & I_{m_i yy}^{m_i} & 0 \\ 0 & 0 & I_{m_i zz}^{m_i} \end{bmatrix} \tag{3.25}$$

It can be shown in [47] that, out of three elements of the motor inertia tensor, only $I_{m_i zz}^{m_i}$ will contribute into the kinetic energy. Therefore, only $I_{m_i zz}^{m_i}$ is taken into account. To simplify the notation, the scalar $I_{m_i zz}^{m_i}$ is written as I_{m_i}.

The control law, as shown in Fig. 3.1, is defined as

$$\mathbf{\Gamma} = \hat{\mathbf{M}}(\mathbf{q})\mathbf{\Gamma}^* + \hat{\mathbf{B}}(\mathbf{q}, \dot{\mathbf{q}})\dot{\mathbf{q}}_r + \hat{\mathbf{g}}(\mathbf{q}) + \hat{\boldsymbol{\tau}}_{vis}\dot{\mathbf{q}}_r + \hat{\boldsymbol{\tau}}_{cou}\,\mathrm{sgn}(\dot{\mathbf{q}}) \tag{3.26}$$

The following terms $\dot{\mathbf{q}}_r$ and $\mathbf{\Gamma}^*$ are defined as

$$\dot{\mathbf{q}}_r = \dot{\mathbf{q}}_d + \mathbf{\Lambda}\mathbf{e} \tag{3.27}$$

$$\mathbf{\Gamma}^* = \ddot{\mathbf{q}}_r + \mathbf{\Lambda}\mathbf{r} \tag{3.28}$$

with the computable terms are defined for computing $\mathbf{\Gamma}^*$ as

$$\ddot{\mathbf{q}}_r = \ddot{\mathbf{q}}_d + \mathbf{\Lambda}\dot{\mathbf{e}} \tag{3.29}$$

$$\mathbf{r} = \dot{\mathbf{q}}_r - \dot{\mathbf{q}} = \dot{\mathbf{e}} + \mathbf{\Lambda}\mathbf{e} \tag{3.30}$$

where $\mathbf{\Lambda} \in \Re^{n\times n}$ is a positive diagonal matrix, $\mathbf{e} = \mathbf{q}_d - \mathbf{x}$ and $\dot{\mathbf{e}} = \dot{\mathbf{q}}_d - \dot{\mathbf{x}}$ are the joint space position and velocity tracking errors, respectively, with $\mathbf{q}_d$, $\dot{\mathbf{q}}_d$ and $\ddot{\mathbf{q}}_d$ are the desired joint space trajectories. A relationship $\tilde{(\cdot)} = (\cdot) - \hat{(\cdot)}$ is defined where $\tilde{(\cdot)}$ is the estimation error dynamics, $(\cdot)$ is the actual dynamics, $\hat{(\cdot)}$ is the estimated dynamics, which will be estimated by the estimated LIP model. Note that, in the implementation, by exploiting its linear model form in (3.12), the controller (3.26) can be simply implemented as

$$\mathbf{\Gamma} = \ \mathbf{Y}(\mathbf{q}, \dot{\mathbf{q}}, \dot{\mathbf{q}}_r, \ddot{\mathbf{q}}_r)\ \hat{\boldsymbol{\pi}} \tag{3.31}$$

where $\hat{\boldsymbol{\pi}} \in \Re^{13n}$ is the vector of estimated inertial parameters. Combining the joint space dynamics (3.11) and direct LIP adaptive control (3.26), and taking into account the first derivative of (3.30), the closed-loop error dynamics can be obtained as as

$$\mathbf{M}(\mathbf{q})\dot{\mathbf{r}} = -\mathbf{M}(\mathbf{q})\mathbf{\Lambda}\mathbf{r} - \mathbf{B}(\mathbf{q}, \dot{\mathbf{q}})\mathbf{r} + \boldsymbol{\eta} \tag{3.32}$$

where the uncertainties $\boldsymbol{\eta}$ is defined as

$$\boldsymbol{\eta} = \tilde{\mathbf{M}}(\mathbf{q})\mathbf{\Gamma}^* + \tilde{\mathbf{B}}(\mathbf{q}, \dot{\mathbf{q}})\dot{\mathbf{q}}_r + \tilde{\mathbf{g}}(\mathbf{q}) + \tilde{\boldsymbol{\tau}}_{vis}\dot{\mathbf{q}}_r + \tilde{\boldsymbol{\tau}}_{cou}\ \text{sgn}(\dot{\mathbf{q}}) \tag{3.33}$$

which can be written using LIP form (3.12) as

$$\boldsymbol{\eta} = \mathbf{Y}(\mathbf{q}, \dot{\mathbf{q}}, \dot{\mathbf{q}}_r, \ddot{\mathbf{q}}_r)\ \tilde{\boldsymbol{\pi}}. \tag{3.34}$$

where $\tilde{\boldsymbol{\pi}} \in \Re^{13n}$ is the vector of closed-loop error dynamics parameters. Substituting (3.34) into the closed-loop error dynamics (3.32), yields

$$\mathbf{M}(\mathbf{q})\dot{\mathbf{r}} = -\mathbf{M}(\mathbf{q})\boldsymbol{\Lambda}\mathbf{r} - \mathbf{B}(\mathbf{q},\dot{\mathbf{q}})\mathbf{r} + \mathbf{Y}(\mathbf{q},\dot{\mathbf{q}},\dot{\mathbf{q}}_r,\ddot{\mathbf{q}}_r)\,\tilde{\boldsymbol{\pi}}. \tag{3.35}$$

3.2.3 Stability Analysis

The chosen Lyapunov function candidate for the closed-loop error dynamics (3.35) with the uncertainties $\boldsymbol{\eta}$ (3.34), is

$$V(\mathbf{r},\tilde{\boldsymbol{\pi}}) = \frac{1}{2}\,\mathbf{r}^{\mathrm{T}}\mathbf{M}(\mathbf{q})\mathbf{r} + \frac{1}{2}\,\tilde{\boldsymbol{\pi}}^{\mathrm{T}}\mathbf{P}^{-1}\tilde{\boldsymbol{\pi}} \tag{3.36}$$

where $\mathbf{P} \in \Re^{13n\times 13n}$ is a constant positive diagonal matrix. Therefore the time derivative of (3.36) can be obtained as

$$\dot{V}(\mathbf{r},\tilde{\boldsymbol{\pi}}) = \mathbf{r}^{\mathrm{T}}\mathbf{M}(\mathbf{q})\dot{\mathbf{r}} + \frac{1}{2}\,\mathbf{r}^{\mathrm{T}}\dot{\mathbf{M}}(\mathbf{q})\mathbf{r} + \tilde{\boldsymbol{\pi}}^{\mathrm{T}}\mathbf{P}^{-1}\dot{\tilde{\boldsymbol{\pi}}} \tag{3.37}$$

Next, we substitute the closed-loop dynamics (3.35) with the uncertainties $\boldsymbol{\eta}$ (3.34) and also take into account Property 3.2.5 into $\dot{V}(\mathbf{r},\tilde{\boldsymbol{\pi}})$ of (3.37), to obtain

$$\dot{V}(\mathbf{r},\tilde{\boldsymbol{\pi}}) = -\mathbf{r}^{\mathrm{T}}\mathbf{M}(\mathbf{q})\boldsymbol{\Lambda}\mathbf{r} + \tilde{\boldsymbol{\pi}}^{\mathrm{T}}\left(\mathbf{P}^{-1}\dot{\tilde{\boldsymbol{\pi}}} + \mathbf{Y}(\mathbf{q},\dot{\mathbf{q}},\dot{\mathbf{q}}_r,\ddot{\mathbf{q}}_r)\mathbf{r}\right) \tag{3.38}$$

Now, if we introduce the parameter updates as

$$\dot{\tilde{\boldsymbol{\pi}}} = \mathbf{P}\left(\mathbf{Y}^{\mathrm{T}}(\mathbf{q},\dot{\mathbf{q}},\dot{\mathbf{q}}_r,\ddot{\mathbf{q}}_r)\,\mathbf{r} + \mathbf{Y}_f^{\mathrm{T}}(\mathbf{q},\dot{\mathbf{q}})\,\tilde{\boldsymbol{\Gamma}}_f\right) \tag{3.39}$$

where $\mathbf{Y}_f(\mathbf{q},\dot{\mathbf{q}})$ and $\tilde{\boldsymbol{\Gamma}}_f$ are computed as

$$\mathbf{Y}_f(\mathbf{q},\dot{\mathbf{q}}) = G(s)\mathbf{Y}(\mathbf{q},\dot{\mathbf{q}},\ddot{\mathbf{q}}) \tag{3.40}$$

and

$$\tilde{\mathbf{\Gamma}}_f = \mathbf{\Gamma}_f - \hat{\mathbf{\Gamma}}_f = \mathbf{Y}_f(\mathbf{q}, \dot{\mathbf{q}})\ \tilde{\boldsymbol{\pi}} \tag{3.41}$$

where $\mathbf{\Gamma}_f$ and $\hat{\mathbf{\Gamma}}_f$ are computed as

$$\mathbf{\Gamma}_f = G(s)\mathbf{\Gamma} \tag{3.42}$$

$$\hat{\mathbf{\Gamma}}_f = \mathbf{Y}_f(\mathbf{q}, \dot{\mathbf{q}})\ \hat{\boldsymbol{\pi}} \tag{3.43}$$

Note that, $G(s)$ is a strictly stable Laplace filter, such as a first order filter $G(s) = \dfrac{\alpha}{s+\alpha},\ \alpha > 0$. It can be shown [48, 49] that $\mathbf{Y}_f(\mathbf{q}, \dot{\mathbf{q}})$ is free from the acceleration signals. Other works to avoid calculating the joint accelerations with different kind of technique, characteristics and requirements were presented in [95, 50, 51, 52]. Henceforth, we can write $\dot{V}(\mathbf{r}, \tilde{\boldsymbol{\pi}})$ (3.38) as

$$\dot{V}(\mathbf{r}, \tilde{\boldsymbol{\pi}}) = -\mathbf{r}^{\mathrm{T}}\mathbf{M}(\mathbf{q})\mathbf{\Lambda}\mathbf{r} - \tilde{\boldsymbol{\pi}}^{\mathrm{T}}\mathbf{Y}_f^{\mathrm{T}}(\mathbf{q}, \dot{\mathbf{q}})\ \mathbf{Y}_f(\mathbf{q}, \dot{\mathbf{q}})\tilde{\boldsymbol{\pi}} \leq 0. \tag{3.44}$$

It can be shown later on that $t \to \infty, \mathbf{r} \to 0$, from (3.30) implies $\mathbf{e}, \dot{\mathbf{e}} \to 0$. While $t \to \infty, \tilde{\boldsymbol{\pi}} \to 0$ can only be achieved if only exciting trajectories are given. In the case the exciting trajectories are not given, then the parameter errors can only be guaranteed to be bounded. Note when the (3.39) employs a constant gain $\mathbf{P}$, then the estimation term (the second term) is often referred as *gradient* estimator.

Now, we are ready to show the stability analysis in details. First, we need to invoke Barbalat's lemma [93] (pp. 123) that if:

- V is bounded as $t \to \infty$, and

- $\ddot{V}$ is bounded,

then $\dot{V} \to 0$ as $t \to \infty$. The first condition can be provided by noticing $\dot{V} \leq 0$ in (3.44) and V is lowerbounded by zero in (3.36), therefore V is bounded as $t \to \infty$. Therefore we are left with proving the boundedness of $\ddot{V}$.

The expression of $\ddot{V}$ can be established from (3.44) as

$$\ddot{V} = -2\,\mathbf{r}^{\mathrm{T}}\mathbf{M}(\mathbf{q})\boldsymbol{\Lambda}\dot{\mathbf{r}} - \mathbf{r}^{\mathrm{T}}\dot{\mathbf{M}}(\mathbf{q})\boldsymbol{\Lambda}\mathbf{r} - 2\,\tilde{\boldsymbol{\pi}}^{\mathrm{T}}\mathbf{Y}_f^{\mathrm{T}}\,\dot{\mathbf{Y}}_f\tilde{\boldsymbol{\pi}} - 2\,\tilde{\boldsymbol{\pi}}^{\mathrm{T}}\mathbf{Y}_f^{\mathrm{T}}\,\mathbf{Y}_f\dot{\tilde{\boldsymbol{\pi}}}. \tag{3.45}$$

The boundedness of $\ddot{V}$ can be shown as follows:

- Since $\dot{V} \leq 0$ (3.38) and V (3.36) is lower bounded by zero, V tends to a constant as $t \to \infty$ and therefore $\underline{V \text{ remains bounded}}$ for $t \in [0, \infty]$. Since V is bounded and $\mathbf{M}(\mathbf{q})$ cannot be zero by Property 3.2.1, therefore from (3.36), $\underline{\mathbf{r} \text{ and } \tilde{\boldsymbol{\pi}}}$ is bounded. The boundedness of $\mathbf{r}$ infers the boundedness of $\underline{\mathbf{e} \text{ and } \dot{\mathbf{e}}}$. The boundedness of $\mathbf{e}, \dot{\mathbf{e}}$ and the trajectories $\mathbf{q}_d, \dot{\mathbf{q}}_d, \ddot{\mathbf{q}}_d$ (by design), infers the boundedness of $\underline{\mathbf{q}, \dot{\mathbf{q}}, \dot{\mathbf{q}}_r, \ddot{\mathbf{q}}_r}$.
- $\dot{\mathbf{M}}(\mathbf{q}) = \dfrac{\mathrm{d}\mathbf{M}(\mathbf{q})}{\mathrm{d}\mathbf{q}}\,\dot{\mathbf{q}}$ can be shown to be bounded since $\mathbf{M}(\mathbf{q})$ and $\dot{\mathbf{q}}$ are bounded, respectively, by Property 3.2.1 and previous point.
- The closed-loop error dynamics (3.35) can be written as

$$\mathbf{M}(\mathbf{q})\dot{\mathbf{r}} + \mathbf{M}(\mathbf{q})\boldsymbol{\Lambda}\mathbf{r} + \mathbf{B}(\mathbf{q}, \dot{\mathbf{q}})\mathbf{r} = \mathbf{Y}(\mathbf{q}, \dot{\mathbf{q}}, \dot{\mathbf{q}}_r, \ddot{\mathbf{q}}_r)\,\tilde{\boldsymbol{\pi}}. \tag{3.46}$$

  Therefore, from properties 3.2.1, 3.2.2 and 3.2.3 and 3.2.4, it can be inferred that $\underline{\mathbf{Y}(\mathbf{q}, \dot{\mathbf{q}}, \ddot{\mathbf{q}})}$ is bounded.

The boundedness of $\mathbf{Y}(\mathbf{q}, \dot{\mathbf{q}}, \dot{\mathbf{q}}_r, \ddot{\mathbf{q}}_r)$ can be inferred from the boundedness of $\mathbf{Y}(\mathbf{q}, \dot{\mathbf{q}}, \ddot{\mathbf{q}})$ and $\dot{\mathbf{q}}_r, \ddot{\mathbf{q}}_r$ (first point). Using (3.46), the boundedness of $\mathbf{Y}(\mathbf{q}, \dot{\mathbf{q}}, \dot{\mathbf{q}}_r, \ddot{\mathbf{q}}_r)$ and the boundedness of $\mathbf{r}$ and $\tilde{\boldsymbol{\pi}}$ (first point), results $\dot{\mathbf{r}}$ is bounded.

- $$\dot{\mathbf{Y}}_f = \frac{d(\mathbf{Y}_f(\mathbf{q}, \dot{\mathbf{q}}))}{dt} = \frac{s\,\alpha}{s+\alpha}\mathbf{Y}(\mathbf{q}, \dot{\mathbf{q}}, \ddot{\mathbf{q}}) \tag{3.47}$$

  Since $\mathbf{Y}(\mathbf{q}, \dot{\mathbf{q}}, \ddot{\mathbf{q}})$ and $\frac{s\,\alpha}{s+\alpha}$ are bounded, therefore $\dot{\mathbf{Y}}_f$ is bounded.

- The boundedness of $\dot{\tilde{\boldsymbol{\pi}}}$ can be directly obtained from (3.39).

Therefore all the terms making up $\ddot{V}$ (3.45) are bounded, therefore by using Barbalat's lemma, we can obtain:

$\dot{V} \to 0$ as $t \to \infty \Rightarrow \mathbf{r} \to 0$ and $\mathbf{Y}_f(\mathbf{q}, \dot{\mathbf{q}})\ \tilde{\boldsymbol{\pi}} \to 0$ as $t \to \infty$. Or, in other words:

- The convergence of $\mathbf{r}$, which implies the convergence of $\mathbf{e}, \dot{\mathbf{e}}$.
- The convergence of $\mathbf{Y}_f(\mathbf{q}, \dot{\mathbf{q}})\tilde{\boldsymbol{\pi}}$.

  However, this does not guarantee the convergence of $\tilde{\boldsymbol{\pi}}$.

The convergence of $\tilde{\boldsymbol{\pi}}$ can be shown as follows [93]: pre-multiplying $\mathbf{Y}_f(\mathbf{q}, \dot{\mathbf{q}})\ \tilde{\boldsymbol{\pi}} \to 0$ with $\mathbf{Y}_f^{\mathrm{T}}(\mathbf{q}, \dot{\mathbf{q}})$, then integrating it over time t, result

$$\int_0^{r=t} \mathbf{Y}_f^{\mathrm{T}}(\mathbf{q}, \dot{\mathbf{q}})\mathbf{Y}_f(\mathbf{q}, \dot{\mathbf{q}})\ \tilde{\boldsymbol{\pi}}\ dr \to 0 \tag{3.48}$$

thus the only way to to enforce $\tilde{\boldsymbol{\pi}} \to 0$ is to make

$$\int_0^{r=t} \mathbf{Y}_f^{\mathrm{T}}(\mathbf{q}, \dot{\mathbf{q}})\mathbf{Y}_f(\mathbf{q}, \dot{\mathbf{q}})\ dr > 0. \tag{3.49}$$

This condition is where the matrix $\mathbf{Y}_f(\mathbf{q}, \dot{\mathbf{q}})$ needs to be persistently exciting, therefore the parameter error $\tilde{\boldsymbol{\pi}}$ will converge to zero, complete proof can be shown in [96, 97].

In practical side, this means that the trajectory tracking errors are always guaranteed to converge and for the parameter errors are only guaranteed to converge if only exciting trajectories are given. In the case the exciting trajectories are not given, then the parameter errors can only be guaranteed to be bounded.

Note that the following aspects are still preferable to be incorporated: (1) two simplified dynamic models for the control and parameter identification, to meet the requirement of the real-time deterministic sampling time (note, ideally, identification model must be acceleration free), and (2) optimal trajectory, to enforce the convergence of the dynamic parameters.

3.3 Operational Space Direct LIP Adaptive Motion Control

For ease of perusal, let's reproduce the end-effector motion dynamics of the non-redundant manipulator (2.27) in Chapter two, which can be described as

$$\mathbf{F} = \mathbf{M}_{\mathbf{x}}(\mathbf{q})\ddot{\mathbf{x}} + \mathbf{B}_{\mathbf{x}}(\mathbf{q}, \dot{\mathbf{q}})\dot{\mathbf{x}} + \mathbf{g}_{\mathbf{x}}(\mathbf{q}) + \boldsymbol{\tau}_{\mathbf{x}}(\mathbf{q}, \dot{\mathbf{q}}) \tag{3.50}$$

where the operational space matrices and vectors $\mathbf{M}_{\mathbf{x}}(\mathbf{q}) \in \Re^{m\times m}$, $\mathbf{B}_{\mathbf{x}}(\mathbf{q}, \dot{\mathbf{q}}) \in \Re^{m\times m}$, $\mathbf{g}_{\mathbf{x}}(\mathbf{q}) \in \Re^{m}$, $\boldsymbol{\tau}_{\mathbf{x}}(\mathbf{q}, \dot{\mathbf{q}}) \in \Re^{m}$ are similar with (2.28) – (2.31), respectively, with slight modification on $\boldsymbol{\tau}_{\mathbf{x}}(\mathbf{q}, \dot{\mathbf{q}})$ as follows:

$$\boldsymbol{\tau}_{\mathbf{x}}(\mathbf{q}, \dot{\mathbf{q}}) = \mathbf{J}^{-\mathrm{T}}(\mathbf{q}) \left(\boldsymbol{\tau}_{vis}\dot{\mathbf{q}} + \boldsymbol{\tau}_{cou}\ \mathrm{sgn}(\dot{\mathbf{q}})\right) \tag{3.51}$$

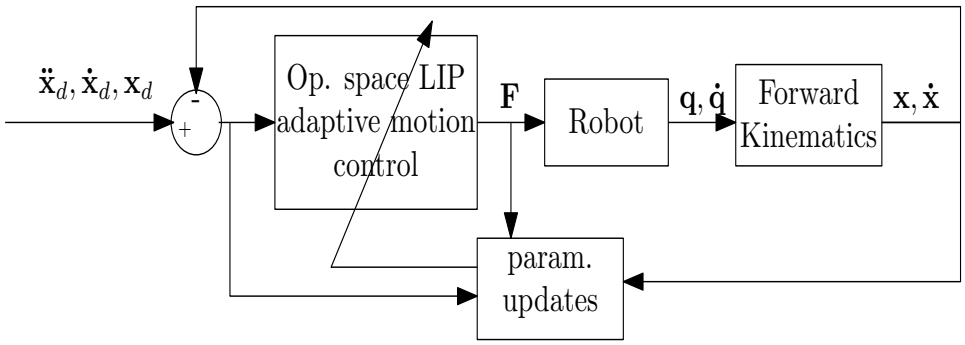

Figure 3.2: The operational space direct LIP adaptive motion control structure.

where it is obtained by considering only viscous and coulomb terms in order to achieve the linearity property.

As the LIP joint space equivalent, by using the linearity property, the operational space dynamics (3.50) can be shown to be linear-in-parameter as follows

$$\mathbf{F} = \bar{\mathbf{Y}}(\mathbf{q}, \dot{\mathbf{q}}, \ddot{\mathbf{q}})\, \boldsymbol{\pi}. \tag{3.52}$$

which can be expanded as

$$\begin{bmatrix} F_1 \\ F_2 \\ \vdots \\ F_m \end{bmatrix} = \begin{bmatrix} \mathbf{y}_{11}^{\mathrm{T}} & \mathbf{y}_{12}^{\mathrm{T}} & \cdots & \mathbf{y}_{1n}^{\mathrm{T}} \\ \mathbf{y}_{21}^{\mathrm{T}} & \mathbf{y}_{22}^{\mathrm{T}} & \cdots & \mathbf{y}_{2n}^{\mathrm{T}} \\ \vdots & \vdots & \ddots & \vdots \\ \mathbf{y}_{n1}^{\mathrm{T}} & \mathbf{y}_{n2}^{\mathrm{T}} & \cdots & \mathbf{y}_{nn}^{\mathrm{T}} \end{bmatrix} \begin{bmatrix} \boldsymbol{\pi}_1 \\ \boldsymbol{\pi}_2 \\ \vdots \\ \boldsymbol{\pi}_n \end{bmatrix} \tag{3.53}$$

where $\bar{\mathbf{Y}}(\mathbf{q}, \dot{\mathbf{q}}, \ddot{\mathbf{q}}) \in \Re^{m \times 13n}$ is the operational space regression matrix and $\boldsymbol{\pi} \in \Re^{13n}$ is the vector of actual inertial parameters, with each element $\boldsymbol{\pi}_i \in \Re^{13}$ has been described in (3.14).

The operational space LIP adaptive force-motion control law, as shown in Fig. 3.2, can be defined as

$$\mathbf{F} = \hat{\mathbf{M}}_{\mathbf{x}}(\mathbf{q})\mathbf{F}^*_{\mathrm{motion}} + \hat{\mathbf{B}}_{\mathbf{x}}(\mathbf{q}, \dot{\mathbf{q}})\dot{\mathbf{x}}_r + \hat{\mathbf{g}}_{\mathbf{x}}(\mathbf{q}) + \hat{\boldsymbol{\tau}}_{\mathbf{x}}(\mathbf{q}, \dot{\mathbf{q}}) \tag{3.54}$$

The following terms $\dot{\mathbf{x}}_r$ and $\mathbf{F}^*_{\text{motion}}$ are defined as

$$\dot{\mathbf{x}}_r = \dot{\mathbf{x}}_d + \mathbf{\Lambda}\mathbf{e} \tag{3.55}$$

$$\mathbf{F}^*_{\text{motion}} = \ddot{\mathbf{x}}_r + \mathbf{\Lambda}\mathbf{r} \tag{3.56}$$

with the computable terms are defined for computing $\mathbf{F}^*_{\text{motion}}$ as

$$\ddot{\mathbf{x}}_r = \ddot{\mathbf{x}}_d + \mathbf{\Lambda}\dot{\mathbf{e}} \tag{3.57}$$

$$\mathbf{r} = \dot{\mathbf{x}}_r - \dot{\mathbf{x}} = \dot{\mathbf{e}} + \mathbf{\Lambda}\mathbf{e} \tag{3.58}$$

where $\mathbf{\Lambda} \in \Re^{m\times m}$ is a positive diagonal matrix, $\mathbf{e} = \mathbf{x}_d - \mathbf{x}$ and $\dot{\mathbf{e}} = \dot{\mathbf{x}}_d - \dot{\mathbf{x}}$ are the operational space position and velocity tracking errors, respectively , $\mathbf{x}_d$, $\dot{\mathbf{x}}_d$ and $\ddot{\mathbf{x}}_d$ are the desired operational space trajectories.

Note that, in the implementation, by exploiting the linearity-in-the-parameter model form in (3.52), the controller (3.54) can be simply implemented as

$$\mathbf{F} = \bar{\mathbf{Y}}(\mathbf{q}, \dot{\mathbf{q}}, \dot{\mathbf{x}}_r, \mathbf{F}^*_{\text{motion}})\, \hat{\boldsymbol{\pi}}. \tag{3.59}$$

Combining the operational space motion dynamics (3.50) and direct LIP adaptive control (3.54), and taking into account the first derivative of (3.58), the closed-loop error dynamics can be obtained as

$$\mathbf{M}_{\mathbf{x}}(\mathbf{q})\dot{\mathbf{r}} = -\mathbf{M}_{\mathbf{x}}(\mathbf{q})\mathbf{\Lambda}\mathbf{r} - \mathbf{B}_{\mathbf{x}}(\mathbf{q}, \dot{\mathbf{q}})\mathbf{r} + \boldsymbol{\eta} \tag{3.60}$$

where the uncertainties $\boldsymbol{\eta}$ is defined as

$$\boldsymbol{\eta} = \tilde{\mathbf{M}}_{\mathbf{x}}(\mathbf{q})\ \mathbf{F}^*_{\text{motion}} + \tilde{\mathbf{B}}_{\mathbf{x}}(\mathbf{q}, \dot{\mathbf{q}})\ \dot{\mathbf{x}}_r + \tilde{\mathbf{g}}(\mathbf{q}) + \tilde{\boldsymbol{\tau}}_{\mathbf{x}}(\mathbf{q}, \dot{\mathbf{q}}). \tag{3.61}$$

which can be written using LIP form (3.12) as

$$\boldsymbol{\eta} = \bar{\mathbf{Y}}(\mathbf{q}, \dot{\mathbf{q}}, \dot{\mathbf{x}}_r, \mathbf{F}^*_{\text{motion}})\ \tilde{\boldsymbol{\pi}}. \tag{3.62}$$

Substituting (3.62) into the closed-loop error dynamics (3.60), yields

$$\mathbf{M}_{\mathbf{x}}(\mathbf{q})\dot{\mathbf{r}} = -\mathbf{M}_{\mathbf{x}}(\mathbf{q})\boldsymbol{\Lambda}\mathbf{r} - \mathbf{B}_{\mathbf{x}}(\mathbf{q}, \dot{\mathbf{q}})\mathbf{r} + \bar{\mathbf{Y}}(\mathbf{q}, \dot{\mathbf{q}}, \dot{\mathbf{x}}_r, \mathbf{F}^*_{\text{motion}})\ \tilde{\boldsymbol{\pi}}. \tag{3.63}$$

The chosen Lyapunov function candidate for the closed-loop error dynamics (3.63) with the uncertainties $\boldsymbol{\eta}$ (3.62), is

$$V(\mathbf{r}, \tilde{\boldsymbol{\pi}}) = \frac{1}{2}\ \mathbf{r}^{\mathrm{T}}\mathbf{M}_{\mathbf{x}}(\mathbf{q})\mathbf{r} + \frac{1}{2}\ \tilde{\boldsymbol{\pi}}^{\mathrm{T}}\mathbf{P}^{-1}\tilde{\boldsymbol{\pi}} \tag{3.64}$$

where $\mathbf{P} \in \Re^{13m \times 13m}$ is a constant positive diagonal matrix. Now, if we introduce the parameter updates as

$$\dot{\hat{\boldsymbol{\pi}}} = \mathbf{P}\left(\bar{\mathbf{Y}}^{\mathrm{T}}(\mathbf{q}, \dot{\mathbf{q}}, \dot{\mathbf{x}}_r, \mathbf{F}^*_{\text{motion}})\ \mathbf{r} + \bar{\mathbf{Y}}_f^{\mathrm{T}}(\mathbf{q}, \dot{\mathbf{q}})\ \tilde{\mathbf{F}}_f\right) \tag{3.65}$$

Note that, the parameter updates (3.65) is similar as in [98], however, the second term is not included in [98].

Next, $\bar{\mathbf{Y}}_f(\mathbf{q}, \dot{\mathbf{q}})$ and $\tilde{\mathbf{F}}_f$ in (3.65) are computed as follows:

$$\bar{\mathbf{Y}}_f(\mathbf{q}, \dot{\mathbf{q}}) = G(s)\bar{\mathbf{Y}}(\mathbf{q}, \dot{\mathbf{q}}, \ddot{\mathbf{q}}) \tag{3.66}$$

and

$$\tilde{\mathbf{F}}_f = \mathbf{F}_f - \hat{\mathbf{F}}_f = \bar{\mathbf{Y}}_f(\mathbf{q}, \dot{\mathbf{q}})\ \tilde{\boldsymbol{\pi}} \tag{3.67}$$

where $\mathbf{F}_f$ and $\hat{\mathbf{F}}_f$ are computed as

$$\mathbf{F}_f = G(s)\mathbf{F} \tag{3.68}$$

$$\hat{\mathbf{F}}_f = \bar{\mathbf{Y}}_f(\mathbf{q}, \dot{\mathbf{q}})\ \hat{\boldsymbol{\pi}}. \tag{3.69}$$

Then by using similar procedure like in Section 3.2.3, it can be shown that

$$\dot{V}(\mathbf{r}, \tilde{\boldsymbol{\pi}}) = -\,\mathbf{r}^{\mathrm{T}}\mathbf{M}_{\mathbf{x}}(\mathbf{q})\boldsymbol{\Lambda}\,\mathbf{r} - \tilde{\boldsymbol{\pi}}^{\mathrm{T}}\bar{\mathbf{Y}}_{f}^{\mathrm{T}}(\mathbf{q}, \dot{\mathbf{q}})\,\bar{\mathbf{Y}}_{f}(\mathbf{q}, \dot{\mathbf{q}})\tilde{\boldsymbol{\pi}} \tag{3.70}$$

It can be shown using Barbalat's lemma as in Section 3.2.3 that as $t \to \infty$, $\mathbf{r} \to 0$. Therefore, from $\mathbf{r}$ (3.58) implies $\mathbf{e}, \dot{\mathbf{e}} \to 0$. For $\tilde{\boldsymbol{\pi}} \to 0$ can only be achieved if only exciting trajectories are given. In the case the exciting trajectories are not given, then the parameter errors can only be guaranteed to be bounded.

Clearly, this operational space extension requires the construction of $\bar{\mathbf{Y}}(\mathbf{q}, \dot{\mathbf{q}}, \ddot{\mathbf{q}})$ (3.52) and $\bar{\mathbf{Y}}_{f}(\mathbf{q}, \dot{\mathbf{q}})$ (3.66), which obviously are more complex than the joint space equivalent.

Note that, a cheaper alternative over direct LIP strategy in operational space can be achieved by employing parameter estimation (either using on-line or off-line method) in joint space. Then non-adaptive model-based control is employed in operational space by transforming the joint space model into the operational model equivalents via (2.28) – (2.31). However, since the operational space control is non-adaptive case, therefore one needs to redo the joint space parameter identification procedure, whenever necessary.

3.4 The Original Joint Space NN Adaptive Motion Control

For ease of perusal, let's reproduce the joint space dynamics in (2.25)

$$\mathbf{M}(\mathbf{q})\ddot{\mathbf{q}} + \mathbf{B}(\mathbf{q}, \dot{\mathbf{q}})\dot{\mathbf{q}} + \mathbf{g}(\mathbf{q}) + \boldsymbol{\tau}_{\text{fric}}(\dot{\mathbf{q}}) = \boldsymbol{\Gamma} \tag{3.71}$$

where $\mathbf{q} \in \Re^n$ denotes the vector of joint space coordinates and $\mathbf{\Gamma} \in \Re^n$ denotes the vector of generalized joint space force. The Lagrangian joint space matrices and vectors: $\mathbf{M}(\mathbf{q}) \in \Re^{n\times n}$, $\mathbf{B}(\mathbf{q}, \dot{\mathbf{q}}) \in \Re^{n\times n}$, $\mathbf{g}(\mathbf{q}) \in \Re^n$, and $\boldsymbol{\tau}_{\text{fric}}(\dot{\mathbf{q}}) \in \Re^n$ denote the inertia matrix, Coriolis/centrifugal matrix, gravity vector and joint friction vector as in (2.31).

Next, we present the original joint space NN motion control [74, 75] as

$$\mathbf{F} = \mathbf{K_v r} + \boldsymbol{\upsilon} + \hat{\mathbf{f}} \tag{3.72}$$

where $\mathbf{K_v} \in \Re^{n\times n}$ is a positive diagonal matrix, $\boldsymbol{\upsilon}$ is a $n \times 1$ robust term vector to be defined later and the term $\hat{\mathbf{f}}$ is a $n \times 1$ vector defined as

$$\hat{\mathbf{f}} = \hat{\mathbf{M}}(\mathbf{q})\ddot{\mathbf{q}}_r + \hat{\mathbf{B}}(\mathbf{q}, \dot{\mathbf{q}})\dot{\mathbf{q}}_r + \hat{\mathbf{g}}(\mathbf{q}) + \hat{\boldsymbol{\tau}}(\mathbf{q}, \dot{\mathbf{q}}). \tag{3.73}$$

Note in (3.73), a relationship $\tilde{(\cdot)} = (\cdot) - \hat{(\cdot)}$ is defined where $\tilde{(\cdot)}$ is the estimation error dynamics, $(\cdot)$ is the actual dynamics, $\hat{(\cdot)}$ is the estimated dynamics, which will be estimated by the estimated NN model. The following terms are also defined

$$\dot{\mathbf{q}}_r = \dot{\mathbf{q}}_d + \mathbf{\Lambda e} \tag{3.74}$$

$$\ddot{\mathbf{q}}_r = \ddot{\mathbf{q}}_d + \mathbf{\Lambda}\dot{\mathbf{e}} \tag{3.75}$$

$$\mathbf{r} = \dot{\mathbf{e}} + \mathbf{\Lambda e} \tag{3.76}$$

where $\mathbf{\Lambda} \in \Re^{n\times n}$ is a positive diagonal matrix, $\mathbf{e} = \mathbf{q}_d - \mathbf{x}$ and $\dot{\mathbf{e}} = \dot{\mathbf{q}}_d - \dot{\mathbf{x}}$ are the joint space position and velocity tracking errors, respectively, $\mathbf{q}_d$, $\dot{\mathbf{q}}_d$ and $\ddot{\mathbf{q}}_d$ are the desired joint space trajectories. The original joint space NN motion control [74, 75] can be shown in Fig. 3.3.

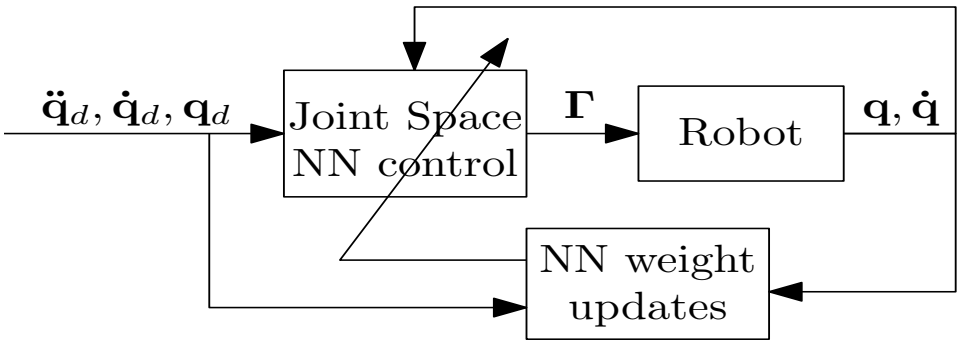

Figure 3.3: The original joint space NN motion control structure.

Next, combining the joint space dynamics (3.71) and NN adaptive motion control (3.72), and taking into account (3.76), the closed-loop error dynamics can be obtained as

$$\mathbf{M}(\mathbf{q})\dot{\mathbf{r}} + \mathbf{K_v}\mathbf{r} + \mathbf{B}(\mathbf{q}, \dot{\mathbf{q}})\mathbf{r} + \boldsymbol{\upsilon} = \boldsymbol{\eta}; \tag{3.77}$$

where the uncertainties $\boldsymbol{\eta}$ in joint space is defined as

$$\boldsymbol{\eta} = \tilde{\mathbf{M}}(\mathbf{q})\ddot{\mathbf{q}}_r + \tilde{\mathbf{B}}(\mathbf{q}, \dot{\mathbf{q}})\dot{\mathbf{q}}_r + \tilde{\mathbf{g}}(\mathbf{q}) + \tilde{\boldsymbol{\tau}}(\mathbf{q}, \dot{\mathbf{q}}) \tag{3.78}$$

and if written in lumped vectors as

$$\boldsymbol{\eta} = \mathbf{f} - \hat{\mathbf{f}}. \tag{3.79}$$

3.4.1 Three-Layer Neural Networks

As shown in Fig. 3.4, in general, a three-layer neural network is defined such that N_1, N_2 and N_3 are the number of neurons in layer 1, layer 2, layer 3, respectively. $\mathbf{z} \in \Re^{N_1}$ is the NN input-layer vector, $\boldsymbol{\sigma} \in \Re^{N_2}$ is the NN hidden-layer vector and $\mathbf{u} \in \Re^{N_3}$ is the NN output-layer vector. v_{kl} is the first-to-second layer weights, with $l = 1, \ldots, N_1$ as the input-layer index and $k = 1, \ldots, N_2$ as the hidden-layer index; θ_k is the threshold offset, and w_{ik} is second-to-third

layer weights for output vector, with $i = 1, \ldots, N_3$ as the output-layer index. Function $\sigma(\cdot)$ is defined to be differentiable throughout, such as sigmoid and hyperbolic functions. In this thesis, sigmoid function $\sigma(s) = 1/(1 + \exp^{-(a \times s)})$ is selected. Therefore each element of output vector $\mathbf{u}$ can be expressed as

$$u_i = \sum_{k=1}^{N_2} w_{ik} \ \sigma_k \left(\sum_{l=1}^{N_1} v_{kl} z_l \ + \ \theta_k \right); \ i = 1, \ldots, N_3, \tag{3.80}$$

Equation (3.80) can be written in a simplified manner in vector-and-matrix form as in [99] as

$$\mathbf{u} = \mathbf{W}^{\mathrm{T}} \, \boldsymbol{\sigma} \left(\mathbf{V}^{\mathrm{T}} \mathbf{z} \right) \tag{3.81}$$

with $\mathbf{W} \in \Re^{N_3 \times N_2}, \mathbf{V} \in \Re^{N_2 \times N_1}$. Note N_3 can be determined from the robot DOF, therefore for non-redundant manipulator with 6 DOF then $N_3 = n = 6$. Also, the addition of the scalar θ_k, in (3.81), has been included in the $\mathbf{V}^{\mathrm{T}}\mathbf{z}$ term. This can be done by appending the vector $\boldsymbol{\theta}^{\mathrm{T}}$ (where each element is θ_k) as the first row of $\mathbf{V}$ and an element containing '1'at the beginning of vector $\mathbf{z}$.

3.4.2 Uncertainties η in NN terms

The uncertainties $\boldsymbol{\eta}$ as lumped vectors as in (3.78) is

$$\boldsymbol{\eta} = \mathbf{f} - \hat{\mathbf{f}} \tag{3.82}$$

From NN theory, given an adequate number of hidden layer nodes, N_2, a three layer NNs with ideal weights is capable of approximating any function [100, 101]. In practice, however, there are only limited number of hidden layer nodes, therefore the actual term $\mathbf{f}$ as a whole, for a given number of hidden neurons,

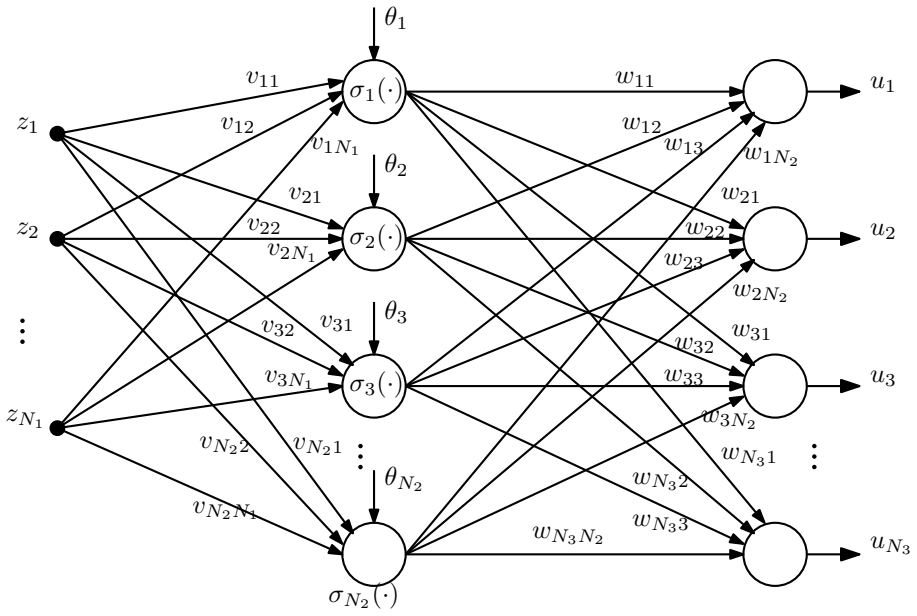

Figure 3.4: Three-layer NN structure (with output vector).

can be described by three-layer NNs with constant *optimum* weights $\mathbf{V}, \mathbf{W}$ and a vector of the lumped approximation error $\boldsymbol{\varepsilon} \in \Re^n$ as follows

$$\mathbf{f}(\mathbf{z}) = \mathbf{W}^{\mathrm{T}} \boldsymbol{\sigma}(\mathbf{V}^{\mathrm{T}} \mathbf{z}) + \boldsymbol{\varepsilon} \tag{3.83}$$

And the selected NN input vector $\mathbf{z}$ in [74, 75] is

$$\mathbf{z} \equiv [\mathbf{e}^{\mathrm{T}} \ \dot{\mathbf{e}}^{\mathrm{T}} \ \mathbf{x}_d^{\mathrm{T}} \ \dot{\mathbf{x}}_d^{\mathrm{T}} \ \ddot{\mathbf{x}}_d^{\mathrm{T}}]^{\mathrm{T}}. \tag{3.84}$$

Likewise the estimated function $\hat{\mathbf{f}}(\mathbf{z})$, can be described by the estimated weights $\hat{\mathbf{V}}, \hat{\mathbf{W}}$ as follows

$$\hat{\mathbf{f}}(\mathbf{z}) = \hat{\mathbf{W}}^{\mathrm{T}} \boldsymbol{\sigma}(\hat{\mathbf{V}}^{\mathrm{T}} \mathbf{z}) \tag{3.85}$$

Therefore, using (3.83) and (3.85), $\boldsymbol{\eta}$ (3.86) can be written as

$$\boldsymbol{\eta} = \ \mathbf{W}^{\mathrm{T}} \boldsymbol{\sigma}(\mathbf{V}^{\mathrm{T}} \mathbf{z}) - \hat{\mathbf{W}}^{\mathrm{T}} \boldsymbol{\sigma}(\hat{\mathbf{V}}^{\mathrm{T}} \mathbf{z}) + \boldsymbol{\varepsilon} \tag{3.86}$$

To compute $\boldsymbol{\eta}$ (3.86), it is necessary to compute the general expression of

$\mathbf{W}^{\mathrm{T}}\boldsymbol{\sigma}(\mathbf{V}^{\mathrm{T}}\mathbf{z})$ - $\hat{\mathbf{W}}^{\mathrm{T}}\boldsymbol{\sigma}(\hat{\mathbf{V}}^{\mathrm{T}}\mathbf{z})$, which can be manipulated, as

$$\begin{aligned}
&\mathbf{W}^{\mathrm{T}}\boldsymbol{\sigma}(\mathbf{V}^{\mathrm{T}}\mathbf{z}) - \hat{\mathbf{W}}^{\mathrm{T}}\boldsymbol{\sigma}(\hat{\mathbf{V}}^{\mathrm{T}}\mathbf{z}) \\
&= \mathbf{W}^{\mathrm{T}}\boldsymbol{\sigma}(\mathbf{V}^{\mathrm{T}}\mathbf{z}) - \hat{\mathbf{W}}^{\mathrm{T}}\boldsymbol{\sigma}(\hat{\mathbf{V}}^{\mathrm{T}}\mathbf{z}) - \mathbf{W}^{\mathrm{T}}\boldsymbol{\sigma}(\hat{\mathbf{V}}^{\mathrm{T}}\mathbf{z}) + \mathbf{W}^{\mathrm{T}}\boldsymbol{\sigma}(\hat{\mathbf{V}}^{\mathrm{T}}\mathbf{z}) \\
&= \tilde{\mathbf{W}}^{\mathrm{T}}\boldsymbol{\sigma}(\hat{\mathbf{V}}^{\mathrm{T}}\mathbf{z}) + \mathbf{W}^{\mathrm{T}}\left(\boldsymbol{\sigma}(\mathbf{V}^{\mathrm{T}}\mathbf{z}) - \boldsymbol{\sigma}(\hat{\mathbf{V}}^{\mathrm{T}}\mathbf{z})\right)
\end{aligned} \tag{3.87}$$

where $\tilde{\mathbf{W}}$ and $\tilde{\mathbf{V}}$ are defined as the NN weight errors.

Therefore, first, we need to compute the error of the sigmoid function as follows

$$\widetilde{\boldsymbol{\sigma}} = \boldsymbol{\sigma}(\mathbf{V}^{\mathrm{T}}\mathbf{z}) - \boldsymbol{\sigma}(\hat{\mathbf{V}}^{\mathrm{T}}\mathbf{z}) \tag{3.88}$$

From the Taylor series expansion, we have

$$\boldsymbol{\sigma}(\mathbf{k})\big|_{\mathbf{k}=\hat{\mathbf{k}}} = \boldsymbol{\sigma}(\hat{\mathbf{k}}) + \frac{d\boldsymbol{\sigma}(\mathbf{k})}{d\mathbf{k}}(\mathbf{k}-\hat{\mathbf{k}}) + O(\mathbf{k}-\hat{\mathbf{k}}) \tag{3.89}$$

where $O(\mathbf{k}-\hat{\mathbf{k}})$ denotes the higher order terms. Note that $\boldsymbol{\sigma}'(\mathbf{k}) = \frac{\mathbf{d}\boldsymbol{\sigma}(\mathbf{k})}{d\mathbf{k}}\big|_{\mathbf{k}=\widehat{\mathbf{k}}}$, and because $\boldsymbol{\sigma}$ is differentiable, $\boldsymbol{\sigma}'$ exists. Hence $\boldsymbol{\sigma}(\mathbf{V}^{\mathrm{T}}\mathbf{z})\big|_{\mathbf{V}^{\mathrm{T}}\mathbf{z}=\hat{\mathbf{V}}^{\mathrm{T}}\mathbf{z}}$ in (3.88) can be written as

$$\boldsymbol{\sigma}(\mathbf{V}^{\mathrm{T}}\mathbf{z}) = \boldsymbol{\sigma}(\hat{\mathbf{V}}^{\mathrm{T}}\mathbf{z}) + \boldsymbol{\sigma}'(\hat{\mathbf{V}}^{\mathrm{T}}\mathbf{z})\tilde{\mathbf{V}}^{\mathrm{T}}\mathbf{z} + O(\tilde{\mathbf{V}}^{\mathrm{T}}\mathbf{z}) \tag{3.90}$$

To simplify the notations, it is defined that $\boldsymbol{\sigma} = \boldsymbol{\sigma}(\mathbf{V}^{\mathrm{T}}\mathbf{z})$, $\hat{\boldsymbol{\sigma}} = \boldsymbol{\sigma}(\hat{\mathbf{V}}^{\mathrm{T}}\mathbf{z})$, and $\boldsymbol{\sigma} = \hat{\boldsymbol{\sigma}} + \tilde{\boldsymbol{\sigma}}$. Therefore, using (3.90), $\widetilde{\boldsymbol{\sigma}}$ (3.88) can be rewritten as:

$$\widetilde{\boldsymbol{\sigma}} = \boldsymbol{\sigma}(\mathbf{V}^{\mathrm{T}}\mathbf{z}) - \boldsymbol{\sigma}(\hat{\mathbf{V}}^{\mathrm{T}}\mathbf{z}) = \hat{\boldsymbol{\sigma}}'\tilde{\mathbf{V}}^{\mathrm{T}}\mathbf{z} + O(\tilde{\mathbf{V}}^{\mathrm{T}}\mathbf{z}), \tag{3.91}$$

Substituting (3.91) into (3.87) and some manipulations, yield:

$$\begin{aligned}
\tilde{\mathbf{W}}^{\mathrm{T}}\hat{\boldsymbol{\sigma}} + \mathbf{W}^{\mathrm{T}}\tilde{\boldsymbol{\sigma}} = \tilde{\mathbf{W}}^{\mathrm{T}}(\hat{\boldsymbol{\sigma}} - \hat{\boldsymbol{\sigma}}'\hat{\mathbf{V}}^{\mathrm{T}}\mathbf{z}) + \hat{\mathbf{W}}^{\mathrm{T}}\hat{\boldsymbol{\sigma}}'\tilde{\mathbf{V}}^{\mathrm{T}}\mathbf{z} + \tilde{\mathbf{W}}^{\mathrm{T}}\hat{\boldsymbol{\sigma}}'\mathbf{V}^{\mathrm{T}}\mathbf{z} \\
+ \mathbf{W}^{\mathrm{T}}O(\tilde{\mathbf{V}}^{\mathrm{T}}\mathbf{z})
\end{aligned} \tag{3.92}$$

Substituting (3.92) into $\boldsymbol{\eta}$ in (3.86), we obtain

$$\boldsymbol{\eta} = \tilde{\mathbf{W}}^{\mathrm{T}}(\hat{\boldsymbol{\sigma}} - \hat{\boldsymbol{\sigma}}'\hat{\mathbf{V}}^{\mathrm{T}}\mathbf{z}) + \hat{\mathbf{W}}^{\mathrm{T}}\hat{\boldsymbol{\sigma}}'\tilde{\mathbf{V}}^{\mathrm{T}}\mathbf{z} + \boldsymbol{\zeta} \tag{3.93}$$

where the term $\boldsymbol{\zeta}$ is defined as

$$\boldsymbol{\zeta} = \tilde{\mathbf{W}}^{\mathrm{T}}\hat{\boldsymbol{\sigma}}'\mathbf{V}^{\mathrm{T}}\mathbf{z} + \mathbf{W}^{\mathrm{T}}O(\tilde{\mathbf{V}}^{\mathrm{T}}\mathbf{z}) + \boldsymbol{\varepsilon} \tag{3.94}$$

Now, to ease for later developments let's define $\mathbf{Z} = diag[\mathbf{W}, \mathbf{V}]$, such that

$$\|\mathbf{Z}\| = \sqrt{\|\mathbf{W}\|^2 + \|\mathbf{V}\|^2} \leq Z_M. \tag{3.95}$$

where Z_M is a positive scalar constant. Note, $\mathbf{W}, \mathbf{V}$ are upper-bounded since the actual dynamic is bounded.

It was shown in [74, 75] that $\boldsymbol{\zeta}$ can be shown to be bounded as follows

$$\|\boldsymbol{\zeta}\| \leq C_0 + C_1 \|\tilde{\mathbf{Z}}\| + C_2 \|\tilde{\mathbf{Z}}\| \|\mathbf{r}\| \tag{3.96}$$

with $C_i's$ are positive constants.

3.4.3 Stability Analysis of the Original Approach

The chosen Lyapunov function candidate for the closed-loop error dynamics (3.77), with the uncertainties $\boldsymbol{\eta}$ (3.93), is

$$V(\mathbf{r}, \tilde{\mathbf{Z}}) = \frac{1}{2}\mathbf{r}^{\mathrm{T}}\mathbf{M}(\mathbf{q})\mathbf{r} + \frac{1}{2}\sum_{i=1}^{n}\tilde{\mathbf{W}}_i^{\mathrm{T}}\mathbf{F}_i^{-1}\tilde{\mathbf{W}}_i + \frac{1}{2}\sum_{k=1}^{N_2}\tilde{\mathbf{V}}_k^{\mathrm{T}}\mathbf{G}_k^{-1}\tilde{\mathbf{V}}_k \tag{3.97}$$

where $\tilde{\mathbf{W}}_i \in \Re^{N_2}, \tilde{\mathbf{V}}_k \in \Re^{N_1}$ are column vectors and $\mathbf{F}_i^{-1} \in \Re^{N_2 \times N_2}, \mathbf{G}_k^{-1} \in \Re^{N_1 \times N_1}$ are positive diagonal matrices.

Taking the derivative of $V(\mathbf{r}, \tilde{\mathbf{Z}})$ with respect to time then substituting the closed-loop error dynamics (3.77), $\boldsymbol{\eta}$ (3.93) and Property 3.2.5 into $\dot{V}(\mathbf{r}, \tilde{\mathbf{Z}})$ (3.97), results

$$\dot{V}(\mathbf{r}, \tilde{\mathbf{Z}}) = -\mathbf{r}^{\mathrm{T}}\mathbf{K_v}\mathbf{r} - \mathbf{r}^{\mathrm{T}}\boldsymbol{\upsilon} + \mathbf{r}^{\mathrm{T}}\boldsymbol{\zeta} + \boldsymbol{\psi} \tag{3.98}$$

where $\boldsymbol{\psi}$ is defined as

$$\begin{aligned}\boldsymbol{\psi} = &\sum_{i=1}^{n} \tilde{\mathbf{W}}_i^{\mathrm{T}} \left(\mathbf{F}_i^{-1}\, \dot{\tilde{\mathbf{W}}}_i + \hat{\boldsymbol{\sigma}}\, r_i - \hat{\boldsymbol{\sigma}}'\hat{\mathbf{V}}\mathbf{z}\, r_i \right) \\ &+ \sum_{k=1}^{N_2} \tilde{\mathbf{V}}_k^{\mathrm{T}} \left(\mathbf{G}_k^{-1}\, \dot{\tilde{\mathbf{V}}}_k + \mathbf{z}\, \hat{\boldsymbol{\sigma}}_k' (\sum_{i=1}^{m} \hat{\mathbf{W}}_{ik} r_i) \right)\end{aligned} \tag{3.99}$$

Now, if we introduce the weight updates as follows

$$\dot{\hat{\mathbf{W}}}_i = \mathbf{F}_i(\hat{\boldsymbol{\sigma}}\, r_i - \hat{\boldsymbol{\sigma}}'\hat{\mathbf{V}}\mathbf{z}\, r_i - \kappa\|\mathbf{r}\|\hat{\mathbf{W}}_i), \tag{3.100}$$

$$\dot{\hat{\mathbf{V}}}_k = \mathbf{G}_k(\mathbf{z}\, \hat{\boldsymbol{\sigma}}_k' (\sum_{i=1}^{m} \hat{\mathbf{W}}_{ik}\, r_i) - \kappa\|\mathbf{r}\|\hat{\mathbf{V}}_k). \tag{3.101}$$

and take into account $-\dot{\tilde{\mathbf{W}}} = \dot{\hat{\mathbf{W}}}$, since $\tilde{\mathbf{W}} = \mathbf{W} - \hat{\mathbf{W}}$ and $\mathbf{W}$ is constant, then $\boldsymbol{\psi}$ (3.99) can be expressed as:

$$\boldsymbol{\psi} = \kappa\|\mathbf{r}\| \sum_{i=1}^{n} \tilde{\mathbf{W}}_i^{\mathrm{T}}\hat{\mathbf{W}}_i + \kappa\|\mathbf{r}\| \sum_{k=1}^{N_2} \tilde{\mathbf{V}}_k^{\mathrm{T}}\hat{\mathbf{V}}_k \tag{3.102}$$

$$\leq -\kappa\|\mathbf{r}\|\|\tilde{\mathbf{Z}}\|^2 + \kappa\|\mathbf{r}\|\|\tilde{\mathbf{Z}}\|Z_M \tag{3.103}$$

where (3.103) is obtained by making use of the following

$$\langle \tilde{\mathbf{W}}, \hat{\mathbf{W}} \rangle = \sum_{i=1}^{n} \tilde{\mathbf{W}}_i^{\mathrm{T}}\hat{\mathbf{W}}_i, \tag{3.104}$$

$$\langle \tilde{\mathbf{V}}, \hat{\mathbf{V}} \rangle = \sum_{k=1}^{N_2} \tilde{\mathbf{V}}_k^{\mathrm{T}}\hat{\mathbf{V}}_k \tag{3.105}$$

$$\langle \tilde{\mathbf{Z}}, \hat{\mathbf{Z}} \rangle = \langle \tilde{\mathbf{V}}, \hat{\mathbf{V}} \rangle + \langle \tilde{\mathbf{W}}, \hat{\mathbf{W}} \rangle \leq \|\tilde{\mathbf{Z}}\|Z_M - \|\tilde{\mathbf{Z}}\|^2. \tag{3.106}$$

Therefore, using $\boldsymbol{\psi}$ (3.103), $\boldsymbol{\zeta}$ (3.96), Property 3.2.1 and defining the robust term as follows

$$\boldsymbol{\upsilon} = K_z(\|\hat{\mathbf{Z}}\| + Z_M)\,\mathbf{r} \tag{3.107}$$

where K_z is a positive scalar constant, then it is possible to show $\dot{V}(\mathbf{r}, \tilde{\mathbf{Z}})$ in (3.98) as

$$\begin{aligned}\dot{V}(\mathbf{r}, \tilde{\mathbf{Z}}) \leq & - K_{v,m}\|\mathbf{r}\|^2 - K_z(\|\hat{\mathbf{Z}}\| + Z_M)\|\mathbf{r}\|^2 \\ & + C_0\|\mathbf{r}\| + C_1\|\tilde{\mathbf{Z}}\|\|\mathbf{r}\| + C_2\|\tilde{\mathbf{Z}}\|\|\mathbf{r}\|^2 \\ & - \kappa\|\mathbf{r}\|\|\tilde{\mathbf{Z}}\|^2 + \kappa\|\mathbf{r}\|\|\tilde{\mathbf{Z}}\|Z_M\end{aligned} \tag{3.108}$$

It was assumed in [74, 75] that it is known that $K_z > C_2$, and since $\|\hat{\mathbf{Z}}\| + Z_M > \|\tilde{\mathbf{Z}}\|$, therefore the term $K_z(\|\hat{\mathbf{Z}}\| + Z_M)\|\mathbf{r}\|^2$ will cancel the term $C_2\|\tilde{\mathbf{Z}}\|\|\mathbf{r}\|^2$, thus

$$\dot{V}(\mathbf{r}, \tilde{\mathbf{Z}}) \leq -\|\mathbf{r}\| \left[K_{v,m}\|\mathbf{r}\| + \kappa\|\tilde{\mathbf{Z}}\| \, (\|\tilde{\mathbf{Z}}\| - \frac{Z_M}{2}) - C_0 - C_1\|\tilde{\mathbf{Z}}\| \right] \tag{3.109}$$

or, by defining $C_3 = Z_M + C_1/\kappa$, we can simplify further

$$\dot{V}(\mathbf{r}, \tilde{\mathbf{Z}}) \leq -\|\mathbf{r}\| \left[K_{v,m}\|\mathbf{r}\| - C_0 + \kappa(\|\tilde{\mathbf{Z}}\| - \frac{C_3}{2})^2 - \frac{\kappa C_3^2}{4} \right] \tag{3.110}$$

Therefore, $\dot{V}(\mathbf{r}, \tilde{\mathbf{Z}}) < 0$ if

$$\|\mathbf{r}\| > \frac{C_0 + \kappa C_3^2/4}{K_{v,m}} \equiv b_{\mathbf{r}}, \quad \text{or} \tag{3.111}$$

$$\|\tilde{\mathbf{Z}}\| > \sqrt{\frac{C_0}{\kappa} + \frac{C_3^2}{4}} + \frac{C_3}{2} \equiv b_{\tilde{\mathbf{Z}}} \tag{3.112}$$

then by applying the Lyapunov's extension theorem [102] then as $t \to \infty$, the errors $\|\mathbf{r}\|$ and $\|\tilde{\mathbf{Z}}\|$ will be bounded, within the boundary of $\mathcal{S}$, as depicted in

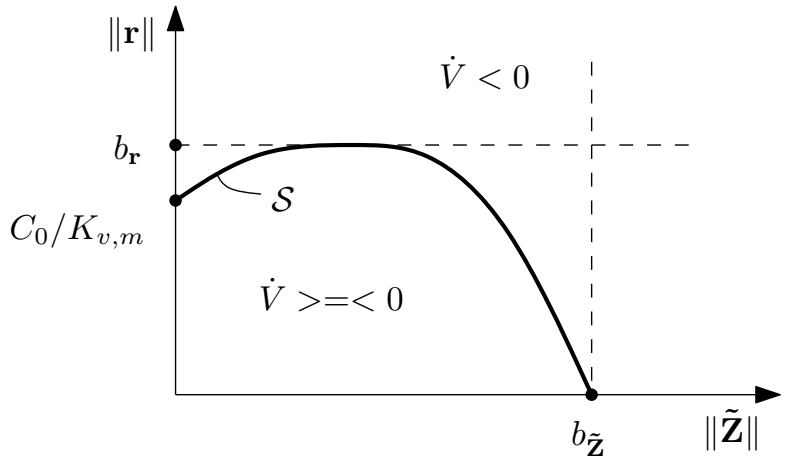

Figure 3.5: $\dot{V}(\mathbf{r}, \tilde{\mathbf{Z}})$ regions of the original joint space NN adaptive motion control.

Fig. 3.5. By using bounded-input-bounded-output (BIBO) property, a bounded input $\mathbf{r}$ in (3.76), yields bounded outputs $\dot{\mathbf{e}}$ and $\mathbf{e}$.

The evolution of the error signals based upon bounded stability can be explained as in [102], as follows: suppose the errors start within the boundary of $\mathcal{S}$, then when they start leaving the boundary of $\mathcal{S}$ since the $V(\mathbf{r}, \tilde{\mathbf{Z}})$ is decreasing ($\dot{V}(\mathbf{r}, \tilde{\mathbf{Z}}) < 0$) hence the errors cannot leave the boundary of $\mathcal{S}$. Now, suppose the errors start at outside the boundary of $\mathcal{S}$ then they tend to go to the equilibrium since $V(\mathbf{r}, \tilde{\mathbf{Z}})$ is decreasing. However, they cannot go to the equilibrium, but only up to entering the boundary of $\mathcal{S}$ and once they enter the boundary of $\mathcal{S}$, we have already shown that they are bounded.

Some notes are in order:

- It was shown in the stability analysis that one of the terms of $\boldsymbol{\zeta}$, $C_2\|\tilde{\mathbf{Z}}\|\|\mathbf{r}\|$, will be canceled by the robust term $\boldsymbol{\upsilon} = K_z(\|\hat{\mathbf{Z}}\| + Z_M)\|\mathbf{r}\|$, under assumption $K_z > C_2$. In other words C_2, C_1, C_0 must be known.

However, in practice we don't know C_2, C_1, C_0 nor we want to compute them, as it is not coherent with the adaptive control philosophy.

- Implementing $\boldsymbol{\upsilon}$ with exorbitantly large K_z might not be suitable for transient condition, albeit $C_2\|\tilde{\mathbf{Z}}\|\|\mathbf{r}\|$ might be truly canceled.

- Therefore, in our approach (the modified version of the original approach), the robust term $\boldsymbol{\upsilon}$ (3.107) is simply omitted and none of the terms of $\boldsymbol{\zeta}$ will be canceled. Therefore $\boldsymbol{\zeta}$ must contain as many as possible the weight errors. Henceforth, we suggest to rewrite $\boldsymbol{\eta}$ (3.93) as

$$\boldsymbol{\eta} = \tilde{\mathbf{W}}^{\mathrm{T}}\hat{\boldsymbol{\sigma}} + \hat{\mathbf{W}}^{\mathrm{T}}\hat{\boldsymbol{\sigma}}'\tilde{\mathbf{V}}^{\mathrm{T}}\mathbf{z} + \boldsymbol{\zeta} \tag{3.113}$$

where the un-cancelable "whole" error $\boldsymbol{\zeta}$ is defined as

$$\boldsymbol{\zeta} = \tilde{\mathbf{W}}^{\mathrm{T}}\hat{\boldsymbol{\sigma}}'\tilde{\mathbf{V}}^{\mathrm{T}}\mathbf{z} + \mathbf{W}^{\mathrm{T}}O(\tilde{\mathbf{V}}^{\mathrm{T}}\mathbf{z}) + \boldsymbol{\varepsilon}. \tag{3.114}$$

We will use the forms in (3.113) and (3.114) throughout our modified approach in the next chapter on Section 4.4.

In the next chapter, we will present our modified NN adaptive motion control implemented in the operational space framework.

CHAPTER 4

NN ADAPTIVE MOTION CONTROL

4.1 Chapter Overview

In this chapter, the operational space NN adaptive motion control is presented. The proposed control law is based upon the original NN adaptive joint space control [74, 75], extended into the operational space free motion formulation [8].

Further, some adjustments are needed in the original control law, so that it becomes more applicable and robust for real-time implementation (note that the original work was only implemented in simulation). The stability analysis of the proposed strategy is also presented in this chapter.

Several useful properties of the end effector dynamics to develop the proposed formulation within the operational space are introduced in this chapter. Simulated and real-time comparison to the performance of the Lagrangian dynamics and the PD-plus-gravity control strategies were also presented.

The preliminary study of this chapter was presented in [103].

4.2 End-effector Motion Dynamics

For controller formulation later, the end-effector free motion dynamics of the non-redundant manipulator (2.27) is reproduced, for ease of perusal, as

$$\mathbf{M_x}(\mathbf{q})\ddot{\mathbf{x}} + \mathbf{B_x}(\mathbf{q}, \dot{\mathbf{q}})\dot{\mathbf{x}} + \mathbf{g_x}(\mathbf{q}) + \boldsymbol{\tau}_{\mathbf{x}}(\mathbf{q}, \dot{\mathbf{q}}) = \mathbf{F} \tag{4.1}$$

where $\mathbf{x} \in \Re^m$ and $\mathbf{q} \in \Re^n$ denote the operational and joint space coordinates, respectively, where for a non-redundant manipulator $m = n$. The matrices $\mathbf{M_x}(\mathbf{q}) \in \Re^{m\times m}$ and $\mathbf{B_x}(\mathbf{q}, \dot{\mathbf{q}}) \in \Re^{m\times m}$ represent the inertia and the Coriolis/centrifugal terms, respectively, while vectors $\mathbf{g_x}(\mathbf{q}) \in \Re^m$ and $\boldsymbol{\tau}_{\mathbf{x}}(\mathbf{q}, \dot{\mathbf{q}}) \in \Re^m$ denote the gravity and joint friction forces, respectively. The vector $\mathbf{F} \in \Re^m$ is the operational space generalized forces.

First, the end-effector properties useful for developing the proposed algorithms need to be introduced, as the previous properties in Section 3.2.1 are only applicable for joint space dynamics.

4.3 Properties of the End-Effector Dynamics

Property 4.3.1 *The operational space kinetic energy matrix* $\mathbf{M_x}(\mathbf{q}) \in \Re^{m\times m}$*, due to* (2.28) *which is valid for all non-singular configurations and the fact that joint space kinetic energy* $\mathbf{M}(\mathbf{q}) > 0$*, is symmetric and positive definite matrix and therefore all its eigenvalues are positive. It follows from Rayleigh-Ritz theorem [93] that: any positive definite matrix* $\mathbf{A}$ *satisfies* $A_m \leq \|\mathbf{A}\| \leq A_M$*, where* $A_m, A_M > 0$ *denote the minimum and maximum eigenvalues of* $\mathbf{A}$*,*

respectively. Therefore $\mathbf{M_x}(\mathbf{q}(t))$ *along* $t \geq 0$ *is lower and upper-bounded by its global minimum and maximum eigenvalues, respectively, as:*

$$M_{x,m} \leq \|\mathbf{M_x}(\mathbf{q}(t))\| \leq M_{x,M}, \quad t \geq 0 \tag{4.2}$$

where $M_{x,m} = min(\lambda_{min}(\mathbf{M_x}(\mathbf{q}(t)))) > 0$ *and* $M_{x,M} = max(\lambda_{max}(\mathbf{M_x}(\mathbf{q}(t))))$ > 0*, where* $\lambda_{min}(\cdot)$ *and* $\lambda_{max}(\cdot)$ *denote the minimum and maximum eigenvalue operators, respectively.*

Property 4.3.2 *The operational space Coriolis and centrifugal matrix can be expressed as a function of* $\mathbf{q}$ *and* $\dot{\mathbf{x}}$ *since*

$$\mathbf{B_x}(\mathbf{q}, \dot{\mathbf{x}}) = [\mathbf{J}^{-\mathrm{T}}(\mathbf{q})\mathbf{B}(\mathbf{q}, \dot{\mathbf{x}}) - \mathbf{M_x}(\mathbf{q})\dot{\mathbf{J}}(\mathbf{q}, \dot{\mathbf{x}})]\mathbf{J}^{-1}(\mathbf{q}). \tag{4.3}$$

Note, $\mathbf{B}(\mathbf{q}, \dot{\mathbf{x}})$ *and* $\dot{\mathbf{J}}(\mathbf{q}, \dot{\mathbf{x}})$ *as functions of* $\mathbf{q}$ *and* $\dot{\mathbf{x}}$ *can be obtained directly by using the fact* $\dot{\mathbf{q}} = \mathbf{J}^{-1}(\mathbf{q})\ \dot{\mathbf{x}}$ *into* $\mathbf{B}(\mathbf{q}, \dot{\mathbf{q}})$ *and* $\dot{\mathbf{J}}(\mathbf{q}, \dot{\mathbf{q}})$*, respectively.*

Property 4.3.3 *The operational space Coriolis and centrifugal matrix* $\mathbf{B_x}(\mathbf{q}, \dot{\mathbf{x}})$ *can be shown to be upper-bounded*

$$\|\mathbf{B_x}(\mathbf{q}, \dot{\mathbf{x}})\| \leq B_{x,M}\ \dot{x}_M \tag{4.4}$$

where $B_{x,M}$ *is a positive scalar constant. This can be obtained directly by substituting the properties in joint space that* $\|\mathbf{B}(\mathbf{q}, \dot{\mathbf{q}})\| \leq B_M\ \dot{q}_M$ *and* $\|\dot{\mathbf{J}}(\mathbf{q}, \dot{\mathbf{q}})\| \leq \dot{J}_M\ \dot{q}_M$ *(*$B_M, \dot{J}_M$ *are positive scalar constants) and the fact* $\dot{\mathbf{q}} = \mathbf{J}^{-1}(\mathbf{q})\ \dot{\mathbf{x}}$*. Note* $\dot{\mathbf{q}}$ *can be assumed to bounded since in reality saturation occurs on the maximum velocity of the motor [47], therefore* $\dot{\mathbf{x}}$ *is bounded.*

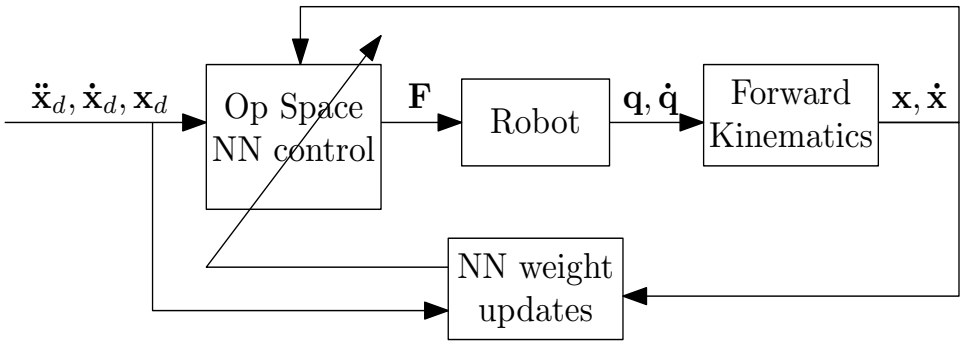

Figure 4.1: The operational space NN motion control structure.

Property 4.3.4 *The operational space gravity vector* $\mathbf{g_x}(\mathbf{q})$ (2.30) *is upper-bounded:*

$$\|\mathbf{g_x}(\mathbf{q})\| \leq g_M < \infty \tag{4.5}$$

Property 4.3.5 *For non-redundant robot,* $\dot{\mathbf{M}}_\mathbf{x}(\mathbf{q}) - 2\mathbf{B_x}(\mathbf{q}, \dot{\mathbf{q}})$ *is a skew-symmetric matrix [98, 90], hence given an operational space vector* $\mathbf{z} \in \Re^m$*, it satisfies*

$$\mathbf{z}^{\mathrm{T}} \left(\dot{\mathbf{M}}_\mathbf{x}(\mathbf{q}) - 2\mathbf{B_x}(\mathbf{q}, \dot{\mathbf{q}}) \right) \mathbf{z} = 0. \tag{4.6}$$

Therefore, it can also be written, using Property 4.3.2, as

$$\mathbf{z}^{\mathrm{T}} \left(\dot{\mathbf{M}}_\mathbf{x}(\mathbf{q}) - 2\mathbf{B_x}(\mathbf{q}, \dot{\mathbf{x}}) \right) \mathbf{z} = 0. \tag{4.7}$$

Property 4.3.6 *It can be shown for non-redundant robot [104], given any two operational space vectors* $\mathbf{y}, \mathbf{z} \in \Re^m$*, that* $\mathbf{B_x}(\mathbf{q}, \dot{\mathbf{x}})$ *satisfies*

$$\mathbf{B_x}(\mathbf{q}, \mathbf{y})\mathbf{z} = \mathbf{B_x}(\mathbf{q}, \mathbf{z})\mathbf{y}. \tag{4.8}$$

4.4 The Modified NN Adaptive Motion Control Law

Next, we present the operational space NN motion control law in Fig. 4.1, as we can see the adaptation from the joint space equivalent is straightforward

$$\mathbf{F} = \hat{\mathbf{M}}_{\mathbf{x}}(\mathbf{q})\mathbf{F}^{*}_{\text{motion}} + \hat{\mathbf{B}}_{\mathbf{x}}(\mathbf{q},\dot{\mathbf{q}})\dot{\mathbf{x}}_r + \hat{\mathbf{g}}_{\mathbf{x}}(\mathbf{q}) + \hat{\boldsymbol{\tau}}_{\mathbf{x}}(\mathbf{q},\dot{\mathbf{q}}) \tag{4.9}$$

where $\dot{\mathbf{x}}_r$ and $\mathbf{F}^{*}_{\text{motion}}$ are defined as

$$\dot{\mathbf{x}}_r = \dot{\mathbf{x}}_d + \boldsymbol{\Lambda}\mathbf{e} \tag{4.10}$$

$$\mathbf{F}^{*}_{\text{motion}} = \ddot{\mathbf{x}}_r + \boldsymbol{\Lambda}\mathbf{r} \tag{4.11}$$

and the computable terms are defined to compute $\mathbf{F}^{*}_{\text{motion}}$ as

$$\ddot{\mathbf{x}}_r = \ddot{\mathbf{x}}_d + \boldsymbol{\Lambda}\dot{\mathbf{e}} \tag{4.12}$$

$$\mathbf{r} = \dot{\mathbf{x}}_r - \dot{\mathbf{x}} = \dot{\mathbf{e}} + \boldsymbol{\Lambda}\mathbf{e} \tag{4.13}$$

where $\boldsymbol{\Lambda} \in \Re^{m\times m}$ is a positive diagonal matrix, $\mathbf{e} = \mathbf{x}_d - \mathbf{x}$ and $\dot{\mathbf{e}} = \dot{\mathbf{x}}_d - \dot{\mathbf{x}}$ are the operational space position and velocity tracking errors, with $\mathbf{x}_d$, $\dot{\mathbf{x}}_d$ and $\ddot{\mathbf{x}}_d$ are the desired operational space trajectories. Note that the estimated NNs within (4.9) will be introduced modularly (not as one lumped vector) i.e. there will be two estimated NN output matrices $\hat{\mathbf{M}}_{\mathbf{x}}(\mathbf{q}), \hat{\mathbf{B}}_{\mathbf{x}}(\mathbf{q},\dot{\mathbf{q}}) \in \Re^{m\times m}$ and two estimated NN output vectors $\hat{\mathbf{g}}_{\mathbf{x}}(\mathbf{q}), \hat{\boldsymbol{\tau}}_{\mathbf{x}}(\mathbf{q},\dot{\mathbf{q}}) \in \Re^{m}$.

Now, let's list the differences between our modified approach with the original approach:

- The robust term $\boldsymbol{\upsilon}$ is omitted. In the original approach, the robust term $\boldsymbol{\upsilon} = K_z(\|\hat{\mathbf{Z}}\| + Z_M)\,\mathbf{r}$ is used to cancel $C_2\|\tilde{\mathbf{Z}}\|\|\mathbf{r}\|$, which is part of

$\|\boldsymbol{\zeta}\|$ (please see (3.96)). However, in reality, we don't know C_2, C_1, C_0. Therefore the robust term $\boldsymbol{\upsilon}$ is not needed.

- The estimated NNs are introduced modularly, not as one lumped vector, and the NN input is defined appropriately to dependent variable, for instance the input for $\hat{\mathbf{B}}_{\mathbf{x}}(\mathbf{q}, \dot{\mathbf{q}})$ is defined as $\mathbf{z}_B = [\mathbf{q}^{\mathrm{T}}\ \dot{\mathbf{q}}^{\mathrm{T}}]^{\mathrm{T}}$. The reason behind the modularity with proper inputs is that it is expected that the NNs can learn more appropriately than one lumped NN vector NN with arbitrary input.

- It can be seen that the controller is only using estimated NNs and therefore, the standard PD term $\mathbf{K_v r}$ "seems "to be omitted.

  However, it can be shown to be similar, as in [93], if $\mathbf{K_v}$ equates to

$$\mathbf{K_v} \equiv \mathbf{M_x}(\mathbf{q})\boldsymbol{\Lambda} \tag{4.14}$$

  and therefore $\mathbf{K_v}$ and $\mathbf{M_x}(\mathbf{q})\boldsymbol{\Lambda}$ all satisfy as positive diagonal matrices. The closed-loop error dynamics for the ideal case can be shown as

$$\mathbf{M_x}(\mathbf{q})\dot{\mathbf{r}} + \mathbf{M_x}(\mathbf{q})\boldsymbol{\Lambda}\mathbf{r} + \mathbf{B_x}(\mathbf{q}, \dot{\mathbf{q}})\mathbf{r} = 0. \tag{4.15}$$

  And the Lyapunov function is chosen as

$$V(\mathbf{r}) = \frac{1}{2}\,\mathbf{r}^{\mathrm{T}}\mathbf{M_x}(\mathbf{q})\mathbf{r} \tag{4.16}$$

  Substituting the closed-loop error dynamics (4.15) into $\dot{V}(\mathbf{r})$, and taking into account Property 4.3.5, we obtain

$$\begin{aligned} \dot{V}(\mathbf{r}) &= -\,\mathbf{r}^{\mathrm{T}}\mathbf{M_x}(\mathbf{q})\boldsymbol{\Lambda}\mathbf{r} + \mathbf{r}^{\mathrm{T}}\left(\dot{\mathbf{M}}_{\mathbf{x}}(\mathbf{q}) - \mathbf{B_x}(\mathbf{q}, \dot{\mathbf{q}})\right)\mathbf{r} \\ &= -\,\mathbf{r}^{\mathrm{T}}\mathbf{M_x}(\mathbf{q})\boldsymbol{\Lambda}\mathbf{r} \leq 0 \end{aligned} \tag{4.17}$$

Where it can be shown using Barbalat's lemma [93] that $t \to \infty, \mathbf{r} \to 0$, from (4.13) implying $\mathbf{e}, \dot{\mathbf{e}} \to 0$.

By combining the operational space motion dynamics (4.1) with the NN adaptive motion control (4.9), and taking into account the first derivative of (4.13), the closed-loop error dynamics can be obtained as

$$\mathbf{M}_{\mathbf{x}}(\mathbf{q})\dot{\mathbf{r}} + \mathbf{M}_{\mathbf{x}}(\mathbf{q})\mathbf{\Lambda}\mathbf{r} + \mathbf{B}_{\mathbf{x}}(\mathbf{q}, \dot{\mathbf{q}})\mathbf{r} = \boldsymbol{\eta}; \tag{4.18}$$

where the uncertainties $\boldsymbol{\eta}$ is defined as

$$\boldsymbol{\eta} = \tilde{\mathbf{M}}_{\mathbf{x}}(\mathbf{q})\mathbf{F}^{*}_{\text{motion}} + \tilde{\mathbf{B}}_{\mathbf{x}}(\mathbf{q}, \dot{\mathbf{q}})\dot{\mathbf{x}}_r + \tilde{\mathbf{g}}_{\mathbf{x}}(\mathbf{q}) + \tilde{\boldsymbol{\tau}}_{\mathbf{x}}. \tag{4.19}$$

4.4.1 Three-Layer Neural Networks

This section is an extension from Section 3.4.1. It explains the construction of NN as an output matrix, as estimated matrices are required in our controller. Each element of output matrix $\mathbf{U} \in \Re^{N_3 \times N_4}$ can be expressed as

$$\begin{gathered} u_{ij} = \sum_{k=1}^{N_2} w_{ijk}\ \sigma_k \left(\sum_{l=1}^{N_1} v_{kl} z_l\ +\ \theta_k \right); \\ i = 1, \ldots, N_3,\ j = 1, \ldots, N_4 \end{gathered} \tag{4.20}$$

where now second-to-third layer weights is w_{ijk} with $i = 1, \ldots, N_3,\ j = 1, \ldots, N_4$ are the output-layer indices. Similarly, (4.20) can be written in a vector-and-matrix form as

$$\mathbf{U} = \mathbf{W}^{\mathrm{T}}\ \boldsymbol{\sigma}\left(\mathbf{V}^{\mathrm{T}}\mathbf{z}\right) \tag{4.21}$$

where now $\mathbf{W} \in \Re^{N_3 \times N_4 \times N_2}, \mathbf{V} \in \Re^{N_2 \times N_1}$. For a non-redundant manipulator with 6 DOF $N_4 = N_3 = m = 6$.

4.4.2 Uncertainties η in NN terms

The procedure is similar to Section 3.4.2. However since it is now done in modular fashion, therefore we will present it completely in this section. This section also serves as a foundation for later algorithms. Using the relationship of error dynamics $\tilde{(\cdot)} = (\cdot) - \hat{(\cdot)}$, the uncertainties $\boldsymbol{\eta}$ in (4.19) can be written as

$$\begin{aligned}\boldsymbol{\eta} = (\mathbf{M}_{\mathbf{x}}(\mathbf{q}) - \hat{\mathbf{M}}_{\mathbf{x}}(\mathbf{q}))\mathbf{F}^{*}_{\text{motion}} + (\mathbf{B}_{\mathbf{x}}(\mathbf{q},\dot{\mathbf{q}}) - \hat{\mathbf{B}}_{\mathbf{x}}(\mathbf{q},\dot{\mathbf{q}}))\dot{\mathbf{x}}_{r} \\ + (\mathbf{g}_{\mathbf{x}}(\mathbf{q}) - \hat{\mathbf{g}}_{\mathbf{x}}(\mathbf{q})) + (\boldsymbol{\tau}_{\mathbf{x}}(\mathbf{q},\dot{\mathbf{q}}) - \hat{\boldsymbol{\tau}}_{\mathbf{x}}(\mathbf{q},\dot{\mathbf{q}}))\end{aligned} \tag{4.22}$$

From NN theory, given an adequate number of hidden layer nodes, N_2, a three layer NNs with ideal weights is capable of approximating any function [100, 101]. In practice, however, there are only limited number of hidden layer nodes, thus the dynamical terms $\mathbf{M}_{\mathbf{x}}(\mathbf{q})$, $\mathbf{B}_{\mathbf{x}}(\mathbf{q},\dot{\mathbf{q}})$, $\mathbf{g}_{\mathbf{x}}(\mathbf{q})$, and $\boldsymbol{\tau}_{\mathbf{x}}(\mathbf{q},\dot{\mathbf{q}})$, for a given number of neurons, can be described by three-layer NNs with constant *optimum* weights $\mathbf{V}_p, \mathbf{W}_p$ and approximation error $\boldsymbol{\varepsilon}_p$, with the subscript $p = M, B, g, \tau$ representing the individual dynamical terms:

$$\mathbf{M}_{\mathbf{x}}(\mathbf{q}) = \mathbf{W}_M^{\mathrm{T}}\, \boldsymbol{\sigma}_M(\mathbf{V}_M^{\mathrm{T}}\, \mathbf{z}_M) + \boldsymbol{\varepsilon}_M \tag{4.23}$$

$$\mathbf{B}_{\mathbf{x}}(\mathbf{q},\dot{\mathbf{q}}) = \mathbf{W}_B^{\mathrm{T}}\, \boldsymbol{\sigma}_B(\mathbf{V}_B^{\mathrm{T}}\, \mathbf{z}_B) + \boldsymbol{\varepsilon}_B \tag{4.24}$$

$$\mathbf{g}_{\mathbf{x}}(\mathbf{q}) = \mathbf{W}_g^{\mathrm{T}}\, \boldsymbol{\sigma}_g(\mathbf{V}_g^{\mathrm{T}}\, \mathbf{z}_g) + \boldsymbol{\varepsilon}_g \tag{4.25}$$

$$\boldsymbol{\tau}_{\mathbf{x}}(\mathbf{q},\dot{\mathbf{q}}) = \mathbf{W}_\tau^{\mathrm{T}}\, \boldsymbol{\sigma}_\tau(\mathbf{V}_\tau^{\mathrm{T}}\, \mathbf{z}_\tau) + \boldsymbol{\varepsilon}_\tau \tag{4.26}$$

Similarly, the estimated dynamic terms $\hat{\mathbf{M}}_{\mathbf{x}}(\mathbf{q})$, $\hat{\mathbf{B}}_{\mathbf{x}}(\mathbf{q},\dot{\mathbf{q}})$, $\hat{\mathbf{g}}_{\mathbf{x}}(\mathbf{q})$, and $\hat{\boldsymbol{\tau}}_{\mathbf{x}}(\mathbf{q},\dot{\mathbf{q}})$ are described by the estimated weights $\hat{\mathbf{V}}_p, \hat{\mathbf{W}}_p$, with subscript $p = M, B, g, \tau$.

It is clear that that $\mathbf{M}_{\mathbf{x}}(\mathbf{q}), \mathbf{B}_{\mathbf{x}}(\mathbf{q},\dot{\mathbf{q}}), \mathbf{g}_{\mathbf{x}}(\mathbf{q})$ can be been shown to be bounded by Properties 4.3.1, 4.3.3, 4.3.4, respectively. The boundedness of $\boldsymbol{\tau}_{\mathbf{x}}(\mathbf{q},\dot{\mathbf{q}})$ can

be shown by using Property 3.2.4 and the fact that $\|\mathbf{J}^{-1}(\mathbf{q})\|$ is bounded for non-singular configuration. Therefore, the optimum weights $\mathbf{W}_p, \mathbf{V}_p$ and the approximation error $\boldsymbol{\varepsilon}_p$ (with subscript $p = M, B, g, \tau$) from (4.23)-(4.26), are also upper-bounded.

For ease of later developments, let us define $\mathbf{Z} = \text{diag}[\mathbf{W}, \mathbf{V}]$ to be upper-bounded as follows

$$\|\mathbf{Z}\| = \sqrt{\|\mathbf{W}\|^2 + \|\mathbf{V}\|^2} \leq Z_M \tag{4.27}$$

where Z_M is a positive scalar constant, $\mathbf{W} = \text{diag}[\mathbf{W}_M, \mathbf{W}_B, \mathbf{W}_g, \mathbf{W}_\tau]$ and $\mathbf{V} = \text{diag}[\mathbf{V}_M, \mathbf{V}_B, \mathbf{V}_g, \mathbf{V}_\tau]$.

Now, for ease of presentation, the following generic NN expressions are defined:

$$\begin{aligned} \mathbf{L}_p &= \mathbf{W}_p^{\mathrm{T}}\, \boldsymbol{\sigma}_p(\mathbf{V}_p^{\mathrm{T}}\, \mathbf{z}_p) \\ \hat{\mathbf{L}}_p &= \hat{\mathbf{W}}_p^{\mathrm{T}}\, \boldsymbol{\sigma}_p(\hat{\mathbf{V}}_p^{\mathrm{T}}\, \mathbf{z}_p) \\ \tilde{\mathbf{L}}_p &= \mathbf{L}_p - \hat{\mathbf{L}}_p; \end{aligned} \tag{4.28}$$

where $\mathbf{L}_p$, $\hat{\mathbf{L}}_p$, and $\tilde{\mathbf{L}}_p$ represent the optimum, estimated, and error, of the respective terms. Hence, using the generic NN expressions, the uncertainties (4.22) can be written as

$$\boldsymbol{\eta} = (\mathbf{L}_M - \hat{\mathbf{L}}_M)\mathbf{F}^*_{\text{motion}} + (\mathbf{L}_B - \hat{\mathbf{L}}_B)\dot{\mathbf{x}}_r + (\mathbf{L}_g - \hat{\mathbf{L}}_g) + (\mathbf{L}_\tau - \hat{\mathbf{L}}_\tau) + \boldsymbol{\varepsilon} \tag{4.29}$$

where the total approximation error $\boldsymbol{\varepsilon} = \boldsymbol{\varepsilon}_M\, \mathbf{F}^*_{\text{motion}} + \boldsymbol{\varepsilon}_B\, \dot{\mathbf{x}}_r + \boldsymbol{\varepsilon}_g + \boldsymbol{\varepsilon}_\tau \leq \varepsilon_M$ (since the actual dynamics are bounded). To compute $\boldsymbol{\eta}$ (4.29), it is necessary

to compute the generic form $\mathbf{L}_p - \hat{\mathbf{L}}_p$, which can be manipulated, as follows

$$\begin{aligned}\mathbf{L}_p - \hat{\mathbf{L}}_p &= \mathbf{W}_p^{\mathrm{T}}\boldsymbol{\sigma}(\mathbf{V}_p^{\mathrm{T}}\mathbf{z}_p) - \hat{\mathbf{W}}_p^{\mathrm{T}}\boldsymbol{\sigma}(\hat{\mathbf{V}}_p^{\mathrm{T}}\mathbf{z}_p) \\ &= \mathbf{W}_p^{\mathrm{T}}\boldsymbol{\sigma}(\mathbf{V}_p^{\mathrm{T}}\mathbf{z}_p) - \hat{\mathbf{W}}_p^{\mathrm{T}}\boldsymbol{\sigma}(\hat{\mathbf{V}}_p^{\mathrm{T}}\mathbf{z}_p) - \mathbf{W}_p^{\mathrm{T}}\boldsymbol{\sigma}(\hat{\mathbf{V}}_p^{\mathrm{T}}\mathbf{z}) + \mathbf{W}_p^{\mathrm{T}}\boldsymbol{\sigma}(\hat{\mathbf{V}}^{\mathrm{T}}\mathbf{z}_p) \\ &= \tilde{\mathbf{W}}_p^{\mathrm{T}}\boldsymbol{\sigma}(\hat{\mathbf{V}}_p^{\mathrm{T}}\mathbf{z}_p) + \mathbf{W}_p^{\mathrm{T}}\left(\boldsymbol{\sigma}(\mathbf{V}_p^{\mathrm{T}}\mathbf{z}_p) - \boldsymbol{\sigma}(\hat{\mathbf{V}}_p^{\mathrm{T}}\mathbf{z}_p)\right)\end{aligned} \tag{4.30}$$

Therefore, first, we need to compute the error of the sigmoid function as:

$$\widetilde{\boldsymbol{\sigma}} = \boldsymbol{\sigma}(\mathbf{V}^{\mathrm{T}}\mathbf{z}) - \boldsymbol{\sigma}(\hat{\mathbf{V}}^{\mathrm{T}}\mathbf{z}). \tag{4.31}$$

From the Taylor series expansion, we have

$$\boldsymbol{\sigma}(\mathbf{k})\big|_{\mathbf{k}=\hat{\mathbf{k}}} = \boldsymbol{\sigma}(\hat{\mathbf{k}}) + \frac{d\boldsymbol{\sigma}(\mathbf{k})}{d\mathbf{k}}(\mathbf{k} - \hat{\mathbf{k}}) + O(\mathbf{k} - \hat{\mathbf{k}}) \tag{4.32}$$

where $O(\mathbf{k} - \hat{\mathbf{k}})$ denotes the higher order terms. Note that $\boldsymbol{\sigma}'(\mathbf{k}) = \frac{\mathbf{d}\boldsymbol{\sigma}(\mathbf{k})}{d\mathbf{k}}\big|_{\mathbf{k}=\widehat{\mathbf{k}}}$, and because $\boldsymbol{\sigma}$ is differentiable, $\boldsymbol{\sigma}'$ exists. Hence $\boldsymbol{\sigma}(\mathbf{V}^{\mathrm{T}}\mathbf{z})\big|_{\mathbf{V}^{\mathrm{T}}\mathbf{z}=\hat{\mathbf{V}}^{\mathrm{T}}\mathbf{z}}$ in (4.31) can be written as

$$\boldsymbol{\sigma}(\mathbf{V}^{\mathrm{T}}\mathbf{z}) = \boldsymbol{\sigma}(\hat{\mathbf{V}}^{\mathrm{T}}\mathbf{z}) + \boldsymbol{\sigma}'(\hat{\mathbf{V}}^{\mathrm{T}}\mathbf{z})\tilde{\mathbf{V}}^{\mathrm{T}}\mathbf{z} + O(\tilde{\mathbf{V}}^{\mathrm{T}}\mathbf{z}) \tag{4.33}$$

To simplify the notations, it is defined that $\boldsymbol{\sigma} = \boldsymbol{\sigma}(\mathbf{V}_p^{\mathrm{T}}\mathbf{z})$, $\hat{\boldsymbol{\sigma}} = \boldsymbol{\sigma}(\hat{\mathbf{V}}^{\mathrm{T}}\mathbf{z})$, and $\boldsymbol{\sigma} = \hat{\boldsymbol{\sigma}} + \tilde{\boldsymbol{\sigma}}$. Therefore, using (4.33), $\widetilde{\boldsymbol{\sigma}}$ (4.31) can be rewritten as:

$$\widetilde{\boldsymbol{\sigma}} = \boldsymbol{\sigma}(\mathbf{V}^{\mathrm{T}}\mathbf{z}) - \boldsymbol{\sigma}(\hat{\mathbf{V}}^{\mathrm{T}}\mathbf{z}) = \hat{\boldsymbol{\sigma}}'\tilde{\mathbf{V}}^{\mathrm{T}}\mathbf{z} + O\left(\tilde{\mathbf{V}}^{\mathrm{T}}\mathbf{z}\right). \tag{4.34}$$

The substitution of (4.34) into (4.30) yields:

$$\begin{aligned}\mathbf{L}_p - \hat{\mathbf{L}}_p &= \tilde{\mathbf{W}}_p^{\mathrm{T}}\hat{\boldsymbol{\sigma}}_p + \mathbf{W}_p^{\mathrm{T}}\tilde{\boldsymbol{\sigma}}_p = \tilde{\mathbf{W}}_p^{\mathrm{T}}\hat{\boldsymbol{\sigma}}_p + \mathbf{W}_p^{\mathrm{T}}\left[\hat{\boldsymbol{\sigma}}_p'\tilde{\mathbf{V}}_p^{\mathrm{T}}\mathbf{z}_p + O(\tilde{\mathbf{V}}_p^{\mathrm{T}}\mathbf{z}_p)\right] \\ &= \tilde{\mathbf{W}}_p^{\mathrm{T}}\hat{\boldsymbol{\sigma}}_p + (\hat{\mathbf{W}}_p^{\mathrm{T}} + \tilde{\mathbf{W}}_p^{\mathrm{T}})\left[\hat{\boldsymbol{\sigma}}_p'\tilde{\mathbf{V}}_p^{\mathrm{T}}\mathbf{z}_p + O(\tilde{\mathbf{V}}_p^{\mathrm{T}}\mathbf{z}_p)\right] \\ &= \left(\tilde{\mathbf{W}}_p^{\mathrm{T}}\hat{\boldsymbol{\sigma}}_p + \hat{\mathbf{W}}_p^{\mathrm{T}}\hat{\boldsymbol{\sigma}}_p'\tilde{\mathbf{V}}_p^{\mathrm{T}}\mathbf{z}_p\right) + \left(\tilde{\mathbf{W}}_p^{\mathrm{T}}\hat{\boldsymbol{\sigma}}_p'\tilde{\mathbf{V}}_p^{\mathrm{T}}\mathbf{z}_p + \mathbf{W}_p^{\mathrm{T}}O(\tilde{\mathbf{V}}_p^{\mathrm{T}}\mathbf{z}_p)\right).\end{aligned} \tag{4.35}$$

Using the general expression (4.35), the uncertainties $\boldsymbol{\eta}$ in (4.29) can be written as

$$\boldsymbol{\eta} = \boldsymbol{\xi} + \boldsymbol{\zeta} \tag{4.36}$$

This division is needed because in the Lyapunov analysis (Section 4.4.3), it becomes evident that only $\boldsymbol{\xi}$ term can be manipulated by the weight updates $\dot{\hat{\mathbf{W}}}, \dot{\hat{\mathbf{V}}}$. The term $\boldsymbol{\xi}$ is defined as

$$\begin{aligned}\boldsymbol{\xi} = & \left(\tilde{\mathbf{W}}_M^{\mathrm{T}}\hat{\boldsymbol{\sigma}}_M\right)\mathbf{F}^*_{\mathrm{motion}} + \left(\tilde{\mathbf{W}}_B^{\mathrm{T}}\hat{\boldsymbol{\sigma}}_B\right)\dot{\mathbf{x}}_r + \tilde{\mathbf{W}}_g^{\mathrm{T}}\hat{\boldsymbol{\sigma}}_g + \tilde{\mathbf{W}}_\tau^{\mathrm{T}}\hat{\boldsymbol{\sigma}}_\tau \\ & + \left(\hat{\mathbf{W}}_M^{\mathrm{T}}\hat{\boldsymbol{\sigma}}'_M\tilde{\mathbf{V}}_M^{\mathrm{T}}\mathbf{z}_M\right)\mathbf{F}^*_{\mathrm{motion}} + \left(\hat{\mathbf{W}}_B^{\mathrm{T}}\hat{\boldsymbol{\sigma}}'_B\tilde{\mathbf{V}}_B^{\mathrm{T}}\mathbf{z}_B\right)\dot{\mathbf{x}}_r \\ & + \hat{\mathbf{W}}_g^{\mathrm{T}}\hat{\boldsymbol{\sigma}}'_g\tilde{\mathbf{V}}_g^{\mathrm{T}}\mathbf{z}_g + \hat{\mathbf{W}}_\tau^{\mathrm{T}}\hat{\boldsymbol{\sigma}}'_\tau\tilde{\mathbf{V}}_\tau^{\mathrm{T}}\mathbf{z}_\tau\end{aligned} \tag{4.37}$$

and the "whole"NN errors $\boldsymbol{\zeta}$ is defined as

$$\begin{aligned}\boldsymbol{\zeta} = & \left(\tilde{\mathbf{W}}_M^{\mathrm{T}}\hat{\boldsymbol{\sigma}}'_M\tilde{\mathbf{V}}_M^{\mathrm{T}}\mathbf{z}_M\right)\mathbf{F}^*_{\mathrm{motion}} + \left(\tilde{\mathbf{W}}_B^{\mathrm{T}}\hat{\boldsymbol{\sigma}}'_B\tilde{\mathbf{V}}_B^{\mathrm{T}}\mathbf{z}_B\right)\dot{\mathbf{x}}_r \\ & + \tilde{\mathbf{W}}_g^{\mathrm{T}}\hat{\boldsymbol{\sigma}}'_g\tilde{\mathbf{V}}_g^{\mathrm{T}}\mathbf{z}_g + \tilde{\mathbf{W}}_\tau^{\mathrm{T}}\hat{\boldsymbol{\sigma}}'_\tau\tilde{\mathbf{V}}_\tau^{\mathrm{T}}\mathbf{z}_\tau \\ & + \left(\mathbf{W}_M^{\mathrm{T}}O(\tilde{\mathbf{V}}_M^{\mathrm{T}}\mathbf{z}_M)\right)\mathbf{F}^*_{\mathrm{motion}} + \left(\mathbf{W}_B^{\mathrm{T}}O(\tilde{\mathbf{V}}_B^{\mathrm{T}}\mathbf{z}_B)\right)\dot{\mathbf{x}}_r \\ & + \mathbf{W}_g^{\mathrm{T}}O(\tilde{\mathbf{V}}_g^{\mathrm{T}}\mathbf{z}_g) + \mathbf{W}_\tau^{\mathrm{T}}O(\tilde{\mathbf{V}}_\tau^{\mathrm{T}}\mathbf{z}_\tau) + \boldsymbol{\varepsilon}\end{aligned} \tag{4.38}$$

Note that, the terms in (4.38) is similar with (3.114).

Now, it can be shown, in incremental manner, that $\boldsymbol{\zeta}$ and $\boldsymbol{\xi}$ possess some upper-boundedness that are useful for the stability analysis to follow in Section 4.4.3.

To prove this, we need the boundedness of the generic expression (4.35)

$$\|\mathbf{L}_p - \hat{\mathbf{L}}_p\| = \left\|\left(\tilde{\mathbf{W}}_p^{\mathrm{T}}\hat{\boldsymbol{\sigma}}_p + \hat{\mathbf{W}}_p^{\mathrm{T}}\hat{\boldsymbol{\sigma}}'_p\tilde{\mathbf{V}}_p^{\mathrm{T}}\mathbf{z}_p\right) + \left(\tilde{\mathbf{W}}_p^{\mathrm{T}}\hat{\boldsymbol{\sigma}}'_p\tilde{\mathbf{V}}_p^{\mathrm{T}}\mathbf{z}_p + \mathbf{W}_p^{\mathrm{T}}O(\tilde{\mathbf{V}}_p^{\mathrm{T}}\mathbf{z}_p)\right)\right\| \tag{4.39}$$

Clearly, the boundedness depends solely on $\tilde{\mathbf{W}}$ and $\tilde{\mathbf{V}}$, this is because the other terms:

- the optimum weights $\mathbf{W}_p, \mathbf{V}_p$ and approximation error $\boldsymbol{\varepsilon}_p$ are upper-bounded, and
- $\boldsymbol{\sigma}$ and $\hat{\boldsymbol{\sigma}}$ are bounded for differentiable functions like sigmoid, tanh, RBF functions.

From the definition of the NN weight errors, $\tilde{\mathbf{W}} = \mathbf{W} - \hat{\mathbf{W}}$, we have

$$\|\tilde{\mathbf{W}}\| \leq \|\mathbf{W}\| + \|\hat{\mathbf{W}}\| \tag{4.40}$$

The boundedness of the NN weight errors $\tilde{\mathbf{W}}$ in (4.40) depends solely on the boundedness of the weight estimate $\hat{\mathbf{W}}$, since $\|\mathbf{W}\|$ is upper-bounded. Note although $\|\hat{\mathbf{W}}\|$ is positive, $\hat{\mathbf{W}}$ is not necessarily a positive definite matrix i.e. its eigenvalues could be negative, zero or positive. Therefore Rayleigh-Ritz theorem is not applicable since the minimum and maximum positive eigenvalues do not exist.

However, it can be shown that the boundedness of $\tilde{\mathbf{W}}$ can be achieved by simply combining the Frobenius norm definition and limiting $\hat{\mathbf{W}}$ in the implementation. From the norm definition of $\|\hat{\mathbf{W}}\|$, for a 3D output matrix $\mathbf{U} \in \Re^{N_3 \times N_4 \times N_2}$ (for a 2D output matrix $N_4 = 1$):

$$\|\hat{\mathbf{W}}\| = \sqrt{\sum_{i}^{N_3} \sum_{j}^{N_4} \sum_{k}^{N_2} \hat{w}_{ijk}^2} \quad . \tag{4.41}$$

In the implementation, $\hat{\mathbf{W}}$ and $\hat{\mathbf{V}}$ can be limited as follows:

$$\begin{aligned} &\text{if } (\|\hat{\mathbf{W}}\| > \hat{W}_M), \text{ then } \dot{\hat{w}}_{ijk} = 0, \text{ and} \\ &\text{if } (\|\hat{\mathbf{V}}\| > \hat{V}_M), \text{ then } \dot{\hat{v}}_{kl} = 0 \end{aligned} \tag{4.42}$$

with $\hat{W}_M > 0$ and $\hat{V}_M > 0$, therefore $\hat{\mathbf{W}}$ and $\hat{\mathbf{V}}$ are upper bounded as follows

$$\begin{aligned} \|\hat{\mathbf{W}}\| \leq & \hat{W}_M, \text{ and} \\ \|\hat{\mathbf{V}}\| \leq & \hat{V}_M. \end{aligned} \tag{4.43}$$

Since $\|\tilde{\mathbf{W}}\| \leq \|\mathbf{W}\| + \|\hat{\mathbf{W}}\|$ and $\|\tilde{\mathbf{V}}\| \leq \|\mathbf{V}\| + \|\hat{\mathbf{V}}\|$ therefore

$$\begin{aligned} \|\tilde{\mathbf{W}}\| \leq & \tilde{W}_M, \text{ and} \\ \|\tilde{\mathbf{V}}\| \leq & \tilde{V}_M \end{aligned} \tag{4.44}$$

with $\tilde{W}_M > 0$ and $\tilde{V}_M > 0$.

Furthermore, it follows that the overall estimated NN weights, $\hat{\mathbf{Z}}$, and NN weight errors, $\tilde{\mathbf{Z}}$, are to be upper bounded as

$$\|\hat{\mathbf{Z}}\| \leq \hat{Z}_M \tag{4.45}$$

$$\|\tilde{\mathbf{Z}}\| \equiv \|\mathbf{Z}\| + \|\hat{\mathbf{Z}}\| \leq Z_M + \hat{Z}_M \equiv \tilde{Z}_M \tag{4.46}$$

with $\hat{Z}_M > 0, \tilde{Z}_M > 0$.

Substituting (4.44) into (4.39), results the generic expression $\|\mathbf{L}_p - \hat{\mathbf{L}}_p\|$ in (4.39) is upper-bounded as

$$\|\mathbf{L}_p - \hat{\mathbf{L}}_p\| \leq (\tilde{L}_p)_M. \tag{4.47}$$

where $(\tilde{L}_p)_M > 0$.

Now, seeing the uncertainties $\boldsymbol{\eta}$ in (4.36) with (4.47), and also exploiting $\mathbf{F}^*_{\text{motion}}$ (4.11) and $\dot{\mathbf{x}}_r$ (4.13), we can write

$$\begin{aligned} \|\boldsymbol{\eta}\| &\leq (\tilde{L}_M)_M \, \|\mathbf{F}^*_{\text{motion}}\| + (\tilde{L}_B)_M \, \|\dot{\mathbf{x}}_r\| + (\tilde{L}_g)_M + (\tilde{L}_\tau)_M + \varepsilon_M \\ &\leq (\tilde{L}_M)_M \, (\|\ddot{\mathbf{x}}_r\| + \boldsymbol{\Lambda}\|\mathbf{r}\|) + (\tilde{L}_B)_M \, (\|\mathbf{r}\| + \|\dot{\mathbf{x}}\|) + (\tilde{L}_g)_M + (\tilde{L}_\tau)_M \\ &\quad + \varepsilon_M \end{aligned} \tag{4.48}$$

Note that $\ddot{\mathbf{x}}_r$ in (4.12) can be assumed to be bounded since the desired trajectories $\ddot{\mathbf{x}}_d, \dot{\mathbf{x}}_d, \mathbf{x}_d$ are bounded by design, $\mathbf{x}$ is bounded by the workspace and $\dot{\mathbf{x}}$ is bounded by motor speed limit.

Therefore $\boldsymbol{\eta}$ can be shown to be bounded as follows

$$\|\boldsymbol{\eta}\| \leq C_0 + C_1 \, \|\mathbf{r}\|. \tag{4.49}$$

where $C_0, C_1 > 0$. And since $\boldsymbol{\eta} = \boldsymbol{\xi} + \boldsymbol{\zeta}$, then clearly the following inequalities are true

$$\|\boldsymbol{\xi}\| \leq C_0 + C_1 \, \|\mathbf{r}\| \tag{4.50}$$

$$\|\boldsymbol{\zeta}\| \leq C_0 + C_1 \, \|\mathbf{r}\|. \tag{4.51}$$

4.4.3 Stability Analysis of Our Modified Approach

For the proposed motion control (4.9), let the weight updates be:

$$\dot{\hat{\mathbf{w}}}_{M_{ij}} = \mathbf{F}_{M_{ij}}(\hat{\boldsymbol{\sigma}}_M \, r_i \, F^*_{\text{motion}\,j} - \kappa\|\mathbf{r}\|\hat{\mathbf{w}}_{M_{ij}}) \tag{4.52}$$

$$\dot{\hat{\mathbf{v}}}_{M_k} = \mathbf{G}_{M_k}(\mathbf{z}_M \, \hat{\boldsymbol{\sigma}}'_{M_k} \, (\sum_{i=1}^{m}\sum_{j=1}^{m} \hat{w}_{M_{ijk}} \, r_i \, F^*_{\text{motion}\,j}) - \kappa\|\mathbf{r}\|\hat{\mathbf{v}}_{M_k}) \tag{4.53}$$

$$\dot{\hat{\mathbf{w}}}_{B_{ij}} = \mathbf{F}_{B_{ij}}(\hat{\boldsymbol{\sigma}}_B \, r_i \, \dot{x}_{rj} - \kappa\|\mathbf{r}\|\hat{\mathbf{w}}_{B_{ij}}) \tag{4.54}$$

$$\dot{\hat{\mathbf{v}}}_{B_k} = \mathbf{G}_{B_k}(\mathbf{z}_B \, \hat{\boldsymbol{\sigma}}'_{B_k} \, (\sum_{i=1}^{m}\sum_{j=1}^{m} \hat{w}_{B_{ijk}} \, r_i \, \dot{x}_{rj}) - \kappa\|\mathbf{r}\|\hat{\mathbf{v}}_{B_k}) \tag{4.55}$$

$$\dot{\hat{\mathbf{w}}}_{g_i} = \mathbf{F}_{g_i}(\hat{\boldsymbol{\sigma}}_g \, r_i - \kappa\|\mathbf{r}\|\hat{\mathbf{w}}_{g_i}) \tag{4.56}$$

$$\dot{\hat{\mathbf{v}}}_{g_k} = \mathbf{G}_{g_k}(\mathbf{z}_g \, \hat{\boldsymbol{\sigma}}'_{g_k} \, (\sum_{i=1}^{m} \hat{w}_{g_{ik}} \, r_i) - \kappa\|\mathbf{r}\|\hat{\mathbf{v}}_{g_k}) \tag{4.57}$$

$$\dot{\hat{\mathbf{w}}}_{\tau_i} = \mathbf{F}_{\tau_i}(\hat{\boldsymbol{\sigma}}_\tau \, r_i - \kappa\|\mathbf{r}\|\hat{\mathbf{w}}_{\tau_i}) \tag{4.58}$$

$$\dot{\hat{\mathbf{v}}}_{\tau_k} = \mathbf{G}_{\tau_k}(\mathbf{z}_\tau \, \hat{\boldsymbol{\sigma}}'_{\tau_k} \, (\sum_{i=1}^{m} \hat{w}_{\tau_{ik}} \, r_i) - \kappa\|\mathbf{r}\|\hat{\mathbf{v}}_{\tau_k}) \tag{4.59}$$

with κ is a positive constant. And the estimated NN weight updates: $\dot{\hat{\mathbf{w}}}_{M_{ij}} \in \Re^{N_2}, \dot{\hat{\mathbf{v}}}_{M_k} \in \Re^{N_{1,M}}, \dot{\hat{\mathbf{w}}}_{B_{ij}} \in \Re^{N_2}, \dot{\hat{\mathbf{v}}}_{B_k} \in \Re^{N_{1,B}}, \dot{\hat{\mathbf{w}}}_{g_i} \in \Re^{N_2}, \dot{\hat{\mathbf{v}}}_{g_k} \in \Re^{N_{1,g}}, \dot{\hat{\mathbf{w}}}_{\tau_i} \in \Re^{N_2}, \dot{\hat{\mathbf{v}}}_{\tau_k} \in \Re^{N_{1,\tau}}$ are all column vector. And the adaptive gains: $\mathbf{F}_{M_{ij}}^{-1} \in \Re^{N_2 \times N_2}, \ldots, \mathbf{F}_{\tau_i}^{-1} \in \Re^{N_2 \times N_2}$ and $\mathbf{G}_{M_k}^{-1} \in \Re^{N_{1,M} \times N_{1,M}}, \ldots, \mathbf{G}_{\tau_k}^{-1} \in \Re^{N_{1,\tau} \times N_{1,\tau}}$ are all positive diagonal matrices. The following indices are defined: $i, j = 1, \ldots, m$ are output-layer indices, $k = 1, \ldots, N_2$ is the hidden-layer index, where to simplify the implementation, the hidden-node size N_2 is set the same for all dynamic terms. While $N_{1,M}, N_{1,B}, N_{1,g}, N_{1,\tau}$ are the respective input-node sizes.

Proposition 4.4.1 *With the assumptions that:*

1. *the controller gain* $\mathbf{\Lambda}$ *meets the condition*

$$\Lambda_m > \frac{C_1}{M_{x,m}} \tag{4.60}$$

where $C_1 > 0, \Lambda_m = min(\mathbf{\Lambda})$ *and* $M_{x,m} = min(\lambda_{min}(\mathbf{M}_\mathbf{x}(t)))$*;*

2. $\hat{Z}_M$*, the upper-bound of the estimated NN weights,* $\hat{\mathbf{Z}}$*, satisfies*

$$\hat{Z}_M < \sqrt{\frac{C_0}{\kappa}}; \tag{4.61}$$

where $C_0, \kappa > 0$*; and*

3. *the initial condition of* $\tilde{\mathbf{Z}}$ *satisfies*

$$\|\tilde{\mathbf{Z}}(0)\| < \tilde{Z}_M; \tag{4.62}$$

where $\tilde{Z}_M$ *is the upper-bound of the NN weight errors,* $\tilde{\mathbf{Z}}$*;*

then using the proposed motion control (4.9) *and the NN weight updates* (4.52)-(4.59)*, it can be shown by Lyapunov's Extension Theorem [102], that as* $t \rightarrow \infty$ *the errors* $\|\mathbf{r}\|$ *and* $\|\tilde{\mathbf{W}}\|, \|\tilde{\mathbf{V}}\|$ *will be bounded to be within the enclosing boundary* $\mathcal{S}$*, which is defined by enclosing region* $\dot{V}(\mathbf{r}, \tilde{\mathbf{Z}}) < 0$*.*

Proof 4.4.1 *The chosen Lyapunov function candidate for the closed-loop error dynamics* (4.18)*, with the uncertainties* $\boldsymbol{\eta}$ (4.36)*, is*

$$\begin{aligned} V(\mathbf{r}, \tilde{\mathbf{Z}}) = & \frac{1}{2}\, \mathbf{r}^{\mathrm{T}} \mathbf{M}_{\mathbf{x}}(\mathbf{q}) \mathbf{r} \\ & + \frac{1}{2} \sum_{i=1}^{m} \sum_{j=1}^{m} \tilde{\mathbf{w}}_{M_{ij}}^{\mathrm{T}}\, \mathbf{F}_{M_{ij}}^{-1}\, \tilde{\mathbf{w}}_{M_{ij}} + \ldots + \frac{1}{2} \sum_{i=1}^{m} \tilde{\mathbf{w}}_{\tau_i}^{\mathrm{T}}\, \mathbf{F}_{\tau_i}^{-1}\, \tilde{\mathbf{w}}_{\tau_i} \\ & + \frac{1}{2} \sum_{k=1}^{N_2} \tilde{\mathbf{v}}_{M_k}^{\mathrm{T}}\, \mathbf{G}_{M_k}^{-1}\, \tilde{\mathbf{v}}_{M_k} + \ldots + \frac{1}{2} \sum_{k=1}^{N_2} \tilde{\mathbf{v}}_{\tau_k}^{\mathrm{T}}\, \mathbf{G}_{\tau_k}^{-1}\, \tilde{\mathbf{v}}_{\tau_k} \end{aligned} \tag{4.63}$$

where the NN weight errors: $\tilde{\mathbf{w}}_{M_{ij}} \in \Re^{N_2}, \tilde{\mathbf{v}}_{M_k} \in \Re^{N_{1,M}}, \tilde{\mathbf{w}}_{B_{ij}} \in \Re^{N_2}, \tilde{\mathbf{v}}_{B_k} \in \Re^{N_{1,B}}, \tilde{\mathbf{w}}_{g_i} \in \Re^{N_2}, \tilde{\mathbf{v}}_{g_k} \in \Re^{N_{1,g}}, \tilde{\mathbf{w}}_{\tau_i} \in \Re^{N_2}, \tilde{\mathbf{v}}_{\tau_k} \in \Re^{N_{1,\tau}}$ *are all column vectors.*

Next, we substitute the closed-loop error dynamics (4.18)*, Property 4.3.5 and also take into account* $\boldsymbol{\eta}$ (4.36)*, with the definition* $\boldsymbol{\xi}$ (4.37) *and the knowledge* $\|\boldsymbol{\zeta}\| \leq C_0 + C_1\|\mathbf{r}\|$ (4.51)*, into* $\dot{V}(\mathbf{r}, \tilde{\mathbf{Z}})$ *of* (4.63)*, to obtain*

$$\dot{V}(\mathbf{r}, \tilde{\mathbf{Z}}) \leq -\mathbf{r}^{\mathrm{T}} \mathbf{M}_{\mathbf{x}}(\mathbf{q}) \boldsymbol{\Lambda} \mathbf{r} + C_1\, \|\mathbf{r}\|^2 + C_0\, \|\mathbf{r}\| + \boldsymbol{\psi} \tag{4.64}$$

where the lump parameter $\boldsymbol{\psi}$ in (4.64) *is defined as*

$$
\begin{aligned}
\boldsymbol{\psi} = & \sum_{i=1}^{m}\sum_{j=1}^{m} \tilde{\mathbf{w}}_{M_{ij}}^{\mathrm{T}} \left(\mathbf{F}_{M_{ij}}^{-1} \dot{\hat{\mathbf{w}}}_{M_{ij}} + \hat{\boldsymbol{\sigma}}_M \, r_i \, F_{\mathrm{motion}j}^{*} \right) \\
& + \sum_{k=1}^{N_2} \tilde{\mathbf{v}}_{M_k}^{\mathrm{T}} \left(\mathbf{G}_{M_k}^{-1} \dot{\hat{\mathbf{v}}}_{M_k} + \mathbf{z}_M \, \hat{\boldsymbol{\sigma}}'_{M_k} (\sum_{i=1}^{m}\sum_{j=1}^{m} \hat{w}_{M_{ijk}} \, r_i \, F_{\mathrm{motion}j}^{*}) \right) \\
& + \sum_{i=1}^{m}\sum_{j=1}^{m} \tilde{\mathbf{w}}_{B_{ij}}^{\mathrm{T}} \left(\mathbf{F}_{B_{ij}}^{-1} \dot{\hat{\mathbf{w}}}_{B_{ij}} + \hat{\boldsymbol{\sigma}}_B \, r_i \, \dot{x}_{rj} \right) \\
& + \sum_{k=1}^{N_2} \tilde{\mathbf{v}}_{B_k}^{\mathrm{T}} \left(\mathbf{G}_{B_k}^{-1} \dot{\hat{\mathbf{v}}}_{B_k} + \mathbf{z}_B \, \hat{\boldsymbol{\sigma}}'_{B_k} (\sum_{i=1}^{m}\sum_{j=1}^{m} \hat{w}_{B_{ijk}} \, r_i \, \dot{x}_{rj}) \right) \\
& + \sum_{i=1}^{m} \tilde{\mathbf{w}}_{g_i}^{\mathrm{T}} \left(\mathbf{F}_{g_i}^{-1} \dot{\tilde{\mathbf{w}}}_{g_i} + \hat{\boldsymbol{\sigma}}_g r_i \right) \\
& + \sum_{k=1}^{N_2} \tilde{\mathbf{v}}_{g_k}^{\mathrm{T}} \left(\mathbf{G}_{g_k}^{-1} \dot{\hat{\mathbf{v}}}_{g_k} + \mathbf{z}_g \, \hat{\boldsymbol{\sigma}}'_{g_k} (\sum_{i=1}^{m} \hat{w}_{g_{ik}} r_i) \right) \\
& + \sum_{i=1}^{m} \tilde{\mathbf{w}}_{\tau_i}^{\mathrm{T}} \left(\mathbf{F}_{\tau_i}^{-1} \dot{\hat{\mathbf{w}}}_{\tau_i} + \hat{\boldsymbol{\sigma}}_\tau r_i \right) \\
& + \sum_{k=1}^{N_2} \tilde{\mathbf{v}}_{\tau_k}^{\mathrm{T}} \left(\mathbf{G}_{\tau_k}^{-1} \dot{\hat{\mathbf{v}}}_{\tau_k} + \mathbf{z}_\tau \, \hat{\boldsymbol{\sigma}}'_{\tau_k} (\sum_{i=1}^{m} \hat{w}_{\tau_{ik}} r_i) \right).
\end{aligned}
\tag{4.65}
$$

Using $\boldsymbol{\xi}$ in (4.37)*, it can be demonstrated that $\boldsymbol{\psi}$ in* (4.65) *is made up of $\dot{\tilde{\mathbf{W}}}$, $\dot{\tilde{\mathbf{V}}}$ and $\mathbf{r}^{\mathrm{T}}\boldsymbol{\xi}$. The idea is to cancel $\mathbf{r}^{\mathrm{T}}\boldsymbol{\xi}$ with $\dot{\tilde{\mathbf{W}}}, \dot{\tilde{\mathbf{V}}}$. Furthermore, $-\dot{\tilde{\mathbf{W}}} = \dot{\hat{\mathbf{W}}}$, since $\tilde{\mathbf{W}} = \mathbf{W} - \hat{\mathbf{W}}$ and $\mathbf{W}$ is constant. With the weight updates* (4.52)– (4.59)*, $\boldsymbol{\psi}$ becomes*

$$
\begin{aligned}
\boldsymbol{\psi} = & \kappa\|\mathbf{r}\| \sum_{i=1}^{m}\sum_{j=1}^{m} \tilde{\mathbf{w}}_{M_{ij}}^{\mathrm{T}} \hat{\mathbf{w}}_{M_{ij}} + \ldots + \kappa\|\mathbf{r}\| \sum_{i=1}^{m} \tilde{\mathbf{w}}_{\tau_i}^{\mathrm{T}} \hat{\mathbf{w}}_{\tau_i} \qquad (4.66) \\
& + \kappa\|\mathbf{r}\| \sum_{k=1}^{N_2} \tilde{\mathbf{v}}_{M_k}^{\mathrm{T}} \hat{\mathbf{v}}_{M_k} + \ldots + \kappa\|\mathbf{r}\| \sum_{k=1}^{N_2} \tilde{\mathbf{v}}_{\tau_k}^{\mathrm{T}} \hat{\mathbf{v}}_{\tau_k} \\
\leq & -\kappa\|\mathbf{r}\|\|\tilde{\mathbf{Z}}\|^2 + \kappa\|\mathbf{r}\|\|\tilde{\mathbf{Z}}\| Z_M \qquad (4.67)
\end{aligned}
$$

Equation (4.67) *is obtained by combining all the inner products as*

$$\langle \tilde{\mathbf{W}}, \hat{\mathbf{W}} \rangle = \sum_{i=1}^{m} \sum_{j=1}^{m} \tilde{\mathbf{w}}_{M_{ij}}^{\mathrm{T}} \hat{\mathbf{w}}_{M_{ij}} + \ldots + \sum_{i=1}^{m} \tilde{\mathbf{w}}_{\tau_i}^{\mathrm{T}} \hat{\mathbf{w}}_{\tau_i} \tag{4.68}$$

$$\langle \tilde{\mathbf{V}}, \hat{\mathbf{V}} \rangle = \sum_{k=1}^{N_2} \tilde{\mathbf{v}}_{M_k}^{\mathrm{T}} \hat{\mathbf{v}}_{M_k} + \ldots + \sum_{k=1}^{N_2} \tilde{\mathbf{v}}_{\tau_k}^{\mathrm{T}} \hat{\mathbf{v}}_{\tau_k} \tag{4.69}$$

$$\langle \tilde{\mathbf{Z}}, \hat{\mathbf{Z}} \rangle = \langle \tilde{\mathbf{V}}, \hat{\mathbf{V}} \rangle + \langle \tilde{\mathbf{W}}, \hat{\mathbf{W}} \rangle \tag{4.70}$$

where $\hat{\mathbf{Z}} = \mathbf{Z} - \tilde{\mathbf{Z}}$*, and therefore*

$$\langle \tilde{\mathbf{Z}}, \hat{\mathbf{Z}} \rangle = \langle \tilde{\mathbf{Z}}, \mathbf{Z} \rangle - \|\tilde{\mathbf{Z}}\|^2 \leq \|\tilde{\mathbf{Z}}\| \|\mathbf{Z}\| - \|\tilde{\mathbf{Z}}\|^2 \leq \|\tilde{\mathbf{Z}}\| Z_M - \|\tilde{\mathbf{Z}}\|^2. \tag{4.71}$$

Substituting ψ *in* (4.67) *and Property 4.3.1, it is possible to show* $\dot{V}(\mathbf{r}, \tilde{\mathbf{Z}})$ (4.64) *that*

$$\dot{V}(\mathbf{r}, \tilde{\mathbf{Z}}) \leq -\|\mathbf{r}\| \left[(M_{x,m}\, \Lambda_m - C_1)\|\mathbf{r}\| - C_0 + \kappa(\|\tilde{\mathbf{Z}}\| - \frac{Z_M}{2})^2 - \frac{\kappa Z_M^2}{4} \right] \tag{4.72}$$

where Λ_m *and* $M_{x,m}$ *are as defined in* (4.60)*, note* $(M_{x,m}\, \Lambda_m - C_1) > 0$ *due to hypothesis* (4.60)*. Hence,* $\dot{V}(\mathbf{r}, \tilde{\mathbf{Z}}) < 0$*, as depicted in Fig. 4.2, if*

$$\|\mathbf{r}\| > \frac{C_0 + \kappa\, Z_M^2/4}{(M_{x,m}\, \Lambda_m - C_1)} \equiv b_r, \quad \textit{or} \tag{4.73}$$

$$\|\tilde{\mathbf{Z}}\| > \sqrt{\frac{C_0}{\kappa} + \frac{Z_M^2}{4}} + \frac{Z_M}{2} \equiv b_{\tilde{Z}}. \tag{4.74}$$

Applying the Lyapunov's Extension Theorem [102] then as $t \to \infty$*, the errors* $\|\mathbf{r}\|$ *and* $\|\tilde{\mathbf{Z}}\|$ *can be shown to be bounded within* $\mathcal{S}$*, as follows: suppose the errors can be shown to start within the boundary of* $\mathcal{S}$*, i.e.* $\|\mathbf{r}(0)\| < b_r$ *and* $\|\tilde{\mathbf{Z}}(0)\| < b_{\tilde{Z}}$*, then they start their course towards the enclosing boundary* $\mathcal{S}$ *and when they start leaving the boundary of* $\mathcal{S}$ *since the* $V(\mathbf{r}, \tilde{\mathbf{Z}})$ *is decreasing*

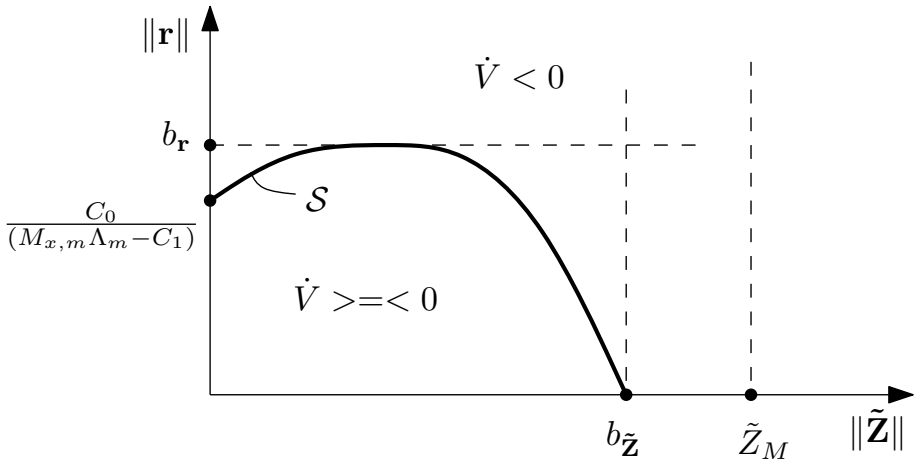

Figure 4.2: $\dot{V}(\mathbf{r}, \tilde{\mathbf{Z}})$ *regions of the modified NN adaptive motion control strategy.*

($\dot{V}(\mathbf{r}, \tilde{\mathbf{Z}}) < 0$*) hence the errors cannot leave the boundary of* $\mathcal{S}$*. Now, suppose the errors start at outside the boundary of* $\mathcal{S}$ *then they tend to go to the equilibrium since* $V(\mathbf{r}, \tilde{\mathbf{Z}})$ *is decreasing. However, they cannot go to the equilibrium, but only up to entering the boundary of* $\mathcal{S}$ *and once they enter the boundary of* $\mathcal{S}$*, we have already shown that they are bounded.*

Using bounded-input-bounded-output (BIBO) property, it can be shown that a bounded input $\mathbf{r}$ *in* (4.13) *yields* $\lim_{t\to\infty} \mathbf{e}, \dot{\mathbf{e}}$ *that are bounded.*

The next part of the proof is to demonstrate the necessity of hypothesis $\hat{Z}_M > \sqrt{\frac{C_0}{\kappa}}$ *in* (4.61)*. Note that,* $\tilde{\mathbf{Z}}$*, in its course towards the enclosing boundary* $\mathcal{S}$*, cannot violate* $\tilde{Z}_M$*, otherwise the Lyapunov's Extension Theorem is no longer applicable. In other words,* $\tilde{Z}_M$ *in* (4.46) *must satisfy*

$$\tilde{Z}_M \equiv Z_M + \hat{Z}_M > b_{\tilde{\mathbf{Z}}}, \tag{4.75}$$

Therefore, it can be shown that if the following is satisfied

$$Z_M + \hat{Z}_M > \sqrt{\frac{C_0}{\kappa}} + Z_M > b_{\tilde{\mathbf{Z}}} \text{ or,} \tag{4.76}$$

$$\hat{Z}_M > \sqrt{\frac{C_0}{\kappa}} \tag{4.77}$$

then $\tilde{Z}_M > b_{\tilde{\mathbf{Z}}}$ *is also satisfied.*

Further, the initial condition $\|\tilde{\mathbf{Z}}(0)\|$ *can be less or greater than* $b_{\tilde{Z}}$*, however in order to comply with the Lyapunov's Extension Theorem, it must be less than* $\tilde{Z}_M$*. The last part of the proof is to demonstrate hypothesis* $\|\tilde{\mathbf{Z}}(0)\| < \tilde{Z}_M$ *in* (4.62) *is to be satisfied in practical implementation.*

By definition $\tilde{\mathbf{Z}} = \mathbf{Z} - \hat{\mathbf{Z}}$*, therefore it is possible to initialize the estimated NN weights with zeroes,* $\|\hat{\mathbf{Z}}(0)\| = 0$*, therefore we can have*

$$\|\tilde{\mathbf{Z}}(0)\| = \|\mathbf{Z}\| \leq Z_M < b_{\tilde{Z}} < \tilde{Z}_M. \tag{4.78}$$

Note that, theoretically, there is no initial condition requirement for $\mathbf{r}$*, however, in practical implementation, it is dangerous to set the desired trajectory further away from the initial end-effector pose i.e.* $\|\mathbf{r}(0)\|$ *starts with large value. In other words, it is a lot safer to set* $\|\mathbf{r}(0)\|$ *as small as possible.*

It can be shown in the implementation that, it is possible to set $\mathbf{r}(0) = \dot{\mathbf{x}}_d(0) - \dot{\mathbf{x}}(0) + \mathbf{\Lambda}_1\mathbf{e}(0) + \mathbf{\Lambda}_i\,\mathbf{e}(0)\,\Delta t$ *in* (4.13) *to be as small as possible through setting the initial points of the desired trajectory equals to the initial end-effector pose i.e.* $\dot{\mathbf{x}}_d(0) = \dot{\mathbf{x}}(0) = 0$*,* $\mathbf{x}_d(0) = \mathbf{x}(0)$*, resulting in* $\dot{\mathbf{e}}(0) = 0$ *and* $\mathbf{e}(0) = 0$*. Therefore,*

$$\|\mathbf{r}(0)\| = 0 < b_r. \tag{4.79}$$

(Therefore, it can be seen that the initial conditions, $\|\mathbf{r}(0)\|$ *and* $\|\tilde{\mathbf{Z}}(0)$*, start within the boundary of* $\mathcal{S}$*).*

It should be noted that:

- It can be seen from (4.73), in steady-state sense, that arbitrarily small tracking error $\mathbf{r}$ can be obtained by setting larger $\min(\mathbf{\Lambda})$. However, care must be exercised as setting too large $\mathbf{\Lambda}$ will affect the transient stability performance.

- Choosing the controller gains, $\mathbf{\Lambda}$, and the parameter update gains, $\mathbf{F}$ and $\mathbf{G}$ matrices, is currently by trial-and-error. In previous simulation studies for a two-link planar manipulator in joint space framework: $\mathbf{\Lambda}$ is chosen to be $5\mathbf{I}$ and $30\mathbf{I}$ in [45] and $5\mathbf{I}$ in [74].

- Recently, there are some preliminary works in optimal adaptive control that can also accommodate the adaptation of the controller gain, $\mathbf{\Lambda}$, and parameter update gains, $\mathbf{G}_p, \mathbf{F}_p$ with subscript $p = M, B, g, \tau$. One is in nonlinear system [105] and another for linear system [106]. Works to accommodate optimal adaptive control for robotic are still in progress.

4.5 Computational Cost

In this section, the computational cost of the proposed NN adaptive strategy is compared with a pure PD control and the classical inverse dynamics strategy. The total computational cost of the proposed NN adaptive strategy can be

shown to be about 163800 arithmetic computations. Inclusive in the presented number are the weight updates and the final computation to obtain the generalized operational space forces (the final computation between of the inertia and the Coriolis/centrifugal matrices and $\mathbf{F}^{*}_{\text{motion}}, \dot{\mathbf{x}}_r$, respectively, with addition of the gravity and joint friction vectors).

In comparison with pure PD control (18 arithmetic operations), the computational cost of proposed NN adaptive strategy is indeed higher. However, it is the nature for the type of dynamics compensation to require additional computation, such as [23] (655 arithmetic operations). Further computation is naturally expected for the adaptive strategy type such as LIP adaptive control, since obviously an adaptation is required. On the other side, however, the proposed NN adaptive strategy does not need the dynamics derivation and its required simplification procedure. Naturally, convenience comes with a cost.

Therefore, the proposed NN adaptive strategy relies on the computer's speed. It can be shown that today's PC is quite fast and cheap enough. For instance, our presented method is implemented on a PC with a single-core 32-bit Pentium IV 3.2GHz using Windows XP (which is relatively cheap in the year 2009 - 2010). Further, as suggested in [91], the required frequency of the NN compensation (200Hz) can be shown to be only $1/5$ of the main sampling frequency (1kHz).

4.6 Performance Evaluation

The proposed strategy (4.9) is studied through simulation and real-time implementation on a PUMA 560 robot. In addition to the proposed NN adaptive motion control in this chapter, two other types of control strategies are performed for comparison: (i) the Lagrangian dynamics motion control (2.27) – without friction compensation, and (ii) Proportional-plus-Derivative (PD) control with gravity term compensation.

A positional periodic circular trajectory – 75 mm radius and 2 second period – with a constant orientation for the effector was set as the desired trajectories for all cases (simulation and real-time implementation). The initial posture of the robot is shown in Fig. 4.3 with the end-effector pointing down and the elbow is

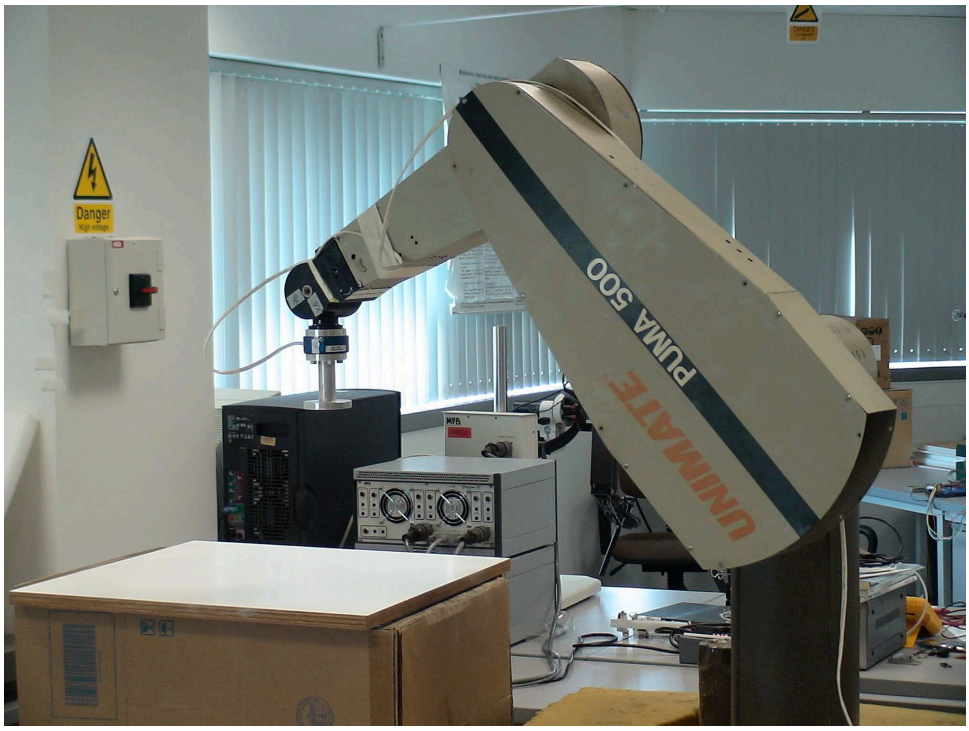

Figure 4.3: The free-motion setup using PUMA 560 robot.

up.

Performances were recorded in term of: (i) desired trajectories along x_{E} and y_{E} axes (the desired trajectory along z_{E} is constant), and (ii) position errors along $x_{\mathrm{E}}, y_{\mathrm{E}}, z_{\mathrm{E}}$.

The planning strategy was carried out as follows: The weights of the proposed NN adaptive motion controller (4.9) were initialized with zero values. Off-line learning simply using the same circular periodic trajectory was performed (for about 5 passes) to achieve an acceptable performance. The NN weights were saved and used to obtain the tracking performances (both simulation and real-time implementation).

4.6.1 Robot Simulation

The proposed NN motion control (4.9) is validated with a 6 DOF PUMA 560 robot dynamic simulator. The Lagrangian dynamics model of PUMA 560 by [19] plus joint model are utilized in the dynamic simulator. Note that joint model is not included in the model-based (Lagrangian only) motion control.

For practical purpose, the Lagrangian dynamics controller does not include the joint friction model, as in the original operational space formulation [8]. Joint friction model (unlike Lagrangian model), varies with time and ambient parameters, and therefore, it must be performed every time prior the operation of the robot. In practical side using Lagrangian dynamics only control: that once a control engineer has obtained the Lagrangian dynamics, then one can easily implement it (where its stability analysis and controller design are well established)

	Lagrangian dynamics motion control	PD + gravity motion control	NN motion control
$\max(\|\mathbf{e}_{\text{pos}}\|)$ (mm)	3.45	18.07	6.63

Table 4.1: Performance comparison in term of the maximum of the magnitude of the end-effector position tracking errors in simulation study.

and to obtain reasonable real time experimental results as shown in [107, 12].

There is a more sophisticated model-based motion control by [108], where an adaptive joint friction compensation is added into Lagrangian model to give improved performance over the Lagrangian only dynamic controller. However, its formulation and stability analysis are rather different and relatively more involved than the original formula [8].

The simulation study performances in term of the magnitude (square root) of the end-effector position tracking errors $\left(\|\mathbf{e}_{\text{pos}}\| = \sqrt{e_{\text{pos},x}^2 + e_{\text{pos},y}^2 + e_{\text{pos},z}^2}\right)$ of: (i) the Lagrangian dynamics control, (ii) the PD + gravity control and (iii) the proposed NN adaptive motion control are shown in Fig. 4.4, Fig. 4.5 and Fig. 4.6, respectively.

Table 4.1 shows that the proposed NN control strategy, without prior knowledge of the robot dynamics, yields comparable performance to that of the Lagrangian dynamics strategy (without joint friction compensation). The bounded stability of the norms of the estimated NN weights is shown in Fig. 4.7.

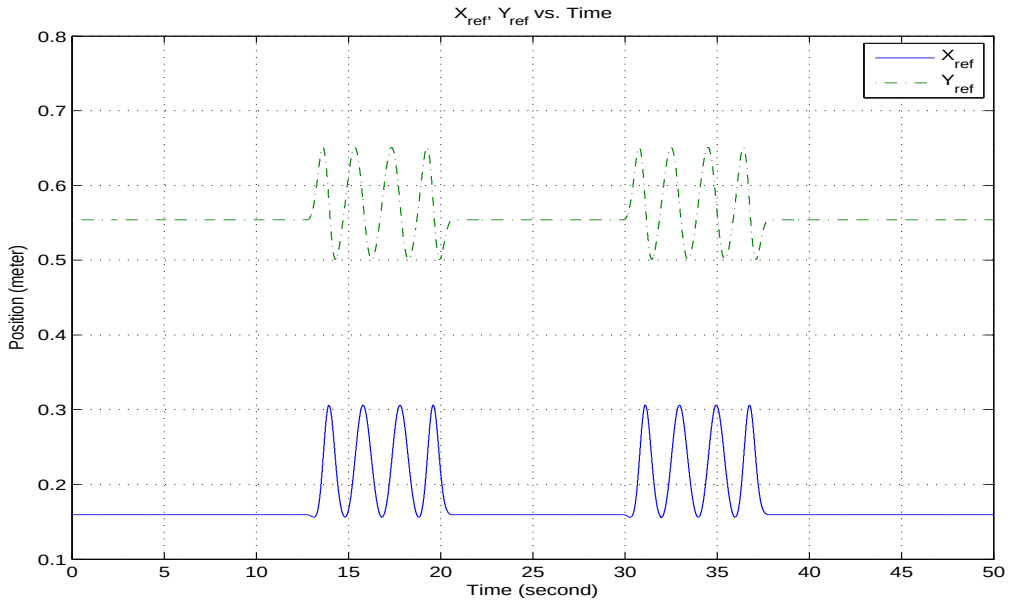

(a) Desired trajectories along $x_{\mathrm{E}}, y_{\mathrm{E}}$.

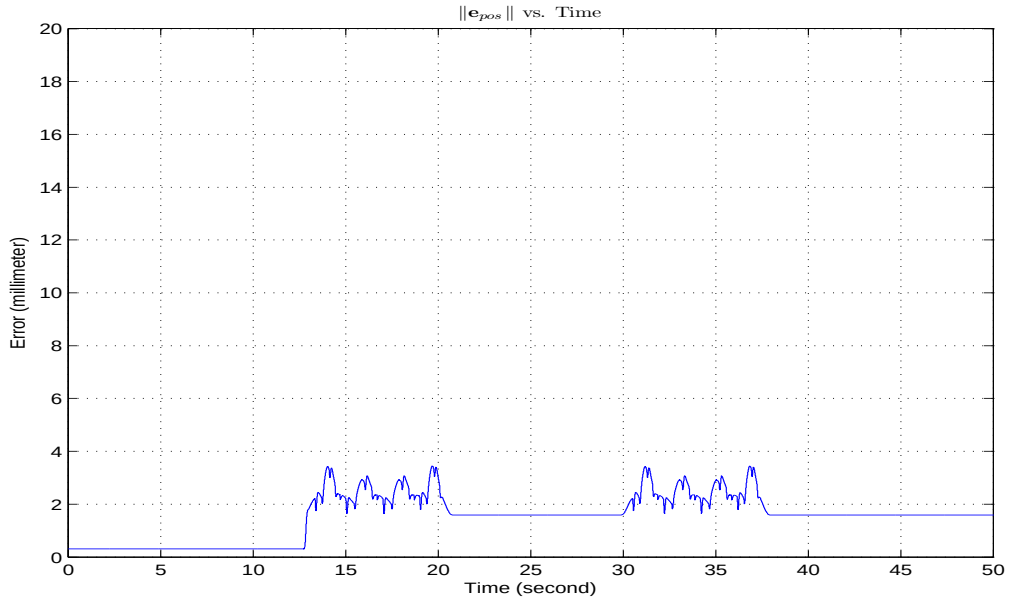

(b) The magnitude of the end-effector position tracking errors.

Figure 4.4: Simulation study using Lagrangian dynamics motion control.

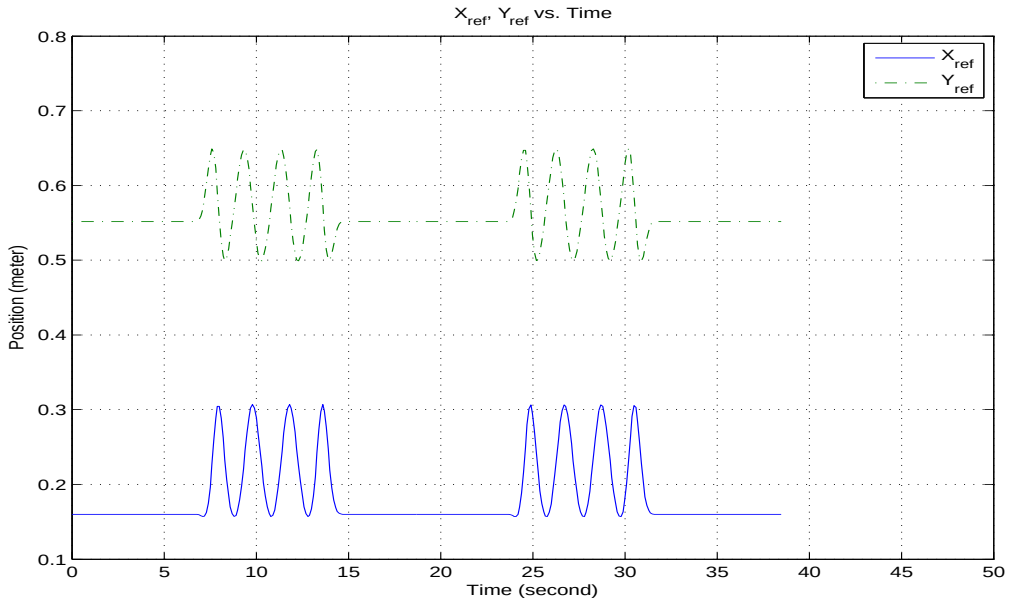

(a) Desired trajectories along $x_{\mathrm{E}}, y_{\mathrm{E}}$.

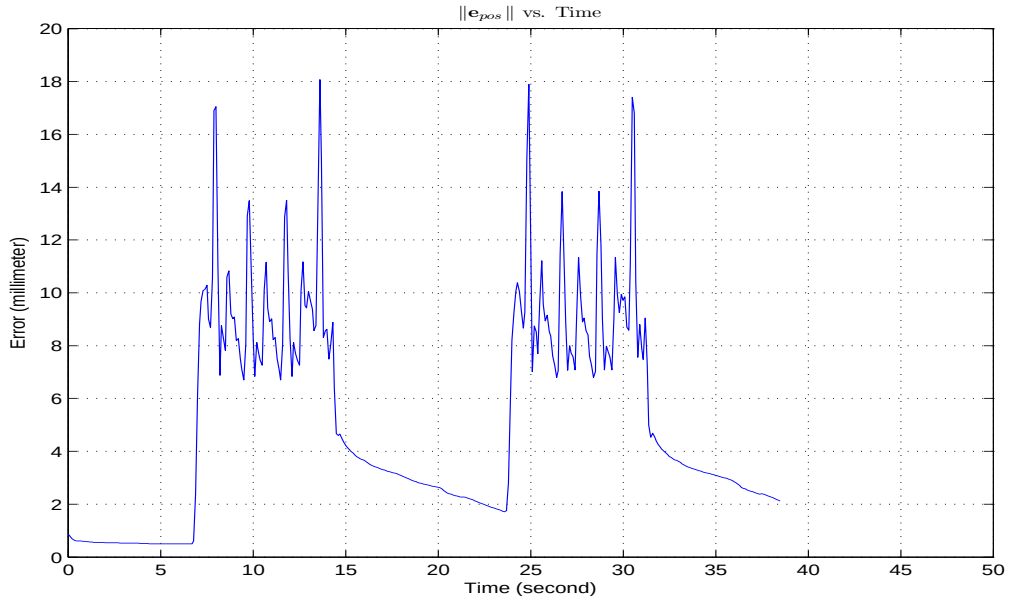

(b) The magnitude of the end-effector position tracking errors.

Figure 4.5: Simulation study using PD + gravity motion control.

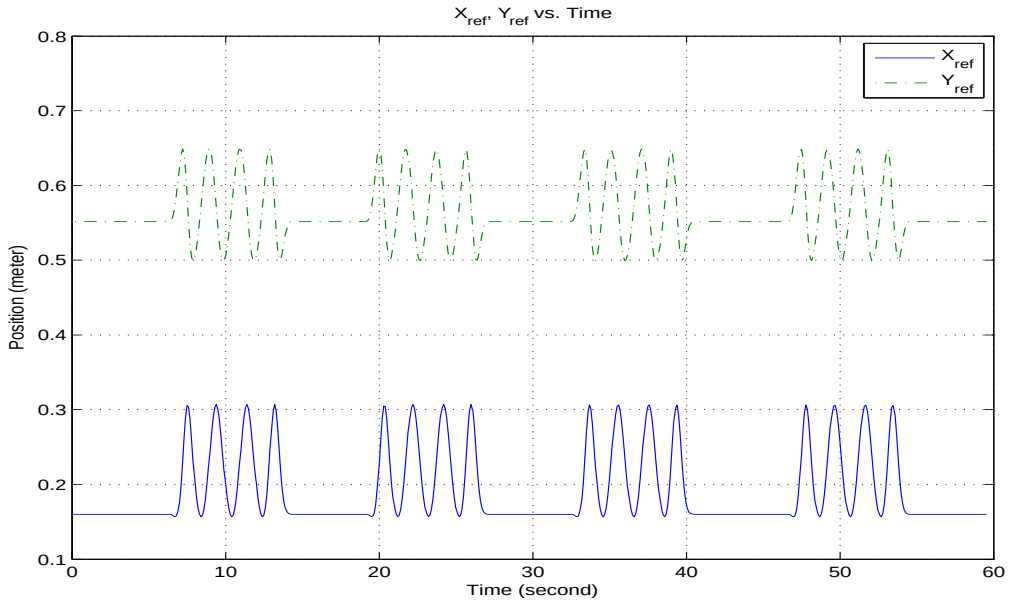

(a) Desired trajectories along $x_{\mathrm{E}}, y_{\mathrm{E}}$.

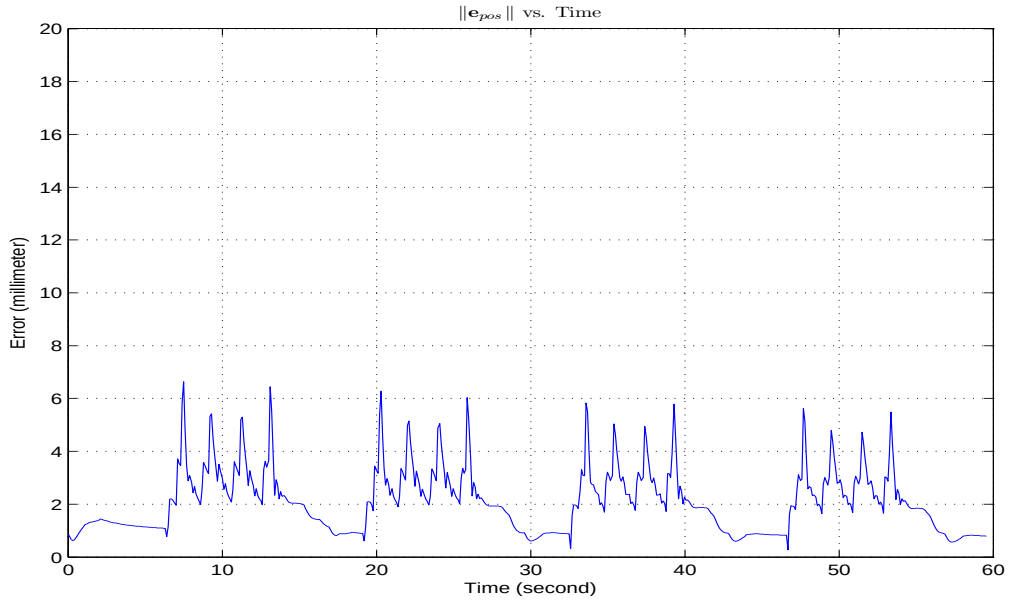

(b) The magnitude of the end-effector position tracking errors.

Figure 4.6: Simulation study using NN adaptive motion control.

The following gains are set for the simulation study of the proposed NN adaptive motion control (4.9): $\kappa = 0.1$, $\mathbf{\Lambda}_1 = \mathbf{\Lambda}_i = 30\mathbf{I} \in \Re^{m\times m}$, $\mathbf{F}_{M_{ij}}^{-1} = \mathbf{I} \in \Re^{N_2\times N_2}$, $\mathbf{F}_{B_{ij}}^{-1} = \mathbf{I} \in \Re^{N_2\times N_2}$, $\mathbf{F}_{g_i}^{-1} = 10\mathbf{I} \in \Re^{N_2\times N_2}$, $\mathbf{F}_{\tau_i}^{-1} = 10\mathbf{I} \in \Re^{N_2\times N_2}$. Note, the hidden-layer size $N_2 = 10$ is chosen throughout this thesis.

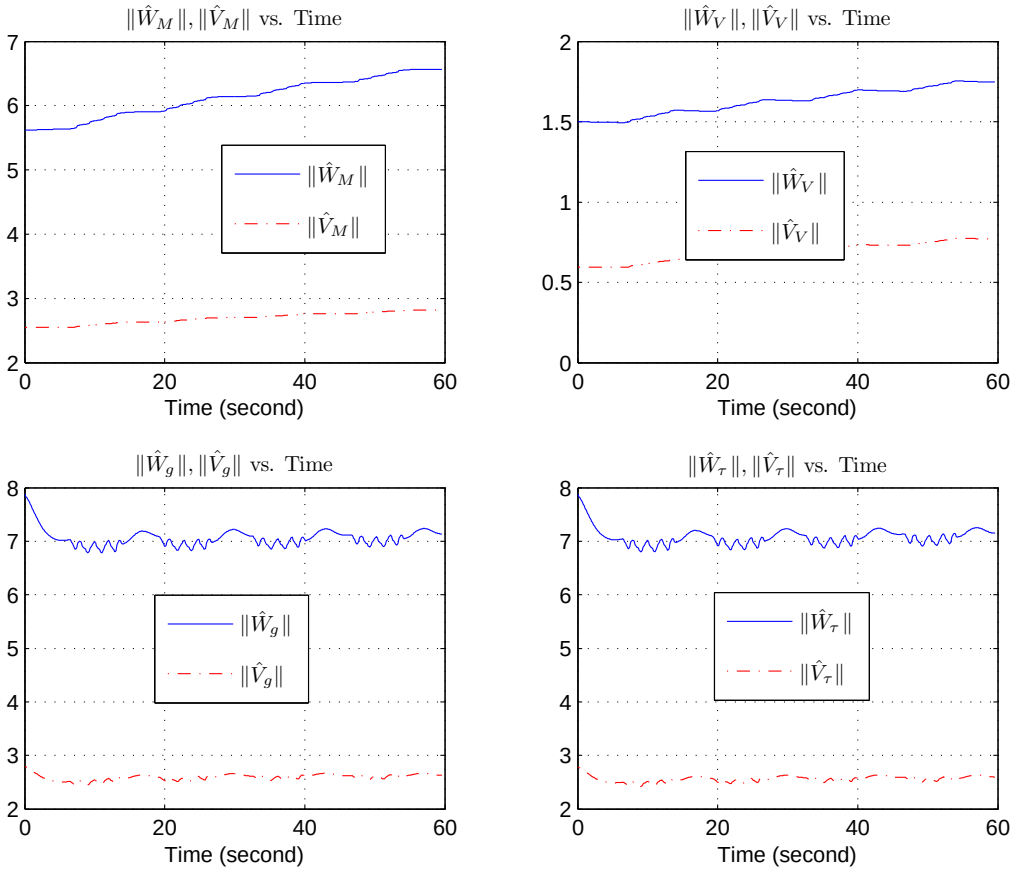

Figure 4.7: Simulation study history of the estimated NN weights of the NN motion controller.

4.6.2 Real-time Robot Experiment

The real-time performances of the Lagrangian dynamics control, the PD + gravity control and the proposed NN adaptive motion control are shown in Fig. 4.8, Fig. 4.9 and Fig. 4.10, respectively. Also the real-time implementation videos are provided in:

- http://guppy.mpe.nus.edu.sg/dandy/Videos/Dynamics-based/Free_motion_control_Dyn.MPG
- http://guppy.mpe.nus.edu.sg/dandy/Videos/Dynamics-based/Free_motion_control_PD.MPG
- http://guppy.mpe.nus.edu.sg/dandy/Videos/NN-based/Free_motion_control_NN_BD.MPG

All the gains are similar with those in Section 4.6.1, with the difference is $\mathbf{\Lambda} = 20\mathbf{I}$.

Fig. 4.10 and Table 4.2 show that the maximum error produced by the NN controller in real-time is a bit larger than that by the simulation study.

Note that all real-time implementations were implemented real-time on a PUMA 560, which does not provide joint velocity feedback. The joint velocities $\dot{\hat{\mathbf{q}}}$ are obtained by employing backward difference algorithm of joint positions $\mathbf{q}$, in conjunction with low pass filter. Hence, only the estimated operational space velocities $\dot{\hat{\mathbf{x}}}$ are available, using $\dot{\hat{\mathbf{x}}} = \mathbf{J}(\mathbf{q})\ \dot{\hat{\mathbf{q}}}$. The filtered velocity signals, $\dot{\hat{\mathbf{q}}}$ and $\dot{\hat{\mathbf{x}}}$, were used for all controllers. It will be revealed that this condition affects the performance of the proposed NN adaptive motion controller.

The evolution of the norms of the estimated NN weights (using filtered velocity) seems to be bounded in Fig. 4.11; this is because, in the implementation, for

	Lagrangian dynamics motion control	PD + gravity motion control	NN motion control with filtered velocity
$\max(\|\mathbf{e}_{pos}\|)$ (mm)	7.90	11.40	28.80

Table 4.2: Performance comparison in term of the maximum of the magnitude of the end-effector position tracking errors in real-time study.

the estimated NN weights are upper bounded by using dead-zone procedure. It was found in the experiments that, without the upper bounds, the estimated NN weights can be unbounded.

In the next Section 4.7, the estimated NN weights cannot be shown to be guaranteed, theoretically.

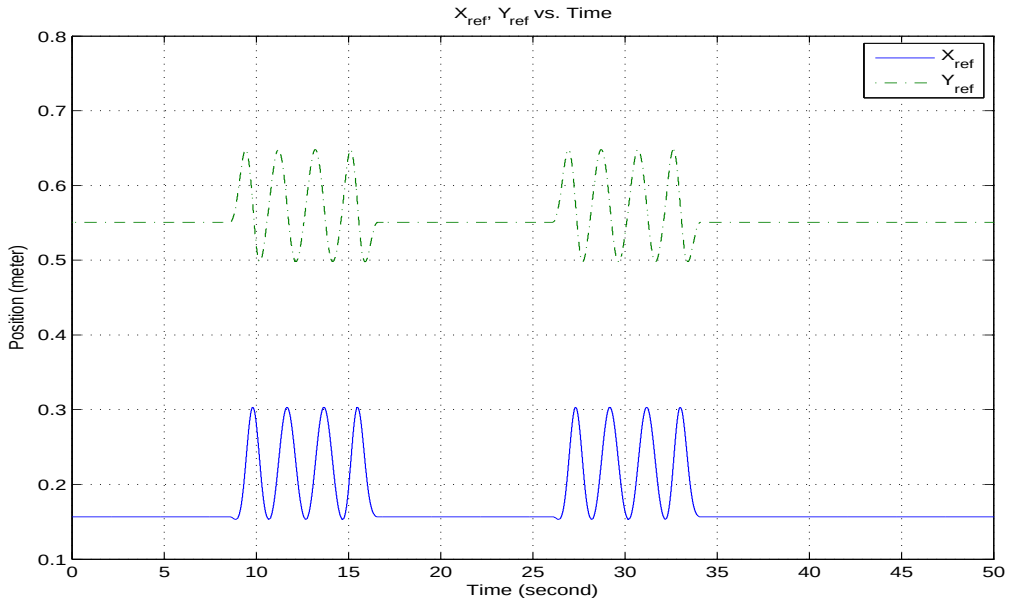

(a) Desired trajectories along $x_{\mathrm{E}}, y_{\mathrm{E}}$.

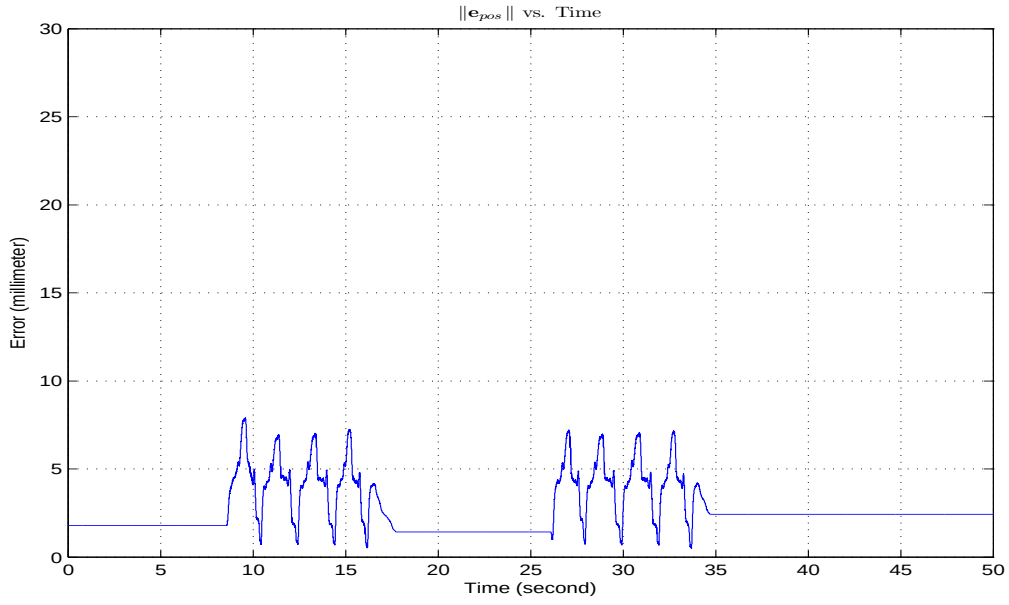

(b) The magnitude of the end-effector position tracking errors.

Figure 4.8: Real-time study using Lagrangian dynamics motion control.

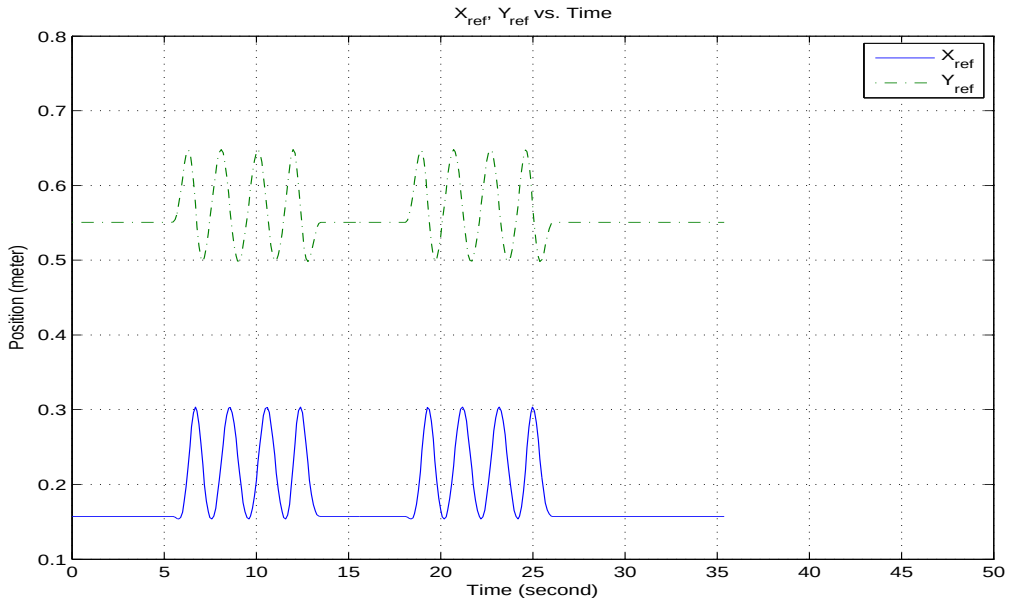

(a) Desired trajectories along $x_{\mathrm{E}}, y_{\mathrm{E}}$.

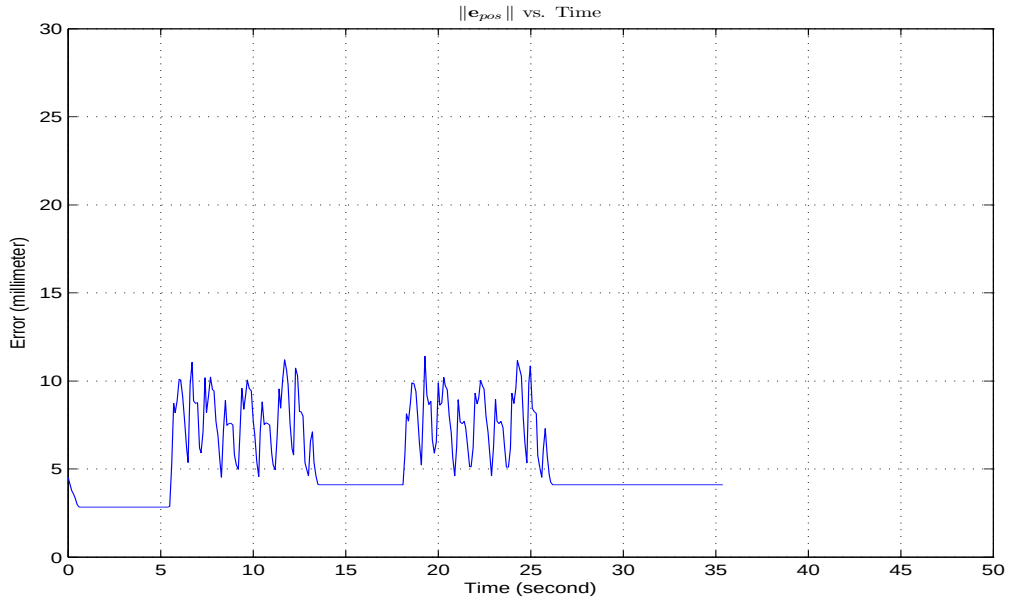

(b) The magnitude of the end-effector position tracking errors.

Figure 4.9: Real-time study using PD + gravity motion control.

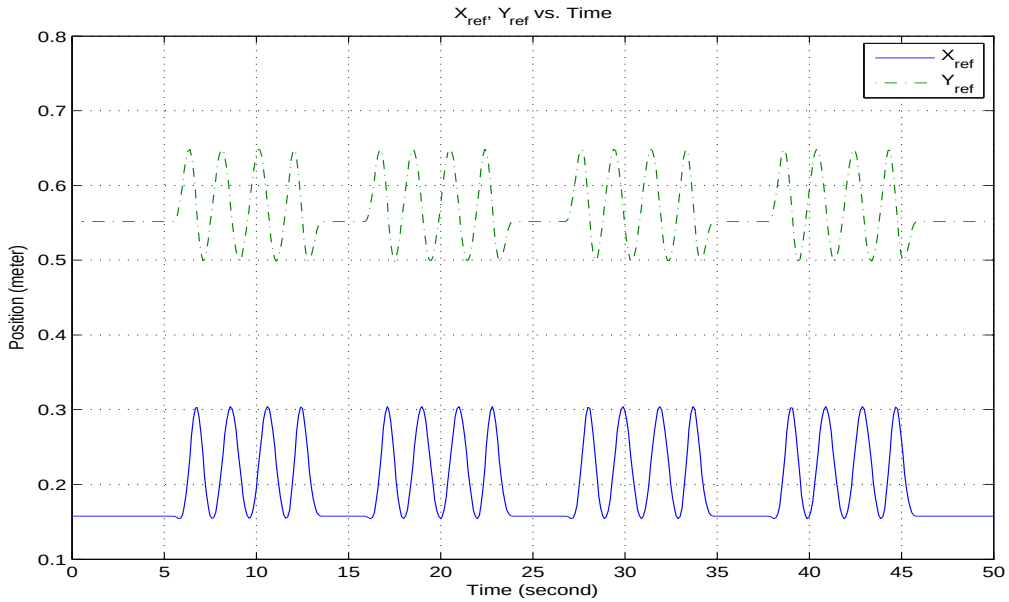

(a) Desired trajectories along $x_{\mathrm{E}}, y_{\mathrm{E}}$.

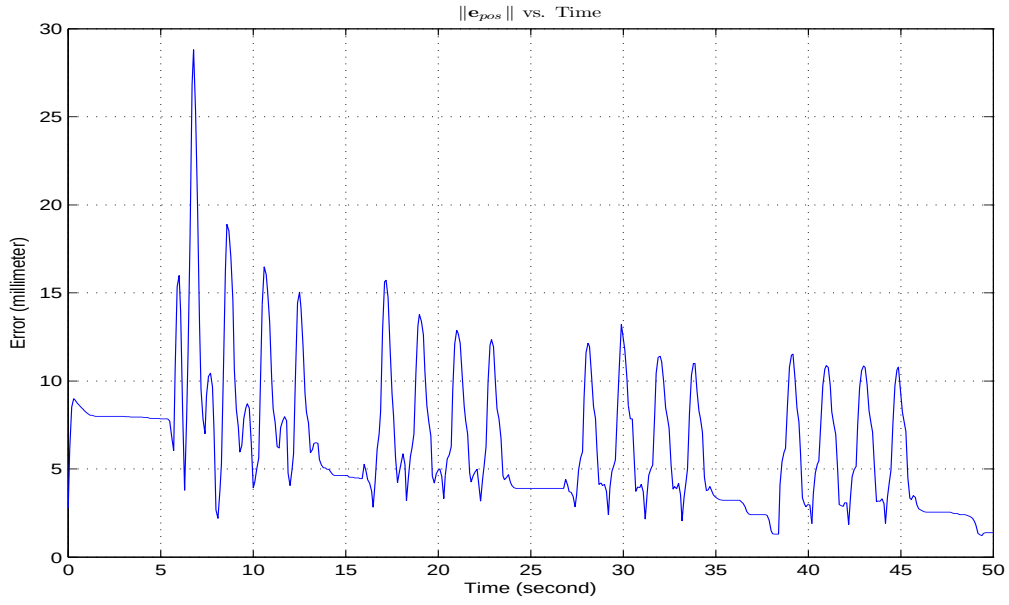

(b) The magnitude of the end-effector position tracking errors.

Figure 4.10: Real-time study NN adaptive motion control with filtered velocity.

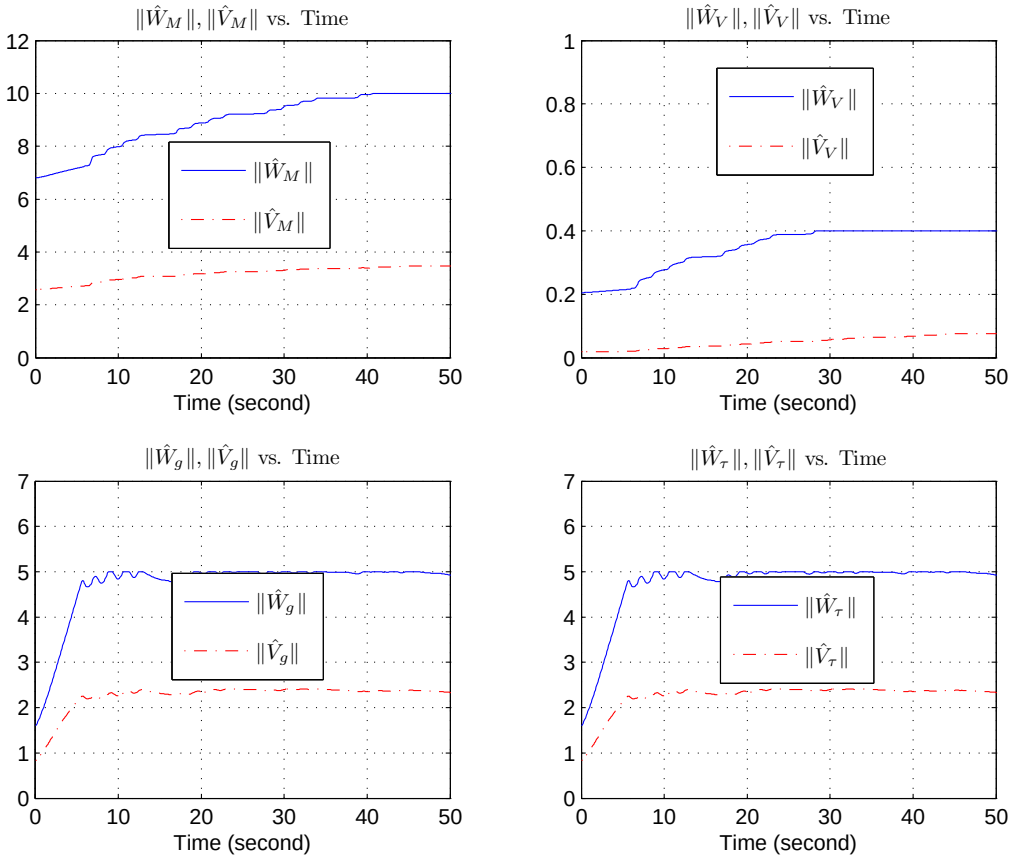

Figure 4.11: Real-time study history of the estimated NN weights of the NN motion controller with filtered velocity.

4.7 Analysis NN Adaptive Motion Control using Filtered Velocity

It is shown in the preliminary study in Section 4.6.1 that the performance on simulation was found to be comparable with that of model-based control, however, performance on real-time experimentation was found to be inferior to the simulation study equivalent. Note that, physically, the PUMA 560 does not have joint velocity sensor.

To fill the non-existing actual velocity in the real-time experimentation, the estimated joint velocities, $\dot{\hat{\mathbf{q}}}$, are obtained by employing backward difference algorithm between the current $\mathbf{q}(t)$ and the previous $\mathbf{q}(t-1)$ actual joint positions, which then followed by low pass filter (LPF). Hence, only the estimated operational space velocities, $\dot{\hat{\mathbf{x}}}$, since $\dot{\hat{\mathbf{x}}} = \mathbf{J}(\mathbf{q})\dot{\hat{\mathbf{q}}}$, are available. The filtered velocity signals, $\dot{\hat{\mathbf{q}}}$ and $\dot{\hat{\mathbf{x}}}$, were used for all controllers in real-time implementation in Section 4.6.2.

In this section, it can be shown by Lyapunov analysis that the filtered velocity signals, $\dot{\hat{\mathbf{q}}}$ and $\dot{\hat{\mathbf{x}}}$, are not suitable replacements to the non-existing actual velocity signals for the proposed adaptive strategy in (4.9).

To properly represent the situation in real-time experiments, the NN adaptive controller in (4.80) can be re-written using estimated velocity signals, $\dot{\hat{\mathbf{q}}}$ and $\dot{\hat{\mathbf{x}}}$, as

$$\mathbf{F} = \mathbf{M}_{\mathbf{x}}(\mathbf{q})\mathbf{F}^{*}_{\text{motion}} + \hat{\mathbf{B}}_{\mathbf{x}}(\mathbf{q}, \dot{\hat{\mathbf{q}}})\dot{\mathbf{x}}_r + \hat{\mathbf{g}}_{\mathbf{x}}(\mathbf{q}) + \hat{\boldsymbol{\tau}}_{\mathbf{x}}(\mathbf{q}, \dot{\hat{\mathbf{q}}}) \qquad (4.80)$$

where $\dot{\mathbf{x}}_r$ and $\mathbf{F}^*_{\text{motion}}$ are defined as

$$\dot{\mathbf{x}}_r = \dot{\mathbf{x}}_d + \mathbf{\Lambda}\mathbf{e} \tag{4.81}$$

$$\mathbf{F}^*_{\text{motion}} = \ddot{\mathbf{x}}'_r + \mathbf{\Lambda}\hat{\mathbf{r}} \tag{4.82}$$

with the following computable terms are defined to compute $\mathbf{F}^*_{\text{motion}}$ as

$$\ddot{\mathbf{x}}'_r = \ddot{\mathbf{x}}_d + \mathbf{\Lambda}(\dot{\mathbf{x}}_d - \dot{\hat{\mathbf{x}}}) \tag{4.83}$$

$$\hat{\mathbf{r}} = \dot{\mathbf{x}}_r - \dot{\tilde{\mathbf{x}}} = \dot{\mathbf{x}}_r - \dot{\mathbf{x}} + \dot{\tilde{\mathbf{x}}} \tag{4.84}$$

where $\mathbf{\Lambda} \in \Re^{m\times m}$ is a positive diagonal matrix, $\mathbf{e} = \mathbf{x}_d - \mathbf{x}$ is the operational space position tracking error, with $\mathbf{x}_d$, $\dot{\mathbf{x}}_d$ and $\ddot{\mathbf{x}}_d$ are the desired operational space trajectories. The velocity estimation error is defined between the actual and estimated velocity, as $\dot{\tilde{\mathbf{x}}} = \dot{\mathbf{x}} - \dot{\hat{\mathbf{x}}}$. It follows that from the first derivative of (4.84) and (4.83), we have

$$\ddot{\mathbf{x}}'_r - \ddot{\mathbf{x}} = \ddot{\mathbf{x}}_r - \dot{\mathbf{x}} + \mathbf{\Lambda}\dot{\tilde{\mathbf{x}}} = \dot{\hat{\mathbf{r}}} - \ddot{\tilde{\mathbf{x}}} + \mathbf{\Lambda}\dot{\tilde{\mathbf{x}}}. \tag{4.85}$$

Combining the operational space motion dynamic (4.1) with the operational space NN motion control using filtered velocity (4.80), and taking into account (4.85) and Property 4.3.2, the closed-loop error dynamics can be obtained as

$$\begin{aligned}\mathbf{M}_{\mathbf{x}}(\mathbf{q})(\dot{\hat{\mathbf{r}}} - \ddot{\tilde{\mathbf{x}}}) = &- \mathbf{M}_{\mathbf{x}}(\mathbf{q})\mathbf{\Lambda}\hat{\mathbf{r}} - \mathbf{M}_{\mathbf{x}}(\mathbf{q})\mathbf{\Lambda}\dot{\tilde{\mathbf{x}}} - \mathbf{B}_{\mathbf{x}}(\mathbf{q},\dot{\hat{\mathbf{x}}})\dot{\mathbf{x}}_r + \mathbf{B}_{\mathbf{x}}(\mathbf{q},\dot{\mathbf{x}})\dot{\mathbf{x}} \\ &+ \boldsymbol{\tau}_{\mathbf{x}}(\mathbf{q},\dot{\mathbf{q}}) - \boldsymbol{\tau}_{\mathbf{x}}(\mathbf{q},\dot{\hat{\mathbf{q}}}) + \boldsymbol{\eta}\end{aligned} \tag{4.86}$$

where the uncertainties of the system, $\boldsymbol{\eta}$, expressed as

$$\boldsymbol{\eta} = \tilde{\mathbf{M}}_{\mathbf{x}}(\mathbf{q})\mathbf{F}^*_{\text{motion}} + \tilde{\mathbf{B}}_{\mathbf{x}}(\mathbf{q},\dot{\hat{\mathbf{q}}})\dot{\mathbf{x}}_r + \tilde{\mathbf{g}}_{\mathbf{x}}(\mathbf{q}) + \tilde{\boldsymbol{\tau}}_{\mathbf{x}}(\mathbf{q},\dot{\hat{\mathbf{q}}}). \tag{4.87}$$

From Property 3.2.4, it is shown that

$$\boldsymbol{\tau}_{\mathbf{x}}(\mathbf{q},\dot{\mathbf{q}}) - \boldsymbol{\tau}_{\mathbf{x}}(\mathbf{q},\dot{\hat{\mathbf{q}}}) = \mathbf{J}^{-\mathrm{T}}[\tau_{vis}\dot{\tilde{\mathbf{q}}} + \tau_{cou}(\mathrm{sgn}(\dot{\mathbf{q}}) - \mathrm{sgn}(\dot{\hat{\mathbf{q}}})) + \boldsymbol{\tau}_{sti}\mathrm{exp}^{(-\tau_{dec}\dot{\mathbf{q}}^2)}\mathrm{sgn}(\dot{\mathbf{q}}) - \boldsymbol{\tau}_{sti}\mathrm{exp}^{(-\tau_{dec}\dot{\hat{\mathbf{q}}}^2)}\mathrm{sgn}(\dot{\hat{\mathbf{q}}})]. \tag{4.88}$$

Using Property 4.3.6 and from (4.84) it can be drawn that $\dot{\mathbf{x}}_r - \dot{\mathbf{x}} = \hat{\mathbf{r}} - \dot{\tilde{\mathbf{x}}}$, and $\mathbf{B}_{\mathbf{x}}(\mathbf{q},\dot{\hat{\mathbf{x}}})\dot{\mathbf{x}}_r - \mathbf{B}_{\mathbf{x}}(\mathbf{q},\dot{\mathbf{x}})\dot{\mathbf{x}}$ in the closed-loop error dynamics (4.86) can be manipulated such as

$$\begin{aligned} &= \mathbf{B}_{\mathbf{x}}(\mathbf{q},\dot{\mathbf{x}} - \dot{\tilde{\mathbf{x}}})(\dot{\mathbf{x}}_d + \boldsymbol{\Lambda}\dot{\mathbf{e}}) - \mathbf{B}_{\mathbf{x}}(\mathbf{q},\dot{\mathbf{x}})\dot{\mathbf{x}} \\ &= \mathbf{B}_{\mathbf{x}}(\mathbf{q},\dot{\mathbf{x}})(\dot{\mathbf{x}}_r - \dot{\mathbf{x}}) - \mathbf{B}_{\mathbf{x}}(\mathbf{q},\dot{\mathbf{x}}_r)\dot{\tilde{\mathbf{x}}} \\ &= \mathbf{B}_{\mathbf{x}}(\mathbf{q},\dot{\mathbf{x}})(\hat{\mathbf{r}} - \dot{\tilde{\mathbf{x}}}) - \mathbf{B}_{\mathbf{x}}(\mathbf{q},\dot{\mathbf{x}}_r)\dot{\tilde{\mathbf{x}}}. \end{aligned} \tag{4.89}$$

Substituting (4.89) into (4.86), yields the closed-loop error dynamics, that is useful for Lyapunov analysis, as

$$\begin{aligned} \mathbf{M}_{\mathbf{x}}(\mathbf{q})(\dot{\hat{\mathbf{r}}} - \ddot{\tilde{\mathbf{x}}}) = &- \mathbf{M}_{\mathbf{x}}(\mathbf{q})\boldsymbol{\Lambda}\hat{\mathbf{r}} - \mathbf{M}_{\mathbf{x}}(\mathbf{q})\boldsymbol{\Lambda}\dot{\tilde{\mathbf{x}}} - \mathbf{B}_{\mathbf{x}}(\mathbf{q},\dot{\mathbf{x}})(\hat{\mathbf{r}} - \dot{\tilde{\mathbf{x}}}) + \mathbf{B}_{\mathbf{x}}(\mathbf{q},\dot{\mathbf{x}}_r)\dot{\tilde{\mathbf{x}}} \\ &+ \boldsymbol{\tau}_{\mathbf{x}}(\mathbf{q},\dot{\mathbf{q}}) - \boldsymbol{\tau}_{\mathbf{x}}(\mathbf{q},\dot{\hat{\mathbf{q}}}) + \boldsymbol{\eta}. \end{aligned} \tag{4.90}$$

Similar with Section 4.4.2, $\mathbf{M}_{\mathbf{x}}(\mathbf{q})$, $\mathbf{B}_{\mathbf{x}}(\mathbf{q},\dot{\hat{\mathbf{q}}})$, $\mathbf{g}_{\mathbf{x}}(\mathbf{q})$, and $\boldsymbol{\tau}_{\mathbf{x}}(\mathbf{q},\dot{\hat{\mathbf{q}}})$ in $\boldsymbol{\eta}$ (4.87) can be described as follows

$$\mathbf{M}_{\mathbf{x}}(\mathbf{q}) = \mathbf{W}_M^{\mathrm{T}}\,\boldsymbol{\sigma}_M(\mathbf{V}_M^{\mathrm{T}}\,\mathbf{z}_M) + \boldsymbol{\varepsilon}_M \tag{4.91}$$

$$\mathbf{B}_{\mathbf{x}}(\mathbf{q},\dot{\hat{\mathbf{q}}}) = \mathbf{W}_B^{\mathrm{T}}\,\boldsymbol{\sigma}_B(\mathbf{V}_B^{\mathrm{T}}\,\mathbf{z}_B) + \boldsymbol{\varepsilon}_B \tag{4.92}$$

$$\mathbf{g}_{\mathbf{x}}(\mathbf{q}) = \mathbf{W}_g^{\mathrm{T}}\,\boldsymbol{\sigma}_g(\mathbf{V}_g^{\mathrm{T}}\,\mathbf{z}_g) + \boldsymbol{\varepsilon}_g \tag{4.93}$$

$$\boldsymbol{\tau}_{\mathbf{x}}(\mathbf{q},\dot{\hat{\mathbf{q}}}) = \mathbf{W}_\tau^{\mathrm{T}}\,\boldsymbol{\sigma}_\tau(\mathbf{V}_\tau^{\mathrm{T}}\,\mathbf{z}_\tau) + \boldsymbol{\varepsilon}_\tau \tag{4.94}$$

Likewise, the estimated dynamic terms $\hat{\mathbf{M}}_{\mathbf{x}}(\mathbf{q})$, $\hat{\mathbf{B}}_{\mathbf{x}}(\mathbf{q},\dot{\hat{\mathbf{q}}})$, $\hat{\mathbf{g}}_{\mathbf{x}}(\mathbf{q})$, and $\hat{\boldsymbol{\tau}}_{\mathbf{x}}(\mathbf{q},\dot{\hat{\mathbf{q}}})$ are described by estimated weights $\hat{\mathbf{V}}_p, \hat{\mathbf{W}}_p$ with subscript $p = M, B, g, \tau$.

As in Section 4.4.2, $\mathbf{M_x(q)}, \mathbf{B_x(q,\dot{\hat{q}})}$, $\mathbf{g_x(q)}, \boldsymbol{\tau}_\mathbf{x}\mathbf{(q,\dot{\hat{q}})}$ can be shown to be bounded by Properties 4.3.1, 4.3.3, 4.3.4, 3.2.4, respectively, and the fact $\dot{\hat{\mathbf{q}}}$ bounded because it is obtained from the backward difference between the current and previous actual position $\mathbf{q}(t)$ and $\mathbf{q}(t-1)$, which are bounded by joint limitation.

Therefore, the optimum weights $\mathbf{W}_p, \mathbf{V}_p$ and the approximation error $\boldsymbol{\varepsilon}_p$ (with subscript $p = M, B, g, \tau, h$) from (4.91)-(4.94), are also upper-bounded.

Using similar development and simplified notations $\boldsymbol{\sigma} \equiv \boldsymbol{\sigma}(\mathbf{V}^\mathrm{T}\mathbf{z})$, $\hat{\boldsymbol{\sigma}} \equiv \boldsymbol{\sigma}(\hat{\mathbf{V}}^\mathrm{T}\mathbf{z})$, and $\boldsymbol{\sigma} = \hat{\boldsymbol{\sigma}} + \tilde{\boldsymbol{\sigma}}$ as in Section 4.4.2, the uncertainties $\boldsymbol{\eta}$ (4.87) can be written as

$$\boldsymbol{\eta} = \boldsymbol{\xi} + \boldsymbol{\zeta} \tag{4.95}$$

This division is needed because only $\boldsymbol{\xi}$ term can be manipulated by the weight updates $\dot{\hat{\mathbf{W}}}, \dot{\hat{\mathbf{V}}}$ as will be shown in Section 4.7.1.

The term $\boldsymbol{\xi}$ is defined as

$$\begin{aligned}\boldsymbol{\xi} = &\left(\tilde{\mathbf{W}}_M^\mathrm{T}\,\hat{\boldsymbol{\sigma}}_M\right)\mathbf{F}^*_\mathrm{motion} + \left(\tilde{\mathbf{W}}_B^\mathrm{T}\,\hat{\boldsymbol{\sigma}}_B\right)\dot{\mathbf{x}}_r + \tilde{\mathbf{W}}_g^\mathrm{T}\,\hat{\boldsymbol{\sigma}}_g + \tilde{\mathbf{W}}_\tau^\mathrm{T}\,\hat{\boldsymbol{\sigma}}_\tau \\ &+ \left(\hat{\mathbf{W}}_M^\mathrm{T}\,\hat{\boldsymbol{\sigma}}'_M\,\tilde{\mathbf{V}}_M^\mathrm{T}\,\mathbf{z}_M\right)\mathbf{F}^*_\mathrm{motion} + \left(\hat{\mathbf{W}}_B^\mathrm{T}\,\hat{\boldsymbol{\sigma}}'_B\,\tilde{\mathbf{V}}_B^\mathrm{T}\,\mathbf{z}_B\right)\dot{\mathbf{x}}_r \\ &+ \hat{\mathbf{W}}_g^\mathrm{T}\,\hat{\boldsymbol{\sigma}}'_g\,\tilde{\mathbf{V}}_g^\mathrm{T}\,\mathbf{z}_g + \hat{\mathbf{W}}_\tau^\mathrm{T}\,\hat{\boldsymbol{\sigma}}'_\tau\,\tilde{\mathbf{V}}_\tau^\mathrm{T}\,\mathbf{z}_\tau\end{aligned} \tag{4.96}$$

and the "whole"NN errors $\boldsymbol{\zeta}$ is defined as

$$\begin{aligned}\boldsymbol{\zeta} = &\left(\tilde{\mathbf{W}}_M^\mathrm{T}\,\hat{\boldsymbol{\sigma}}'_M\,\tilde{\mathbf{V}}_M^\mathrm{T}\,\mathbf{z}_M\right)\mathbf{F}^*_\mathrm{motion} + \left(\tilde{\mathbf{W}}_B^\mathrm{T}\,\hat{\boldsymbol{\sigma}}'_B\,\tilde{\mathbf{V}}_B^\mathrm{T}\,\mathbf{z}_B\right)\dot{\mathbf{x}}_r \\ &+ \tilde{\mathbf{W}}_g^\mathrm{T}\hat{\boldsymbol{\sigma}}'_g\tilde{\mathbf{V}}_g^\mathrm{T}\mathbf{z}_g + \tilde{\mathbf{W}}_\tau^\mathrm{T}\hat{\boldsymbol{\sigma}}'_\tau\tilde{\mathbf{V}}_\tau^\mathrm{T}\,\mathbf{z}_\tau \\ &+ \left(\mathbf{W}_M^\mathrm{T}\,O(\tilde{\mathbf{V}}_M^\mathrm{T}\,\mathbf{z}_M)\right)\mathbf{F}^*_\mathrm{motion} + \left(\mathbf{W}_B^\mathrm{T}\,O(\tilde{\mathbf{V}}_B^\mathrm{T}\,\mathbf{z}_B)\right)\dot{\mathbf{x}}_r \\ &+ \mathbf{W}_g^\mathrm{T}\,O(\tilde{\mathbf{V}}_g^\mathrm{T}\,\mathbf{z}_g) + \mathbf{W}_\tau^\mathrm{T}\,O(\tilde{\mathbf{V}}_\tau^\mathrm{T}\,\mathbf{z}_\tau) + \boldsymbol{\varepsilon}\end{aligned} \tag{4.97}$$

where the total approximation error $\boldsymbol{\varepsilon} = \boldsymbol{\varepsilon}_M \, \mathbf{F}^*_{\text{motion}} + \boldsymbol{\varepsilon}_B \, \dot{\mathbf{x}}_r + \boldsymbol{\varepsilon}_g + \boldsymbol{\varepsilon}_\tau \leq \varepsilon_M$ (since the actual dynamics are bounded).

Note that, the driving signals $\dot{\mathbf{x}}_r$ (4.81) and $\mathbf{F}^*_{\text{motion}}$ (4.82), used in (4.96) and (4.97), are different than $\dot{\mathbf{x}}_r$ and $\mathbf{F}^*_{\text{motion}}$ in Section 4.4.2.

As in Section 4.4.2, the uncertainties $\boldsymbol{\eta}$ (4.95) can be seen to be bounded with the generic expression $\|\mathbf{L}_p - \hat{\mathbf{L}}_p\| \leq (\tilde{L}_p)_M$ in (4.47) and also $\mathbf{F}^*_{\text{motion}}$ (4.82) and $\dot{\mathbf{x}}_r$ in (4.84), as follows

$$\begin{aligned}\|\boldsymbol{\eta}\| &\leq (\tilde{L}_M)_M \, \|\mathbf{F}^*_{\text{motion}}\| + (\tilde{L}_B)_M \, \|\dot{\mathbf{x}}_r\| + (\tilde{L}_g)_M + (\tilde{L}_\tau)_M + \varepsilon_M \\ &\leq (\tilde{L}_M)_M \, (\|\ddot{\mathbf{x}}'_r\| + \boldsymbol{\Lambda}\|\hat{\mathbf{r}}\|) + (\tilde{L}_B)_M \, (\|\hat{\mathbf{r}}\| + \|\dot{\hat{\mathbf{x}}}\|) + (\tilde{L}_g)_M + (\tilde{L}_\tau)_M \\ &\quad + \varepsilon_M\end{aligned} \tag{4.98}$$

Note that $\ddot{\mathbf{x}}_r$ in (4.12) can be assumed to be bounded since the desired trajectories $\ddot{\mathbf{x}}_d, \dot{\mathbf{x}}_d, \mathbf{x}_d$ are bounded by design, $\mathbf{x}$ is bounded by the workspace and the filtered estimated velocity $\dot{\hat{\mathbf{x}}}$ is bounded, since it is obtained from $\dot{\hat{\mathbf{x}}} = \mathbf{J} \, \dot{\hat{\mathbf{q}}}$.

Therefore $\boldsymbol{\eta}$ can be shown to be bounded as

$$\|\boldsymbol{\eta}\| \leq C_0 + C_1 \, \|\hat{\mathbf{r}}\|. \tag{4.99}$$

where $C_0, C_1 > 0$. And since $\boldsymbol{\eta} = \boldsymbol{\xi} + \boldsymbol{\zeta}$, then clearly the following inequalities are true

$$\|\boldsymbol{\xi}\| \leq C_0 + C_1 \, \|\hat{\mathbf{r}}\| \tag{4.100}$$

$$\|\boldsymbol{\zeta}\| \leq C_0 + C_1 \, \|\hat{\mathbf{r}}\|. \tag{4.101}$$

Note that, the definition of $\hat{\mathbf{r}}$ (4.84) in this section, is <u>different</u> with the definition of $\mathbf{r}$ in Section 4.4.2.

4.7.1 Stability Analysis using Filtered Velocity

The chosen Lyapunov function candidate for the closed-loop error dynamics (4.90), with the uncertainties $\boldsymbol{\eta}$ (4.95), can be chosen as

$$\begin{aligned} V(\hat{\mathbf{r}}, \dot{\tilde{\mathbf{x}}}, \tilde{\mathbf{Z}}) = & \frac{1}{2}(\hat{\mathbf{r}} - \dot{\tilde{\mathbf{x}}})^{\mathrm{T}} \mathbf{M}_{\mathbf{x}}(\mathbf{q})(\hat{\mathbf{r}} - \dot{\tilde{\mathbf{x}}}) \\ & + \frac{1}{2} \sum_{i=1}^{m} \sum_{j=1}^{m} \tilde{\mathbf{w}}_{M_{ij}}^{\mathrm{T}} \, \mathbf{F}_{M_{ij}}^{-1} \, \tilde{\mathbf{w}}_{M_{ij}} + \ldots + \frac{1}{2} \sum_{i=1}^{m} \tilde{\mathbf{w}}_{\tau_i}^{\mathrm{T}} \, \mathbf{F}_{\tau_i}^{-1} \, \tilde{\mathbf{w}}_{\tau_i} \\ & + \frac{1}{2} \sum_{k=1}^{N_2} \tilde{\mathbf{v}}_{M_k}^{\mathrm{T}} \, \mathbf{G}_{M_k}^{-1} \, \tilde{\mathbf{v}}_{M_k} + \ldots + \frac{1}{2} \sum_{k=1}^{N_2} \tilde{\mathbf{v}}_{\tau_k}^{\mathrm{T}} \, \mathbf{G}_{\tau_k}^{-1} \, \tilde{\mathbf{v}}_{\tau_k} \end{aligned} \tag{4.102}$$

where the NN weight errors: $\tilde{\mathbf{w}}_{M_{ij}} \in \Re^{N_2}, \tilde{\mathbf{v}}_{M_k} \in \Re^{N_{1,M}}, \tilde{\mathbf{w}}_{B_{ij}} \in \Re^{N_2}, \tilde{\mathbf{v}}_{B_k} \in \Re^{N_{1,B}}, \tilde{\mathbf{w}}_{g_i} \in \Re^{N_2}, \tilde{\mathbf{v}}_{g_k} \in \Re^{N_{1,g}}, \tilde{\mathbf{w}}_{\tau_i} \in \Re^{N_2}, \tilde{\mathbf{v}}_{\tau_k} \in \Re^{N_{1,\tau}}$ are all column vector. And the adaptive gains: $\mathbf{F}_{M_{ij}}^{-1} \in \Re^{N_2 \times N_2}, \ldots, \mathbf{F}_{\tau_i}^{-1} \in \Re^{N_2 \times N_2}$ and $\mathbf{G}_{M_k}^{-1} \in \Re^{N_{1,M} \times N_{1,M}}, \ldots,$

$\mathbf{G}_{\tau_k}^{-1} \in \Re^{N_{1,\tau} \times N_{1,\tau}}$ are all positive diagonal matrices. The following indices are defined: $i, j = 1, \ldots, m$ are output-node indices, $k = 1, \ldots, N_2$ is the hidden-node index. While $N_{1,M}, N_{1,B}, N_{1,g}, N_{1,\tau}$ are respective input-node sizes.

Next, we substitute the closed-loop error dynamics (4.86), Property 4.3.5 and also take into account $\boldsymbol{\eta}$ (4.95), with the definition $\boldsymbol{\xi}$ (4.96) and the knowledge $\|\boldsymbol{\zeta}\| \leq C_0 + C_1 \|\hat{\mathbf{r}}\|$ (4.101), into $\dot{V}(\mathbf{r}, \tilde{\mathbf{Z}})$ of (4.102), to obtain

$$\begin{aligned} \dot{V}(\hat{\mathbf{r}}, \dot{\tilde{\mathbf{x}}}, \tilde{\mathbf{Z}}) \leq & - \hat{\mathbf{r}}^{\mathrm{T}} \mathbf{M}_{\mathbf{x}}(\mathbf{q}) \boldsymbol{\Lambda} \hat{\mathbf{r}} + \dot{\tilde{\mathbf{x}}}^{\mathrm{T}} \mathbf{M}_{\mathbf{x}}(\mathbf{q}) \boldsymbol{\Lambda} \dot{\tilde{\mathbf{x}}} \\ & + (\hat{\mathbf{r}}^{\mathrm{T}} - \dot{\tilde{\mathbf{x}}}^{\mathrm{T}}) \mathbf{B}_{\mathbf{x}}(\mathbf{q}, \dot{\mathbf{x}}_r) \dot{\tilde{\mathbf{x}}} \\ & + (\hat{\mathbf{r}}^{\mathrm{T}} - \dot{\tilde{\mathbf{x}}}^{\mathrm{T}}) (\boldsymbol{\tau}_{\mathbf{x}}(\mathbf{q}, \dot{\mathbf{q}}) - \boldsymbol{\tau}_{\mathbf{x}}(\mathbf{q}, \dot{\tilde{\mathbf{q}}})) \\ & + C_0 \|\hat{\mathbf{r}}\| + C_0 \|\dot{\tilde{\mathbf{x}}}\| + C_1 \|\hat{\mathbf{r}}\|^2 + C_1 \|\hat{\mathbf{r}}\| \, \|\dot{\tilde{\mathbf{x}}}\| + \boldsymbol{\psi} \end{aligned} \tag{4.103}$$

where the lump parameter $\boldsymbol{\psi}$ in (4.103) is defined as

$$
\begin{aligned}
\boldsymbol{\psi} = & \sum_{i=1}^{m}\sum_{j=1}^{m} \tilde{\mathbf{w}}_{M_{ij}}^{\mathrm{T}} \left(\mathbf{F}_{M_{ij}}^{-1} \dot{\tilde{\mathbf{w}}}_{M_{ij}} + \hat{\boldsymbol{\sigma}}_M \, (\hat{r}_i - \dot{\tilde{x}}_i) \, F_{\mathrm{motion}j}^{*} \right) \\
& + \sum_{k=1}^{N_2} \tilde{\mathbf{v}}_{M_k}^{\mathrm{T}} \left(\mathbf{G}_{M_k}^{-1} \dot{\tilde{\mathbf{v}}}_{M_k} + \mathbf{z}_M \, \hat{\boldsymbol{\sigma}}'_{M_k} (\sum_{i=1}^{m}\sum_{j=1}^{m} \hat{w}_{M_{ijk}} \, (\hat{r}_i - \dot{\tilde{x}}_i) \, F_{\mathrm{motion}j}^{*}) \right) \\
& + \sum_{i=1}^{m}\sum_{j=1}^{m} \tilde{\mathbf{w}}_{B_{ij}}^{\mathrm{T}} \left(\mathbf{F}_{B_{ij}}^{-1} \dot{\tilde{\mathbf{w}}}_{B_{ij}} + \hat{\boldsymbol{\sigma}}_B \, (\hat{r}_i - \dot{\tilde{x}}_i) \, \dot{x}_{rj} \right) \\
& + \sum_{k=1}^{N_2} \tilde{\mathbf{v}}_{B_k}^{\mathrm{T}} \left(\mathbf{G}_{B_k}^{-1} \dot{\tilde{\mathbf{v}}}_{B_k} + \mathbf{z}_B \, \hat{\boldsymbol{\sigma}}'_{B_k} (\sum_{i=1}^{m}\sum_{j=1}^{m} \hat{w}_{B_{ijk}} \, (\hat{r}_i - \dot{\tilde{x}}_i) \, \dot{x}_{rj}) \right) \\
& + \sum_{i=1}^{m} \tilde{\mathbf{w}}_{g_i}^{\mathrm{T}} \left(\mathbf{F}_{g_i}^{-1} \dot{\tilde{\mathbf{w}}}_{g_i} + \hat{\boldsymbol{\sigma}}_g (\hat{r}_i - \dot{\tilde{x}}_i) \right) \\
& + \sum_{k=1}^{N_2} \tilde{\mathbf{v}}_{g_k}^{\mathrm{T}} \left(\mathbf{G}_{g_k}^{-1} \dot{\tilde{\mathbf{v}}}_{g_k} + \mathbf{z}_g \, \hat{\boldsymbol{\sigma}}'_{g_k} (\sum_{i=1}^{m} \hat{w}_{g_{ik}} (\hat{r}_i - \dot{\tilde{x}}_i)) \right) \\
& + \sum_{i=1}^{m} \tilde{\mathbf{w}}_{\tau_i}^{\mathrm{T}} \left(\mathbf{F}_{\tau_i}^{-1} \dot{\tilde{\mathbf{w}}}_{\tau_i} + \hat{\boldsymbol{\sigma}}_\tau (\hat{r}_i - \dot{\tilde{x}}_i) \right) \\
& + \sum_{k=1}^{N_2} \tilde{\mathbf{v}}_{\tau_k}^{\mathrm{T}} \left(\mathbf{G}_{\tau_k}^{-1} \dot{\tilde{\mathbf{v}}}_{\tau_k} + \mathbf{z}_\tau \, \hat{\boldsymbol{\sigma}}'_{\tau_k} (\sum_{i=1}^{m} \hat{w}_{\tau_{ik}} (\hat{r}_i - \dot{\tilde{x}}_i)) \right).
\end{aligned}
\tag{4.104}
$$

Using $\boldsymbol{\xi}$ (4.96), it can be demonstrated that $\boldsymbol{\psi}$ (4.104) is made up of $\dot{\tilde{\mathbf{W}}}$, $\dot{\tilde{\mathbf{V}}}$ and $(\hat{\mathbf{r}} - \dot{\tilde{\mathbf{x}}})^{\mathrm{T}}\boldsymbol{\xi}$. The idea is to cancel $(\hat{\mathbf{r}} - \dot{\tilde{\mathbf{x}}})^{\mathrm{T}}\boldsymbol{\xi}$ with $\dot{\tilde{\mathbf{W}}}, \dot{\tilde{\mathbf{V}}}$. However only $\hat{\mathbf{r}}$ is available, hence only $\hat{\mathbf{r}}^{\mathrm{T}}\boldsymbol{\xi}$ can be canceled by $\dot{\tilde{\mathbf{W}}}, \dot{\tilde{\mathbf{V}}}$.

Therefore, if we introduce the weight updates as follows

$$\dot{\hat{\mathbf{w}}}_{M_{ij}} = \mathbf{F}_{M_{ij}}(\hat{\boldsymbol{\sigma}}_M\ \hat{r}_i\ F^*_{\text{motion}j} - \kappa\|\hat{\mathbf{r}}\|\hat{\mathbf{w}}_{M_{ij}}) \tag{4.105}$$

$$\dot{\hat{\mathbf{v}}}_{M_k} = \mathbf{G}_{M_k}(\mathbf{z}_M\ \hat{\boldsymbol{\sigma}}'_{M_k}\ (\sum_{i=1}^{m}\sum_{j=1}^{m}\hat{w}_{M_{ijk}}\ \hat{r}_i\ F^*_{\text{motion}j}) - \kappa\|\hat{\mathbf{r}}\|\hat{\mathbf{v}}_{M_k}) \tag{4.106}$$

$$\dot{\hat{\mathbf{w}}}_{B_{ij}} = \mathbf{F}_{B_{ij}}(\hat{\boldsymbol{\sigma}}_B\ \hat{r}_i\ \dot{x}_{rj} - \kappa\|\hat{\mathbf{r}}\|\hat{\mathbf{w}}_{B_{ij}}) \tag{4.107}$$

$$\dot{\hat{\mathbf{v}}}_{B_k} = \mathbf{G}_{B_k}(\mathbf{z}_B\ \hat{\boldsymbol{\sigma}}'_{B_k}\ (\sum_{i=1}^{m}\sum_{j=1}^{m}\hat{w}_{B_{ijk}}\ \hat{r}_i\ \dot{x}_{rj}) - \kappa\|\hat{\mathbf{r}}\|\hat{\mathbf{v}}_{B_k}) \tag{4.108}$$

$$\dot{\hat{\mathbf{w}}}_{g_i} = \mathbf{F}_{g_i}(\hat{\boldsymbol{\sigma}}_g\ \hat{r}_i - \kappa\|\hat{\mathbf{r}}\|\hat{\mathbf{w}}_{g_i}) \tag{4.109}$$

$$\dot{\hat{\mathbf{v}}}_{g_k} = \mathbf{G}_{g_k}(\mathbf{z}_g\ \hat{\boldsymbol{\sigma}}'_{g_k}\ (\sum_{i=1}^{m}\hat{w}_{g_{ik}}\ \hat{r}_i) - \kappa\|\hat{\mathbf{r}}\|\hat{\mathbf{v}}_{g_k}) \tag{4.110}$$

$$\dot{\hat{\mathbf{w}}}_{\tau_i} = \mathbf{F}_{\tau_i}(\hat{\boldsymbol{\sigma}}_\tau\ \hat{r}_i - \kappa\|\hat{\mathbf{r}}\|\hat{\mathbf{w}}_{\tau_i}) \tag{4.111}$$

$$\dot{\hat{\mathbf{v}}}_{\tau_k} = \mathbf{G}_{\tau_k}(\mathbf{z}_\tau\ \hat{\boldsymbol{\sigma}}'_{\tau_k}\ (\sum_{i=1}^{m}\hat{w}_{\tau_{ik}}\ \hat{r}_i) - \kappa\|\hat{\mathbf{r}}\|\hat{\mathbf{v}}_{\tau_k}) \tag{4.112}$$

and take into account $-\dot{\tilde{\mathbf{W}}} = \dot{\hat{\mathbf{W}}}$, since $\tilde{\mathbf{W}} = \mathbf{W} - \hat{\mathbf{W}}$ and $\mathbf{W}$ is constant, and the knowledge $\|\boldsymbol{\xi}\| \leq\ C_0 + C_1\ \|\hat{\mathbf{r}}\|$ in (4.100) and some inner products in (4.68) – (4.71), then $\boldsymbol{\psi}$ (4.104) can be expressed as:

$$\begin{aligned}\boldsymbol{\psi} &\leq -\kappa\ \|\hat{\mathbf{r}}\|\ \|\tilde{\mathbf{Z}}\|^2 + \kappa\ \|\hat{\mathbf{r}}\|\ \|\tilde{\mathbf{Z}}\|\ Z_M - \dot{\tilde{\mathbf{x}}}^{\mathrm{T}}\ \boldsymbol{\xi} \\ &\leq -\kappa\ \|\hat{\mathbf{r}}\|\ \|\tilde{\mathbf{Z}}\|^2 + \kappa\ \|\hat{\mathbf{r}}\|\ \|\tilde{\mathbf{Z}}\|\ Z_M + C_0\ \|\dot{\tilde{\mathbf{x}}}\| + C_1\ \|\hat{\mathbf{r}}\|\ \|\dot{\tilde{\mathbf{x}}}\|\end{aligned} \tag{4.113}$$

The substitution of $\boldsymbol{\psi}$ (4.113) into $\dot{V}(\mathbf{r}, \tilde{\mathbf{Z}})$ (4.103), yields

$$\begin{aligned}\dot{V}(\hat{\mathbf{r}}, \dot{\tilde{\mathbf{x}}}, \tilde{\mathbf{Z}}) = &-\hat{\mathbf{r}}^{\mathrm{T}}\ \mathbf{M}_{\mathbf{x}}(\mathbf{q})\boldsymbol{\Lambda}\hat{\mathbf{r}} + \dot{\tilde{\mathbf{x}}}^{\mathrm{T}}\ \mathbf{M}_{\mathbf{x}}(\mathbf{q})\boldsymbol{\Lambda}\dot{\tilde{\mathbf{x}}} + (\hat{\mathbf{r}}^{\mathrm{T}} - \dot{\tilde{\mathbf{x}}}^{\mathrm{T}})\mathbf{B}_{\mathbf{x}}(\mathbf{q}, \dot{\mathbf{x}}_r)\dot{\tilde{\mathbf{x}}} \\ &+ (\hat{\mathbf{r}}^{\mathrm{T}} - \dot{\tilde{\mathbf{x}}}^{\mathrm{T}})(\boldsymbol{\tau}_{\mathbf{x}}(\mathbf{q}, \dot{\mathbf{q}}) - \boldsymbol{\tau}_{\mathbf{x}}(\mathbf{q}, \dot{\hat{\mathbf{q}}})) \\ &+ C_0\ \|\hat{\mathbf{r}}\| + 2\ C_0\ \|\dot{\tilde{\mathbf{x}}}\| + C_1\ \|\hat{\mathbf{r}}\|^2 + 2\ C_1\ \|\hat{\mathbf{r}}\|\|\dot{\tilde{\mathbf{x}}}\| \\ &- \kappa\|\hat{\mathbf{r}}\|\|\tilde{\mathbf{Z}}\|^2 + \kappa\|\hat{\mathbf{r}}\|\|\tilde{\mathbf{Z}}\|Z_M\end{aligned} \tag{4.114}$$

The terms in (4.114) can be analyzed for its boundedness. The following terms,

using Property 4.3.1, can be written as

$$-\hat{\mathbf{r}}^{\mathrm{T}}\mathbf{M}_{\mathbf{x}}(\mathbf{q})\mathbf{\Lambda}\hat{\mathbf{r}} \leq -M_{x,m}\Lambda_m \left\|\hat{\mathbf{r}}\right\|^2 \tag{4.115}$$

$$\dot{\tilde{\mathbf{x}}}^{\mathrm{T}}\mathbf{M}_{\mathbf{x}}(\mathbf{q})\mathbf{\Lambda}\dot{\tilde{\mathbf{x}}} \leq \ M_{x,M}\Lambda_M \left\|\tilde{\mathbf{x}}\right\|^2 \tag{4.116}$$

where $M_{x,m} = \lambda_{min}(\mathbf{M}_{\mathbf{x}}(\mathbf{q}))$, $M_{x,M} = \lambda_{max}(\mathbf{M}_{\mathbf{x}}(\mathbf{q}))$, $\Lambda_m = \min(\mathbf{\Lambda})$, $\Lambda_M = \max(\mathbf{\Lambda})$.

The next term in (4.114), using Property 4.3.3, can be written as:

$$\begin{aligned}&\|(\hat{\mathbf{r}}^{\mathrm{T}} - \dot{\tilde{\mathbf{x}}}^{\mathrm{T}})\mathbf{B}_{\mathbf{x}}(\mathbf{q}, \dot{\mathbf{x}}_r)\dot{\tilde{\mathbf{x}}}\| \leq (\|\hat{\mathbf{r}}^{\mathrm{T}}\| + \|\dot{\tilde{\mathbf{x}}}\|) \left\|\mathbf{B}_{\mathbf{x}}(\mathbf{q}, \dot{\mathbf{x}}_r)\right\| \left\|\dot{\tilde{\mathbf{x}}}\right\| \leq \\ &\|\hat{\mathbf{r}}\|\|\dot{\tilde{\mathbf{x}}}\| \ B_{x,M}\left(\|\hat{\mathbf{r}}\| + \|\dot{\tilde{\mathbf{x}}}\| + \dot{x}_M\right) + \ \|\dot{\tilde{\mathbf{x}}}\|^2 \ B_{x,M}\left(\|\hat{\mathbf{r}}\| + \|\dot{\tilde{\mathbf{x}}}\| + \dot{x}_M\right)\end{aligned} \tag{4.117}$$

This is due from (4.84) $\|\dot{\mathbf{x}}_r\| = \|\hat{\mathbf{r}} + \dot{\hat{\mathbf{x}}}\| = \|\hat{\mathbf{r}} + \dot{\mathbf{x}} - \dot{\tilde{\mathbf{x}}}\| \leq \|\hat{\mathbf{r}}\| + \|\dot{\mathbf{x}}\| + \|\dot{\tilde{\mathbf{x}}}\| \leq \|\hat{\mathbf{r}}\| + \|\dot{\tilde{\mathbf{x}}}\| + \dot{x}_M$.

And the term $\boldsymbol{\tau}_{\mathbf{x}}(\mathbf{q}, \dot{\mathbf{q}}) - \boldsymbol{\tau}_{\mathbf{x}}(\mathbf{q}, \dot{\hat{\mathbf{q}}})$ in (4.114) can be shown to be bounded by

$$\|\boldsymbol{\tau}_{\mathbf{x}}(\mathbf{q}, \dot{\mathbf{q}}) - \boldsymbol{\tau}_{\mathbf{x}}(\mathbf{q}, \dot{\hat{\mathbf{q}}})\| \leq (\tau_{\text{fric}})_M \tag{4.118}$$

which is obtained from (4.88), Property 3.2.4 and the followings:

1. $\|\mathbf{J}^{-\mathrm{T}}\boldsymbol{\tau}_{vis}\mathbf{J}^{-1}\dot{\tilde{\mathbf{x}}}\|$ is bounded because $\boldsymbol{\tau}_{vis}$ is bounded (as shown in (3.7)), $\|\mathbf{J}^{-1}\|$ is bounded for non-singular configuration of the manipulator and it was assumed that $\|\dot{\tilde{\mathbf{x}}}\|$ is bounded.

2. $\|\boldsymbol{\tau}_{cou}(\text{sgn}(\dot{\mathbf{q}}) - \text{sgn}(\dot{\hat{\mathbf{q}}}))\|$ is bounded because $\boldsymbol{\tau}_{cou}$ is shown to be bounded in (3.8) and because $(\text{sgn}(\dot{q}_i) - \text{sgn}(\dot{\hat{q}}_i))$ is bounded.

3. $\|\boldsymbol{\tau}_{sti}(\exp^{(-\boldsymbol{\tau}_{dec}\dot{\mathbf{q}}^2)}\text{sgn}(\dot{\mathbf{q}}) - \exp^{(-\boldsymbol{\tau}_{dec}\dot{\hat{\mathbf{q}}}^2)}\text{sgn}(\dot{\hat{\mathbf{q}}}))\|$ is bounded because $\boldsymbol{\tau}_{sti}$ is shown to be bounded in (3.9) and because both $\text{sgn}(\cdot)$ and $\exp^{-|a|}$ are bounded.

Substituting (4.115) – (4.118) into $\dot{V}(\hat{\mathbf{r}}, \dot{\tilde{\mathbf{x}}}, \tilde{\mathbf{Z}})$ in (4.114), yield

$$\begin{aligned}\dot{V}(\hat{\mathbf{r}}, \dot{\tilde{\mathbf{x}}}, \tilde{\mathbf{Z}}) \leq & -(M_{x,m}\Lambda_m - C_1)\|\hat{\mathbf{r}}\|^2 + M_{x,M}\Lambda_M\|\tilde{\mathbf{x}}\|^2 \\ & + \|\hat{\mathbf{r}}\|\|\dot{\tilde{\mathbf{x}}}\| \ \left(B_{x,M}(\|\hat{\mathbf{r}}\| + \|\dot{\tilde{\mathbf{x}}}\| + \dot{x}_M) + 2\,C_1\right) \\ & + \|\dot{\tilde{\mathbf{x}}}\|^2\, B_{x,M}(\|\hat{\mathbf{r}}\| + \|\dot{\tilde{\mathbf{x}}}\| + \dot{x}_M) \\ & + ((\tau_{\text{fric}})_M + C_0)\ \|\hat{\mathbf{r}}\| + ((\tau_{\text{fric}})_M + 2\,C_0)\ \|\dot{\tilde{\mathbf{x}}}\| \\ & - \kappa\|\hat{\mathbf{r}}\|\|\tilde{\mathbf{Z}}\|^2 + \kappa\|\hat{\mathbf{r}}\|\|\tilde{\mathbf{Z}}\|Z_M\end{aligned} \tag{4.119}$$

Defining $\mathbf{y}^{\mathrm{T}} = \begin{bmatrix}\hat{\mathbf{r}}^{\mathrm{T}} & \dot{\tilde{\mathbf{x}}}^{\mathrm{T}}\end{bmatrix}$, then $\dot{V}(\hat{\mathbf{r}}, \dot{\tilde{\mathbf{x}}}, \tilde{\mathbf{Z}})$ in (4.119) can be written as

$$\begin{aligned}\dot{V}(\mathbf{y}, \tilde{\mathbf{Z}}) \leq & -\mathbf{y}^{\mathrm{T}}\mathbf{\Psi}\mathbf{y} + \begin{bmatrix}(\tau_{\text{fric}})_M + C_0 & 0 \\ 0 & (\tau_{\text{fric}})_M + 2\,C_0\end{bmatrix}\mathbf{y} \\ & - \kappa\|\tilde{\mathbf{Z}}\|^2 + \kappa\|\tilde{\mathbf{Z}}\|Z_M\end{aligned} \tag{4.120}$$

where

$$\mathbf{\Psi} = \begin{bmatrix}M_{x,m}\Lambda_m - C_1 & -\frac{1}{2}p \\ -\frac{1}{2}p & -p - M_{x,M}\Lambda_M\end{bmatrix} \tag{4.121}$$

with p is defined as

$$p = B_{x,M}(\|\hat{\mathbf{r}}\| + \|\dot{\tilde{\mathbf{x}}}\| + \dot{x}_M) + 2\,C_1 \tag{4.122}$$

Note that, the positivity of the first diagonal of $\mathbf{\Psi}$, $(M_{x,m}\ \Lambda_m - C_1)$ can be achieved by setting $\Lambda_m > \dfrac{C_1}{M_{x,m}}$. However, unfortunately, the matrix $\mathbf{\Psi}$ in (4.120) is not positive definite since its second diagonal element is negative, hence the existence of an enclosing region $\dot{V} < 0$ had failed to be established and therefore bounded stability cannot be achieved.

In practice, $|\mathbf{\Psi}|$ depends on the quality of the filtered velocity feedback obtained, i.e. $|\mathbf{\Psi}| < 0$ for $\dot{\tilde{\mathbf{x}}} \neq 0$, or, $|\mathbf{\Psi}| > 0$ for $\dot{\tilde{\mathbf{x}}} = 0$ especially when the robot is not moving (hence it is bounded stable as shown in Section 4.4.3), and therefore

stability and unstability could alternate. This also explains why, in real-time, the controller gain $\mathbf{\Lambda} = 20\mathbf{I}$ that can be selected is lower than that in simulation ($\mathbf{\Lambda} = 30\mathbf{I}$), this is due to the quality of the velocity feedback signal that can be obtained.

It is therefore signifies the need of an improved formulation to overcome the deficiency of actual velocity feedback by providing the enclosing region $\dot{V} < 0$, where bounded stability can be ensured.

4.8 Conclusion

At this point, it is possible to conclude that:

- it is feasible in simulation study to construct an NN adaptive controller in operational space, without any prior knowledge of the system dynamic, with a potential performance comparable to that of Lagrangian dynamics strategy (without joint friction compensation), however
- it does highlight the problem in real robot implementation where joint velocity feedback does not exist. It was shown that the filtered velocity signal feedback can significantly affect the performance of the adaptive NN controller.

Therefore, in the next chapter, a controller with velocity observer strategy is proposed to address this limitation.

CHAPTER 5

NN ADAPTIVE MOTION CONTROL WITH VELOCITY OBSERVER

5.1 Chapter Overview

In this chapter, an NN adaptive motion control in operational space with velocity observer is presented, to overcome the absence of an actual velocity signal in the real robot. This work was extended from the previous formulation in Chapter three, by taking into account the model-based motion control with velocity observer in joint space introduced by [109].

The stability analysis of the proposed strategy is presented in this chapter. The improved NN formulation was validated with a six DOF PUMA 560 manipulator in real-time experiment.

It is worth to mention that a NN adaptive motion control with velocity observer in joint space was presented in [110]; it is based upon the model-based controller with velocity observer by [111]. However, the proposed approach by [110] still requires the knowledge of kinetic energy matrix. Also, a model-based motion control with velocity observer in operational space was presented in [92] where the joint friction model is estimated adaptively, giving a more improved performance than the Lagrangian only dynamics controller. However, its formulation

and stability analysis are rather different and relatively more involved than the original operational space Lagrangian dynamics formulation [8].

Another algorithm, the projection algorithm can be used to achieve faster convergence rate for the estimated parameters for LIP case [112, 113] or NN weights for NN case [114] (by de-correlating the system inputs). Projection algorithm can be seen as an improvement from a working algorithm / strategy. However, it is not a solution for a non-working algorithm.

Thus, our approach is to propose a solution for a non-working NN adaptive motion control in real time implementation by introducing the NN adaptive motion controller with velocity observer. Note that, it is still theoretically feasible, though, to improve the NN adaptive motion controller - observer with the projection algorithm.

The preliminary work of this chapter was presented in [115], where the more complete version is presented in [116].

5.2 End-effector Motion Dynamics

To ease the formulation development in this chapter, let's reproduce the end-effector motion dynamics of the non-redundant manipulator (2.27) in Chapter Two, which can be described as

$$\mathbf{M_x}(\mathbf{q})\ddot{\mathbf{x}} + \mathbf{B_x}(\mathbf{q},\dot{\mathbf{q}})\dot{\mathbf{x}} + \mathbf{g_x}(\mathbf{q}) + \boldsymbol{\tau}_{\mathbf{x}}(\mathbf{q},\dot{\mathbf{q}}) = \mathbf{F} \tag{5.1}$$

where $\mathbf{x} \in \Re^m$ and $\mathbf{q} \in \Re^n$ denote the operational and joint space coordinates, respectively, where for a non-redundant manipulator $m = n$. The

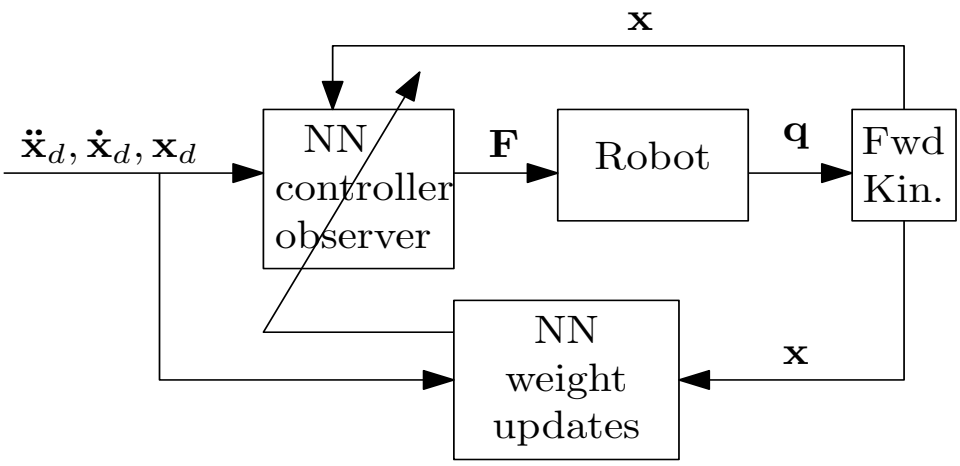

Figure 5.1: The operational space NN motion NN controller-observer structure.

matrices $\mathbf{M}_{\mathbf{x}}(\mathbf{q}) \in \Re^{m\times m}$ and $\mathbf{B}_{\mathbf{x}}(\mathbf{q},\dot{\mathbf{q}}) \in \Re^{m\times m}$ represent the inertia and the Coriolis/centrifugal terms, respectively, while vectors $\mathbf{g}_{\mathbf{x}}(\mathbf{q}) \in \Re^m$ and $\boldsymbol{\tau}_{\mathbf{x}}(\mathbf{q},\dot{\mathbf{q}}) \in \Re^m$ denote the gravity and joint friction forces, respectively. The vector $\mathbf{F} \in \Re^m$ is the operational space generalized forces.

5.3 NN Adaptive Motion Controller - Observer Formulation

5.3.1 NN Adaptive Motion Controller-Observer

In this section, a NN adaptive motion controller with velocity observer is proposed. The controller-observer structure is shown in Fig. 5.1. The control law is defined as:

$$\mathbf{F} = \hat{\mathbf{M}}_{\mathbf{x}}(\mathbf{q})\mathbf{F}^*_{\text{motion}} + \hat{\mathbf{B}}_{\mathbf{x}}(\mathbf{q},\dot{\mathbf{x}}_0)\dot{\mathbf{x}}_r + \hat{\mathbf{g}}_{\mathbf{x}}(\mathbf{q}) + \hat{\boldsymbol{\tau}}_{\mathbf{x}}(\mathbf{q},\dot{\hat{\mathbf{q}}}) \tag{5.2}$$

where $\dot{\mathbf{x}}_r, \dot{\mathbf{x}}_0$ and $\mathbf{F}^*_{\text{motion}}$ are defined as

$$\dot{\mathbf{x}}_r = \dot{\mathbf{x}}_d + \mathbf{\Lambda}_1(\mathbf{x}_d - \hat{\mathbf{x}}) \tag{5.3}$$

$$\dot{\mathbf{x}}_0 = \dot{\hat{\mathbf{x}}} - \mathbf{\Lambda}_2\tilde{\mathbf{x}} \tag{5.4}$$

$$\mathbf{F}^*_{\text{motion}} = \ddot{\mathbf{x}}_r + \mathbf{\Lambda}_1(\mathbf{r}_1 + \mathbf{r}_2) \tag{5.5}$$

with the computable terms to compute $\mathbf{F}^*_{\text{motion}}$ are defined as

$$\ddot{\mathbf{x}}_r = \ddot{\mathbf{x}}_d + \mathbf{\Lambda}_1(\dot{\mathbf{x}}_d - \dot{\hat{\mathbf{x}}}) \tag{5.6}$$

$$\mathbf{r}_1 + \mathbf{r}_2 = \dot{\mathbf{x}}_r - \dot{\mathbf{x}}_0 \tag{5.7}$$

It follows from (5.7) that we can write

$$\mathbf{r}_1 + \mathbf{r}_2 = (\dot{\mathbf{x}}_r - \dot{\mathbf{x}}) + (\dot{\mathbf{x}} - \dot{\mathbf{x}}_0), \tag{5.8}$$

where it can be defined

$$\mathbf{r}_1 = \dot{\mathbf{x}}_r - \dot{\mathbf{x}} = \dot{\mathbf{e}} + \mathbf{\Lambda}_1\mathbf{e} + \mathbf{\Lambda}_1\tilde{\mathbf{x}} \tag{5.9}$$

$$\mathbf{r}_2 = \dot{\mathbf{x}} - \dot{\mathbf{x}}_0 = \dot{\tilde{\mathbf{x}}} + \mathbf{\Lambda}_2\tilde{\mathbf{x}}. \tag{5.10}$$

Note: $\mathbf{\Lambda}_1, \mathbf{\Lambda}_2 \in \Re^{m\times m}$ are positive diagonal matrices, $\mathbf{e} = \mathbf{x}_d - \mathbf{x}$ and $\dot{\mathbf{e}} = \dot{\mathbf{x}}_d - \dot{\mathbf{x}}$ are defined as the position and velocity tracking errors, respectively, and $\mathbf{x}_d$, $\dot{\mathbf{x}}_d$ and $\ddot{\mathbf{x}}_d$ are the desired operational space trajectories. The estimated position and velocity errors, $\tilde{\mathbf{x}} = \mathbf{x} - \hat{\mathbf{x}}$ and $\dot{\tilde{\mathbf{x}}} = \dot{\mathbf{x}} - \dot{\hat{\mathbf{x}}}$, denote the difference between the actual position and velocity $\mathbf{x}, \dot{\mathbf{x}}$ and the estimated position and velocity $\hat{\mathbf{x}}, \dot{\hat{\mathbf{x}}}$, respectively. The computation to obtain $\hat{\mathbf{x}}$ and $\tilde{\mathbf{x}}$ will be given on Section 5.4.

Combining the robot dynamics (5.1) and the proposed controller (5.2), and taking into account the first derivative of (5.9) and Property 4.3.2, a *general closed-loop dynamics* is obtained as:

$$\begin{aligned}\mathbf{M_x}(\mathbf{q})\dot{\mathbf{r}}_1 =& -\mathbf{M_x}(\mathbf{q})\boldsymbol{\Lambda}_1(\mathbf{r}_1+\mathbf{r}_2) - \mathbf{B_x}(\mathbf{q},\dot{\mathbf{x}}_0)\dot{\mathbf{x}}_r + \mathbf{B_x}(\mathbf{q},\dot{\mathbf{x}})\dot{\mathbf{x}} \\ &+ \boldsymbol{\tau}_{\mathbf{x}}(\mathbf{q},\dot{\mathbf{q}}) - \boldsymbol{\tau}_{\mathbf{x}}(\mathbf{q},\dot{\hat{\mathbf{q}}}) + \boldsymbol{\eta}\end{aligned} \tag{5.11}$$

where the uncertainties of the system, $\boldsymbol{\eta}$, expressed as

$$\boldsymbol{\eta} = \tilde{\mathbf{M}}_{\mathbf{x}}(\mathbf{q})\mathbf{F}^*_{\text{motion}} + \tilde{\mathbf{B}}_{\mathbf{x}}(\mathbf{q},\dot{\mathbf{x}}_0)\dot{\mathbf{x}}_r + \tilde{\mathbf{g}}_{\mathbf{x}}(\mathbf{q}) + \tilde{\boldsymbol{\tau}}_{\mathbf{x}}(\mathbf{q},\dot{\hat{\mathbf{q}}}). \tag{5.12}$$

and $\boldsymbol{\tau}_{\mathbf{x}}(\mathbf{q},\dot{\mathbf{q}}) - \boldsymbol{\tau}_{\mathbf{x}}(\mathbf{q},\dot{\hat{\mathbf{q}}})$ is similar with (4.88), however it is reproduced for ease of perusal as

$$\begin{aligned}\boldsymbol{\tau}_{\mathbf{x}}(\mathbf{q},\dot{\mathbf{q}}) - \boldsymbol{\tau}_{\mathbf{x}}(\mathbf{q},\dot{\hat{\mathbf{q}}}) =& \mathbf{J}^{-\mathrm{T}}[\tau_{vis}\dot{\tilde{\mathbf{q}}} + \tau_{cou}(\text{sgn}(\dot{\mathbf{q}}) - \text{sgn}(\dot{\hat{\mathbf{q}}})) \\ &+ \boldsymbol{\tau}_{sti}\text{exp}^{(-\boldsymbol{\tau}_{dec}\dot{\mathbf{q}}^2)}\text{sgn}(\dot{\mathbf{q}}) - \boldsymbol{\tau}_{sti}\text{exp}^{(-\boldsymbol{\tau}_{dec}\dot{\hat{\mathbf{q}}}^2)}\text{sgn}(\dot{\hat{\mathbf{q}}})].\end{aligned} \tag{5.13}$$

The general closed-loop dynamics (5.11) cannot be used directly into stability analysis. It must be converted into useful controller closed-loop dynamics (Section 5.3.2) and observer closed-loop dynamics (Section 5.3.3):

5.3.2 Controller closed-loop dynamics

Using (5.9), (5.10) and Property 4.3.6, $\mathbf{B_x}(\mathbf{q},\dot{\mathbf{x}}_0)\dot{\mathbf{x}}_r - \mathbf{B_x}(\mathbf{q},\dot{\mathbf{x}})\dot{\mathbf{x}}$ in (5.11) can be rearranged such that

$$\begin{aligned}&= \mathbf{B_x}(\mathbf{q},\dot{\mathbf{x}}-\mathbf{r}_2)(\mathbf{r}_1+\dot{\mathbf{x}}) - \mathbf{B_x}(\mathbf{q},\dot{\mathbf{x}})\dot{\mathbf{x}} \\ &= \mathbf{B_x}(\mathbf{q},\dot{\mathbf{x}})\mathbf{r}_1 - \mathbf{B_x}(\mathbf{q},\dot{\mathbf{x}}_r)\mathbf{r}_2.\end{aligned} \tag{5.14}$$

Substituting (5.14) into the general closed-loop dynamics (5.11) yields the useful *controller closed-loop dynamics*:

$$\begin{aligned}\mathbf{M_x}(\mathbf{q})\dot{\mathbf{r}}_1 =& -\mathbf{M_x}(\mathbf{q})\boldsymbol{\Lambda}_1(\mathbf{r}_1+\mathbf{r}_2) - \mathbf{B_x}(\mathbf{q},\dot{\mathbf{x}})\mathbf{r}_1 + \mathbf{B_x}(\mathbf{q},\dot{\mathbf{x}}_r)\mathbf{r}_2 \\ &+ \boldsymbol{\tau}_{\mathbf{x}}(\mathbf{q},\dot{\mathbf{q}}) - \boldsymbol{\tau}_{\mathbf{x}}(\mathbf{q},\dot{\hat{\mathbf{q}}}) + \boldsymbol{\eta}\end{aligned} \tag{5.15}$$

5.3.3 Observer closed-loop dynamics

An observer can be designed as in [109]:

$$\dot{\hat{\mathbf{x}}} = \dot{\mathbf{x}} - \dot{\tilde{\mathbf{x}}} = \mathbf{z} + (\mathbf{l}_D + \mathbf{\Lambda}_2)\tilde{\mathbf{x}} \tag{5.16}$$

$$\dot{\mathbf{z}} = \ddot{\mathbf{x}}_r + (\mathbf{l}_D \cdot \mathbf{\Lambda}_2)\tilde{\mathbf{x}} \tag{5.17}$$

where $\mathbf{l}_D = \text{diag}(l_{D,ii} > 0) \in \Re^{m\times m}$. Combining the first derivative of (5.16) with (5.17), and taking into account the first derivative of (5.9), results in:

$$\ddot{\tilde{\mathbf{x}}} + (\mathbf{l}_D + \mathbf{\Lambda}_2)\dot{\tilde{\mathbf{x}}} + (\mathbf{l}_D \cdot \mathbf{\Lambda}_2)\tilde{\mathbf{x}} = -(\ddot{\mathbf{x}}_r - \ddot{\mathbf{x}}) = -\dot{\mathbf{r}}_1. \tag{5.18}$$

Substituting (5.10) and its derivative into the left-hand-side (LHS) of (5.18) and multiplying both sides with $\mathbf{M}_\mathbf{x}(\mathbf{q})$, yield

$$\mathbf{M}_\mathbf{x}(\mathbf{q})\dot{\mathbf{r}}_2 + \mathbf{M}_\mathbf{x}(\mathbf{q})\mathbf{l}_D\mathbf{r}_2 = -\mathbf{M}_\mathbf{x}(\mathbf{q})\dot{\mathbf{r}}_1 \tag{5.19}$$

Using (5.9), (5.10) and Property 4.3.6, $\mathbf{B}_\mathbf{x}(\mathbf{q},\dot{\mathbf{x}}_0)\dot{\mathbf{x}}_r - \mathbf{B}_\mathbf{x}(\mathbf{q},\dot{\mathbf{x}})\dot{\mathbf{x}}$ in (5.11) can be manipulated such that

$$\begin{aligned} &= \mathbf{B}_\mathbf{x}(\mathbf{q},\dot{\mathbf{x}}_0)(\mathbf{r}_1 + \dot{\mathbf{x}}) - \mathbf{B}_\mathbf{x}(\mathbf{q},\dot{\mathbf{x}}_0 + \mathbf{r}_2)\dot{\mathbf{x}} \\ &= \mathbf{B}_\mathbf{x}(\mathbf{q},\dot{\mathbf{x}}_0)\mathbf{r}_1 - \mathbf{B}_\mathbf{x}(\mathbf{q},\dot{\mathbf{x}})\mathbf{r}_2. \end{aligned} \tag{5.20}$$

Substituting (5.20) into the general closed-loop dynamics (5.11) yields

$$\begin{aligned} -\mathbf{M}_\mathbf{x}(\mathbf{q})\dot{\mathbf{r}}_1 = \mathbf{M}_\mathbf{x}(\mathbf{q})\mathbf{\Lambda}_1(\mathbf{r}_1 + \mathbf{r}_2) + \mathbf{B}_\mathbf{x}(\mathbf{q},\dot{\mathbf{x}}_0)\mathbf{r}_1 - \mathbf{B}_\mathbf{x}(\mathbf{q},\dot{\mathbf{x}})\mathbf{r}_2 \\ - (\boldsymbol{\tau}_\mathbf{x}(\mathbf{q},\dot{\mathbf{q}}) - \boldsymbol{\tau}_\mathbf{x}(\mathbf{q},\dot{\hat{\mathbf{q}}})) - \boldsymbol{\eta} \end{aligned} \tag{5.21}$$

Substituting (5.21) into (5.19), the *observer closed-loop dynamics* can be obtained as:

$$\begin{aligned} \mathbf{M}_\mathbf{x}(\mathbf{q})\dot{\mathbf{r}}_2 = &- (\mathbf{M}_\mathbf{x}(\mathbf{q})\mathbf{l}_D - \mathbf{M}_\mathbf{x}(\mathbf{q})\mathbf{\Lambda}_1)\mathbf{r}_2 + \mathbf{M}_\mathbf{x}(\mathbf{q})\mathbf{\Lambda}_1\mathbf{r}_1 \\ &- \mathbf{B}_\mathbf{x}(\mathbf{q},\dot{\mathbf{x}})\mathbf{r}_2 + \mathbf{B}_\mathbf{x}(\mathbf{q},\dot{\mathbf{x}}_0)\mathbf{r}_1 - (\boldsymbol{\tau}_\mathbf{x}(\mathbf{q},\dot{\mathbf{q}}) - \boldsymbol{\tau}_\mathbf{x}(\mathbf{q},\dot{\hat{\mathbf{q}}})) - \boldsymbol{\eta}. \end{aligned} \tag{5.22}$$

It can be shown that, the model-based equivalent [109] of the motion control (5.2) with its observer (5.16) - (5.17), i.e. $\boldsymbol{\eta} = 0$ in (5.15) and (5.22), showed that the local asymptotic stability can be achieved.

5.3.4 Uncertainties η in NN terms

Now, similar with Section 4.4.2, $\mathbf{M}_{\mathbf{x}}(\mathbf{q})$, $\mathbf{B}_{\mathbf{x}}(\mathbf{q}, \dot{\mathbf{x}}_0)$, $\mathbf{g}_{\mathbf{x}}(\mathbf{q})$, and $\boldsymbol{\tau}_{\mathbf{x}}(\mathbf{q}, \dot{\hat{\mathbf{q}}})$ in $\boldsymbol{\eta}$ (5.12) can be described as follows

$$\mathbf{M}_{\mathbf{x}}(\mathbf{q}) = \mathbf{W}_M^{\mathrm{T}} \, \boldsymbol{\sigma}_M(\mathbf{V}_M^{\mathrm{T}} \, \mathbf{z}_M) + \boldsymbol{\varepsilon}_M \tag{5.23}$$

$$\mathbf{B}_{\mathbf{x}}(\mathbf{q}, \dot{\mathbf{x}}_0) = \mathbf{W}_B^{\mathrm{T}} \, \boldsymbol{\sigma}_B(\mathbf{V}_B^{\mathrm{T}} \, \mathbf{z}_B) + \boldsymbol{\varepsilon}_B \tag{5.24}$$

$$\mathbf{g}_{\mathbf{x}}(\mathbf{q}) = \mathbf{W}_g^{\mathrm{T}} \, \boldsymbol{\sigma}_g(\mathbf{V}_g^{\mathrm{T}} \, \mathbf{z}_g) + \boldsymbol{\varepsilon}_g \tag{5.25}$$

$$\boldsymbol{\tau}_{\mathbf{x}}(\mathbf{q}, \dot{\hat{\mathbf{q}}}) = \mathbf{W}_\tau^{\mathrm{T}} \, \boldsymbol{\sigma}_\tau(\mathbf{V}_\tau^{\mathrm{T}} \, \mathbf{z}_\tau) + \boldsymbol{\varepsilon}_\tau \tag{5.26}$$

Similarly, the estimated dynamic terms $\hat{\mathbf{M}}_{\mathbf{x}}(\mathbf{q})$, $\hat{\mathbf{B}}_{\mathbf{x}}(\mathbf{q}, \dot{\mathbf{x}}_0)$, $\hat{\mathbf{g}}_{\mathbf{x}}(\mathbf{q})$, and $\hat{\boldsymbol{\tau}}_{\mathbf{x}}(\mathbf{q}, \dot{\hat{\mathbf{q}}})$ are described by estimated weights $\hat{\mathbf{V}}_p, \hat{\mathbf{W}}_p$, with subscript $p = M, B, g, \tau$.

It is clear that $\mathbf{M}_{\mathbf{x}}(\mathbf{q})$ and $\mathbf{g}_{\mathbf{x}}(\mathbf{q})$ can be been shown to be bounded by Properties 4.3.1 and 4.3.4, respectively. Using Property 4.3.3, the boundedness of $\mathbf{B}_{\mathbf{x}}(\mathbf{q}, \dot{\mathbf{x}}_0)$ depends on $\|\dot{\mathbf{x}}_0\|$ (5.4), which in turn depends on $\|\dot{\hat{\mathbf{x}}}\|, \|\hat{\mathbf{x}}\|$ and $\|\mathbf{x}\|$: $\mathbf{x}$ is directly bounded by the workspace. The estimated velocity, $\|\dot{\hat{\mathbf{x}}}\|$, can be assumed to be bounded, $\|\dot{\hat{\mathbf{x}}}\| \leq \dot{\hat{x}}_M$, since in the implementation it is possible to set $-\dot{\hat{x}}_M \leq \dot{\hat{\mathbf{x}}} \leq \dot{\hat{x}}_M$. This implies that $\|\hat{\mathbf{x}}\|$ is bounded since it is obtained from $\dot{\hat{\mathbf{x}}}$ (see Section 5.4. Computation of Estimated Operational Space Coordinates). Therefore $\|\dot{\mathbf{x}}_0\|$ is bounded. The boundedness of $\boldsymbol{\tau}_{\mathbf{x}}(\mathbf{q}, \dot{\hat{\mathbf{q}}})$ can be shown by using Property 3.2.4 and the fact that $\|\mathbf{J}^{-1}(\mathbf{q})\|$ is bounded for non-singular configuration and $\dot{\hat{\mathbf{x}}}$ is bounded, implying $\dot{\hat{\mathbf{q}}}$ is bounded. Therefore, the optimum

weights $\mathbf{W}_p, \mathbf{V}_p$ and the approximation error $\boldsymbol{\varepsilon}_p$ (with subscript $p = M, B, g, \tau$) from (5.23)-(5.26), are also upper-bounded.

Using similar development and simplified notations $\boldsymbol{\sigma} \equiv \boldsymbol{\sigma}(\mathbf{V}^{\mathrm{T}}\mathbf{z})$, $\hat{\boldsymbol{\sigma}} \equiv \boldsymbol{\sigma}(\hat{\mathbf{V}}^{\mathrm{T}}\mathbf{z})$, and $\boldsymbol{\sigma} = \hat{\boldsymbol{\sigma}} + \tilde{\boldsymbol{\sigma}}$ as in Section 4.4.2, the uncertainties $\boldsymbol{\eta}$ (5.12) can be written as

$$\boldsymbol{\eta} = \boldsymbol{\xi} + \boldsymbol{\zeta}. \tag{5.27}$$

This division is needed because only $\boldsymbol{\xi}$ term can be manipulated by the weight updates $\dot{\hat{\mathbf{W}}}, \dot{\hat{\mathbf{V}}}$ as will be shown in Section 5.3.5.

The term $\boldsymbol{\xi}$ is defined as

$$\begin{aligned}\boldsymbol{\xi} = &\left(\tilde{\mathbf{W}}_M^{\mathrm{T}}\hat{\boldsymbol{\sigma}}_M\right)\mathbf{F}^*_{\mathrm{motion}} + \left(\tilde{\mathbf{W}}_B^{\mathrm{T}}\hat{\boldsymbol{\sigma}}_B\right)\dot{\mathbf{x}}_r + \tilde{\mathbf{W}}_g^{\mathrm{T}}\hat{\boldsymbol{\sigma}}_g + \tilde{\mathbf{W}}_\tau^{\mathrm{T}}\hat{\boldsymbol{\sigma}}_\tau \\ &+ \left(\hat{\mathbf{W}}_M^{\mathrm{T}}\hat{\boldsymbol{\sigma}}'_M\tilde{\mathbf{V}}_M^{\mathrm{T}}\mathbf{z}_M\right)\mathbf{F}^*_{\mathrm{motion}} + \left(\hat{\mathbf{W}}_B^{\mathrm{T}}\hat{\boldsymbol{\sigma}}'_B\tilde{\mathbf{V}}_B^{\mathrm{T}}\mathbf{z}_B\right)\dot{\mathbf{x}}_r \\ &+ \hat{\mathbf{W}}_g^{\mathrm{T}}\hat{\boldsymbol{\sigma}}'_g\tilde{\mathbf{V}}_g^{\mathrm{T}}\mathbf{z}_g + \hat{\mathbf{W}}_\tau^{\mathrm{T}}\hat{\boldsymbol{\sigma}}'_\tau\tilde{\mathbf{V}}_\tau^{\mathrm{T}}\mathbf{z}_\tau\end{aligned} \tag{5.28}$$

and the "whole"NN errors $\boldsymbol{\zeta}$ is defined as

$$\begin{aligned}\boldsymbol{\zeta} = &\left(\tilde{\mathbf{W}}_M^{\mathrm{T}}\hat{\boldsymbol{\sigma}}'_M\tilde{\mathbf{V}}_M^{\mathrm{T}}\mathbf{z}_M\right)\mathbf{F}^*_{\mathrm{motion}} + \left(\tilde{\mathbf{W}}_B^{\mathrm{T}}\hat{\boldsymbol{\sigma}}'_B\tilde{\mathbf{V}}_B^{\mathrm{T}}\mathbf{z}_B\right)\dot{\mathbf{x}}_r \\ &+ \tilde{\mathbf{W}}_g^{\mathrm{T}}\hat{\boldsymbol{\sigma}}'_g\tilde{\mathbf{V}}_g^{\mathrm{T}}\mathbf{z}_g + \tilde{\mathbf{W}}_\tau^{\mathrm{T}}\hat{\boldsymbol{\sigma}}'_\tau\tilde{\mathbf{V}}_\tau^{\mathrm{T}}\mathbf{z}_\tau \\ &+ \left(\mathbf{W}_M^{\mathrm{T}}O(\tilde{\mathbf{V}}_M^{\mathrm{T}}\mathbf{z}_M)\right)\mathbf{F}^*_{\mathrm{motion}} + \left(\mathbf{W}_B^{\mathrm{T}}O(\tilde{\mathbf{V}}_B^{\mathrm{T}}\mathbf{z}_B)\right)\dot{\mathbf{x}}_r \\ &+ \mathbf{W}_g^{\mathrm{T}}O(\tilde{\mathbf{V}}_g^{\mathrm{T}}\mathbf{z}_g) + \mathbf{W}_\tau^{\mathrm{T}}O(\tilde{\mathbf{V}}_\tau^{\mathrm{T}}\mathbf{z}_\tau) + \boldsymbol{\varepsilon}\end{aligned} \tag{5.29}$$

where the total approximation error $\boldsymbol{\varepsilon} = \boldsymbol{\varepsilon}_M\,\mathbf{F}^*_{\mathrm{motion}} + \boldsymbol{\varepsilon}_B\,\dot{\mathbf{x}}_r + \boldsymbol{\varepsilon}_g + \boldsymbol{\varepsilon}_\tau \leq \varepsilon_M$ (since the actual dynamics are bounded). Note that, the driving signals $\dot{\mathbf{x}}_r$ (5.3) and $\mathbf{F}^*_{\mathrm{motion}}$ (5.5), used in (5.28) and (5.29), are different with $\dot{\mathbf{x}}_r$ and $\mathbf{F}^*_{\mathrm{motion}}$ in Section 4.4.2.

As in Section 4.4.2, the uncertainties $\boldsymbol{\eta}$ (5.27) can be seen to be bounded with the generic expression $\|\mathbf{L}_p - \hat{\mathbf{L}}_p\| \leq (\tilde{L}_p)_M$ in (4.47) and also $\mathbf{F}^*_{\mathrm{motion}}$ (5.5) and

$\dot{\mathbf{x}}_r$ in (5.7), as follows

$$\begin{aligned}\|\boldsymbol{\eta}\| &\leq (\tilde{L}_M)_M \, \|\mathbf{F}^*_{\text{motion}}\| + (\tilde{L}_B)_M \, \|\dot{\mathbf{x}}_r\| + (\tilde{L}_g)_M + (\tilde{L}_\tau)_M + \varepsilon_M \\ &\leq (\tilde{L}_M)_M \, (\|\ddot{\mathbf{x}}_r\| + \boldsymbol{\Lambda}_1(\|\mathbf{r}_1\| + \|\mathbf{r}_2\|)) + (\tilde{L}_B)_M \, (\|\mathbf{r}_1\| + \|\mathbf{r}_2\| + \|\dot{\mathbf{x}}_0\|) \\ &\quad + (\tilde{L}_g)_M + (\tilde{L}_\tau)_M + \varepsilon_M\end{aligned} \tag{5.30}$$

Note that $\ddot{\mathbf{x}}_r$ in (5.6) can be assumed to be bounded since the desired trajectories $\ddot{\mathbf{x}}_d, \dot{\mathbf{x}}_d, \mathbf{x}_d$ are bounded by design, $\mathbf{x}$ is bounded by the workspace and $\hat{\mathbf{x}}$ is bounded due to $\dot{\hat{\mathbf{x}}}$ can be shown to be bounded. And $\dot{\mathbf{x}}_0$ in (5.4) can be shown to be bounded due to $\dot{\hat{\mathbf{x}}}$ and $\hat{\mathbf{x}}$ can be shown to be bounded.

Therefore $\boldsymbol{\eta}$ can be shown to be bounded as

$$\|\boldsymbol{\eta}\| \leq C_0 + C_1 \, (\|\mathbf{r}_1\| + \|\mathbf{r}_2\|). \tag{5.31}$$

where $C_0, C_1 > 0$. And since $\boldsymbol{\eta} = \boldsymbol{\xi} + \boldsymbol{\zeta}$, then clearly the following inequalities are true

$$\|\boldsymbol{\xi}\| \leq C_0 + C_1 \, (\|\mathbf{r}_1\| + \|\mathbf{r}_2\|) \tag{5.32}$$

$$\|\boldsymbol{\zeta}\| \leq C_0 + C_1 \, (\|\mathbf{r}_1\| + \|\mathbf{r}_2\|). \tag{5.33}$$

Note that, the definitions of $\mathbf{r}_1$ (5.9) and $\mathbf{r}_2$ (5.10) in this section, are different with the definition of $\mathbf{r}$ in Section 4.4.2.

For ease of later developments, let us define $\mathbf{Z} = \text{diag}[\mathbf{W}, \mathbf{V}]$ to be upper-bounded as follows

$$\|\mathbf{Z}\| = \sqrt{\|\mathbf{W}\|^2 + \|\mathbf{V}\|^2} \leq Z_M \tag{5.34}$$

where Z_M is a positive scalar constant, $\mathbf{W} = \text{diag}[\mathbf{W}_M, \mathbf{W}_B, \mathbf{W}_g, \mathbf{W}_\tau]$ and $\mathbf{V} = \text{diag}[\mathbf{V}_M, \mathbf{V}_B, \mathbf{V}_g, \mathbf{V}_\tau]$.

5.3.5 Stability Analysis

For the motion control (5.2) and the observer (5.16), (5.17), let the NN weight updates be provided as

$$\dot{\hat{\mathbf{w}}}_{M_{ij}} = \mathbf{F}_{M_{ij}}(\hat{\boldsymbol{\sigma}}_M\ (r_{1,i} + r_{2,i})\ F^*_{\text{motion}j} - \kappa\ \hat{\mathbf{w}}_{M_{ij}}) \tag{5.35}$$

$$\dot{\hat{\mathbf{v}}}_{M_k} = \mathbf{G}_{M_k}(\mathbf{z}_M\ \hat{\boldsymbol{\sigma}}'_{M_k}\ (\sum_{i=1}^{m}\sum_{j=1}^{m} \hat{w}_{M_{ijk}}\ (r_{1,i} + r_{2,i})\ F^*_{\text{motion}j}) - \kappa\ \hat{\mathbf{v}}_{M_k}) \tag{5.36}$$

$$\dot{\hat{\mathbf{w}}}_{B_{ij}} = \mathbf{F}_{B_{ij}}(\hat{\boldsymbol{\sigma}}_B\ (r_{1,i} + r_{2,i})\ \dot{x}_{rj} - \kappa\ \hat{\mathbf{w}}_{B_{ij}}) \tag{5.37}$$

$$\dot{\hat{\mathbf{v}}}_{B_k} = \mathbf{G}_{B_k}(\mathbf{z}_B\ \hat{\boldsymbol{\sigma}}'_{B_k}\ (\sum_{i=1}^{m}\sum_{j=1}^{m} \hat{w}_{B_{ijk}}\ (r_{1,i} + r_{2,i})\ \dot{x}_{rj}) - \kappa\ \hat{\mathbf{v}}_{B_k}) \tag{5.38}$$

$$\dot{\hat{\mathbf{w}}}_{g_i} = \mathbf{F}_{g_i}(\hat{\boldsymbol{\sigma}}_g\ (r_{1,i} + r_{2,i}) - \kappa\ \hat{\mathbf{w}}_{g_i}) \tag{5.39}$$

$$\dot{\hat{\mathbf{v}}}_{g_k} = \mathbf{G}_{g_k}(\mathbf{z}_g\ \hat{\boldsymbol{\sigma}}'_{g_k}\ (\sum_{i=1}^{m} \hat{w}_{g_{ik}}\ (r_{1,i} + r_{2,i})) - \kappa\ \hat{\mathbf{v}}_{g_k}) \tag{5.40}$$

$$\dot{\hat{\mathbf{w}}}_{\tau_i} = \mathbf{F}_{\tau_i}(\hat{\boldsymbol{\sigma}}_\tau\ (r_{1,i} + r_{2,i}) - \kappa\ \hat{\mathbf{w}}_{\tau_i}) \tag{5.41}$$

$$\dot{\hat{\mathbf{v}}}_{\tau_k} = \mathbf{G}_{\tau_k}(\mathbf{z}_\tau\ \hat{\boldsymbol{\sigma}}'_{\tau_k}\ (\sum_{i=1}^{m} \hat{w}_{\boldsymbol{\tau}ik}\ (r_{1,i} + r_{2,i})) - \kappa\ \hat{\mathbf{v}}_{\tau_k}) \tag{5.42}$$

with κ is a positive constant. And the estimated NN weight updates: $\dot{\hat{\mathbf{w}}}_{M_{ij}} \in \Re^{N_2}, \dot{\hat{\mathbf{v}}}_{M_k} \in \Re^{N_{1,M}}, \dot{\hat{\mathbf{w}}}_{B_{ij}} \in \Re^{N_2}, \dot{\hat{\mathbf{v}}}_{B_k} \in \Re^{N_{1,B}}, \dot{\hat{\mathbf{w}}}_{g_i} \in \Re^{N_2}, \dot{\hat{\mathbf{v}}}_{g_k} \in \Re^{N_{1,g}}, \dot{\hat{\mathbf{w}}}_{\tau_i} \in \Re^{N_2}$, $\dot{\hat{\mathbf{v}}}_{\tau_k} \in \Re^{N_{1,\tau}}$ are all column vector. And the adaptive gains: $\mathbf{F}^{-1}_{M_{ij}} \in \Re^{N_2 \times N_2}, \ldots$, $\mathbf{F}^{-1}_{\tau_i} \in \Re^{N_2 \times N_2}$ and $\mathbf{G}^{-1}_{M_k} \in \Re^{N_{1,M} \times N_{1,M}}, \ldots, \mathbf{G}^{-1}_{\tau_k} \in \Re^{N_{1,\tau} \times N_{1,\tau}}$ are all positive diagonal matrices. The following indices are defined: $i, j = 1, \ldots, m$ are output-layer indices, $k = 1, \ldots, N_2$ is the hidden-layer index, where to simplify the implementation, the hidden-node size N_2 is set the same for all dynamic parameters. While $N_{1,M}, N_{1,B}, N_{1,g}, N_{1,\tau}$ are the respective input-node sizes.

Proposition 5.3.1 *Let* $\mathbf{y} = [\mathbf{r}_1^{\mathrm{T}}\ \mathbf{r}_2^{\mathrm{T}}]^{\mathrm{T}}$. *With the assumptions that:*

1. *the controller gain* $\mathbf{\Lambda}_1$ *and the observer gain* l_D *meet the conditions*

$$\Lambda_{1,m} > \frac{C_1}{M_{x,m}} \tag{5.43}$$

$$l_{D,m} > \frac{M_{x,M}\ \Lambda_{1,M} + \ 3\ C_1}{M_{x,m}} \tag{5.44}$$

where $C_1 > 0$, $\Lambda_{1,m} = min(\mathbf{\Lambda}_1)$, $\Lambda_{1,M} = max(\mathbf{\Lambda}_1)$, $M_{x,m} = min(\lambda_{min}(\mathbf{M}_{\mathbf{x}}(t)))$, $M_{x,M} = min(\lambda_{max}(\mathbf{M}_{\mathbf{x}}(t)))$ *and* $l_{D,m} = min(\mathrm{l}_D)$*;*

2. y_M*, the upper-bound constraint of* $\mathbf{y}$*, and,* $\hat{Z}_M$*, the upper-bound of the estimated NN weights,* $\hat{\mathbf{Z}}$*, satisfy*

$$y_M > \ b_y \tag{5.45}$$

$$\hat{Z}_M > \ \sqrt{\frac{((\tau_{fric})_M + 3\ C_0)^2}{4\ \kappa\ \Psi_m}} \tag{5.46}$$

where $C_0, \kappa > 0$, $(\tau_{fric})_M$ *is the upper-bound of* $\|\boldsymbol{\tau}_{\mathbf{x}}(\mathbf{q}, \dot{\mathbf{q}}) - \boldsymbol{\tau}_{\mathbf{x}}(\mathbf{q}, \dot{\hat{\mathbf{q}}})\|$, $\Psi_m = min(\mathbf{\Psi})$ *with* $\mathbf{\Psi}$ *is to be defined in* (5.60)*, and* b_y *is to be defined in* (5.64)*; and*

3. *both initial conditions of* $\mathbf{y}$ *and* $\tilde{\mathbf{Z}}$ *satisfy*

$$\|\mathbf{y}(0)\| < y_M \tag{5.47}$$

$$\|\tilde{\mathbf{Z}}(0)\| < \tilde{Z}_M \tag{5.48}$$

where $\tilde{Z}_M$ *is the upper-bound of the NN weight errors,* $\tilde{\mathbf{Z}}$*;*

then using the proposed motion control (5.2)*, the observer* (5.16) – (5.17) *and the NN weight updates* (5.35)-(5.42)*, it can be shown by Lyapunov's Extension Theorem [102] that as* $t \to \infty$*, the errors* $\|\mathbf{r}_1\|$, $\|\mathbf{r}_2\|$ *and* $\|\tilde{\mathbf{W}}\|, \|\tilde{\mathbf{V}}\|$

will be bounded by enclosing boundary $\mathcal{S}$, which is defined by enclosing region $\dot{V}(\mathbf{y}, \tilde{\mathbf{Z}}) < 0$.

Proof 5.3.1 *The chosen Lyapunov function candidate for the closed-loop error dynamics* (5.15) *and* (5.22)*, with the uncertainties* $\boldsymbol{\eta}$ (5.27)*, is*

$$\begin{aligned} V(\mathbf{r}_1, \mathbf{r}_2, \tilde{\mathbf{Z}}) = & \frac{1}{2}\, \mathbf{r}_1^{\mathrm{T}} \mathbf{M}_{\mathbf{x}}(\mathbf{q}) \mathbf{r}_1 + \frac{1}{2}\, \mathbf{r}_2^{\mathrm{T}} \mathbf{M}_{\mathbf{x}}(\mathbf{q}) \mathbf{r}_2 \\ & + \frac{1}{2} \sum_{i=1}^{m} \sum_{j=1}^{m} \tilde{\mathbf{w}}_{M_{ij}}^{\mathrm{T}}\, \mathbf{F}_{M_{ij}}^{-1}\, \tilde{\mathbf{w}}_{M_{ij}} + \ldots + \frac{1}{2} \sum_{i=1}^{m} \tilde{\mathbf{w}}_{\tau_i}^{\mathrm{T}}\, \mathbf{F}_{\tau_i}^{-1}\, \tilde{\mathbf{w}}_{\tau_i} \\ & + \frac{1}{2} \sum_{k=1}^{N_2} \tilde{\mathbf{v}}_{M_k}^{\mathrm{T}}\, \mathbf{G}_{M_k}^{-1}\, \tilde{\mathbf{v}}_{M_k} + \ldots + \frac{1}{2} \sum_{k=1}^{N_2} \tilde{\mathbf{v}}_{\tau_k}^{\mathrm{T}}\, \mathbf{G}_{\tau_k}^{-1}\, \tilde{\mathbf{v}}_{\tau_k} \end{aligned} \tag{5.49}$$

where the NN weight errors: $\tilde{\mathbf{w}}_{M_{ij}} \in \Re^{N_2}, \tilde{\mathbf{v}}_{M_k} \in \Re^{N_{1,M}}, \tilde{\mathbf{w}}_{B_{ij}} \in \Re^{N_2}, \tilde{\mathbf{v}}_{B_k} \in \Re^{N_{1,B}}, \tilde{\mathbf{w}}_{g_i} \in \Re^{N_2}, \tilde{\mathbf{v}}_{g_k} \in \Re^{N_{1,g}}, \tilde{\mathbf{w}}_{\tau_i} \in \Re^{N_2}, \tilde{\mathbf{v}}_{\tau_k} \in \Re^{N_{1,\tau}}$ *are all column vector.*

Next, we substitute the closed-loop error dynamics (5.15)*,* (5.22)*, Property 4.3.5 and also take into account* $\boldsymbol{\eta}$ (5.27)*, with the definition* $\boldsymbol{\xi}$ (5.28) *and the knowledge* $\|\boldsymbol{\zeta}\| \leq C_0 + C_1(\|\mathbf{r}_1\| + \|\mathbf{r}_2\|)$ (5.33)*, into* $\dot{V}(\mathbf{r}_1, \mathbf{r}_2, \tilde{\mathbf{Z}})$ *of* (5.49)*, to obtain*

$$\begin{aligned} \dot{V}(\mathbf{r}_1, \mathbf{r}_2, \tilde{\mathbf{Z}}) \leq & - \mathbf{r}_1^{\mathrm{T}} \mathbf{M}_{\mathbf{x}}(\mathbf{q}) \boldsymbol{\Lambda}_1 \mathbf{r}_1 - \mathbf{r}_2^{\mathrm{T}} (\mathbf{M}_{\mathbf{x}}(\mathbf{q}) \mathbf{l}_D - \mathbf{M}_{\mathbf{x}}(\mathbf{q}) \boldsymbol{\Lambda}_1) \mathbf{r}_2 \\ & + \mathbf{r}_1^{\mathrm{T}} \mathbf{B}_{\mathbf{x}}(\mathbf{q}, \dot{\mathbf{x}}_r) \mathbf{r}_2 + \mathbf{r}_2^{\mathrm{T}} \mathbf{B}_{\mathbf{x}}(\mathbf{q}, \dot{\mathbf{x}}_0) \mathbf{r}_1 \\ & + (\mathbf{r}_1^{\mathrm{T}} - \mathbf{r}_2^{\mathrm{T}})\, (\boldsymbol{\tau}_{\mathbf{x}}(\mathbf{q}, \dot{\mathbf{q}}) - \boldsymbol{\tau}_{\mathbf{x}}(\mathbf{q}, \dot{\hat{\mathbf{q}}})) \\ & + C_0 \|\mathbf{r}_1\| + C_0 \|\mathbf{r}_2\| + C_1 \|\mathbf{r}_1\|^2 + 2\, C_1 \|\mathbf{r}_1\| \|\mathbf{r}_2\| + C_2 \|\mathbf{r}_2\|^2 \\ & + \boldsymbol{\psi} \end{aligned} \tag{5.50}$$

where the lump parameter $\boldsymbol{\psi}$ *in* (5.50) *is defined as*

$$
\begin{aligned}
\boldsymbol{\psi} = & \sum_{i=1}^{m}\sum_{j=1}^{m} \tilde{\mathbf{w}}_{M_{ij}}^{\mathrm{T}} \left(\mathbf{F}_{M_{ij}}^{-1} \, \dot{\tilde{\mathbf{w}}}_{M_{ij}} + \hat{\boldsymbol{\sigma}}_M \, (r_{1,i} - r_{2,i}) \, F^*_{\mathrm{motion}j} \right) \\
& + \sum_{k=1}^{N_2} \tilde{\mathbf{v}}_{M_k}^{\mathrm{T}} \left(\mathbf{G}_{M_k}^{-1} \, \dot{\tilde{\mathbf{v}}}_{M_k} + \mathbf{z}_M \, \hat{\boldsymbol{\sigma}}'_{M_k} (\sum_{i=1}^{m}\sum_{j=1}^{m} \hat{w}_{M_{ijk}} \, (r_{1,i} - r_{2,i}) \, F^*_{\mathrm{motion}j}) \right) \\
& + \sum_{i=1}^{m}\sum_{j=1}^{m} \tilde{\mathbf{w}}_{B_{ij}}^{\mathrm{T}} \left(\mathbf{F}_{B_{ij}}^{-1} \, \dot{\tilde{\mathbf{w}}}_{B_{ij}} + \hat{\boldsymbol{\sigma}}_B \, (r_{1,i} - r_{2,i}) \, \dot{x}_{rj} \right) \\
& + \sum_{k=1}^{N_2} \tilde{\mathbf{v}}_{B_k}^{\mathrm{T}} \left(\mathbf{G}_{B_k}^{-1} \, \dot{\tilde{\mathbf{v}}}_{B_k} + \mathbf{z}_B \, \hat{\boldsymbol{\sigma}}'_{B_k} (\sum_{i=1}^{m}\sum_{j=1}^{m} \hat{w}_{B_{ijk}} \, (r_{1,i} - r_{2,i}) \, \dot{x}_{rj}) \right) \\
& + \sum_{i=1}^{m} \tilde{\mathbf{w}}_{g_i}^{\mathrm{T}} \left(\mathbf{F}_{g_i}^{-1} \, \dot{\tilde{\mathbf{w}}}_{g_i} + \hat{\boldsymbol{\sigma}}_g \, (r_{1,i} - r_{2,i}) \right) \\
& + \sum_{k=1}^{N_2} \tilde{\mathbf{v}}_{g_k}^{\mathrm{T}} \left(\mathbf{G}_{g_k}^{-1} \, \dot{\tilde{\mathbf{v}}}_{g_k} + \mathbf{z}_g \, \hat{\boldsymbol{\sigma}}'_{g_k} (\sum_{i=1}^{m} \hat{w}_{g_{ik}} \, (r_{1,i} - r_{2,i})) \right) \\
& + \sum_{i=1}^{m} \tilde{\mathbf{w}}_{\tau_i}^{\mathrm{T}} \left(\mathbf{F}_{\tau_i}^{-1} \, \dot{\tilde{\mathbf{w}}}_{\tau_i} + \hat{\boldsymbol{\sigma}}_\tau \, (r_{1,i} - r_{2,i}) \right) \\
& + \sum_{k=1}^{N_2} \tilde{\mathbf{v}}_{\tau_k}^{\mathrm{T}} \left(\mathbf{G}_{\tau_k}^{-1} \, \dot{\tilde{\mathbf{v}}}_{\tau_k} + \mathbf{z}_\tau \, \hat{\boldsymbol{\sigma}}'_{\tau_k} (\sum_{i=1}^{m} \hat{w}_{\boldsymbol{\tau}_{ik}} \, (r_{1,i} - r_{2,i})) \right).
\end{aligned}
\tag{5.51}
$$

Using $\boldsymbol{\xi}$ (5.28)*, it can be demonstrated that* $\boldsymbol{\psi}$ (5.51) *is made up of* $\dot{\tilde{\mathbf{W}}}, \dot{\tilde{\mathbf{V}}}$ *and* $(\mathbf{r}_1 - \mathbf{r}_2)^{\mathrm{T}} \, \boldsymbol{\xi}$*. The idea is to cancel* $(\mathbf{r}_1 - \mathbf{r}_2)^{\mathrm{T}} \, \boldsymbol{\xi}$ *with* $\dot{\tilde{\mathbf{W}}}, \dot{\tilde{\mathbf{V}}}$*. Unfortunately, only* $(\mathbf{r}_1 + \mathbf{r}_2)$ *can be computed (see* (5.7)*), hence only* $\mathbf{r}_1^{\mathrm{T}} \, \boldsymbol{\xi}$ *can be canceled by* $\dot{\hat{\mathbf{W}}}, \dot{\hat{\mathbf{V}}}$*. With the weight updates* $\dot{\hat{\mathbf{W}}}, \dot{\hat{\mathbf{V}}}$ (5.35) – (5.42) *(note that* $-\dot{\tilde{\mathbf{W}}} = \dot{\hat{\mathbf{W}}}$*, since* $\tilde{\mathbf{W}} = \mathbf{W} - \hat{\mathbf{W}}$ *and* $\mathbf{W}$ *is constant), and taking into consideration* $\|\boldsymbol{\xi}\| \leq \; C_0 + C_1(\|\mathbf{r}_1\| + \|\mathbf{r}_2\|)$ (5.32)*,* $\boldsymbol{\psi}$ (5.51) *can be expressed as:*

$$
\begin{aligned}
\boldsymbol{\psi} &= \kappa \sum_{i=1}^{m}\sum_{j=1}^{m} \tilde{\mathbf{w}}_{M_{ij}}^{\mathrm{T}} \hat{\mathbf{w}}_{M_{ij}} + \ldots + \kappa \sum_{k=1}^{N_2} \tilde{\mathbf{v}}_{\tau_k}^{\mathrm{T}} \hat{\mathbf{v}}_{\tau_k} - 2 \, \mathbf{r}_2^{\mathrm{T}} \, \boldsymbol{\xi} \\
&\leq - \kappa \|\tilde{\mathbf{Z}}\|^2 + \kappa \|\tilde{\mathbf{Z}}\| Z_M + 2 \, C_0 \|\mathbf{r}_2\| + 2 \, C_1 \|\mathbf{r}_1\| \|\mathbf{r}_2\| + 2 \, C_1 \|\mathbf{r}_2\|^2.
\end{aligned}
\tag{5.52}
$$

Equation (5.52) *is obtained by using the inner products in* (4.68) – (4.71)*.*

The substitution of $\boldsymbol{\psi}$ (5.52) *into* $\dot{V}(\mathbf{r}_1, \mathbf{r}_2, \tilde{\mathbf{Z}})$ (5.50)*, yields*

$$\begin{aligned}\dot{V}(\mathbf{r}_1, \mathbf{r}_2, \tilde{\mathbf{Z}}) \leq & -\mathbf{r}_1^{\mathrm{T}}(\mathbf{M}_{\mathbf{x}}(\mathbf{q})\boldsymbol{\Lambda}_1)\mathbf{r}_1 - \mathbf{r}_2^{\mathrm{T}}(\mathbf{M}_{\mathbf{x}}(\mathbf{q})\mathbf{l}_D - \mathbf{M}_{\mathbf{x}}(\mathbf{q})\boldsymbol{\Lambda}_1)\mathbf{r}_2 \\ & + \mathbf{r}_1^{\mathrm{T}}\mathbf{B}_{\mathbf{x}}(\mathbf{q}, \dot{\mathbf{x}}_r)\mathbf{r}_2 + \mathbf{r}_2^{\mathrm{T}}\mathbf{B}_{\mathbf{x}}(\mathbf{q}, \dot{\mathbf{x}}_0)\mathbf{r}_1 \\ & + (\mathbf{r}_1^{\mathrm{T}} - \mathbf{r}_2^{\mathrm{T}})\left(\boldsymbol{\tau}_{\mathbf{x}}(\mathbf{q}, \dot{\mathbf{q}}) - \boldsymbol{\tau}_{\mathbf{x}}(\mathbf{q}, \dot{\hat{\mathbf{q}}})\right) \\ & + C_0\|\mathbf{r}_1\| + 3\,C_0\|\mathbf{r}_2\| + C_1\|\mathbf{r}_1\|^2 + 4\,C_1\|\mathbf{r}_1\|\|\mathbf{r}_2\| + 3\,C_1\|\mathbf{r}_2\|^2 \\ & - \kappa\|\tilde{\mathbf{Z}}\|^2 + \kappa\|\tilde{\mathbf{Z}}\|Z_M\end{aligned} \tag{5.53}$$

The terms in (5.53) *can be analysed for its boundedness: The following terms, using Property 4.2, can be written as:*

$$-\mathbf{r}_1^{\mathrm{T}}\mathbf{M}_{\mathbf{x}}(\mathbf{q})\boldsymbol{\Lambda}_1\mathbf{r}_1 \leq -M_{x,m}\,\Lambda_{1,m}\|\mathbf{r}_1\|^2 \tag{5.54}$$

$$-\mathbf{r}_2^{\mathrm{T}}(\mathbf{M}_{\mathbf{x}}(\mathbf{q})\mathbf{l}_D - \mathbf{M}_{\mathbf{x}}(\mathbf{q})\boldsymbol{\Lambda}_1)\mathbf{r}_2 \leq -(M_{x,m}l_{D,m} - M_{x,M}\Lambda_{1,M})\|\mathbf{r}_2\|^2 \tag{5.55}$$

where $\Lambda_{1,m}, \Lambda_{1,M}, M_{x,m}, M_{x,M}, l_{D,m}$ *are as defined in* (5.43) *and* (5.44)*.*

The next terms, by taking into account Property 4.3.3, can be written as:

$$\begin{aligned}&\|\mathbf{r}_1^{\mathrm{T}}\mathbf{B}_{\mathbf{x}}(\mathbf{q}, \dot{\mathbf{x}}_r)\mathbf{r}_2\| + \|\mathbf{r}_2^{\mathrm{T}}\mathbf{B}_{\mathbf{x}}(\mathbf{q}, \dot{\mathbf{x}}_0)\mathbf{r}_1\| \\ \leq &\|\mathbf{r}_1\|\|\mathbf{r}_2\|B_{x,M}(\|\mathbf{r}_1\| + \|\mathbf{r}_2\| + 2\dot{x}_M).\end{aligned} \tag{5.56}$$

This is due to the facts $\dot{\mathbf{x}}_r = \mathbf{r}_1 + \dot{\mathbf{x}}$ *in* (5.9) *and* $\dot{\mathbf{x}}_0 = \dot{\mathbf{x}} - \mathbf{r}_2$ *in* (5.10)*.*

And the final term, $\boldsymbol{\tau}_{\mathbf{x}}(\mathbf{q}, \dot{\mathbf{q}}) - \boldsymbol{\tau}_{\mathbf{x}}(\mathbf{q}, \dot{\hat{\mathbf{q}}})$*, had been shown to be bounded in* (4.118)*, however, it is reproduced here for ease of perusal:*

$$\|\boldsymbol{\tau}_{\mathbf{x}}(\mathbf{q}, \dot{\mathbf{q}}) - \boldsymbol{\tau}_{\mathbf{x}}(\mathbf{q}, \dot{\hat{\mathbf{q}}})\| \leq (\tau_{fric})_M. \tag{5.57}$$

which is obtained from (5.13)*, Property 3.2.4 and the followings:*

1. $\|\mathbf{J}^{-\mathrm{T}}\boldsymbol{\tau}_{vis}\mathbf{J}^{-1}\dot{\tilde{\mathbf{x}}}\|$ *is bounded because* $\boldsymbol{\tau}_{vis}$ *is bounded (as shown in* (3.7)*),* $\|\mathbf{J}^{-1}\|$ *is bounded for non-singular configuration of the manipulator and it was assumed that* $\|\dot{\tilde{\mathbf{x}}}\|$ *is bounded.*

2. $\|\boldsymbol{\tau}_{cou}(sgn(\dot{\mathbf{q}}) - sgn(\dot{\hat{\mathbf{q}}}))\|$ *is bounded because* $\boldsymbol{\tau}_{cou}$ *is shown to be bounded in* (3.8) *and because* $(sgn(\dot{q}_i) - sgn(\dot{\hat{q}}_i))$ *is bounded.*

3. $\|\boldsymbol{\tau}_{sti}(exp^{(-\boldsymbol{\tau}_{dec}\dot{\mathbf{q}}^2)}sgn(\dot{\mathbf{q}}) - exp^{(-\boldsymbol{\tau}_{dec}\dot{\hat{\mathbf{q}}}^2)}sgn(\dot{\hat{\mathbf{q}}}))\|$ *is bounded because* $\boldsymbol{\tau}_{sti}$ *is shown to be bounded in* (3.9) *and because both* $sgn(\cdot)$ *and* $exp^{-|a|}$ *are bounded.*

Substituting (5.54)–(5.57) *into* $\dot{V}(\mathbf{r}_1, \mathbf{r}_2, \tilde{\mathbf{Z}})$ *in* (5.53)*, we have*

$$\begin{aligned}\dot{V}(\mathbf{r}_1, \mathbf{r}_2, \tilde{\mathbf{Z}}) \leq & -(M_{x,m}\,\Lambda_{1,m} - C_1)\,\|\mathbf{r}_1\|^2 \\ & -(M_{x,m}l_{D,m} - M_{x,M}\Lambda_{1,M} - \,3\,C_1)\,\|\mathbf{r}_2\|^2 \\ & +\|\mathbf{r}_1\|\|\mathbf{r}_2\|\,[B_{x,M}(\|\mathbf{r}_1\| + \|\mathbf{r}_2\| + 2\dot{x}_M) + 4\,C_1] \\ & +((\tau_{fric})_M + C_0)\,\|\mathbf{r}_1\| + ((\tau_{fric})_M + 3\,C_0)\,\|\mathbf{r}_2\| \\ & -\kappa\|\tilde{\mathbf{Z}}\|^2 + \kappa\|\tilde{\mathbf{Z}}\|Z_M.\end{aligned} \tag{5.58}$$

Defining $\mathbf{y}^{\mathrm{T}} = \begin{bmatrix}\mathbf{r}_1^{\mathrm{T}} & \mathbf{r}_2^{\mathrm{T}}\end{bmatrix}$*,* $\dot{V}(\mathbf{r}_1, \mathbf{r}_2, \tilde{\mathbf{Z}})$ (5.58) *can be written as*

$$\begin{aligned}\dot{V}(\mathbf{y}, \tilde{\mathbf{Z}}) \leq & -\mathbf{y}^{\mathrm{T}}\boldsymbol{\Psi}\mathbf{y} + \begin{bmatrix}(\tau_{fric})_M + C_0 & 0 \\ 0 & (\tau_{fric})_M + \,3\,C_0\end{bmatrix}\mathbf{y} \\ & -\kappa\|\tilde{\mathbf{Z}}\|^2 + \kappa\|\tilde{\mathbf{Z}}\|Z_M,\end{aligned} \tag{5.59}$$

where

$$\boldsymbol{\Psi} = \begin{bmatrix}(M_{x,m}\,\Lambda_{1,m} - C_1) & -\frac{1}{2}p \\ -\frac{1}{2}p & (M_{x,m}l_{D,m} - M_{x,M}\Lambda_{1,M} - \,3\,C_1)\end{bmatrix} \tag{5.60}$$

$$p = B_{x,M}(\|\mathbf{r}_1\| + \|\mathbf{r}_2\| + 2\dot{x}_M) + 4\,C_1. \tag{5.61}$$

The matrix $\boldsymbol{\Psi}$ (5.60) *is greater than zero (positive definite) if*

$$p < 2\sqrt{(M_{x,m}\,\Lambda_{1,m} - C_1)(M_{x,m}l_{D,m} - M_{x,M}\,\Lambda_{1,M} - \,3\,C_1)}; \tag{5.62}$$

where the right-hand side is positive due to hypotheses (5.43) *and* (5.44)*. Equation* (5.59) *can be written as*

$$\begin{aligned}\dot{V}(\mathbf{y},\tilde{\mathbf{Z}}) \leq & -\Psi_m\left[\|\mathbf{y}\| - \frac{(\tau_{fric})_M + 3\,C_0}{2\Psi_m}\right]^2 - \kappa\left[\|\tilde{\mathbf{Z}}\| - \frac{Z_M}{2}\right]^2 \\ & + \frac{((\tau_{fric})_M + 3\,C_0)^2}{4\Psi_m} + \frac{\kappa Z_M^2}{4}\end{aligned} \tag{5.63}$$

Hence, $\dot{V}(\mathbf{y},\tilde{\mathbf{Z}}) < 0$*, as depicted in Fig. 5.2, if*

$$\|\mathbf{y}\| > \sqrt{\frac{((\tau_{fric})_M + 3\,C_0)^2}{4\Psi_m^2} + \frac{\kappa Z_M^2}{4\Psi_m}} + \frac{(\tau_{fric})_M + 3\,C_0}{2\Psi_m} \equiv b_y, \quad \textit{or} \tag{5.64}$$

$$\|\tilde{\mathbf{Z}}\| > \sqrt{\frac{((\tau_{fric})_M + 3\,C_0)^2}{4\,\kappa\,\Psi_m} + \frac{Z_M^2}{4}} + \frac{Z_M}{2} \equiv b_{\tilde{Z}} \tag{5.65}$$

Applying the Lyapunov's Extension Theorem [102] then as $t \to \infty$*, the errors* $\|\mathbf{y}\|$ *and* $\|\tilde{\mathbf{Z}}\|$ *can be shown to be bounded within* $\mathcal{S}$*, as follows:*

Suppose the errors start within the boundary of $\mathcal{S}$*, i.e.* $\|\mathbf{y}(0)\| < b_y$ *and* $\|\tilde{\mathbf{Z}}(0)\| < b_{\tilde{Z}}$*, then they start their course towards the enclosing boundary* $\mathcal{S}$ *since* $\dot{V}(\mathbf{y},\tilde{\mathbf{Z}})$ *can not be guaranteed to be less than zero, within this boundary. However, when they are leaving the boundary and entering the region* $\dot{V}(\mathbf{y},\tilde{\mathbf{Z}}) < 0$*, they will return to the boundary. Now, suppose the errors start at outside the boundary of* $\mathcal{S}$ *then they tend to go to the equilibrium since* $V(\mathbf{y},\tilde{\mathbf{Z}})$ *is decreasing. However, they cannot go to the equilibrium, but only up to entering the boundary of* $\mathcal{S}$ *and once they enter the boundary of* $\mathcal{S}$*, we have already shown that they are bounded.*

Using bounded-input-bounded-output (BIBO) property, it can be shown that a bounded $\mathbf{r}_2$ *in* (5.10)*, yields bounded outputs* $\dot{\tilde{\mathbf{x}}}$ *and* $\tilde{\mathbf{x}}$*. Bounded input* $\mathbf{r}_1$ *together with* $\tilde{\mathbf{x}}$ *in* (5.9) *yield* $\lim_{t\to\infty} \mathbf{e}, \dot{\mathbf{e}}$ *that are bounded.*

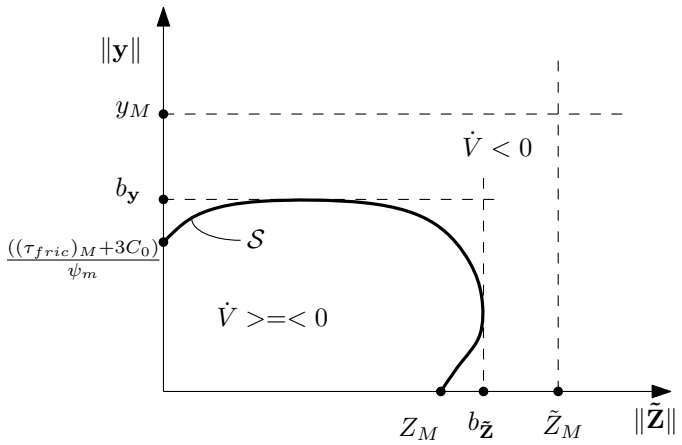

Figure 5.2: $\dot{V}(\mathbf{y}, \tilde{\mathbf{Z}})$ regions of the NN adaptive motion control with velocity observer.

The next part of the proof is to demonstrate the necessity of hypothesis $y_M > b_y$ in (5.45) *and $\hat{Z}_M > \sqrt{\frac{((\tau_{fric})_M + 3\ C_0)^2}{4\ \kappa\ \Psi_m}}$ in* (5.46)*, as follows:*

- *The error* $\mathbf{y}$ *can be shown to be upper-bounded by combining* (5.62) *and the definition of* p *in* (5.61)*:*

$$\|\mathbf{r}_1\| + \|\mathbf{r}_2\| < 2(1/B_{x,M}[\sqrt{\alpha} - 4\ C_1] - \ \dot{x}_M) \tag{5.66}$$

where $\alpha = (M_{x,m}\ \Lambda_{1,m} - C_1)(M_{x,m} l_{D,m} - M_{x,M}\ \Lambda_{1,M} - \ 3\ C_1) > 0$ *due to hypothesis* (5.43) *and* (5.44)*, and it is still true that*

$$\|\mathbf{y}\| = \sqrt{\|\mathbf{r}_1\|^2 + \|\mathbf{r}_2\|^2} < \sqrt{2}(1/B_{x,M}[\sqrt{\alpha} - 4\ C_1] - \ \dot{x}_M) \equiv \ y_M \tag{5.67}$$

where the right-hand side of (5.67) *can be defined as the upper-bound of* $\mathbf{y}$*. The last equation signifies the need of hypothesis $y_M > b_y$ in* (5.45)*; since* $\mathbf{y}$*, in its course towards the enclosing boundary* $\mathcal{S}$*, cannot violate the constraint y_M, otherwise, the Lyapunov's Extension Theorem is no longer applicable.*

- *Note that,* $\tilde{\mathbf{Z}}$*, in its course towards the enclosing boundary* $\mathcal{S}$*, cannot violate* $\tilde{Z}_M$*, otherwise the Lyapunov's Extension Theorem is no longer applicable. In other words,* $\tilde{Z}_M$ *in* (4.46) *must satisfy*

$$\tilde{Z}_M \equiv Z_M + \hat{Z}_M > b_{\tilde{\mathbf{Z}}}, \tag{5.68}$$

Therefore, it can be shown that if the following is satisfied

$$Z_M + \hat{Z}_M > \sqrt{\frac{((\tau_{fric})_M + 3\,C_0)^2}{4\kappa\Psi_m}} + Z_M > b_{\tilde{\mathbf{Z}}} \text{ or,} \tag{5.69}$$

$$\hat{Z}_M > \sqrt{\frac{((\tau_{fric})_M + 3\,C_0)^2}{4\kappa\Psi_m}} \tag{5.70}$$

then $\tilde{Z}_M > b_{\tilde{\mathbf{Z}}}$ *is also satisfied.*

Further, the initial condition $\|\mathbf{y}(0)\|$ *can be less or greater than* b_y*, however in order to comply with the Lyapunovs Extension Theorem, it must be less than* y_M*. Similarly,* $\|\tilde{\mathbf{Z}}(0)\|$ *must be less than* $\tilde{Z}_M$*. The last part of the proof is to demonstrate hypotheses* $\|\mathbf{y}(0)\| < y_M$ *in* (5.47) *and* $\|\tilde{\mathbf{Z}}(0)\| < \tilde{Z}_M$ *in* (5.48) *are to be satisfied in practical implementation:*

1. *In the implementation, it is possible to set* $\|\mathbf{y}(0)\|$ *to be as small as possible. As* $\|\mathbf{y}\| = \sqrt{\|\mathbf{r}_1\|^2 + \|\mathbf{r}_2\|^2}$*, obtaining as small* $\|\mathbf{y}(0)\|$ *as possible can be achieved through:*

   - *From* (5.10)*,* $\mathbf{r}_2(0) = \dot{\tilde{\mathbf{x}}}(0) + \mathbf{\Lambda}_2\tilde{\mathbf{x}}(0)$*: it is acceptable to assume that the end-effector starts from stationary. Setting* $\dot{\hat{\mathbf{x}}}(0) = \dot{\mathbf{x}}(0) = 0$ *results in* $\dot{\tilde{\mathbf{x}}}(0) = 0$*. Setting the initial estimate of* $\mathbf{x}$ *equal to the actual end-effector pose, i.e.* $\hat{\mathbf{x}}(0) = \mathbf{x}(0)$*, results in zero estimation error* $\tilde{\mathbf{x}}(0) = 0$*. Hence,* $\mathbf{r}_2(0) = 0$*.*

- *From* (5.9), $\mathbf{r}_1(0) = \dot{\mathbf{x}}_d(0) - \dot{\mathbf{x}}(0) + \mathbf{\Lambda}_1\mathbf{e}(0) + \mathbf{\Lambda}_1\tilde{\mathbf{x}}(0) + \mathbf{\Lambda}_i\mathbf{e}(0)\Delta t$*:* *as in the previous point,* $\tilde{\mathbf{x}}(0) = 0$*. The initial point of the desired trajectory can be set equal to the initial end-effector pose i.e.* $\dot{\mathbf{x}}_d(0) = \dot{\mathbf{x}}(0) = 0$*,* $\mathbf{x}_d(0) = \mathbf{x}(0)$*, resulting in* $\dot{\mathbf{e}}(0) = 0$ *and* $\mathbf{e}(0) = 0$*. Hence* $\mathbf{r}_1(0) = 0$*.*

Therefore,

$$\|\mathbf{y}(0)\| = 0 < b_y < y_M. \tag{5.71}$$

2. *By definition* $\tilde{\mathbf{Z}} = \mathbf{Z} - \hat{\mathbf{Z}}$*, therefore it is possible to initialize the estimated NN weights with zeroes,* $\|\hat{\mathbf{Z}}(0)\| = 0$*, therefore we can have*

$$\|\tilde{\mathbf{Z}}(0)\| = \|\mathbf{Z}\| \leq Z_M < b_{\tilde{Z}} < \tilde{Z}_M. \tag{5.72}$$

It can be seen that the initial conditions, $\|\mathbf{y}(0)\|$ *and* $\|\tilde{\mathbf{Z}}(0)\|$*, start within the boundary of* $\mathcal{S}$*.*

5.4 Computation of Estimated Operational Space Coordinates

Note that the the estimated velocities $\dot{\hat{\mathbf{x}}}$ are prescribed in operational space. And for the proposed controller observer we need to obtain $\tilde{\mathbf{x}} = \mathbf{x} - \hat{\mathbf{x}}$. However, the problem is we cannot do direct integration of $\dot{\hat{\mathbf{x}}}$ to obtain $\hat{\mathbf{x}}$. In this section, we also show how to obtain $\tilde{\mathbf{x}}$.

First, we need to calculate the estimated joint velocity, which for non-redundant manipulator is given by the formula

$$\dot{\hat{\mathbf{q}}} = \mathbf{J}^{-1}(\mathbf{q})\, \dot{\hat{\mathbf{x}}} \tag{5.73}$$

Now we can integrate $\dot{\hat{\mathbf{q}}}$ to get the estimated joint positions $\hat{\mathbf{q}}$.

Then, we can compute forward kinematics to obtain the estimated end-effector configuration parameters $\hat{\mathbf{x}} \equiv \mathbf{T}(\hat{\mathbf{q}})$, by using (2.7) and (2.8), which consists the estimated position and rotation of the end-effector

$$\hat{\mathbf{x}} = \begin{bmatrix} \hat{\mathbf{x}}_p \\ \hat{\mathbf{x}}_r \end{bmatrix}. \tag{5.74}$$

The positional estimated errors, $\tilde{\mathbf{x}}_p$, can be calculated as

$$\tilde{\mathbf{x}}_p = \mathbf{x}_p - \hat{\mathbf{x}}_p, \tag{5.75}$$

and the rotational estimated errors, $\delta\boldsymbol{\phi}$, can be computed as

$$\delta\boldsymbol{\phi} = -\frac{1}{2}([\mathbf{s}_1\times]\,\hat{\mathbf{s}}_1 \;+\; [\mathbf{s}_2\times]\,\hat{\mathbf{s}}_2 \;+\; [\mathbf{s}_3\times]\,\hat{\mathbf{s}}_3) \tag{5.76}$$

by using the actual orientation $\mathbf{x}_r = \begin{bmatrix} \mathbf{s}_1^{\mathrm{T}}(\mathbf{q}) & \mathbf{s}_2^{\mathrm{T}}(\mathbf{q}) & \mathbf{s}_3^{\mathrm{T}}(\mathbf{q}) \end{bmatrix}^{\mathrm{T}}$ and estimated orientation $\hat{\mathbf{x}}_r = \begin{bmatrix} \hat{\mathbf{s}}_1^{\mathrm{T}}(\mathbf{q}) & \hat{\mathbf{s}}_2^{\mathrm{T}}(\mathbf{q}) & \hat{\mathbf{s}}_3^{\mathrm{T}}(\mathbf{q}) \end{bmatrix}^{\mathrm{T}}$. The operator $[\mathbf{s}\times]$, is a 3×3 skew-symmetric matrix defined as

$$[\mathbf{s}\times] = \begin{pmatrix} 0 & -s_z & s_y \\ s_z & 0 & -s_x \\ -s_y & s_x & 0 \end{pmatrix} \tag{5.77}$$

given a 3×1 vector $\mathbf{s} = \begin{pmatrix} s_x & s_y & s_z \end{pmatrix}^{\mathrm{T}}$. Finally the close form of the positional and rotational estimated error can be written as

$$\tilde{\mathbf{x}} = \begin{bmatrix} \tilde{\mathbf{x}}_p^{\mathrm{T}} & \delta\boldsymbol{\phi}^{\mathrm{T}} \end{bmatrix}^{\mathrm{T}}. \tag{5.78}$$

5.5 Real-time Robot Experiment

The proposed NN motion control with velocity observer (5.2) is validated with the 6 DOF PUMA 560 manipulator, which does not have velocity feedback sensors, in real-time experiment.

Similar setup as in previous chapter is set as follows:

- A positional periodic circular trajectory – 75 mm radius and 2 second period – with a constant orientation for the effector was set as the desired trajectory.
- The initial posture of the robot is shown in Fig. 4.3 where the end-effector pointing down and the elbow is up.
- Performances were recorded in term of: (i) desired trajectories along x_{E} and y_{E} axes, and (ii) position errors along $x_{\mathrm{E}}, y_{\mathrm{E}}, z_{\mathrm{E}}$.

The real-time implementation video of the proposed NN adaptive motion controller-observer (5.2) is provided in:

http://guppy.mpe.nus.edu.sg/dandy/Videos/NN-based/
Free_motion_control_NN_obs.MPG

The planning strategy is similar as previously: the weights of the proposed NN adaptive motion controller with velocity observer (5.2) were initialized with zero values. Off-line learning simply using the same circular periodic trajectory was performed (for about 5 passes) to achieve an acceptable performance. The recorded weights were then used for the performance shown in Fig. 5.3.

Control type	Lagrangian dynamics	NN controller w/ filtered vel.	NN controller w/ vel. obs.
$\max(\|\mathbf{e}_{\text{pos}}\|)$ (mm)	7.90	28.80	6.80

Table 5.1: Performance comparison in term of the maximum of the magnitude of the end-effector position tracking errors in real-time study.

Table 5.1 shows that the proposed NN controller with velocity observer yields comparable performance to that of the Lagrangian dynamics strategy (without joint friction compensation). Also notice that the performance of the NN controller-observer strategy is better in comparison with the NN strategy without velocity observer. The bounded stability of the norms of the estimated NN weights is shown in Fig. 5.4.

The following gains are set for the proposed NN adaptive motion controller-observer (5.2): $\kappa = 0.1$, $\mathbf{\Lambda}_1 = \mathbf{\Lambda}_i = 30\mathbf{I} \in \Re^{m\times m}$, $\mathbf{F}_{M_{ij}}^{-1} = \mathbf{I} \in \Re^{N_2\times N_2}$, $\mathbf{F}_{B_{ij}}^{-1} = \mathbf{I} \in \Re^{N_2\times N_2}$, $\mathbf{F}_{g_i}^{-1} = 10\mathbf{I} \in \Re^{N_2\times N_2}$, $\mathbf{F}_{\tau_i}^{-1} = 10\mathbf{I} \in \Re^{N_2\times N_2}$, $\mathbf{\Lambda}_2 = 0.200\mathbf{I} \in \Re^{m\times m}$ and $\mathbf{l}_D = 400\mathbf{I} \in \Re^{m\times m}$.

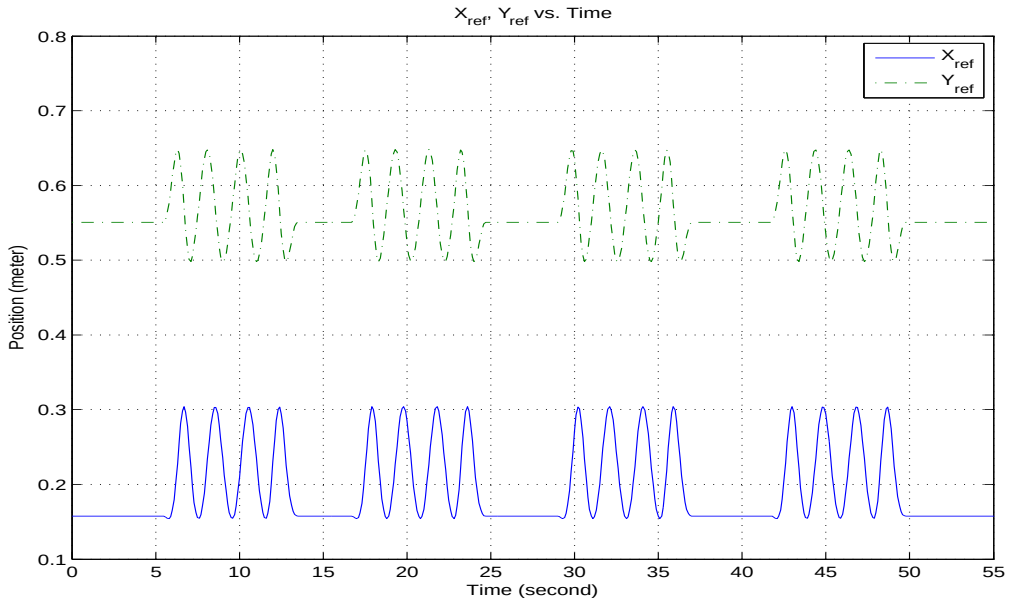

(a) Desired trajectories along $x_{\mathrm{E}}, y_{\mathrm{E}}$.

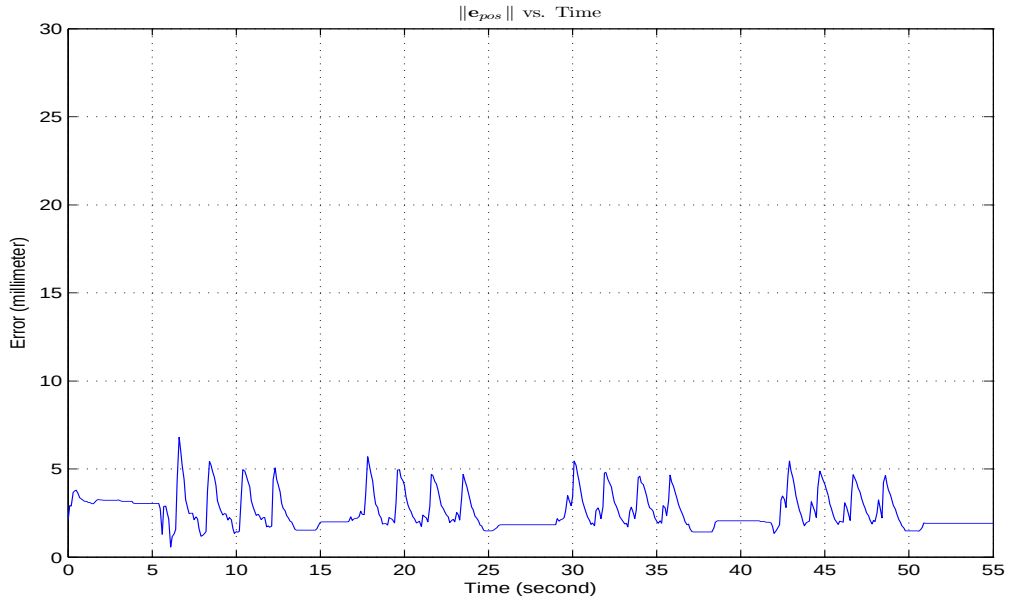

(b) The magnitude of the end-effector position tracking errors.

Figure 5.3: Real-time study NN adaptive motion control with velocity observer.

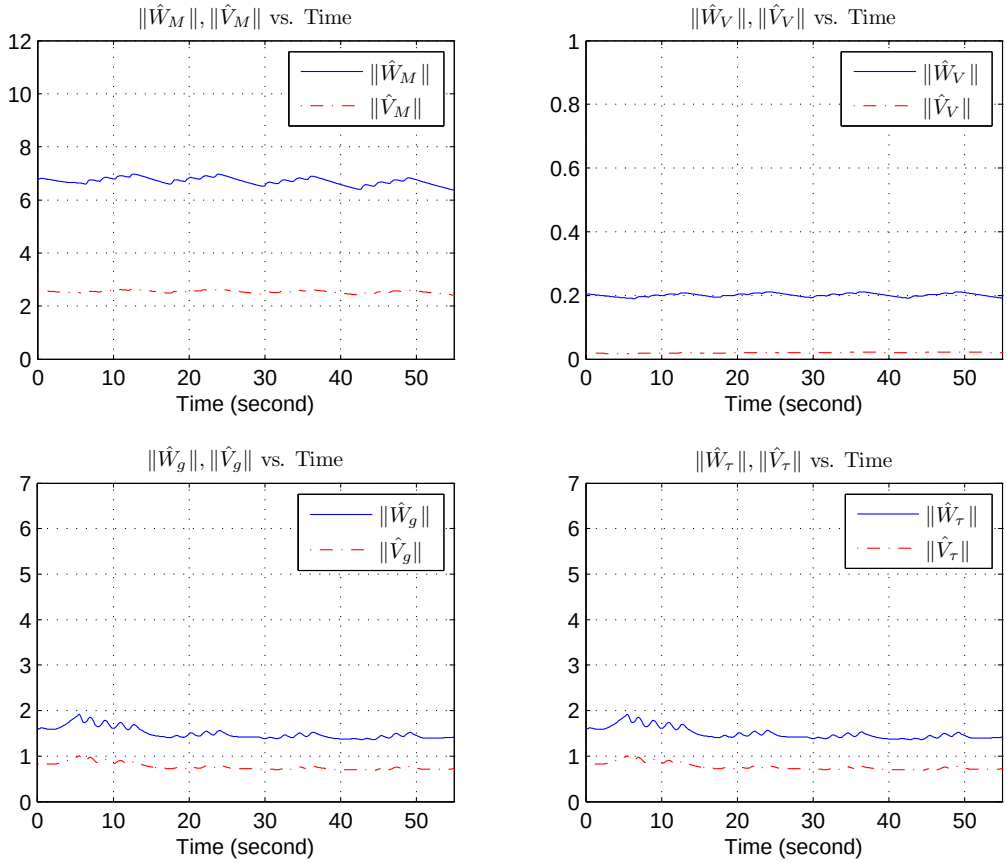

Figure 5.4: Real-time study history of the estimated NN weights of the NN motion controller with velocity observer.

5.6 Conclusion

In this chapter, the NN adaptive operational space motion formulation with velocity observer (5.2) was developed and validated through real-time experiment.

It can be concluded that the proposed strategy produces:

- a comparable performance to that of the Lagrangian dynamics strategy in real-time experiment.
- better performance than that of the NN motion control (4.80) (where filtered velocity is used to replace the actual velocity).

Therefore, the outcome of the study is a promising alternative, for real-time robotic implementation, to the Lagrangian dynamic strategy, in term of without the need of deriving and identifying Lagrangian dynamics.

In the next chapter, the current strategy which is done in free motion will be extended into the full unified force-motion control strategy in the operational space framework.

CHAPTER 6

NN ADAPTIVE FORCE-MOTION CONTROL WITH VELOCITY OBSERVER

6.1 Chapter Overview

In this chapter, a NN adaptive force and motion control in operational space (with velocity observer) is presented. This work is extended from previous formulation in Chapter four, by incorporating selection matrices Ω and $\bar{\Omega}$ (2.41) which are instrumental in decoupling force and motion subsystems in operational space formulation. A NN adaptive impact strategy is also proposed to dissipate the impact force produced after the end-effector hits the working surface from using NN adaptive motion control. Lyapunov stability analyzes for both NN adaptive force-motion and impact control are also presented.

Real-time experimentations were performed on a PUMA 560 robot, with comparison to the performance of a well-tuned Lagrangian dynamics control. It can be shown that the proposed strategy yielded comparable performance to that of the Lagrangian dynamics strategy. An adaptive impact strategy and its stability analysis, to complement the proposed strategy in real-time experiment, were also given.

Details can also be found in [117].

6.2 End-effector Constrained Motion Dynamics

To ease the formulation development in this chapter, let's reproduce the end-effector constrained motion dynamics of the non-redundant manipulator interacting with the environment (2.35) in Chapter two, which can be described as

$$\mathbf{M_x}(\mathbf{q})\ddot{\mathbf{x}} + \mathbf{B_x}(\mathbf{q},\dot{\mathbf{q}})\dot{\mathbf{x}} + \mathbf{g_x}(\mathbf{q}) + \boldsymbol{\tau}_{\mathbf{x}}(\mathbf{q},\dot{\mathbf{q}}) + \mathbf{f}_{\text{contact}} = \mathbf{F} \tag{6.1}$$

where the vector $\mathbf{f} \in \Re^m$, as in (2.36), represents the contact force vector exerted by the effector onto the contact surface. The operational space matrices and vectors $\mathbf{M_x}(\mathbf{q}) \in \Re^{m\times m}$, $\mathbf{B_x}(\mathbf{q},\dot{\mathbf{q}}) \in \Re^{m\times m}$, $\mathbf{g_x}(\mathbf{q}) \in \Re^m$ and $\boldsymbol{\tau}_{\mathbf{x}}(\mathbf{q},\dot{\mathbf{q}}) \in \Re^m$ are identical with (2.28) – (2.31), respectively.

The constrained motion equation (6.1) needs to be rearranged to accommodate the proposed controller-observer formulation. Using selection matrices $\boldsymbol{\Omega}$ and $\bar{\boldsymbol{\Omega}}$ in (2.41), and Property 4.3.2 $\mathbf{B_x}(\mathbf{q},\dot{\mathbf{x}}) = \mathbf{B_x}(\mathbf{q},\dot{\mathbf{q}})$, then the effector constrained dynamic (6.1) can be written as

$$\mathbf{M_x}(\mathbf{q})(\boldsymbol{\Omega}\ddot{\mathbf{x}} + \bar{\boldsymbol{\Omega}}\ddot{\mathbf{x}}) + \mathbf{B_x}(\mathbf{q},\dot{\mathbf{x}})(\boldsymbol{\Omega}\dot{\mathbf{x}} + \bar{\boldsymbol{\Omega}}\dot{\mathbf{x}}) + \mathbf{g_x}(\mathbf{q}) + \boldsymbol{\tau}_{\mathbf{x}}(\mathbf{q},\dot{\mathbf{q}}) + \mathbf{f}_{\text{contact}} = \mathbf{F} \tag{6.2}$$

6.3 NN Adaptive Force-Motion Control - Observer Formulation

6.3.1 NN Adaptive Force-Motion Controller-Observer

In this section, the NN adaptive force - motion controller with velocity observer is proposed. The controller-observer structure is shown in Fig. 6.1. To start, the

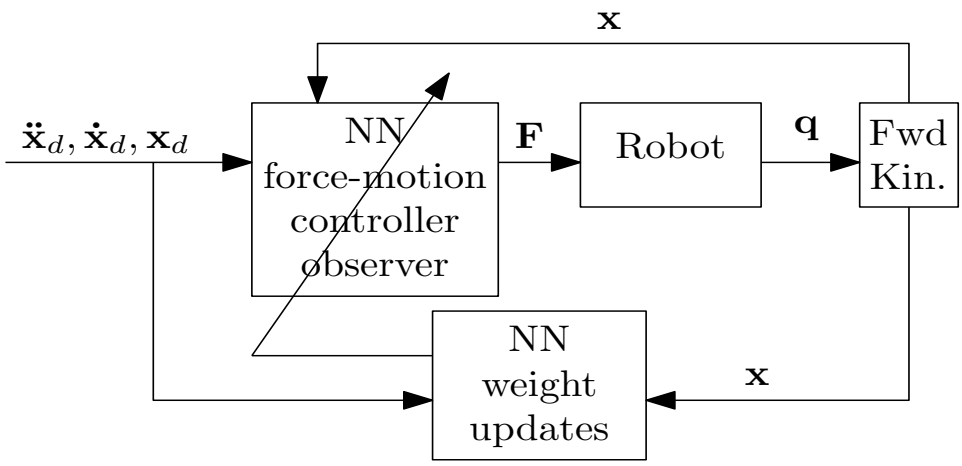

Figure 6.1: The operational space NN force - motion controller-observer structure.

control law is defined as:

$$\begin{aligned}\mathbf{F} = \hat{\mathrm{M}}_{\mathbf{x}}(\mathbf{q})(\boldsymbol{\Omega}\mathbf{F}^*_{\text{motion}} + \bar{\boldsymbol{\Omega}}\mathbf{F}^*_{\text{force}}) + \hat{\mathbf{B}}_{\mathbf{x}}(\mathbf{q}, \dot{\mathbf{x}}_0)(\boldsymbol{\Omega}\dot{\mathbf{x}}_r + \bar{\boldsymbol{\Omega}}\dot{\mathbf{f}}_r) \\ + \hat{\mathbf{g}}_{\mathbf{x}}(\mathbf{q}) + \hat{\boldsymbol{\tau}}_{\mathbf{x}}(\mathbf{q}, \dot{\hat{\mathbf{q}}}) + \mathbf{f}_{\text{sensor}}\end{aligned} \tag{6.3}$$

where $\dot{\mathbf{x}}_0, \dot{\mathbf{x}}_r, \dot{\mathbf{f}}_r, \mathbf{F}^*_{\text{motion}}$ and $\mathbf{F}^*_{\text{force}}$ are defined as

$$\begin{aligned}\dot{\mathbf{x}}_r &= \dot{\mathbf{x}}_d + \boldsymbol{\Lambda}_1(\mathbf{x}_d - \hat{\mathbf{x}}) \qquad (6.4)\\ &= \dot{\mathbf{x}}_d + \boldsymbol{\Lambda}_1\mathbf{e}_{\mathbf{x}} + \boldsymbol{\Lambda}_1\tilde{\mathbf{x}}\end{aligned}$$

$$\dot{\mathbf{x}}_0 = \dot{\hat{\mathbf{x}}} - \boldsymbol{\Lambda}_2\tilde{\mathbf{x}} \tag{6.5}$$

$$\dot{\mathbf{f}}_r = \mathbf{K}_e^{-1}(\boldsymbol{\Lambda}_1\mathbf{e}_{\mathbf{f}} + \boldsymbol{\Lambda}_i \int_0^{\tau=t} \mathbf{e}_{\mathbf{f}}\, \mathrm{d}\tau) \tag{6.6}$$

$$\mathbf{F}^*_{\text{motion}} = \ddot{\mathbf{x}}_r + \boldsymbol{\Lambda}_1(\mathbf{r}_{\mathbf{x}1} + \mathbf{r}_{\mathbf{x}2}) \tag{6.7}$$

$$\mathbf{F}^*_{\text{force}} = \ddot{\mathbf{f}}'_r + \boldsymbol{\Lambda}_1(\mathbf{r}_{\mathbf{f}} + \mathbf{r}_{\mathbf{x}2}) \tag{6.8}$$

with the computable terms to compute $\mathbf{F}^*_{\text{motion}}$ and $\mathbf{F}^*_{\text{force}}$ are defined as

$$\ddot{\mathbf{x}}_r = \ddot{\mathbf{x}}_d + \mathbf{\Lambda}_1(\dot{\mathbf{x}}_d - \dot{\hat{\mathbf{x}}}) \tag{6.9}$$

$$\mathbf{r}_{\mathbf{x}1} + \mathbf{r}_{\mathbf{x}2} = \dot{\mathbf{x}}_r - \dot{\mathbf{x}}_0 \tag{6.10}$$

$$\ddot{\mathbf{f}}'_r = -\mathbf{\Lambda}_1\dot{\mathbf{x}}_0 + \mathbf{K}_e^{-1}\mathbf{\Lambda}_i\mathbf{e}_\mathbf{f} \tag{6.11}$$

$$\mathbf{r}_\mathbf{f} + \mathbf{r}_{\mathbf{x}2} = \dot{\mathbf{f}}_r - \dot{\mathbf{x}}_0 \tag{6.12}$$

It follows from (6.11) that we can write

$$\begin{aligned}\ddot{\mathbf{f}}'_r &= -\mathbf{\Lambda}_1\dot{\mathbf{x}} + \mathbf{\Lambda}_1(\dot{\tilde{\mathbf{x}}} + \mathbf{\Lambda}_2\tilde{\mathbf{x}}) + \mathbf{K}_e^{-1}\mathbf{\Lambda}_i\mathbf{e}_\mathbf{f} \\ &= \ddot{\mathbf{f}}_r + \mathbf{\Lambda}_1\mathbf{r}_{\mathbf{x}2}\end{aligned} \tag{6.13}$$

where it can be defined

$$\ddot{\mathbf{f}}_r = -\mathbf{\Lambda}_1\dot{\mathbf{x}} + \mathbf{K}_e^{-1}\mathbf{\Lambda}_i\mathbf{e}_\mathbf{f} = \mathbf{K}_e^{-1}\mathbf{\Lambda}_1\dot{\mathbf{e}}_\mathbf{f} + \mathbf{K}_e^{-1}\mathbf{\Lambda}_i\mathbf{e}_\mathbf{f} \tag{6.14}$$

confirming the derivative of (6.6).

It follows that from (6.10), (6.4) and (6.5) we can write

$$\mathbf{r}_{\mathbf{x}1} + \mathbf{r}_{\mathbf{x}2} = (\dot{\mathbf{x}}_r - \dot{\mathbf{x}}) + (\dot{\mathbf{x}} - \dot{\mathbf{x}}_0), \tag{6.15}$$

where it can be defined

$$\mathbf{r}_{\mathbf{x}1} = \dot{\mathbf{x}}_r - \dot{\mathbf{x}} = \dot{\mathbf{e}}_\mathbf{x} + \mathbf{\Lambda}_1\mathbf{e}_\mathbf{x} + \mathbf{\Lambda}_1\tilde{\mathbf{x}} \tag{6.16}$$

$$\mathbf{r}_{\mathbf{x}2} = \dot{\mathbf{x}} - \dot{\mathbf{x}}_0 = \dot{\tilde{\mathbf{x}}} + \mathbf{\Lambda}_2\tilde{\mathbf{x}}. \tag{6.17}$$

It follows from (6.12), (6.6) and (6.5) that we can write

$$\mathbf{r}_\mathbf{f} + \mathbf{r}_{\mathbf{x}2} = (\dot{\mathbf{f}}_r - \dot{\mathbf{x}}) + (\dot{\mathbf{x}} - \dot{\mathbf{x}}_0), \tag{6.18}$$

where it can be defined

$$\begin{aligned}\mathbf{r_f} = \dot{\mathbf{f}}_r - \dot{\mathbf{x}} &= -\dot{\mathbf{x}} + \mathbf{K}_e^{-1}(\mathbf{\Lambda}_1\mathbf{e_f} + \mathbf{\Lambda}_i \int_0^{\tau=t} \mathbf{e_f}\, \mathrm{d}\tau) \\ &= \mathbf{K}_e^{-1}\, \dot{\mathbf{e}}_\mathbf{f} + \mathbf{K}_e^{-1}(\mathbf{\Lambda}_1\mathbf{e_f} + \mathbf{\Lambda}_i \int_0^{\tau=t} \mathbf{e_f}\, \mathrm{d}\tau).\end{aligned} \tag{6.19}$$

where $\mathbf{\Lambda}_1, \mathbf{\Lambda}_2, \mathbf{\Lambda}_i \in \Re^{m\times m}$ are positive diagonal matrices, $\mathbf{e_x} = \mathbf{x}_d - \mathbf{x}$ and $\dot{\mathbf{e}}_\mathbf{x} = \dot{\mathbf{x}}_d - \dot{\mathbf{x}}$ are the trajectory tracking errors and $\mathbf{x}_d$, $\dot{\mathbf{x}}_d$ and $\ddot{\mathbf{x}}_d$ are the desired operational space trajectories. The estimated errors between the actual terms $\mathbf{x}, \dot{\mathbf{x}}$ and their estimates $\hat{\mathbf{x}}, \dot{\hat{\mathbf{x}}}$ are defined by $\tilde{\mathbf{x}} = \mathbf{x} - \hat{\mathbf{x}}$ and $\dot{\tilde{\mathbf{x}}} = \dot{\mathbf{x}} - \dot{\hat{\mathbf{x}}}$, respectively. The computation to obtain $\hat{\mathbf{x}}$ and $\tilde{\mathbf{x}}$ is given already on Section 5.4. $\mathbf{e_f} = \mathbf{f}_d - \mathbf{f}$ and $\dot{\mathbf{e}}_\mathbf{f} = -\dot{\mathbf{f}} = -\mathbf{K}_e\, \dot{\mathbf{x}}$ are the force tracking errors, where $\mathbf{f}_d$ is a constant desired active-force. Note that the linear spring matrix $\mathbf{K}_e^{-1}$ is assumed to be known, however, in the implementation it can be seen as tunable gain i.e. a positive diagonal matrix.

Now, combining robot dynamics (6.2) and the proposed controller (6.20), and taking into account (6.13) and the first derivatives of (6.16), (6.19) and also Property 4.3.2, a *general closed-loop dynamic* can be obtained as

$$\begin{aligned}\mathbf{M_x}(\mathbf{q})(\mathbf{\Omega}\dot{\mathbf{r}}_{\mathbf{x}1} + \bar{\mathbf{\Omega}}\dot{\mathbf{r}}_\mathbf{f}) = &-\mathbf{M_x}(\mathbf{q})\mathbf{\Lambda}_1(\mathbf{\Omega}\mathbf{r}_{\mathbf{x}1} + \bar{\mathbf{\Omega}}\mathbf{r_f}) - \mathbf{M_x}(\mathbf{q})\mathbf{\Lambda}_1(\mathbf{I} + \bar{\mathbf{\Omega}})\mathbf{r}_{\mathbf{x}2} \\ &- \mathbf{B_x}(\mathbf{q}, \dot{\mathbf{x}}_0)(\mathbf{\Omega}\dot{\mathbf{x}}_r + \bar{\mathbf{\Omega}}\dot{\mathbf{f}}_r) + \mathbf{B_x}(\mathbf{q}, \dot{\mathbf{x}})(\mathbf{\Omega}\dot{\mathbf{x}} + \bar{\mathbf{\Omega}}\dot{\mathbf{x}}) \\ &+ (\boldsymbol{\tau}_\mathbf{x}(\mathbf{q}, \dot{\mathbf{q}}) - \boldsymbol{\tau}_\mathbf{x}(\mathbf{q}, \dot{\hat{\mathbf{q}}})) + \boldsymbol{\eta}\end{aligned} \tag{6.20}$$

where uncertainties $\boldsymbol{\eta}$

$$\begin{aligned}\boldsymbol{\eta} = &\tilde{\mathbf{M}}_\mathbf{x}(\mathbf{q})(\mathbf{\Omega}\mathbf{F}^*_{\text{motion}} + \bar{\mathbf{\Omega}}\mathbf{F}^*_{\text{force}}) + \tilde{\mathbf{B}}_\mathbf{x}(\mathbf{q}, \dot{\mathbf{x}}_0)(\mathbf{\Omega}\dot{\mathbf{x}}_r + \bar{\mathbf{\Omega}}\dot{\mathbf{f}}_r) \\ &+ \tilde{\mathbf{g}}_\mathbf{x}(\mathbf{q}) + \tilde{\boldsymbol{\tau}}_\mathbf{x}(\mathbf{q}, \dot{\hat{\mathbf{q}}}).\end{aligned} \tag{6.21}$$

and $\boldsymbol{\tau}_\mathbf{x}(\mathbf{q}, \dot{\mathbf{q}}) - \boldsymbol{\tau}_\mathbf{x}(\mathbf{q}, \dot{\hat{\mathbf{q}}})$, is similar with (4.88), however it is reproduced for

ease of perusal as

$$\boldsymbol{\tau}_{\mathbf{x}}(\mathbf{q},\dot{\mathbf{q}}) - \boldsymbol{\tau}_{\mathbf{x}}(\mathbf{q},\dot{\hat{\mathbf{q}}}) = \mathbf{J}^{-\mathrm{T}}[\tau_{vis}\dot{\tilde{\mathbf{q}}} + \tau_{cou}(\mathrm{sgn}(\dot{\mathbf{q}}) - \mathrm{sgn}(\dot{\hat{\mathbf{q}}})) + \boldsymbol{\tau}_{sti}\mathrm{exp}^{(-\boldsymbol{\tau}_{dec}\dot{\mathbf{q}}^2)}\mathrm{sgn}(\dot{\mathbf{q}}) - \boldsymbol{\tau}_{sti}\mathrm{exp}^{(-\boldsymbol{\tau}_{dec}\dot{\hat{\mathbf{q}}}^2)}\mathrm{sgn}(\dot{\hat{\mathbf{q}}})]. \tag{6.22}$$

The general closed-loop dynamics (6.20) cannot be used directly into stability analysis. It must be converted into useful closed-loop controller (Section 6.3.2) and observer (Section 6.3.3) dynamics:

6.3.2 Controller closed-loop dynamics

Using (6.16), (6.17), (6.19) and Property 4.3.6, $\mathbf{B}_{\mathbf{x}}(\mathbf{q},\dot{\mathbf{x}}_0)(\boldsymbol{\Omega}\dot{\mathbf{x}}_r + \bar{\boldsymbol{\Omega}}\dot{\mathbf{f}}_r) - \mathbf{B}_{\mathbf{x}}(\mathbf{q},\dot{\mathbf{x}})(\boldsymbol{\Omega}\dot{\mathbf{x}} + \bar{\boldsymbol{\Omega}}\dot{\mathbf{x}})$ in (6.20), can be arranged such that

$$= \mathbf{B}_{\mathbf{x}}(\mathbf{q},\dot{\mathbf{x}})(\boldsymbol{\Omega}\mathbf{r}_{\mathbf{x}1} + \bar{\boldsymbol{\Omega}}\mathbf{r}_{\mathbf{f}}) - \mathbf{B}_{\mathbf{x}}(\mathbf{q},\boldsymbol{\Omega}\dot{\mathbf{x}}_r + \bar{\boldsymbol{\Omega}}\dot{\mathbf{f}}_r)\mathbf{r}_{\mathbf{x}2} \tag{6.23}$$

Substituting it into (6.20), yields the *controller closed-loop dynamics* as

$$\begin{aligned}\mathbf{M}_{\mathbf{x}}(\mathbf{q})(\boldsymbol{\Omega}\dot{\mathbf{r}}_{\mathbf{x}1} + \bar{\boldsymbol{\Omega}}\dot{\mathbf{r}}_{\mathbf{f}}) = &- \mathbf{M}_{\mathbf{x}}(\mathbf{q})\boldsymbol{\Lambda}_1(\boldsymbol{\Omega}\mathbf{r}_{\mathbf{x}1} + \bar{\boldsymbol{\Omega}}\mathbf{r}_{\mathbf{f}}) - \mathbf{M}_{\mathbf{x}}(\mathbf{q})\boldsymbol{\Lambda}_1(\mathbf{I} + \bar{\boldsymbol{\Omega}})\mathbf{r}_{\mathbf{x}2} \\ &- \mathbf{B}_{\mathbf{x}}(\mathbf{q},\dot{\mathbf{x}})(\boldsymbol{\Omega}\mathbf{r}_{\mathbf{x}1} + \bar{\boldsymbol{\Omega}}\mathbf{r}_{\mathbf{f}}) + \mathbf{B}_{\mathbf{x}}(\mathbf{q},\boldsymbol{\Omega}\dot{\mathbf{x}}_r + \bar{\boldsymbol{\Omega}}\dot{\mathbf{f}}_r)\mathbf{r}_{\mathbf{x}2} \\ &+ (\boldsymbol{\tau}_{\mathbf{x}}(\mathbf{q},\dot{\mathbf{q}}) - \boldsymbol{\tau}_{\mathbf{x}}(\mathbf{q},\dot{\hat{\mathbf{q}}})) + \boldsymbol{\eta}.\end{aligned} \tag{6.24}$$

6.3.3 Observer closed-loop dynamics

An observer can be designed (based upon [109]):

$$\dot{\tilde{\mathbf{x}}} = \dot{\mathbf{x}} - \dot{\hat{\mathbf{x}}} = \mathbf{z} + (\mathbf{l}_D + \boldsymbol{\Lambda}_2)\tilde{\mathbf{x}} \tag{6.25}$$

$$\begin{aligned}\dot{\mathbf{z}} = &\boldsymbol{\Omega}\ddot{\mathbf{x}}_r + \bar{\boldsymbol{\Omega}}\ddot{\mathbf{f}}_r' + ((\mathbf{l}_D \cdot \boldsymbol{\Lambda}_2))\tilde{\mathbf{x}} \\ &- \bar{\boldsymbol{\Omega}}\boldsymbol{\Lambda}_1\left[\boldsymbol{\Omega}(\mathbf{r}_{\mathbf{x}1} + \mathbf{r}_{\mathbf{x}2}) + \bar{\boldsymbol{\Omega}}(\mathbf{r}_{\mathbf{f}} + \mathbf{r}_{\mathbf{x}2})\right],\end{aligned} \tag{6.26}$$

where $\mathbf{l}_D = \text{diag}(l_{D,ii} > 0) \in \Re^{m \times m}$. Combining the first derivative of (6.25) with (6.26), and taking into account (6.13) and the first derivatives of (6.16), (6.19), yield

$$\begin{aligned}\ddot{\tilde{\mathbf{x}}} + (\mathbf{l}_D + \mathbf{\Lambda}_2)\dot{\tilde{\mathbf{x}}} + ((\mathbf{l}_D \cdot \mathbf{\Lambda}_2))\tilde{\mathbf{x}} = &- \mathbf{\Omega}(\ddot{\mathbf{x}}_r - \ddot{\mathbf{x}}) - \bar{\mathbf{\Omega}}(\ddot{\mathbf{f}}_r - \ddot{\mathbf{x}}) - \bar{\mathbf{\Omega}}\mathbf{\Lambda}_1\mathbf{r}_{\mathbf{x}2} \\ &+ \bar{\mathbf{\Omega}}\mathbf{\Lambda}_1\left[\mathbf{\Omega}(\mathbf{r}_{\mathbf{x}1} + \mathbf{r}_{\mathbf{x}2}) + \bar{\mathbf{\Omega}}(\mathbf{r}_{\mathbf{f}} + \mathbf{r}_{\mathbf{x}2})\right] \\ = &- (\mathbf{\Omega}\dot{\mathbf{r}}_{\mathbf{x}1} + \bar{\mathbf{\Omega}}\dot{\mathbf{r}}_{\mathbf{f}}) + \bar{\mathbf{\Omega}}\mathbf{\Lambda}_1(\mathbf{\Omega}\mathbf{r}_{\mathbf{x}1} + \bar{\mathbf{\Omega}}\mathbf{r}_{\mathbf{f}})\end{aligned} \tag{6.27}$$

Substituting (6.17) and its derivative into the left-hand-side (LHS) of (6.27) and multiplying both sides with $\mathbf{M}_{\mathbf{x}}(\mathbf{q})$, yield

$$\begin{aligned}&\mathbf{M}_{\mathbf{x}}(\mathbf{q})\dot{\mathbf{r}}_{\mathbf{x}2} + \mathbf{M}_{\mathbf{x}}(\mathbf{q})\mathbf{l}_D\mathbf{r}_{\mathbf{x}2} = \\ &- \mathbf{M}_{\mathbf{x}}(\mathbf{q})(\mathbf{\Omega}\dot{\mathbf{r}}_{\mathbf{x}1} + \bar{\mathbf{\Omega}}\dot{\mathbf{r}}_{\mathbf{f}}) + \mathbf{M}_{\mathbf{x}}(\mathbf{q})\bar{\mathbf{\Omega}}\mathbf{\Lambda}_1(\mathbf{\Omega}\mathbf{r}_{\mathbf{x}1} + \bar{\mathbf{\Omega}}\mathbf{r}_{\mathbf{f}}).\end{aligned} \tag{6.28}$$

Using (6.16), (6.17), (6.19) and Property 4.3.6, $\mathbf{B}_{\mathbf{x}}(\mathbf{q}, \dot{\mathbf{x}}_0)(\mathbf{\Omega}\dot{\mathbf{x}}_r + \bar{\mathbf{\Omega}}\dot{\mathbf{f}}_r) - \mathbf{B}_{\mathbf{x}}(\mathbf{q}, \dot{\mathbf{x}})(\mathbf{\Omega}\dot{\mathbf{x}} + \bar{\mathbf{\Omega}}\dot{\mathbf{x}})$ in (6.20), can be arranged such that

$$= \mathbf{B}_{\mathbf{x}}(\mathbf{q}, \dot{\mathbf{x}}_0)(\mathbf{\Omega}\mathbf{r}_{\mathbf{x}1} + \bar{\mathbf{\Omega}}\mathbf{r}_{\mathbf{f}}) - \mathbf{B}_{\mathbf{x}}(\mathbf{q}, \dot{\mathbf{x}})\mathbf{r}_{\mathbf{x}2} \tag{6.29}$$

Substituting it with into the general closed-loop dynamics (6.20), yields

$$\begin{aligned}-\mathbf{M}_{\mathbf{x}}(\mathbf{q})(\mathbf{\Omega}\dot{\mathbf{r}}_{\mathbf{x}1} + \bar{\mathbf{\Omega}}\dot{\mathbf{r}}_{\mathbf{f}}) = &\ \mathbf{M}_{\mathbf{x}}(\mathbf{q})\mathbf{\Lambda}_1(\mathbf{\Omega}\mathbf{r}_{\mathbf{x}1} + \bar{\mathbf{\Omega}}\mathbf{r}_{\mathbf{f}}) + \mathbf{M}_{\mathbf{x}}(\mathbf{q})\mathbf{\Lambda}_1(\mathbf{I} + \bar{\mathbf{\Omega}})\mathbf{r}_{\mathbf{x}2} \\ &+ \mathbf{B}_{\mathbf{x}}(\mathbf{q}, \dot{\mathbf{x}}_0)(\mathbf{\Omega}\mathbf{r}_{\mathbf{x}1} + \bar{\mathbf{\Omega}}\mathbf{r}_{\mathbf{f}}) - \mathbf{B}_{\mathbf{x}}(\mathbf{q}, \dot{\mathbf{x}})\mathbf{r}_{\mathbf{x}2} \\ &- (\boldsymbol{\tau}_{\mathbf{x}}(\mathbf{q}, \dot{\mathbf{q}}) - \boldsymbol{\tau}_{\mathbf{x}}(\mathbf{q}, \dot{\hat{\mathbf{q}}})) - \boldsymbol{\eta}\end{aligned} \tag{6.30}$$

Substituting (6.30) into (6.28), the *observer closed-loop dynamics* can be obtained as:

$$\begin{aligned}\mathbf{M}_{\mathbf{x}}(\mathbf{q})\dot{\mathbf{r}}_{\mathbf{x}2} = &- \mathbf{M}_{\mathbf{x}}(\mathbf{q})(\mathbf{l}_D - \mathbf{\Lambda}_1(\mathbf{I} + \bar{\mathbf{\Omega}}))\mathbf{r}_{\mathbf{x}2} \\ &+ \mathbf{M}_{\mathbf{x}}(\mathbf{q})\mathbf{\Lambda}_1(\mathbf{I} + \bar{\mathbf{\Omega}})(\mathbf{\Omega}\mathbf{r}_{\mathbf{x}1} + \bar{\mathbf{\Omega}}\mathbf{r}_{\mathbf{f}}) \\ &- \mathbf{B}_{\mathbf{x}}(\mathbf{q}, \dot{\mathbf{x}})\mathbf{r}_{\mathbf{x}2} + \mathbf{B}_{\mathbf{x}}(\mathbf{q}, \dot{\mathbf{x}}_0)(\mathbf{\Omega}\mathbf{r}_{\mathbf{x}1} + \bar{\mathbf{\Omega}}\mathbf{r}_{\mathbf{f}}) \\ &- (\boldsymbol{\tau}_{\mathbf{x}}(\mathbf{q}, \dot{\mathbf{q}}) - \boldsymbol{\tau}_{\mathbf{x}}(\mathbf{q}, \dot{\hat{\mathbf{q}}})) - \boldsymbol{\eta}.\end{aligned} \tag{6.31}$$

6.3.4 Uncertainties $\boldsymbol{\eta}$ in NN terms

Similar with Section 4.4.2, $\mathbf{M_x(q)}$, $\mathbf{B_x(q,\dot{x}_0)}$, $\mathbf{g_x(q)}$ and $\boldsymbol{\tau}_\mathbf{x}(\mathbf{q},\dot{\hat{\mathbf{q}}})$ in $\boldsymbol{\eta}$ (6.21) can be described as follows

$$\mathbf{M_x(q)} = \mathbf{W}_M^{\mathrm{T}}\, \boldsymbol{\sigma}_M(\mathbf{V}_M^{\mathrm{T}}\, \mathbf{z}_M) + \boldsymbol{\varepsilon}_M \tag{6.32}$$

$$\mathbf{B_x(q,\dot{x}_0)} = \mathbf{W}_B^{\mathrm{T}}\, \boldsymbol{\sigma}_B(\mathbf{V}_B^{\mathrm{T}}\, \mathbf{z}_B) + \boldsymbol{\varepsilon}_B \tag{6.33}$$

$$\mathbf{g_x(q)} = \mathbf{W}_g^{\mathrm{T}}\, \boldsymbol{\sigma}_g(\mathbf{V}_g^{\mathrm{T}}\, \mathbf{z}_g) + \boldsymbol{\varepsilon}_g \tag{6.34}$$

$$\boldsymbol{\tau}_\mathbf{x}(\mathbf{q},\dot{\hat{\mathbf{q}}}) = \mathbf{W}_\tau^{\mathrm{T}}\, \boldsymbol{\sigma}_\tau(\mathbf{V}_\tau^{\mathrm{T}}\, \mathbf{z}_\tau) + \boldsymbol{\varepsilon}_\tau \tag{6.35}$$

Similarly, the estimated dynamic terms $\hat{\mathbf{M}}_\mathbf{x}(\mathbf{q})$, $\hat{\mathbf{B}}_\mathbf{x}(\mathbf{q},\dot{\mathbf{x}}_0)$, $\hat{\mathbf{g}}_\mathbf{x}(\mathbf{q})$, $\hat{\boldsymbol{\tau}}_\mathbf{x}(\mathbf{q},\dot{\hat{\mathbf{q}}})$ are described by the estimated weights $\{\hat{\mathbf{V}}_p\}, \{\hat{\mathbf{W}}_p\}$, with subscript $p = M, B, g, \tau$.

Similar with Section 5.3.4, $\mathbf{M_x(q)}, \mathbf{B_x(q,\dot{q})}, \mathbf{g_x(q)}, \boldsymbol{\tau}_\mathbf{x}(\mathbf{q},\dot{\hat{\mathbf{q}}})$ can be shown to be bounded. Therefore, the optimum weights $\mathbf{W}_p, \mathbf{V}_p$ and the approximation error $\boldsymbol{\varepsilon}_p$ (with subscript $p = M, B, g, \tau$) from (6.32)-(6.35), are also upper-bounded.

Using similar development and simplified notations $\boldsymbol{\sigma} \equiv \boldsymbol{\sigma}(\mathbf{V}^{\mathrm{T}}\mathbf{z})$, $\hat{\boldsymbol{\sigma}} \equiv \boldsymbol{\sigma}(\hat{\mathbf{V}}^{\mathrm{T}}\mathbf{z})$, and $\boldsymbol{\sigma} = \hat{\boldsymbol{\sigma}} + \tilde{\boldsymbol{\sigma}}$ as in Section 4.4.2, the uncertainties $\boldsymbol{\eta}$ (6.21) can be written as

$$\boldsymbol{\eta} = \boldsymbol{\xi} + \boldsymbol{\zeta} \tag{6.36}$$

This division is needed because only $\boldsymbol{\xi}$ term can be manipulated by the weight updates $\dot{\hat{\mathbf{W}}}, \dot{\hat{\mathbf{V}}}$ as will be shown in Section 6.3.5.

The term $\boldsymbol{\xi}$ is defined as

$$\begin{aligned}\boldsymbol{\xi} = & \left(\tilde{\mathbf{W}}_M^{\mathrm{T}}\hat{\boldsymbol{\sigma}}_M\right)(\boldsymbol{\Omega}\mathbf{F}^*_{\mathrm{motion}} + \bar{\boldsymbol{\Omega}}\mathbf{F}^*_{\mathrm{force}}) \\ & + \left(\tilde{\mathbf{W}}_B^{\mathrm{T}}\hat{\boldsymbol{\sigma}}_B\right)(\boldsymbol{\Omega}\dot{\mathbf{x}}_r + \bar{\boldsymbol{\Omega}}\dot{\mathbf{f}}_r) \\ & + \tilde{\mathbf{W}}_g^{\mathrm{T}}\hat{\boldsymbol{\sigma}}_g + \tilde{\mathbf{W}}_\tau^{\mathrm{T}}\hat{\boldsymbol{\sigma}}_\tau \\ & + \left(\hat{\mathbf{W}}_M^{\mathrm{T}}\,\boldsymbol{\sigma}'_M\tilde{\mathbf{V}}_M^{\mathrm{T}}\,\mathbf{z}_M\right)(\boldsymbol{\Omega}\mathbf{F}^*_{\mathrm{motion}} + \bar{\boldsymbol{\Omega}}\mathbf{F}^*_{\mathrm{force}}) \\ & + \left(\hat{\mathbf{W}}_B^{\mathrm{T}}\,\boldsymbol{\sigma}'_B\tilde{\mathbf{V}}_B^{\mathrm{T}}\,\mathbf{z}_B\right)(\boldsymbol{\Omega}\dot{\mathbf{x}}_r + \bar{\boldsymbol{\Omega}}\dot{\mathbf{f}}_r) \\ & + \hat{\mathbf{W}}_g^{\mathrm{T}}\,\boldsymbol{\sigma}'_g\tilde{\mathbf{V}}_g^{\mathrm{T}}\,\mathbf{z}_g + \hat{\mathbf{W}}_\tau^{\mathrm{T}}\,\boldsymbol{\sigma}'_\tau\tilde{\mathbf{V}}_\tau^{\mathrm{T}}\,\mathbf{z}_\tau\end{aligned} \tag{6.37}$$

and the "whole"NN errors $\boldsymbol{\zeta}$ is defined as

$$\begin{aligned}\boldsymbol{\zeta} = & \left(\tilde{\mathbf{W}}_M^{\mathrm{T}}\,\boldsymbol{\sigma}'_M\tilde{\mathbf{V}}_M^{\mathrm{T}}\,\mathbf{z}_M\right)(\boldsymbol{\Omega}\mathbf{F}^*_{\mathrm{motion}} + \bar{\boldsymbol{\Omega}}\mathbf{F}^*_{\mathrm{force}}) \\ & + \left(\tilde{\mathbf{W}}_B^{\mathrm{T}}\,\boldsymbol{\sigma}'_B\tilde{\mathbf{V}}_B^{\mathrm{T}}\,\mathbf{z}_B\right)(\boldsymbol{\Omega}\dot{\mathbf{x}}_r + \bar{\boldsymbol{\Omega}}\dot{\mathbf{f}}_r) \\ & + \tilde{\mathbf{W}}_g^{\mathrm{T}}\,\boldsymbol{\sigma}'_g\tilde{\mathbf{V}}_g^{\mathrm{T}}\,\mathbf{z}_g + \tilde{\mathbf{W}}_\tau^{\mathrm{T}}\,\boldsymbol{\sigma}'_\tau\tilde{\mathbf{V}}_\tau^{\mathrm{T}}\,\mathbf{z}_\tau \\ & + \left(\mathbf{W}_M^{\mathrm{T}}O(\tilde{\mathbf{V}}_M^{\mathrm{T}}\,\mathbf{z}_M)\right)(\boldsymbol{\Omega}\mathbf{F}^*_{\mathrm{motion}} + \bar{\boldsymbol{\Omega}}\mathbf{F}^*_{\mathrm{force}}) \\ & + \left(\mathbf{W}_B^{\mathrm{T}}O(\tilde{\mathbf{V}}_B^{\mathrm{T}}\,\mathbf{z}_B)\right)(\boldsymbol{\Omega}\dot{\mathbf{x}}_r + \bar{\boldsymbol{\Omega}}\dot{\mathbf{f}}_r) \\ & + \mathbf{W}_g^{\mathrm{T}}O(\tilde{\mathbf{V}}_g^{\mathrm{T}}\,\mathbf{z}_g) + \mathbf{W}_\tau^{\mathrm{T}}O(\tilde{\mathbf{V}}_\tau^{\mathrm{T}}\,\mathbf{z}_\tau) \\ & + \boldsymbol{\varepsilon}\end{aligned} \tag{6.38}$$

where the total approximation error $\boldsymbol{\varepsilon} = \boldsymbol{\varepsilon}_M(\boldsymbol{\Omega}\mathbf{F}^*_{\mathrm{motion}} + \bar{\boldsymbol{\Omega}}\mathbf{F}^*_{\mathrm{force}}) + \boldsymbol{\varepsilon}_B(\boldsymbol{\Omega}\dot{\mathbf{x}}_r + \bar{\boldsymbol{\Omega}}\dot{\mathbf{f}}_r) + \boldsymbol{\varepsilon}_g + \boldsymbol{\varepsilon}_\tau \leq \varepsilon_M$ (since the actual dynamics are bounded).

Note that, the driving signals $\dot{\mathbf{x}}_r$ (6.4) and $\mathbf{F}^*_{\mathrm{motion}}$ (6.7), used in (6.37) and (6.38), are different with $\dot{\mathbf{x}}_r$ and $\mathbf{F}^*_{\mathrm{motion}}$ in Section 4.4.2.

As in Section 4.4.2, the uncertainties $\boldsymbol{\eta}$ (6.36) can be shown to be bounded by using $\|\mathbf{L}_p - \hat{\mathbf{L}}_p\| \leq (\tilde{L}_p)_M$ in (4.47) and also $\mathbf{F}^*_{\mathrm{motion}}$ (6.7), $\mathbf{F}^*_{\mathrm{force}}$ (6.8) and $\dot{\mathbf{x}}_r$ defined in (6.10), $\dot{\mathbf{f}}_r$ defined in (6.12), as follows

$$\begin{aligned}\|\boldsymbol{\eta}\| &\leq (\tilde{L}_M)_M \ \left\|(\boldsymbol{\Omega}\mathbf{F}^*_{\text{motion}} + \bar{\boldsymbol{\Omega}}\mathbf{F}^*_{\text{force}})\right\| + (\tilde{L}_B)_M \ \left\|(\boldsymbol{\Omega}\dot{\mathbf{x}}_r + \bar{\boldsymbol{\Omega}}\dot{\mathbf{f}}_r)\right\| \\ &\quad + (\tilde{L}_g)_M + (\tilde{L}_\tau)_M + \varepsilon_M \\ &\leq (\tilde{L}_M)_M \ \left\|[\boldsymbol{\Omega}\ (\ddot{\mathbf{x}}_r + \boldsymbol{\Lambda}_1(\mathbf{r}_{\mathbf{x}1} + \mathbf{r}_{\mathbf{x}2})) + \bar{\boldsymbol{\Omega}}\ (\ddot{\mathbf{f}}'_r + \boldsymbol{\Lambda}_1(\mathbf{r}_{\mathbf{f}} + \mathbf{r}_{\mathbf{x}2}))]\right\| \\ &\quad + (\tilde{L}_B)_M \ \left\|[\boldsymbol{\Omega}\ (\mathbf{r}_{\mathbf{x}1} + \mathbf{r}_{\mathbf{x}2} + \dot{\mathbf{x}}_0) + \bar{\boldsymbol{\Omega}}\ (\mathbf{r}_{\mathbf{f}} + \mathbf{r}_{\mathbf{x}2} + \dot{\mathbf{x}}_0)]\right\| \\ &\quad + (\tilde{L}_g)_M + (\tilde{L}_\tau)_M + \varepsilon_M\end{aligned} \tag{6.39}$$

Note that $\ddot{\mathbf{x}}_r$ (6.9) can be assumed to be bounded since the desired trajectories $\ddot{\mathbf{x}}_d, \dot{\mathbf{x}}_d, \mathbf{x}_d$ are bounded by design, $\mathbf{x}$ is bounded by the workspace and $\dot{\hat{\mathbf{x}}}$ can be shown to be bounded. And $\dot{\mathbf{x}}_0$ in (6.5) can be shown to be bounded due to $\dot{\hat{\mathbf{x}}}$ and $\hat{\mathbf{x}}$ can be shown to be bounded. And $\ddot{\mathbf{f}}'_r$ in (6.11) can be shown to be bounded since $\dot{\mathbf{x}}_0$ can be shown to be bounded, $\mathbf{f}_d$ is bound by design and $\mathbf{f}$ can be safely assumed to be bounded. Now, for ease of representation, let's define

$$\mathbf{r}_1 = \boldsymbol{\Omega}\mathbf{r}_{\mathbf{x}1} + \bar{\boldsymbol{\Omega}}\mathbf{r}_{\mathbf{f}} \tag{6.40}$$

$$\mathbf{r}_2 = \mathbf{r}_{\mathbf{x}2} \tag{6.41}$$

therefore

$$\mathbf{r}_1 + \mathbf{r}_2 = (\boldsymbol{\Omega}\mathbf{r}_{\mathbf{x}1} + \bar{\boldsymbol{\Omega}}\mathbf{r}_{\mathbf{f}}) + (\boldsymbol{\Omega}\mathbf{r}_{\mathbf{x}2} + \bar{\boldsymbol{\Omega}}\mathbf{r}_{\mathbf{x}2}). \tag{6.42}$$

Hence $\boldsymbol{\eta}$, by taking into account (6.42), can be shown to be bounded as

$$\begin{aligned}\|\boldsymbol{\eta}\| &\leq C_0 + C_1 \ \left\|[\boldsymbol{\Omega}\ (\mathbf{r}_{\mathbf{x}1} + \mathbf{r}_{\mathbf{x}2}) + \bar{\boldsymbol{\Omega}}\ (\mathbf{r}_{\mathbf{f}} + \mathbf{r}_{\mathbf{x}2})]\right\| \\ &\leq C_0 + C_1\ (\|\mathbf{r}_1\| + \|\mathbf{r}_2\|).\end{aligned} \tag{6.43}$$

where $C_0, C_1 > 0$. And since $\boldsymbol{\eta} = \boldsymbol{\xi} + \boldsymbol{\zeta}$, then clearly the following inequalities are true

$$\boldsymbol{\xi} \leq C_0 + C_1\ (\|\mathbf{r}_1\| + \|\mathbf{r}_2\|) \tag{6.44}$$

$$\boldsymbol{\zeta} \leq C_0 + C_1\ (\|\mathbf{r}_1\| + \|\mathbf{r}_2\|). \tag{6.45}$$

Note that, the definitions of $\mathbf{r}_1$ (6.40) and $\mathbf{r}_2$ (6.41) in this section, are different with the definitions of $\mathbf{r}_1$ (5.9) and $\mathbf{r}_2$ (5.10) in Section 5.3.4.

For ease of later developments, let us define $\mathbf{Z} = \text{diag}[\mathbf{W}, \mathbf{V}]$ to be upper-bounded as follows

$$\|\mathbf{Z}\| = \sqrt{\|\mathbf{W}\|^2 + \|\mathbf{V}\|^2} \leq Z_M \tag{6.46}$$

where Z_M is a positive scalar constant, $\mathbf{W} = \text{diag}[\mathbf{W}_M, \mathbf{W}_B, \mathbf{W}_g, \mathbf{W}_\tau]$ and $\mathbf{V} = \text{diag}[\mathbf{V}_M, \mathbf{V}_B, \mathbf{V}_g, \mathbf{V}_\tau]$.

6.3.5 Stability Analysis

For the force - motion controller (6.3) and the observer (6.25), (6.26), let the NN weight updates be provided as

$$\dot{\hat{\mathbf{w}}}_{M_{ij}} = \mathbf{F}_{M_{ij}}(\hat{\boldsymbol{\sigma}}_M\ (r_{1,i} + r_{2,i})\ (\Omega_j\ F^*_{\text{motion},j} + \bar{\Omega}_j\ F^*_{\text{force},j}) - \kappa\ \hat{\mathbf{w}}_{M_{ij}}) \tag{6.47}$$

$$\begin{aligned}\dot{\hat{\mathbf{v}}}_{M_k} = \mathbf{G}_{M_k}(\mathbf{z}_M\ \hat{\boldsymbol{\sigma}}'_{M_k}\ (\sum_{i=1}^{m}\sum_{j=1}^{m} \hat{w}_{M_{ijk}}\ (r_{1,i} + r_{2,i})(\Omega_j F^*_{\text{motion},j} + \bar{\Omega}_j F^*_{\text{force},j})) \\ - \kappa\ \hat{\mathbf{v}}_{M_k})\end{aligned} \tag{6.48}$$

$$\dot{\hat{\mathbf{w}}}_{B_{ij}} = \mathbf{F}_{B_{ij}}(\hat{\boldsymbol{\sigma}}_B\ (r_{1,i} + r_{2,i})\ (\Omega_j\ \dot{x}_{r,j} + \bar{\Omega}_j\ \dot{f}_{r,j}) - \kappa\ \hat{\mathbf{w}}_{B_{ij}}) \tag{6.49}$$

$$\begin{aligned}\dot{\hat{\mathbf{v}}}_{B_k} = \mathbf{G}_{B_k}(\mathbf{z}_B\ \hat{\boldsymbol{\sigma}}'_{B_k}\ (\sum_{i=1}^{m}\sum_{j=1}^{m} \hat{w}_{B_{ijk}}\ (r_{1,i} + r_{2,i})\ (\Omega_j\ \dot{x}_{r,j} + \bar{\Omega}_j\ \dot{f}_{r,j})) \\ - \kappa\ \hat{\mathbf{v}}_{B_k})\end{aligned} \tag{6.50}$$

$$\dot{\hat{\mathbf{w}}}_{g_i} = \mathbf{F}_{g_i}(\hat{\boldsymbol{\sigma}}_g\ (r_{1,i} + r_{2,i}) - \kappa\ \hat{\mathbf{w}}_{g_i}) \tag{6.51}$$

$$\dot{\hat{\mathbf{v}}}_{g_k} = \mathbf{G}_{g_k}(\mathbf{z}_g\ \hat{\boldsymbol{\sigma}}'_{g_k}\ (\sum_{i=1}^{m} \hat{w}_{g_{ik}}\ (r_{1,i} + r_{2,i})) - \kappa\ \hat{\mathbf{v}}_{g_k}) \tag{6.52}$$

$$\dot{\hat{\mathbf{w}}}_{\tau_i} = \mathbf{F}_{\tau_i}(\hat{\boldsymbol{\sigma}}_\tau\ (r_{1,i} + r_{2,i}) - \kappa\ \hat{\mathbf{w}}_{\tau_i}) \tag{6.53}$$

$$\dot{\hat{\mathbf{v}}}_{\tau_k} = \mathbf{G}_{\tau_k}(\mathbf{z}_\tau\ \hat{\boldsymbol{\sigma}}'_{\tau_k}\ (\sum_{i=1}^{m} \hat{w}_{\boldsymbol{\tau}_{ik}}\ (r_{1,i} + r_{2,i})) - \kappa\ \hat{\mathbf{v}}_{\tau_k}) \tag{6.54}$$

with κ is a positive constant. And the estimated NN weight updates: $\dot{\hat{\mathbf{w}}}_{M_{ij}} \in \Re^{N_2}, \dot{\hat{\mathbf{v}}}_{M_k} \in \Re^{N_{1,M}}, \dot{\hat{\mathbf{w}}}_{B_{ij}} \in \Re^{N_2}, \dot{\hat{\mathbf{v}}}_{B_k} \in \Re^{N_{1,B}}, \dot{\hat{\mathbf{w}}}_{g_i} \in \Re^{N_2}, \dot{\hat{\mathbf{v}}}_{g_k} \in \Re^{N_{1,g}}, \dot{\hat{\mathbf{w}}}_{\tau_i} \in \Re^{N_2}$, $\dot{\hat{\mathbf{v}}}_{\tau_k} \in \Re^{N_{1,\tau}}$ are all column vector. And the adaptive gains: $\mathbf{F}_{M_{ij}}^{-1} \in \Re^{N_2 \times N_2}$, ..., $\mathbf{F}_{\tau_i}^{-1} \in \Re^{N_2 \times N_2}$ and $\mathbf{G}_{M_k}^{-1} \in \Re^{N_{1,M} \times N_{1,M}}, \ldots, \mathbf{G}_{\tau_k}^{-1} \in \Re^{N_{1,\tau} \times N_{1,\tau}}$ are all positive diagonal matrices. The following indices are defined: $i, j = 1, \ldots, m$ are output-layer indices, $k = 1, \ldots, N_2$ is the hidden-layer index, where to simplify the implementation, the hidden-node size N_2 is set the same throughout. While $N_{1,M}, N_{1,B}, N_{1,g}, N_{1,\tau}$ are the respective input-node sizes.

Proposition 6.3.1 *Let* $\mathbf{y} = [\mathbf{r}_1^{\mathrm{T}} \ \mathbf{r}_2^{\mathrm{T}}]^{\mathrm{T}}$. *With the assumptions that:*

1. *the controller gain* $\mathbf{\Lambda}_1$ *and the observer gain* $\mathbf{l}_D$ *meet the conditions*

$$\Lambda_{1,m} > \frac{C_1}{M_{x,m}} \tag{6.55}$$

$$l_{D,m} > \frac{M_{x,M}\ \Lambda_{1,M} + \ 3\ C_1}{M_{x,m}} \tag{6.56}$$

   where $C_1 > 0$, $\Lambda_{1,m} = min(\mathbf{\Lambda}_1)$, $\Lambda_{1,M} = max(\mathbf{\Lambda}_1)$, $M_{x,m} = min(\lambda_{min}(\mathbf{M}_{\mathbf{x}}(t)))$, $M_{x,M} = min(\lambda_{max}(\mathbf{M}_{\mathbf{x}}(t)))$ *and* $l_{D,m} = min(\mathbf{l}_D)$*;*

2. y_M*, the upper-bound constraint of* $\mathbf{y}$*, and,* $\hat{Z}_M$*, the upper-bound of the estimated NN weights,* $\hat{\mathbf{Z}}$*, satisfy*

$$y_M > \ b_y \tag{6.57}$$

$$\hat{Z}_M > \ \sqrt{\frac{((\tau_{fric})_M + 3\ C_0)^2}{4\ \kappa\ \Psi_m}} \tag{6.58}$$

   where $C_0, \kappa > 0$, $(\tau_{fric})_M$ *is the upper-bound of* $\|\boldsymbol{\tau}_{\mathbf{x}}(\mathbf{q}, \dot{\mathbf{q}}) - \boldsymbol{\tau}_{\mathbf{x}}(\mathbf{q}, \dot{\hat{\mathbf{q}}})\|$, $\Psi_m = min(\mathbf{\Psi})$ *with* $\mathbf{\Psi}$ *is to be defined in* (6.72)*, and* b_y *is to be defined in* (6.76)*; and*

3. *both initial conditions of* $\mathbf{y}$ *and* $\tilde{\mathbf{Z}}$ *satisfy*

$$\|\mathbf{y}(0)\| < y_M \tag{6.59}$$

$$\|\tilde{\mathbf{Z}}(0)\| < \tilde{Z}_M; \tag{6.60}$$

where y_M *is the upper-bound of* y *and* $\tilde{Z}_M$ *is the upper-bound of the NN weight errors,* $\tilde{\mathbf{Z}}$*;*

then using the proposed motion control (6.3)*, the observer* (6.25) – (6.26) *and the NN weight updates* (6.47)-(6.54)*, it can be shown by Lyapunov's extension theorem [102] that as* $t \to \infty$*, the errors* $\|\mathbf{r}_1\|$*,* $\|\mathbf{r}_2\|$ *and* $\|\tilde{\mathbf{W}}\|, \|\tilde{\mathbf{V}}\|$ *will be bounded by enclosing boundary* $\mathcal{S}$*, which is defined by enclosing region* $\dot{V}(\mathbf{y}, \tilde{\mathbf{Z}}) < 0$*.*

Proof 6.3.1 *The chosen Lyapunov function candidate for error dynamics* (6.24) *and* (6.31)*, with the uncertainties* $\boldsymbol{\eta}$ (6.36)*, is*

$$\begin{aligned} V(\mathbf{r}_1, \mathbf{r}_2, \tilde{\mathbf{Z}}) = \frac{1}{2}\, \mathbf{r}_1^{\mathrm{T}} \mathbf{M}_{\mathbf{x}}(\mathbf{q}) \mathbf{r}_1 + \frac{1}{2}\, \mathbf{r}_2^{\mathrm{T}} \mathbf{M}_{\mathbf{x}}(\mathbf{q}) \mathbf{r}_2 \\ + \frac{1}{2} \sum_{i=1}^{m} \sum_{j=1}^{m} \tilde{\mathbf{w}}_{M_{ij}}^{\mathrm{T}}\, \mathbf{F}_{M_{ij}}^{-1}\, \tilde{\mathbf{w}}_{M_{ij}} + \ldots + \frac{1}{2} \sum_{i=1}^{m} \tilde{\mathbf{w}}_{\tau_i}^{\mathrm{T}}\, \mathbf{F}_{\tau_i}^{-1}\, \tilde{\mathbf{w}}_{\tau_i} \\ + \frac{1}{2} \sum_{k=1}^{N_2} \tilde{\mathbf{v}}_{M_k}^{\mathrm{T}}\, \mathbf{G}_{M_k}^{-1}\, \tilde{\mathbf{v}}_{M_k} + \ldots + \frac{1}{2} \sum_{k=1}^{N_2} \tilde{\mathbf{v}}_{\tau_k}^{\mathrm{T}}\, \mathbf{G}_{\tau_k}^{-1}\, \tilde{\mathbf{v}}_{\tau_k} \end{aligned} \tag{6.61}$$

where the NN weight errors: $\tilde{\mathbf{w}}_{M_{ij}} \in \Re^{N_2}, \tilde{\mathbf{v}}_{M_k} \in \Re^{N_{1,M}}, \tilde{\mathbf{w}}_{B_{ij}} \in \Re^{N_2}, \tilde{\mathbf{v}}_{B_k} \in \Re^{N_{1,B}}, \tilde{\mathbf{w}}_{g_i} \in \Re^{N_2}, \tilde{\mathbf{v}}_{g_k} \in \Re^{N_{1,g}}, \tilde{\mathbf{w}}_{\tau_i} \in \Re^{N_2}, \tilde{\mathbf{v}}_{\tau_k} \in \Re^{N_{1,\tau}}$ *are all column vector.*

Next, we substitute the closed-loop dynamics (6.24)*,* (6.31)*, Property 4.3.5 and also take into account* $\boldsymbol{\eta}$ (6.36)*, the definition* $\boldsymbol{\xi}$ (6.37) *and the knowledge* $\|\boldsymbol{\zeta}\| \leq$

$C_0 + C_1(\|\mathbf{r}_1\| + \|\mathbf{r}_2\|)$ (6.45) *and also we take the fact that* $\mathbf{\Omega A \bar{\Omega}} = \mathbf{\bar{\Omega} A \Omega} = \mathbf{0}$ *for any positive diagonal matrix* $\mathbf{A}$*, into* $\dot{V}(\mathbf{r}_1, \mathbf{r}_2, \tilde{\mathbf{Z}})$ *of* (6.61)*, to obtain*

$$\begin{aligned}\dot{V}(\mathbf{r}_1, \mathbf{r}_2, \tilde{\mathbf{Z}}) = &- \mathbf{r}_1^{\mathrm{T}} \mathbf{M}_{\mathbf{x}}(\mathbf{q}) \mathbf{\Lambda}_1 \mathbf{r}_1 - \mathbf{r}_2^{\mathrm{T}} \mathbf{M}_{\mathbf{x}}(\mathbf{q})(\mathbf{l}_D - \mathbf{\Lambda}_1)\mathbf{r}_2 \\ &+ \mathbf{r}_1^{\mathrm{T}} \mathbf{B}_{\mathbf{x}}(\mathbf{q}, \mathbf{\Omega}\dot{\mathbf{x}}_r + \bar{\mathbf{\Omega}}\dot{\mathbf{f}}_r)\mathbf{r}_2 + \mathbf{r}_2^{\mathrm{T}} \mathbf{B}_{\mathbf{x}}(\mathbf{q}, \dot{\mathbf{x}}_0)\mathbf{r}_1 \\ &+ (\mathbf{r}_1^{\mathrm{T}} - \mathbf{r}_2^{\mathrm{T}})(\boldsymbol{\tau}_{\mathbf{x}}(\mathbf{q}, \dot{\mathbf{q}}) - \boldsymbol{\tau}_{\mathbf{x}}(\mathbf{q}, \dot{\hat{\mathbf{q}}})) \\ &+ C_0\|\mathbf{r}_1\| + C_0\|\mathbf{r}_2\| + C_1\|\mathbf{r}_1\|^2 + 2\, C_1\|\mathbf{r}_1\|\|\mathbf{r}_2\| + C_2\|\mathbf{r}_1\|^2 \\ &+ \boldsymbol{\psi}\end{aligned} \tag{6.62}$$

where the lump parameter $\boldsymbol{\psi}$ *in* (6.62) *is defined as*

$$\begin{aligned}\boldsymbol{\psi} = &\sum_{i=1}^{m}\sum_{j=1}^{m} \tilde{\mathbf{w}}_{M_{ij}}^{\mathrm{T}} \left(\mathbf{F}_{M_{ij}}^{-1}\, \dot{\tilde{\mathbf{w}}}_{M_{ij}} + \hat{\boldsymbol{\sigma}}_M\, (r_{1,i} - r_{2,i})(\Omega_j\, F^*_{\mathrm{motion},j} + \bar{\Omega}_j\, F^*_{\mathrm{force},j}) \right) \\ &+ \sum_{k=1}^{N_2} \tilde{\mathbf{v}}_{M_k}^{\mathrm{T}} (\mathbf{G}_{M_k}^{-1}\, \dot{\tilde{\mathbf{v}}}_{M_k} + \mathbf{z}_M\, \hat{\boldsymbol{\sigma}}'_{M_k} (\sum_{i=1}^{m}\sum_{j=1}^{m} \hat{w}_{M_{ijk}}\, (r_{1,i} - r_{2,i}) \\ &\quad (\Omega_j\, F^*_{\mathrm{motion},j} + \bar{\Omega}_j\, F^*_{\mathrm{force},j}))) \\ &+ \sum_{i=1}^{m}\sum_{j=1}^{m} \tilde{\mathbf{w}}_{B_{ij}}^{\mathrm{T}} \left(\mathbf{F}_{B_{ij}}^{-1}\, \dot{\tilde{\mathbf{w}}}_{B_{ij}} + \hat{\boldsymbol{\sigma}}_B\, (r_{1,i} - r_{2,i})(\Omega_j\, \dot{x}_{r,j} + \bar{\Omega}_j\, \dot{f}_{r,j}) \right) \\ &+ \sum_{k=1}^{N_2} \tilde{\mathbf{v}}_{B_k}^{\mathrm{T}} (\mathbf{G}_{B_k}^{-1}\, \dot{\tilde{\mathbf{v}}}_{B_k} + \mathbf{z}_B\, \hat{\boldsymbol{\sigma}}'_{B_k} (\sum_{i=1}^{m}\sum_{j=1}^{m} \hat{w}_{B_{ijk}}\, (r_{1,i} - r_{2,i}) \\ &\quad (\Omega_j\, \dot{x}_{r,j} + \bar{\Omega}_j\, \dot{f}_{r,j}))) \\ &+ \sum_{i=1}^{m} \tilde{\mathbf{w}}_{g_i}^{\mathrm{T}} \left(\mathbf{F}_{g_i}^{-1}\, \dot{\tilde{\mathbf{w}}}_{g_i} + \hat{\boldsymbol{\sigma}}_g\, (r_{1,i} - r_{2,i}) \right) \\ &+ \sum_{k=1}^{N_2} \tilde{\mathbf{v}}_{g_k}^{\mathrm{T}} \left(\mathbf{G}_{g_k}^{-1}\, \dot{\tilde{\mathbf{v}}}_{g_k} + \mathbf{z}_g\, \hat{\boldsymbol{\sigma}}'_{g_k} (\sum_{i=1}^{m} \hat{w}_{g_{ik}}\, (r_{1,i} - r_{2,i})) \right) \\ &+ \sum_{i=1}^{m} \tilde{\mathbf{w}}_{\tau_i}^{\mathrm{T}} \left(\mathbf{F}_{\tau_i}^{-1}\, \dot{\tilde{\mathbf{w}}}_{\tau_i} + \hat{\boldsymbol{\sigma}}_\tau\, (r_{1,i} - r_{2,i}) \right) \\ &+ \sum_{k=1}^{N_2} \tilde{\mathbf{v}}_{\tau_k}^{\mathrm{T}} \left(\mathbf{G}_{\tau_k}^{-1}\, \dot{\tilde{\mathbf{v}}}_{\tau_k} + \mathbf{z}_\tau\, \hat{\boldsymbol{\sigma}}'_{M_k} (\sum_{i=1}^{m} \hat{w}_{\boldsymbol{\tau}_{ik}}\, (r_{1,i} - r_{2,i})) \right)\end{aligned} \tag{6.63}$$

Using $\boldsymbol{\xi}$ (6.37)*, it can be demonstrated that* $\boldsymbol{\psi}$ (6.63) *is made up of* $\dot{\hat{\mathbf{W}}}$, $\dot{\hat{\mathbf{V}}}$ *and* $(\mathbf{r}_1 - \mathbf{r}_2)^{\mathrm{T}}\ \boldsymbol{\xi}$*. The idea is to cancel* $(\mathbf{r}_1 - \mathbf{r}_2)^{\mathrm{T}}\ \boldsymbol{\xi}$ *with* $\dot{\hat{\mathbf{W}}}, \dot{\hat{\mathbf{V}}}$*. Unfortunately, only* $(\mathbf{r}_1 + \mathbf{r}_2)$ *can be computed (see* (6.42)*), hence only* $\mathbf{r}_1^{\mathrm{T}}\ \boldsymbol{\xi}$ *can be canceled by* $\dot{\hat{\mathbf{W}}}, \dot{\hat{\mathbf{V}}}$*. With the weight updates* $\dot{\hat{\mathbf{W}}}, \dot{\hat{\mathbf{V}}}$ (6.47) – (6.54) *(note that* $-\dot{\hat{\mathbf{W}}} = \dot{\hat{\mathbf{W}}}$*, since* $\tilde{\mathbf{W}} = \mathbf{W} - \hat{\mathbf{W}}$ *and* $\mathbf{W}$ *is constant), and taking into consideration* $\|\boldsymbol{\xi}\| \leq\ C_0 + C_1(\|\mathbf{r}_1\| + \|\mathbf{r}_2\|)$ (6.44)*,* $\boldsymbol{\psi}$ (6.63) *can be expressed as:*

$$\begin{aligned}\boldsymbol{\psi} &= \kappa \sum_{i=1}^{m}\sum_{j=1}^{m} \tilde{\mathbf{w}}_{M_{ij}}^{\mathrm{T}} \hat{\mathbf{w}}_{M_{ij}} + \ldots + \kappa \sum_{k=1}^{N_2} \tilde{\mathbf{v}}_{\tau_k}^{\mathrm{T}} \hat{\mathbf{v}}_{\tau_k} - 2\ \mathbf{r}_2^{\mathrm{T}}\ \boldsymbol{\xi} \\ &\leq -\kappa\|\tilde{\mathbf{Z}}\|^2 + \kappa\|\tilde{\mathbf{Z}}\| Z_M + 2\ C_0\|\mathbf{r}_2\| + 2\ C_1\|\mathbf{r}_1\|\|\mathbf{r}_2\| + 2\ C_1\|\mathbf{r}_2\|^2.\end{aligned} \tag{6.64}$$

Note, equation (6.64) *is obtained by using the inner products in* (4.68) – (4.71)*.*

The substitution of $\boldsymbol{\psi}$ (6.64) *into* $\dot{V}(\mathbf{r}_1, \mathbf{r}_2, \tilde{\mathbf{Z}})$ (6.62)*, yields*

$$\begin{aligned}\dot{V}(\mathbf{r}_1, \mathbf{r}_2, \tilde{\mathbf{Z}}) =& -\mathbf{r}_1^{\mathrm{T}}\mathbf{M}_{\mathbf{x}}(\mathbf{q})\boldsymbol{\Lambda}_1\mathbf{r}_1 - \mathbf{r}_2^{\mathrm{T}}\mathbf{M}_{\mathbf{x}}(\mathbf{q})(\mathbf{l}_D - \boldsymbol{\Lambda}_1)\mathbf{r}_2 \\ &+ \mathbf{r}_1^{\mathrm{T}}\mathbf{B}_{\mathbf{x}}(\mathbf{q}, \boldsymbol{\Omega}\dot{\mathbf{x}}_r + \bar{\boldsymbol{\Omega}}\dot{\mathbf{f}}_r)\mathbf{r}_2 + \mathbf{r}_2^{\mathrm{T}}\mathbf{B}_{\mathbf{x}}(\mathbf{q}, \dot{\mathbf{x}}_0)\mathbf{r}_1 \\ &+ (\mathbf{r}_1^{\mathrm{T}} - \mathbf{r}_2^{\mathrm{T}})(\boldsymbol{\tau}_{\mathbf{x}}(\mathbf{q}, \dot{\mathbf{q}}) - \boldsymbol{\tau}_{\mathbf{x}}(\mathbf{q}, \dot{\hat{\mathbf{q}}})) \\ &+ C_0\|\mathbf{r}_1\| + 3\ C_0\|\mathbf{r}_2\| + C_1\|\mathbf{r}_1\|^2 + 4\ C_1\|\mathbf{r}_1\|\|\mathbf{r}_2\| + 3\ C_1\|\mathbf{r}_2\|^2 \\ &- \kappa\|\tilde{\mathbf{Z}}\|^2 + \kappa\|\tilde{\mathbf{Z}}\| Z_M\end{aligned} \tag{6.65}$$

The following terms, using Property 4.2, can be written as:

$$-\mathbf{r}_1^{\mathrm{T}}\mathbf{M}_{\mathbf{x}}(\mathbf{q})\boldsymbol{\Lambda}_1\mathbf{r}_1 \leq -\ M_{x,m}\ \Lambda_{1,m}\|\mathbf{r}_1\|^2 \tag{6.66}$$

$$-\mathbf{r}_2^{\mathrm{T}}(\mathbf{M}_{\mathbf{x}}(\mathbf{q})\mathbf{l}_D - \mathbf{M}_{\mathbf{x}}(\mathbf{q})\boldsymbol{\Lambda}_1)\mathbf{r}_2 \leq -\ (M_{x,m}l_{D,m} - M_{x,M}\Lambda_{1,M})\|\mathbf{r}_2\|^2 \tag{6.67}$$

where $\Lambda_{1,m}, \Lambda_{1,M}, M_{x,m}, M_{x,M}, l_{D,m}$ *are as defined in* (6.55) *and* (6.56)*.*

The next terms, by taking into account Property 4.3.3, can be written as:

$$\begin{aligned}&\|\mathbf{r}_1^{\mathrm{T}}\mathbf{B}_{\mathbf{x}}(\mathbf{q}, \boldsymbol{\Omega}\dot{\mathbf{x}}_r + \bar{\boldsymbol{\Omega}}\dot{\mathbf{f}}_r)\mathbf{r}_2\| + \|\mathbf{r}_2^{\mathrm{T}}\mathbf{B}_{\mathbf{x}}(\mathbf{q}, \dot{\mathbf{x}}_0)\mathbf{r}_1\| \\ \leq& \|\mathbf{r}_1\|\|\mathbf{r}_2\| B_{x,M}(\|\mathbf{r}_1\| + \|\mathbf{r}_2\| + 2\dot{x}_M).\end{aligned} \tag{6.68}$$

This is due to the fact $\dot{\mathbf{x}}_r = \mathbf{r}_{\mathbf{x}1} + \dot{\mathbf{x}}$ *in* (6.16), $\dot{\mathbf{f}}_r = \mathbf{r}_{\mathbf{f}1} + \dot{\mathbf{x}}$ *in* (6.19) *and* $\dot{\mathbf{x}}_0 = \dot{\mathbf{x}} - \mathbf{r}_{\mathbf{x}2}$ *in* (6.17).

The remaining two terms can be shown to be bounded as:

$$\|\boldsymbol{\tau}_{\mathbf{x}}(\mathbf{q}, \dot{\mathbf{q}}) - \boldsymbol{\tau}_{\mathbf{x}}(\mathbf{q}, \dot{\hat{\mathbf{q}}})\| \leq (\tau_{fric})_M. \tag{6.69}$$

which is obtained from (6.22)*, Property 3.2.4 and the followings:*

1. $\|\mathbf{J}^{-\mathrm{T}}\boldsymbol{\tau}_{vis}\mathbf{J}^{-1}\dot{\tilde{\mathbf{x}}}\|$ *is bounded because* $\boldsymbol{\tau}_{vis}$ *is bounded (as shown in* (3.7)*),* $\|\mathbf{J}^{-1}\|$ *is bounded for non-singular configuration of the manipulator and it was assumed that* $\|\dot{\tilde{\mathbf{x}}}\|$ *is bounded.*

2. $\|\boldsymbol{\tau}_{cou}(sgn(\dot{\mathbf{q}}) - sgn(\dot{\hat{\mathbf{q}}}))\|$ *is bounded because* $\boldsymbol{\tau}_{cou}$ *is shown to be bounded in* (3.8) *and because* $(sgn(\dot{q}_i) - sgn(\dot{\hat{q}}_i))$ *is bounded.*

3. $\|\boldsymbol{\tau}_{sti}(exp^{(-\boldsymbol{\tau}_{dec}\dot{\mathbf{q}}^2)}sgn(\dot{\mathbf{q}}) - exp^{(-\boldsymbol{\tau}_{dec}\dot{\hat{\mathbf{q}}}^2)}sgn(\dot{\hat{\mathbf{q}}}))\|$ *is bounded because* $\boldsymbol{\tau}_{sti}$ *is shown to be bounded in* (3.9) *and because both* $sgn(\cdot)$ *and* $exp^{-|a|}$ *are bounded.*

Substituting (6.66)–(6.69) *into* $\dot{V}(\mathbf{r}_1, \mathbf{r}_2, \tilde{\mathbf{Z}})$ *in* (6.65)*, we have*

$$\begin{aligned}
\dot{V}(\mathbf{r}_1, \mathbf{r}_2, \tilde{\mathbf{Z}}) \leq & -(M_{x,m}\,\Lambda_{1,m} - C_1)\,\|\mathbf{r}_1\|^2 \\
& -(M_{x,m}l_{D,m} - M_{x,M}\Lambda_{1,M} - 3\,C_1)\,\|\mathbf{r}_2\|^2 \\
& +\|\mathbf{r}_1\|\|\mathbf{r}_2\|\,[B_{x,M}(\|\mathbf{r}_1\| + \|\mathbf{r}_2\| + 2\dot{x}_M) + 4\,C_1] \\
& +((\tau_{fric})_M + C_0)\,\|\mathbf{r}_1\| + ((\tau_{fric})_M + 3\,C_0)\,\|\mathbf{r}_2\| \\
& -\kappa\|\tilde{\mathbf{Z}}\|^2 + \kappa\|\tilde{\mathbf{Z}}\|Z_M.
\end{aligned} \tag{6.70}$$

Defining $\mathbf{y}^{\mathrm{T}} = \begin{bmatrix}\mathbf{r}_1^{\mathrm{T}} & \mathbf{r}_2^{\mathrm{T}}\end{bmatrix}$, $\dot{V}(\mathbf{r}_1, \mathbf{r}_2, \tilde{\mathbf{Z}})$ (6.70) *can be written as*

$$\begin{aligned}\dot{V}(\mathbf{y}, \tilde{\mathbf{Z}}) \leq & -\mathbf{y}^{\mathrm{T}}\mathbf{\Psi}\mathbf{y} + \begin{bmatrix}(\tau_{fric})_M + C_0 & 0 \\ 0 & (\tau_{fric})_M + 3\,C_0\end{bmatrix}\mathbf{y} \\ & - \kappa\|\tilde{\mathbf{Z}}\|^2 + \kappa\|\tilde{\mathbf{Z}}\|Z_M,\end{aligned} \tag{6.71}$$

where

$$\mathbf{\Psi} = \begin{bmatrix}(M_{x,m}\,\Lambda_{1,m} - C_1) & -\frac{1}{2}p \\ -\frac{1}{2}p & (M_{x,m}l_{D,m} - M_{x,M}\Lambda_{1,M} - 3\,C_1)\end{bmatrix} \tag{6.72}$$

$$p = B_{x,M}(\|\mathbf{r}_1\| + \|\mathbf{r}_2\| + 2\dot{x}_M) + 4\,C_1. \tag{6.73}$$

The matrix $\mathbf{\Psi}$ (6.72) *is greater than zero (positive definite) if*

$$p < 2\sqrt{(M_{x,m}\,\Lambda_{1,m} - C_1)(M_{x,m}l_{D,m} - M_{x,M}\,\Lambda_{1,M} - 3\,C_1)}; \tag{6.74}$$

where the right-hand side is positive due to hypotheses (6.55) *and* (6.56)*. Equation* (6.71) *can be written as*

$$\begin{aligned}\dot{V}(\mathbf{y}, \tilde{\mathbf{Z}}) \leq & -\Psi_m\left[\|\mathbf{y}\| - \frac{(\tau_{fric})_M + 3\,C_0}{2\Psi_m}\right]^2 - \kappa\left[\|\tilde{\mathbf{Z}}\| - \frac{Z_M}{2}\right]^2 \\ & + \frac{((\tau_{fric})_M + 3\,C_0)^2}{4\Psi_m} + \frac{\kappa Z_M^2}{4}\end{aligned} \tag{6.75}$$

Hence, $\dot{V}(\mathbf{y}, \tilde{\mathbf{Z}}) < 0$*, as depicted in Fig. 6.2, if*

$$\|\mathbf{y}\| > \sqrt{\frac{((\tau_{fric})_M + 3\,C_0)^2}{4\Psi_m^2} + \frac{\kappa Z_M^2}{4\Psi_m}} + \frac{(\tau_{fric})_M + 3\,C_0}{2\Psi_m} \equiv b_y, \qquad \textit{or} \tag{6.76}$$

$$\|\tilde{\mathbf{Z}}\| > \sqrt{\frac{((\tau_{fric})_M + 3\,C_0)^2}{4\kappa\Psi_m} + \frac{Z_M^2}{4}} + \frac{Z_M}{2} \equiv b_{\tilde{Z}} \tag{6.77}$$

Applying the Lyapunov's extension theorem [102] then as $t \to \infty$*, the errors* $\|\mathbf{y}\|$ *and* $\|\tilde{\mathbf{Z}}\|$ *can be shown to be bounded within* $\mathcal{S}$*, as follows:*

Suppose the errors start within the boundary of $\mathcal{S}$*, i.e.* $\|\mathbf{y}(0)\| < b_y$ *and* $\|\tilde{\mathbf{Z}}(0)\| < b_{\tilde{Z}} < \tilde{Z}_M$*, then they start their course towards the enclosing boundary* $\mathcal{S}$ *and when they start leaving the boundary of* $\mathcal{S}$ *since the* $V(\mathbf{y}, \tilde{\mathbf{Z}})$ *is decreasing (*$\dot{V}(\mathbf{y}, \tilde{\mathbf{Z}}) < 0$*) hence the errors cannot leave the boundary of* $\mathcal{S}$*. Note,*

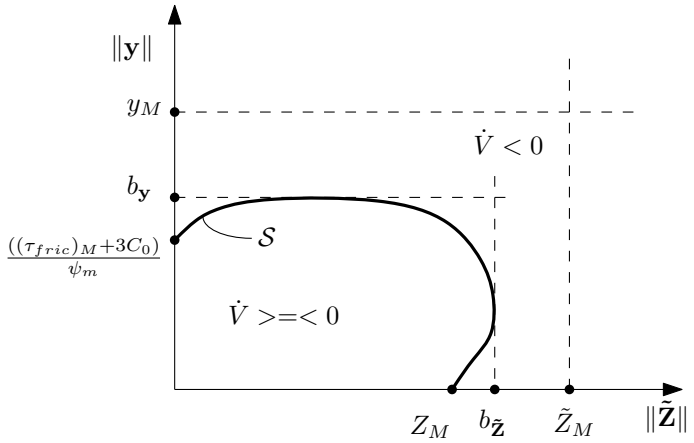

Figure 6.2: $\dot{V}(\mathbf{y}, \tilde{\mathbf{Z}})$ regions of the proposed NN adaptive force and motion strategy.

however, in its course towards the enclosing boundary $\mathcal{S}$, the error $\mathbf{y}$ cannot violate the constraint $\|\mathbf{y}\| < y_M$, therefore it signifies the last hypothesis $b_y < y_M$ in (6.57)*, as shown in Fig. 6.2. Now, suppose the errors start at outside the boundary of $\mathcal{S}$ then they tend to go to the equilibrium since $V(\mathbf{y}, \tilde{\mathbf{Z}})$ is decreasing. However, they cannot go to the equilibrium, but only up to entering the boundary of $\mathcal{S}$ and once they enter the boundary of $\mathcal{S}$, we have already shown that they are bounded.*

Using bounded-input-bounded-output (BIBO) property it can be shown that a bounded input $\mathbf{r}_2 = \mathbf{r}_{\mathbf{x}2}$, in (6.17)*, yields bounded outputs $\dot{\tilde{\mathbf{x}}}$ and $\tilde{\mathbf{x}}$. Bounded input $\mathbf{r}_1$* (6.40) *yields bounded output $\mathbf{\Omega r}_{\mathbf{x}1}$ and $\bar{\mathbf{\Omega}}\mathbf{r}_{\mathbf{f}}$. Bounded input $\mathbf{\Omega r}_{\mathbf{x}1}$* (6.16) *together with bounded $\mathbf{\Omega}\tilde{\mathbf{x}}$ yield $\lim_{t\to\infty} \mathbf{\Omega e}_{\mathbf{x}}, \mathbf{\Omega}\dot{\mathbf{e}}_{\mathbf{x}}$ that are bounded. Similarly, by using BIBO property and and taking into account the final-value-theorem (FVT) of Laplace transform, it can be shown that a bounded input $\bar{\mathbf{\Omega}}\mathbf{r}_{\mathbf{f}}$ in* (6.19) *yields error signals $\lim_{t\to\infty} \bar{\mathbf{\Omega}}\mathbf{e}_{\mathbf{f}} = 0$ and $\bar{\mathbf{\Omega}}\dot{\mathbf{e}}_{\mathbf{f}}$, $\int_0^{\tau=t} \bar{\mathbf{\Omega}}\ \mathbf{e}_{\mathbf{f}}\, d\tau$ that are bounded.*

The next part of the proof is to demonstrate the necessity of hypothesis $y_M > b_y$

in (6.57) *and* $\hat{Z}_M > \sqrt{\frac{((\tau_{fric})_M + 3\ C_0)^2}{4\ \kappa\ \Psi_m}}$ *in* (6.58)*, as follows:*

- *The error* $\mathbf{y}$ *can be shown to be upper-bounded by combining* (6.74) *and the definition of* p *in* (6.73)*:*

$$\|\mathbf{r}_1\| + \|\mathbf{r}_2\| < 2(1/B_{x,M}[\sqrt{\alpha} - 4\ C_1] - \ \dot{x}_M) \tag{6.78}$$

where $\alpha = (M_{x,m}\ \Lambda_{1,m} - C_1)(M_{x,m} l_{D,m} - M_{x,M}\ \Lambda_{1,M} - \ 3\ C_1) > 0$ *due to hypothesis* (6.55) *and* (6.56)*, and it is still true that*

$$\|\mathbf{y}\| = \sqrt{\|\mathbf{r}_1\|^2 + \|\mathbf{r}_2\|^2} < \sqrt{2}(1/B_{x,M}[\sqrt{\alpha} - 4\ C_1] - \ \dot{x}_M) \equiv \ y_M \tag{6.79}$$

where the right-hand side of (6.79) *can be defined as the upper-bound of* $\mathbf{y}$*. The last equation signifies the need of hypothesis* $y_M > b_y$ *in* (6.57)*; since* $\mathbf{y}$*, in its course towards the enclosing boundary* $\mathcal{S}$*, cannot violate the constraint* y_M*, otherwise, the Lyapunov's Extension Theorem is no longer applicable.*

- *Note that,* $\tilde{\mathbf{Z}}$*, in its course towards the enclosing boundary* $\mathcal{S}$*, cannot violate* $\tilde{Z}_M$*, otherwise the Lyapunov's Extension Theorem is no longer applicable. In other words,* $\tilde{Z}_M$ *in* (4.46) *must satisfy*

$$\tilde{Z}_M \equiv Z_M + \hat{Z}_M > b_{\tilde{\mathbf{Z}}}, \tag{6.80}$$

Therefore, it can be shown that if the following is satisfied

$$Z_M + \hat{Z}_M > \ \sqrt{\frac{((\tau_{fric})_M + 3\ C_0)^2}{4\kappa\Psi_m}} + Z_M > b_{\tilde{\mathbf{Z}}} \text{ or,} \tag{6.81}$$

$$\hat{Z}_M > \ \sqrt{\frac{((\tau_{fric})_M + 3\ C_0)^2}{4\kappa\Psi_m}} \tag{6.82}$$

then $\tilde{Z}_M > b_{\tilde{\mathbf{Z}}}$ *is also satisfied.*

Further, the initial condition $\|\mathbf{y}(0)\|$ *can be less or greater than* b_y*, however in order to comply with the Lyapunovs Extension Theorem, it must be less than* y_M*. Similarly,* $\|\tilde{\mathbf{Z}}(0)\|$ *must be less than* $\tilde{Z}_M$*. The last part of the proof is to demonstrate hypotheses* $\|\mathbf{y}(0)\| < y_M$ *in* (6.59) *and* $\|\tilde{\mathbf{Z}}(0)\| < \tilde{Z}_M$ *in* (6.60) *are to be satisfied in practical implementation:*

1. *In the implementation, it is possible to set* $\|\mathbf{y}(0)\|$ *to be as small as possible. As* $\|\mathbf{y}\| = \sqrt{\|\mathbf{r}_1\|^2 + \|\mathbf{r}_2\|^2}$ *comprises* $\mathbf{r}_2 = \mathbf{r}_{\mathbf{x}2}$ *and* $\mathbf{r}_1 = \mathbf{\Omega}\mathbf{r}_{\mathbf{x}1} + \bar{\mathbf{\Omega}}\mathbf{r}_{\mathbf{f}}$*, obtaining as small* $\|\mathbf{y}(0)\|$ *as possible can be achieved through:*

   - *The logic to make* $\mathbf{r}_{\mathbf{x}1}$ *and* $\mathbf{r}_{\mathbf{x}2}$ *as small as possible can be shown to be similar as in Section 5.3.5:*
     - *From* (6.16)*,* $\mathbf{r}_{\mathbf{x}2}(0) = \dot{\tilde{\mathbf{x}}}(0) + \mathbf{\Lambda}_2\tilde{\mathbf{x}}(0)$*: in practice, the force-motion control follows the impact control, which will make the system into low velocity* $\dot{\mathbf{x}}(0) \approx 0$*. Setting* $\dot{\hat{\mathbf{x}}}(0) = 0$ *results in* $\dot{\tilde{\mathbf{x}}}(0) = \dot{\mathbf{x}}(0) - \dot{\hat{\mathbf{x}}}(0) \approx 0$*. Setting the initial estimate of* $\mathbf{x}$ *equal to the actual end-effector pose, i.e.* $\hat{\mathbf{x}}(0) = \mathbf{x}(0)$*, results in zero estimation error* $\tilde{\mathbf{x}}(0) = 0$*. Hence,* $\mathbf{r}_2(0) \approx 0$*.*
     - *From* (6.17)*,* $\mathbf{r}_{\mathbf{x}1}(0) = \dot{\mathbf{x}}_d(0) - \dot{\mathbf{x}}(0) + \mathbf{\Lambda}_1\mathbf{e}_{\mathbf{x}}(0) + \mathbf{\Lambda}_1\tilde{\mathbf{x}}(0) + \mathbf{\Lambda}_i\mathbf{e}_{\mathbf{x}}(0)\Delta t$*: as in the previous point,* $\tilde{\mathbf{x}}(0) = 0$ *and* $\dot{\mathbf{x}}(0) \approx 0$*. The initial point of the desired trajectory can be set as* $\dot{\mathbf{x}}_d(0) = 0$ *and* $\mathbf{x}_d(0) = \mathbf{x}(0)$*, resulting in* $\dot{\mathbf{e}}_{\mathbf{x}}(0) = \dot{\mathbf{x}}_d(0) - \dot{\mathbf{x}}(0) \approx 0$ *and* $\mathbf{e}_{\mathbf{x}}(0) = 0$*. Hence* $\mathbf{r}_{\mathbf{x}1}(0) \approx 0$*.*
   - *From* (6.19)*,* $\mathbf{r}_{\mathbf{f}}(0) = -\dot{\mathbf{x}}(0) + \mathbf{K}_e^{-1}(\mathbf{\Lambda}_1\mathbf{e}_{\mathbf{f}}(0) + \mathbf{\Lambda}_i\mathbf{e}_{\mathbf{f}}(0)\Delta t)$*: as in the first point,* $\dot{\mathbf{x}}(0) \approx 0$*. The initial point of the desired force can be*

set equal to the actual force i.e. $\mathbf{f}_d(0) = \mathbf{f}(0)$*, resulting in* $\mathbf{e_f}(0) = 0$*. Hence* $\mathbf{r_f}(0) \approx 0$*.*

Therefore,

$$\|\mathbf{y}(0)\| \approx 0 < y_M. \tag{6.83}$$

2. *Hypothesis* $\|\tilde{\mathbf{Z}}(0)\| < \tilde{Z}_M$ *in* (6.60) *can be equally satisfied, if the following condition from* (4.46) *is satisfied*

$$\|\tilde{\mathbf{Z}}(0)\| \equiv \|\mathbf{Z}(0)\| + \|\hat{\mathbf{Z}}(0)\| \leq Z_M + \hat{Z}_M \equiv \tilde{Z}_M, \text{ or} \tag{6.84}$$

$$\|\hat{\mathbf{Z}}(0)\| \leq \hat{Z}_M. \tag{6.85}$$

In the implementation, the last equation can be achieved by simply initializing the NN force - motion weights (in this section) with the NN impact's stabilized weights as follows

$$\hat{\mathbf{Z}}(0)_{\textit{force-motion}} = \hat{\mathbf{Z}}_{\textit{impact}}, \tag{6.86}$$

where in practice, $\|\hat{\mathbf{Z}}\|_{\textit{impact}}$ *can be limited by design i.e.* $\|\hat{\mathbf{Z}}\|_{\textit{impact}} \leq \hat{Z}_M$*.*

6.4 NN Adaptive Impact Control Formulation

For fully automatic application, force - motion control can not be implemented directly after motion control. When the end-effector hits the working surface (contact state) it will produce impact force which need to be dissipated. In this section we propose NN adaptive impact force control, based upon motion dynamics as

$$\mathbf{M_x}(\mathbf{q})\ddot{\mathbf{x}} + \mathbf{B_x}(\mathbf{q}, \dot{\mathbf{q}})\dot{\mathbf{x}} + \mathbf{g_x}(\mathbf{q}) + \boldsymbol{\tau}_{\mathbf{x}}(\mathbf{q}, \dot{\mathbf{q}}) = \mathbf{F} \tag{6.87}$$

The NN adaptive impact control law is proposed as

$$\mathbf{F} = -\hat{\mathbf{M}}_{\mathbf{x}}(\mathbf{q})\mathbf{\Lambda}\,\dot{\mathbf{x}} + \hat{\mathbf{g}}_{\mathbf{x}}(\mathbf{q}) + \hat{\boldsymbol{\tau}}_{\mathbf{x}}(\mathbf{q}, \dot{\mathbf{q}}) \tag{6.88}$$

Note that we use impact control in short period to dissipate the impact force as quickly as possible, thus the availability of the actual velocity $\dot{\mathbf{x}}$ is assumed (although in practice it is obtained from filtered backward difference of joint position).

Combining the manipulator dynamics (6.87) and the proposed impact control (6.88), yields

$$\mathbf{M}_{\mathbf{x}}(\mathbf{q})\ddot{\mathbf{x}} = -\mathbf{M}_{\mathbf{x}}(\mathbf{q})\mathbf{\Lambda}\,\dot{\mathbf{x}} - \mathbf{B}_{\mathbf{x}}(\mathbf{q}, \dot{\mathbf{q}})\dot{\mathbf{x}} + \boldsymbol{\eta}; \tag{6.89}$$

where the uncertainties of the system $\boldsymbol{\eta}$

$$\boldsymbol{\eta} = \tilde{\mathbf{M}}_{\mathbf{x}}(\mathbf{q})\mathbf{\Lambda}\,\dot{\mathbf{x}} + \tilde{\mathbf{g}}_{\mathbf{x}}(\mathbf{q}) + \tilde{\boldsymbol{\tau}}_{\mathbf{x}}(\mathbf{q}, \dot{\mathbf{q}}). \tag{6.90}$$

6.4.1 Uncertainties η in NN terms

Now, similar with Section 4.4.2, $\mathbf{M}_{\mathbf{x}}(\mathbf{q})$, $\mathbf{g}_{\mathbf{x}}(\mathbf{q})$, and $\boldsymbol{\tau}_{\mathbf{x}}(\mathbf{q}, \dot{\mathbf{q}})$ in $\boldsymbol{\eta}$ (6.90) can be described as follows

$$\mathbf{M}_{\mathbf{x}}(\mathbf{q}) = \mathbf{W}_M^{\mathrm{T}}\,\boldsymbol{\sigma}_M(\mathbf{V}_M^{\mathrm{T}}\,\mathbf{z}_M) + \boldsymbol{\varepsilon}_M \tag{6.91}$$

$$\mathbf{g}_{\mathbf{x}}(\mathbf{q}) = \mathbf{W}_g^{\mathrm{T}}\,\boldsymbol{\sigma}_g(\mathbf{V}_g^{\mathrm{T}}\,\mathbf{z}_g) + \boldsymbol{\varepsilon}_g \tag{6.92}$$

$$\boldsymbol{\tau}_{\mathbf{x}}(\mathbf{q}, \dot{\mathbf{q}}) = \mathbf{W}_\tau^{\mathrm{T}}\,\boldsymbol{\sigma}_\tau(\mathbf{V}_\tau^{\mathrm{T}}\,\mathbf{z}_\tau) + \boldsymbol{\varepsilon}_\tau \tag{6.93}$$

Similarly, the estimated dynamic terms $\hat{\mathbf{M}}_{\mathbf{x}}(\mathbf{q})$, $\hat{\mathbf{g}}_{\mathbf{x}}(\mathbf{q})$, and $\hat{\boldsymbol{\tau}}_{\mathbf{x}}(\mathbf{q}, \dot{\mathbf{q}})$ are described by estimated weights $\hat{\mathbf{V}}_p, \hat{\mathbf{W}}_p$ with subscript $p = M, g, \tau$.

Similar with Section 4.4.2, $\mathbf{M_x(q)}, \mathbf{g_x(q)}, \boldsymbol{\tau_x(q, \dot{\hat{q}})}$ can be shown to be bounded. Therefore, the optimum weights $\mathbf{W}_p, \mathbf{V}_p$ and the approximation error $\boldsymbol{\varepsilon}_p$ (with subscript $p = M, g, \tau$) from (6.91)-(6.93), are also upper-bounded.

Using similar development and simplified notations $\boldsymbol{\sigma} \equiv \boldsymbol{\sigma}(\mathbf{V}^{\mathrm{T}}\mathbf{z})$, $\hat{\boldsymbol{\sigma}} \equiv \boldsymbol{\sigma}(\hat{\mathbf{V}}^{\mathrm{T}}\mathbf{z})$, and $\boldsymbol{\sigma} = \hat{\boldsymbol{\sigma}} + \tilde{\boldsymbol{\sigma}}$ as in Section 4.4.2, the uncertainties $\boldsymbol{\eta}$ (6.90) can be written as

$$\boldsymbol{\eta} = \boldsymbol{\xi} + \boldsymbol{\zeta}. \tag{6.94}$$

This division is needed because only $\boldsymbol{\xi}$ term can be manipulated by the weight updates $\dot{\hat{\mathbf{W}}}, \dot{\hat{\mathbf{V}}}$ as will be shown in Section 6.4.2.

The term $\boldsymbol{\xi}$ is defined as

$$\begin{aligned} \boldsymbol{\xi} = & \left(\tilde{\mathbf{W}}_M^{\mathrm{T}}\hat{\boldsymbol{\sigma}}_M\right)\boldsymbol{\Lambda}\dot{\mathbf{x}} + \tilde{\mathbf{W}}_g^{\mathrm{T}}\hat{\boldsymbol{\sigma}}_g + \tilde{\mathbf{W}}_\tau^{\mathrm{T}}\hat{\boldsymbol{\sigma}}_\tau \\ & + \left(\hat{\mathbf{W}}_M^{\mathrm{T}}\hat{\boldsymbol{\sigma}}'_M\tilde{\mathbf{V}}_M^{\mathrm{T}}\mathbf{z}_M\right)\boldsymbol{\Lambda}\dot{\mathbf{x}} + \hat{\mathbf{W}}_g^{\mathrm{T}}\hat{\boldsymbol{\sigma}}'_g\tilde{\mathbf{V}}_g^{\mathrm{T}}\mathbf{z}_g + \hat{\mathbf{W}}_\tau^{\mathrm{T}}\hat{\boldsymbol{\sigma}}'_\tau\tilde{\mathbf{V}}_\tau^{\mathrm{T}}\mathbf{z}_\tau \end{aligned} \tag{6.95}$$

and the "whole"NN errors $\boldsymbol{\zeta}$ is defined as

$$\begin{aligned} \boldsymbol{\zeta} = & \left(\tilde{\mathbf{W}}_M^{\mathrm{T}}\hat{\boldsymbol{\sigma}}'_M\tilde{\mathbf{V}}_M^{\mathrm{T}}\mathbf{z}_M\right)\boldsymbol{\Lambda}\dot{\mathbf{x}} + \tilde{\mathbf{W}}_g^{\mathrm{T}}\hat{\boldsymbol{\sigma}}'_g\tilde{\mathbf{V}}_g^{\mathrm{T}}\mathbf{z}_g + \tilde{\mathbf{W}}_\tau^{\mathrm{T}}\hat{\boldsymbol{\sigma}}'_\tau\tilde{\mathbf{V}}_\tau^{\mathrm{T}}\mathbf{z}_\tau \\ & + \left(\mathbf{W}_M^{\mathrm{T}}O(\tilde{\mathbf{V}}_M^{\mathrm{T}}\mathbf{z}_M)\right)\boldsymbol{\Lambda}\dot{\mathbf{x}} + \mathbf{W}_g^{\mathrm{T}}O(\tilde{\mathbf{V}}_g^{\mathrm{T}}\mathbf{z}_g) + \mathbf{W}_\tau^{\mathrm{T}}O(\tilde{\mathbf{V}}_\tau^{\mathrm{T}}\mathbf{z}_\tau) + \boldsymbol{\varepsilon} \end{aligned} \tag{6.96}$$

As in Section 4.4.2, the uncertainties $\boldsymbol{\eta}$ (6.94) can be seen to be bounded with the generic expression $\|\mathbf{L}_p - \hat{\mathbf{L}}_p\| \leq (\tilde{L}_p)_M$ in (4.47), as follows

$$\|\boldsymbol{\eta}\| \leq (\tilde{L}_M)_M\, \boldsymbol{\Lambda}\|\dot{\mathbf{x}}\| + (\tilde{L}_g)_M + (\tilde{L}_\tau)_M + \varepsilon_M \tag{6.97}$$

Note that $\dot{\mathbf{x}}$ is bounded by motor speed limit. Therefore $\boldsymbol{\eta}$ can be simply shown to be bounded as

$$\|\boldsymbol{\eta}\| \leq C_0 + C_1\, \|\dot{\mathbf{x}}\|. \tag{6.98}$$

where $C_0, C_1 > 0$. And since $\boldsymbol{\eta} = \boldsymbol{\xi} + \boldsymbol{\zeta}$, then clearly the following inequalities are true

$$\|\boldsymbol{\xi}\| \leq C_0 + C_1 \, \|\dot{\mathbf{x}}\| \tag{6.99}$$

$$\|\boldsymbol{\zeta}\| \leq C_0 + C_1 \, \|\dot{\mathbf{x}}\|. \tag{6.100}$$

Let us redefine in this section $\mathbf{Z} = \text{diag}[\mathbf{W}, \mathbf{V}]$ to be upper-bounded as follows

$$\|\mathbf{Z}\| = \sqrt{\|\mathbf{W}\|^2 + \|\mathbf{V}\|^2} \leq Z_M \tag{6.101}$$

where Z_M is a positive scalar constant, $\mathbf{W} = \text{diag}[\mathbf{W}_M, \mathbf{W}_g, \mathbf{W}_\tau]$ and $\mathbf{V} = \text{diag}[\mathbf{V}_M, \mathbf{V}_g, \mathbf{V}_\tau]$.

6.4.2 Stability Analysis

For the proposed impact control (6.88), let the weight updates be provided as:

$$\dot{\hat{\mathbf{w}}}_{M_{ij}} = \mathbf{F}_{M_{ij}}(\hat{\boldsymbol{\sigma}}_M \, \dot{x}_i \, \Lambda_{jj} \, \dot{x}_j - \kappa \|\dot{\mathbf{x}}\| \hat{\mathbf{w}}_{M_{ij}}) \tag{6.102}$$

$$\dot{\hat{\mathbf{v}}}_{M_k} = \mathbf{G}_{M_k}(\mathbf{z}_M \, \hat{\boldsymbol{\sigma}}'_{M_k} \, (\sum_{i=1}^{m} \sum_{j=1}^{m} \hat{\mathbf{w}}_{M_{ijk}} \, \dot{x}_i \, \Lambda_{jj} \, \dot{x}_j) - \kappa \|\dot{\mathbf{x}}\| \hat{\mathbf{v}}_{M_k}) \tag{6.103}$$

$$\dot{\hat{\mathbf{w}}}_{g_i} = \mathbf{F}_{g_i}(\hat{\boldsymbol{\sigma}}_g \, \dot{x}_i - \kappa \|\dot{\mathbf{x}}\| \hat{\mathbf{w}}_{g_i}) \tag{6.104}$$

$$\dot{\hat{\mathbf{v}}}_{g_k} = \mathbf{G}_{g_k}(\mathbf{z}_g \, \hat{\boldsymbol{\sigma}}'_{g_k} \, (\sum_{i=1}^{m} \hat{\mathbf{w}}_{\mathbf{g}_{ik}} \, \dot{x}_i) - \kappa \|\dot{\mathbf{x}}\| \hat{\mathbf{v}}_{g_k}) \tag{6.105}$$

$$\dot{\hat{\mathbf{w}}}_{\tau_i} = \mathbf{F}_{\tau_i}(\hat{\boldsymbol{\sigma}}_\tau \, \dot{x}_i - \kappa \|\dot{\mathbf{x}}\| \hat{\mathbf{w}}_{\tau_i}) \tag{6.106}$$

$$\dot{\hat{\mathbf{v}}}_{\tau_k} = \mathbf{G}_{\tau_k}(\mathbf{z}_\tau \, \hat{\boldsymbol{\sigma}}'_{\tau_k} \, (\sum_{i=1}^{m} \hat{\mathbf{w}}_{\boldsymbol{\tau}_{ik}} \, \dot{x}_i) - \kappa \|\dot{\mathbf{x}}\| \hat{\mathbf{v}}_{\tau_k}) \tag{6.107}$$

with κ is a positive constant. And the estimated NN weight updates: $\dot{\hat{\mathbf{w}}}_{M_{ij}} \in \Re^{N_2}, \dot{\hat{\mathbf{v}}}_{M_k} \in \Re^{N_{1,M}}, \dot{\hat{\mathbf{w}}}_{g_i} \in \Re^{N_2}, \dot{\hat{\mathbf{v}}}_{g_k} \in \Re^{N_{1,g}}, \dot{\hat{\mathbf{w}}}_{\tau_i} \in \Re^{N_2}, \dot{\hat{\mathbf{v}}}_{\tau_k} \in \Re^{N_{1,\tau}}$ are all column vector. And the adaptive gains: $\mathbf{F}_{M_{ij}}^{-1} \in \Re^{N_2 \times N_2}, \ldots, \mathbf{F}_{\tau_i}^{-1} \in \Re^{N_2 \times N_2}$

and $\mathbf{G}_{M_k}^{-1} \in \Re^{N_{1,M} \times N_{1,M}}, \ldots, \mathbf{G}_{\tau_k}^{-1} \in \Re^{N_{1,\tau} \times N_{1,\tau}}$ are all positive diagonal matrices. The following indices are defined: $i, j = 1, \ldots, m$ are output-layer indices, $k = 1, \ldots, N_2$ is the hidden-layer index, where to simplify the implementation, the hidden-node size N_2 is set the same throughout. While $N_{1,M}, N_{1,g}, N_{1,\tau}$ are the respective input-node sizes.

Proposition 6.4.1 *With the assumptions that:*

1. *the controller gain* $\mathbf{\Lambda}$ *meets the condition*

$$\Lambda_m > \frac{C_1}{M_{x,m}} \tag{6.108}$$

where $C_1 > 0, \Lambda_m = min(\mathbf{\Lambda})$ *and* $M_{x,m} = min(\lambda_{min}(\mathbf{M}_\mathbf{x}(t)))$*;*

2. $\hat{Z}_M$*, the upper-bound of the estimated NN weights* $\hat{\mathbf{Z}}$*, satisfies*

$$\hat{Z}_M > \sqrt{\frac{C_0}{\kappa}}; \tag{6.109}$$

where $C_0, \kappa > 0$*; and*

3. *the initial condition of* $\tilde{\mathbf{Z}}$ *satisfies*

$$\|\tilde{\mathbf{Z}}(0)\| < \tilde{Z}_M; \tag{6.110}$$

$\tilde{Z}_M$ *is the upper-bound of the NN weight errors,* $\tilde{\mathbf{Z}}$*;*

then using the proposed motion control (6.88) *and the NN weight updates* (6.102)-(6.107)*, it can be shown by Lyapunov's extension theorem [102] that as* $t \to \infty$*, the errors* $\|\dot{\mathbf{x}}\|$ *and* $\|\tilde{\mathbf{W}}\|, \|\tilde{\mathbf{V}}\|$ *will be bounded by enclosing boundary* $\mathcal{S}$*, which is defined by enclosing region* $\dot{V}(\dot{\mathbf{x}}, \tilde{\mathbf{Z}}) < 0$.

Proof 6.4.1 *The chosen Lyapunov function candidate for error dynamics* (6.89)*, with the uncertainties* $\boldsymbol{\eta}$ (6.94)*, is*

$$\begin{aligned} V(\dot{\mathbf{x}}, \tilde{\mathbf{Z}}) = & \frac{1}{2}\dot{\mathbf{x}}^{\mathrm{T}}\mathbf{M}_{\mathbf{x}}(\mathbf{q})\dot{\mathbf{x}} \\ & + \frac{1}{2}\sum_{i=1}^{m}\sum_{j=1}^{m}\tilde{\mathbf{w}}_{M_{ij}}^{\mathrm{T}}\,\mathbf{F}_{M_{ij}}^{-1}\,\tilde{\mathbf{w}}_{M_{ij}} + \frac{1}{2}\sum_{i=1}^{m}\tilde{\mathbf{w}}_{g_i}^{\mathrm{T}}\,\mathbf{F}_{g_i}^{-1}\,\tilde{\mathbf{w}}_{g_i} + \frac{1}{2}\sum_{i=1}^{m}\tilde{\mathbf{w}}_{\tau_i}^{\mathrm{T}}\,\mathbf{F}_{\tau_i}^{-1}\,\tilde{\mathbf{w}}_{\tau_i} \\ & + \frac{1}{2}\sum_{k=1}^{N_2}\tilde{\mathbf{v}}_{M_k}^{\mathrm{T}}\,\mathbf{G}_{M_k}^{-1}\,\tilde{\mathbf{v}}_{M_k} + \frac{1}{2}\sum_{k=1}^{N_2}\tilde{\mathbf{v}}_{g_k}^{\mathrm{T}}\,\mathbf{G}_{g_k}^{-1}\,\tilde{\mathbf{v}}_{g_k} + \frac{1}{2}\sum_{k=1}^{N_2}\tilde{\mathbf{v}}_{\tau_k}^{\mathrm{T}}\,\mathbf{G}_{\tau_k}^{-1}\,\tilde{\mathbf{v}}_{\tau_k} \end{aligned} \tag{6.111}$$

where the NN weight errors: $\tilde{\mathbf{w}}_{M_{ij}} \in \Re^{N_2}, \tilde{\mathbf{v}}_{M_k} \in \Re^{N_{1,M}}, \tilde{\mathbf{w}}_{g_i} \in \Re^{N_2}, \tilde{\mathbf{v}}_{g_k} \in \Re^{N_{1,g}}, \tilde{\mathbf{w}}_{\tau_i} \in \Re^{N_2}, \tilde{\mathbf{v}}_{\tau_k} \in \Re^{N_{1,\tau}}$ *are all column vector.*

Next, we substitute the closed-loop dynamics (6.89)*, Property 4.3.5 and also take into account* $\boldsymbol{\eta}$ (6.94)*, with the definition* $\boldsymbol{\xi}$ (6.95) *and the knowledge* $\|\boldsymbol{\zeta}\| \leq C_0 + C_1\|\mathbf{r}\|$ (6.100)*, into* $\dot{V}(\mathbf{r}, \tilde{\mathbf{Z}})$ *of* (6.111)*, to obtain*

$$\dot{V}(\dot{\mathbf{x}}, \tilde{\mathbf{Z}}) \leq -\dot{\mathbf{x}}^{\mathrm{T}}\mathbf{M}_{\mathbf{x}}(\mathbf{q})\boldsymbol{\Lambda}\dot{\mathbf{x}} + C_1\,\|\mathbf{r}\|^2 + C_0\,\|\mathbf{r}\| + \boldsymbol{\psi} \tag{6.112}$$

where the lump parameter $\boldsymbol{\psi}$ *in* (6.112) *is defined as*

$$\begin{aligned} \boldsymbol{\psi} = & \sum_{i=1}^{m}\sum_{j=1}^{m}\tilde{\mathbf{w}}_{M_{ij}}^{\mathrm{T}}\left(\mathbf{F}_{M_{ij}}^{-1}\,\dot{\tilde{\mathbf{w}}}_{M_{ij}} + \hat{\boldsymbol{\sigma}}_M\,\dot{x}_i\,\Lambda_{jj}\,\dot{x}_j\right) \\ & + \sum_{k=1}^{N_2}\tilde{\mathbf{v}}_{M_k}^{\mathrm{T}}\left(\mathbf{G}_{M_k}^{-1}\,\dot{\tilde{\mathbf{v}}}_{M_k} + \mathbf{z}_M\,\hat{\boldsymbol{\sigma}}'_{M_k}(\sum_{i=1}^{m}\sum_{j=1}^{m}\hat{w}_{M_{ijk}}\,\dot{x}_i\,\Lambda_{jj}\,\dot{x}_j)\right) \\ & + \sum_{i=1}^{m}\tilde{\mathbf{w}}_{g_i}^{\mathrm{T}}\left(\mathbf{F}_{g_i}^{-1}\dot{\tilde{\mathbf{w}}}_{g_i} + \hat{\boldsymbol{\sigma}}_g\,\dot{x}_i\right) \\ & + \sum_{k=1}^{N_2}\tilde{\mathbf{v}}_{g_k}^{\mathrm{T}}\left(\mathbf{G}_{g_k}^{-1}\,\dot{\tilde{\mathbf{v}}}_{g_k} + \mathbf{z}_g\,\hat{\boldsymbol{\sigma}}'_{g_k}(\sum_{i=1}^{m}\hat{w}_{g_{ik}}\,\dot{x}_i)\right) \\ & + \sum_{i=1}^{m}\tilde{\mathbf{w}}_{\tau_i}^{\mathrm{T}}\left(\mathbf{F}_{\tau_i}^{-1}\,\dot{\tilde{\mathbf{w}}}_{\tau_i} + \hat{\boldsymbol{\sigma}}_\tau\,\dot{x}_i\right) \\ & + \sum_{k=1}^{N_2}\tilde{\mathbf{v}}_{\tau_k}^{\mathrm{T}}\left(\mathbf{G}_{\tau_k}^{-1}\,\dot{\tilde{\mathbf{v}}}_{\tau_k} + \mathbf{z}_\tau\,\hat{\boldsymbol{\sigma}}'_{\tau_k}(\sum_{i=1}^{m}\hat{w}_{\tau_{ik}}\,\dot{x}_i)\right). \end{aligned} \tag{6.113}$$

Using $\boldsymbol{\xi}$ *in* (6.95)*, it can be demonstrated that* ψ *in* (6.113) *is made up of* $\dot{\tilde{\mathbf{W}}}$, $\dot{\tilde{\mathbf{V}}}$ *and* $\mathbf{r}^{\mathrm{T}}\boldsymbol{\xi}$*. The idea is to cancel* $\mathbf{r}^{\mathrm{T}}\boldsymbol{\xi}$ *with* $\dot{\tilde{\mathbf{W}}}, \dot{\tilde{\mathbf{V}}}$*. Furthermore,* $-\dot{\tilde{\mathbf{W}}} = \dot{\hat{\mathbf{W}}}$*, since* $\tilde{\mathbf{W}} = \mathbf{W} - \hat{\mathbf{W}}$ *and* $\mathbf{W}$ *is constant. With the weight updates* (6.102)– (6.107)*,* ψ *becomes*

$$\begin{aligned}\psi = &\kappa\|\dot{\mathbf{x}}\| \sum_{i=1}^{m}\sum_{j=1}^{m} \tilde{\mathbf{w}}_{M_{ij}}^{\mathrm{T}} \hat{\mathbf{w}}_{M_{ij}} + \kappa\|\dot{\mathbf{x}}\| \sum_{i=1}^{m} \tilde{\mathbf{w}}_{g_i}^{\mathrm{T}} \hat{\mathbf{w}}_{g_i} + \kappa\|\dot{\mathbf{x}}\| \sum_{i=1}^{m} \tilde{\mathbf{W}}_{\tau_i}^{\mathrm{T}} \tilde{\mathbf{w}}_{\tau_i} \\ &+ \kappa\|\dot{\mathbf{x}}\| \sum_{k=1}^{N_2} \tilde{\mathbf{v}}_{M_k}^{\mathrm{T}} \hat{\mathbf{v}}_{M_k} + \kappa\|\dot{\mathbf{x}}\| \sum_{k=1}^{N_2} \tilde{\mathbf{v}}_{g_k}^{\mathrm{T}} \hat{\mathbf{v}}_{g_k} + \kappa\|\dot{\mathbf{x}}\| \sum_{k=1}^{N_2} \tilde{\mathbf{v}}_{\tau_k}^{\mathrm{T}} \hat{\mathbf{v}}_{\tau_k} \\ \leq &-\kappa\|\dot{\mathbf{x}}\|\|\tilde{\mathbf{Z}}\|^2 + \kappa\|\dot{\mathbf{x}}\|\|\tilde{\mathbf{Z}}\| Z_M\end{aligned} \tag{6.114}$$

Equation (6.114) *is obtained by combining all the inner products as*

$$\langle \tilde{\mathbf{W}}, \hat{\mathbf{W}} \rangle = \sum_{i=1}^{m}\sum_{j=1}^{m} \tilde{\mathbf{w}}_{M_{ij}}^{\mathrm{T}} \hat{\mathbf{w}}_{M_{ij}} + \sum_{i=1}^{m} \tilde{\mathbf{w}}_{g_i}^{\mathrm{T}} \hat{\mathbf{w}}_{g_i} + \sum_{i=1}^{m} \tilde{\mathbf{w}}_{\tau_i}^{\mathrm{T}} \hat{\mathbf{w}}_{\tau_i} \tag{6.115}$$

$$\langle \tilde{\mathbf{V}}, \hat{\mathbf{V}} \rangle = \sum_{k=1}^{N_2} \tilde{\mathbf{v}}_{M_k}^{\mathrm{T}} \hat{\mathbf{v}}_{M_k} + \sum_{k=1}^{N_2} \tilde{\mathbf{v}}_{g_k}^{\mathrm{T}} \hat{\mathbf{v}}_{g_k} + \sum_{k=1}^{N_2} \tilde{\mathbf{v}}_{\tau_k}^{\mathrm{T}} \hat{\mathbf{v}}_{\tau_k} \tag{6.116}$$

$$\langle \tilde{\mathbf{Z}}, \hat{\mathbf{Z}} \rangle = \langle \tilde{\mathbf{V}}, \hat{\mathbf{V}} \rangle + \langle \tilde{\mathbf{W}}, \hat{\mathbf{W}} \rangle \tag{6.117}$$

where $\hat{\mathbf{Z}} = \mathbf{Z} - \tilde{\mathbf{Z}}$*, and therefore*

$$\langle \tilde{\mathbf{Z}}, \hat{\mathbf{Z}} \rangle = \langle \tilde{\mathbf{Z}}, \mathbf{Z} \rangle - \|\tilde{\mathbf{Z}}\|^2 \leq \|\tilde{\mathbf{Z}}\|\|\mathbf{Z}\| - \|\tilde{\mathbf{Z}}\|^2 \leq \|\tilde{\mathbf{Z}}\| Z_M - \|\tilde{\mathbf{Z}}\|^2. \tag{6.118}$$

Substituting ψ (6.114) *and Property 4.3.1, it is possible to show* $\dot{V}(\dot{\mathbf{x}}, \tilde{\mathbf{Z}})$ (6.112) *that*

$$\dot{V}(\dot{\mathbf{x}}, \tilde{\mathbf{Z}}) \leq -\|\dot{\mathbf{x}}\| \left[(M_{x,m}\, \Lambda_m - C_1)\|\dot{\mathbf{x}}\| - C_0 + \kappa(\|\tilde{\mathbf{Z}}\| - \frac{Z_M}{2})^2 - \frac{\kappa Z_M^2}{4} \right] \tag{6.119}$$

where Λ_m *and* $M_{x,m}$ *are as defined in* (6.108)*, note* $(M_{x,m}\, \Lambda_m - C_1) > 0$ *is due to hypothesis* (6.108)*. Hence,* $\dot{V}(\dot{\mathbf{x}}, \tilde{\mathbf{Z}}) < 0$*, as depicted in Fig. 6.3, when*

$$\|\dot{\mathbf{x}}\| > \frac{C_0 + \kappa Z_M^2/4}{(M_{x,m}\, \Lambda_m - C_1)} \equiv b_{\dot{x}}, \quad \textit{or} \tag{6.120}$$

$$\|\tilde{\mathbf{Z}}\| > \sqrt{\frac{C_0}{\kappa} + \frac{Z_M^2}{4}} + \frac{Z_M}{2} \equiv b_{\tilde{Z}} \tag{6.121}$$

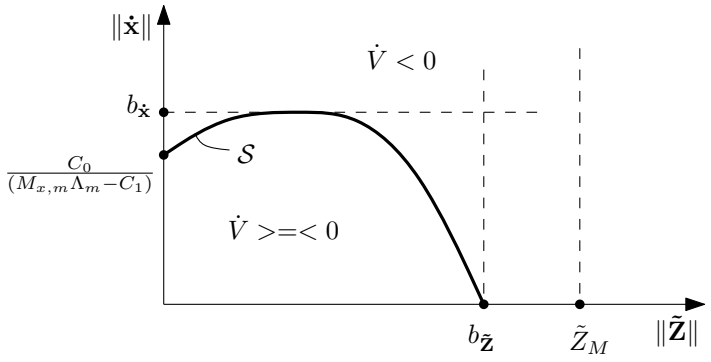

Figure 6.3: $\dot{V}(\dot{\mathbf{x}}, \tilde{\mathbf{Z}})$ regions of the proposed NN adaptive impact strategy.

Applying the Lyapunov's extension theorem [102] then as $t \to \infty$, the errors $\|\dot{\mathbf{x}}\|$ and $\|\tilde{\mathbf{Z}}\|$ can be shown to be bounded within the boundary of $\mathcal{S}$, as follow:

Suppose the errors start within the boundary of $\mathcal{S}$, i.e. $\|\dot{\mathbf{x}}(0)\| < b_{\dot{x}}$ and $\|\tilde{\mathbf{Z}}(0)\| < b_{\tilde{Z}}$, then they start their course towards the enclosing boundary $\mathcal{S}$ since $\dot{V}(\dot{\mathbf{x}}, \tilde{\mathbf{Z}})$ can not be guaranteed to be less than zero, within this boundary. However, when they are leaving the boundary and entering the region $\dot{V}(\dot{\mathbf{x}}, \tilde{\mathbf{Z}}) < 0$, they will return to the boundary. Now, suppose the errors start at outside the boundary of $\mathcal{S}$ then they tend to go to the equilibrium since $V(\dot{\mathbf{x}}, \tilde{\mathbf{Z}})$ is decreasing. However, they cannot go to the equilibrium, but only up to entering the boundary of $\mathcal{S}$ and once they enter the boundary of $\mathcal{S}$, we have already shown that they are bounded.

The next part of the proof is to demonstrate the necessity of hypothesis $\hat{Z}_M > \sqrt{\frac{C_0}{\kappa}}$ in (6.109)*. Note that, $\tilde{\mathbf{Z}}$, in its course towards the enclosing boundary $\mathcal{S}$, cannot violate $\tilde{Z}_M$, otherwise the Lyapunov's Extension Theorem is no longer applicable. In other words, $\tilde{Z}_M$ in* (4.46) *must satisfy*

$$\tilde{Z}_M \equiv Z_M + \hat{Z}_M > b_{\tilde{\mathbf{Z}}}, \tag{6.122}$$

Therefore, it can be shown that if the following is satisfied

$$Z_M + \hat{Z}_M > \sqrt{\frac{C_0}{\kappa}} + Z_M > b_{\tilde{\mathbf{Z}}} \text{ or,} \tag{6.123}$$

$$\hat{Z}_M > \sqrt{\frac{C_0}{\kappa}} \tag{6.124}$$

then $\tilde{Z}_M > b_{\tilde{\mathbf{Z}}}$ *is also satisfied.*

Further, the initial condition $\|\tilde{\mathbf{Z}}(0)\|$ *can be less or greater than* $b_{\tilde{\mathbf{Z}}}$*, however in order to comply with the Lyapunovs Extension Theorem, it must be less than* $\tilde{Z}_M$*. The last part of the proof is to demonstrate hypothesis* $\|\tilde{\mathbf{Z}}(0)\| < \tilde{Z}_M$ *in* (6.110) *is to be satisfied in practical implementation. This hypothesis can be equally achieved, if the following condition from* (4.46) *is satisfied*

$$\begin{gathered} \|\tilde{\mathbf{Z}}(0)\| \equiv \|\mathbf{Z}(0)\| + \|\hat{\mathbf{Z}}(0)\| \leq Z_M + \hat{Z}_M \equiv \tilde{Z}_M, \text{ or} \\ \|\hat{\mathbf{Z}}(0)\| \leq \hat{Z}_M. \end{gathered} \tag{6.125}$$

In the implementation, the last equation can be achieved by simply initializing the NN impact weights with the bounded weights of the NN free motion controller - observer (in Section 5.3.5) as follows

$$\hat{\mathbf{Z}}(0)_{impact} = \hat{\mathbf{Z}}_{motion}. \tag{6.126}$$

Note: theoretically and practically, there is no initial condition requirement for $\dot{\mathbf{x}}$*. The purpose of impact control is to stabilize the system from whatever its initial velocity is into low velocity.*

6.5 Real-time Robot Experiment

The proposed NN adaptive force - motion controller with velocity observer (6.3) is validated with the 6 DOF PUMA 560 manipulator (which does not have velocity feedback sensors). For comparison purpose, the Lagrangian dynamics force - motion control (2.35), without friction compensation, is also implemented.

The setup is set as follows:

- A positional periodic circular trajectory – 75 mm radius and 2 second period – with a constant orientation for the effector was set as the desired trajectory.
- A horizontal plane surface is used for this compliant motion experiment as shown in Fig. 6.4, with the end-effector pointing down and the elbow is up.
- Performances were recorded in term of: (i) desired trajectories along $x_{\rm E}$ and $y_{\rm E}$ axes, and (ii) position errors along $x_{\rm E}$ and $y_{\rm E}$, (iii) normal force F_z with desired 20N normal force, and (iv) the zero-moment controls M_x and M_y.

Note that there is a more sophisticated model-based force - motion control by [118], where an adaptive joint friction compensation and a velocity observer are added along with the Lagrangian dynamics control, giving more improved performance than the Lagrangian dynamics controller along. However, its formulation and stability analysis are rather different and relatively more involved

than the original formula [8]. Also, the compliant motion requires a proper planning strategy that needs to be met.

In compliant motion, we cannot directly apply the force - motion control. It is equally important to design a proper planning for the force - motion control to deliver the compliant motion. For the ease of implementation, the original Lagrangian dynamics operational space force - motion formulation [8] was employed and complemented with the model-based impact force control strategy as in [12].

The planning design for NN adaptive strategies can be described as follows: (i) the NN weights were initialized with the recorded weights of the NN adaptive motion controller with velocity observer (5.2) in Chapter 5, then followed by (ii) the NN adaptive impact control in (6.88) and then followed by (iii) the circular

Figure 6.4: The compliant motion setup using PUMA 560 robot.

Errors	Lagrange dynamics force - motion	NN force - motion controller - observer.
$\max(\sqrt{e_{\text{pos},x}^2 + e_{\text{pos},y}^2})$ (mm)	13.68	19.41
$F_{z,\text{error}}$ (N)	28.0	17.0
$M_{x,\text{error}}$ (N-m)	0.7	1.0
$M_{y,\text{error}}$ (N-m)	0.8	1.0

Table 6.1: Real-time compliant motion performance comparison.

compliant motion using NN adaptive force - motion control in (6.3).

The performances of the Lagrangian dynamics force - motion control are shown in Fig. 6.5 and Fig. 6.6. While the performances of the proposed NN adaptive force - motion controller-observer are shown in Fig. 6.7 and Fig. 6.8. The bounded stability of the norms of the estimated NN weights is shown in Fig. 6.9.

It can be shown in Table 6.1, that the performances of the NN adaptive experiments were comparable with those of the Lagrangian dynamics strategy:

1. In term of position errors along x_{E} and y_{E} axes and zero-moment controls (M_x, M_y): both strategies produced relatively similar performances.

2. In term of the normal force error the NN adaptive strategy can be shown to produce smaller error (17 N) in comparison with the that of Lagrangian dynamics strategy (28 N).

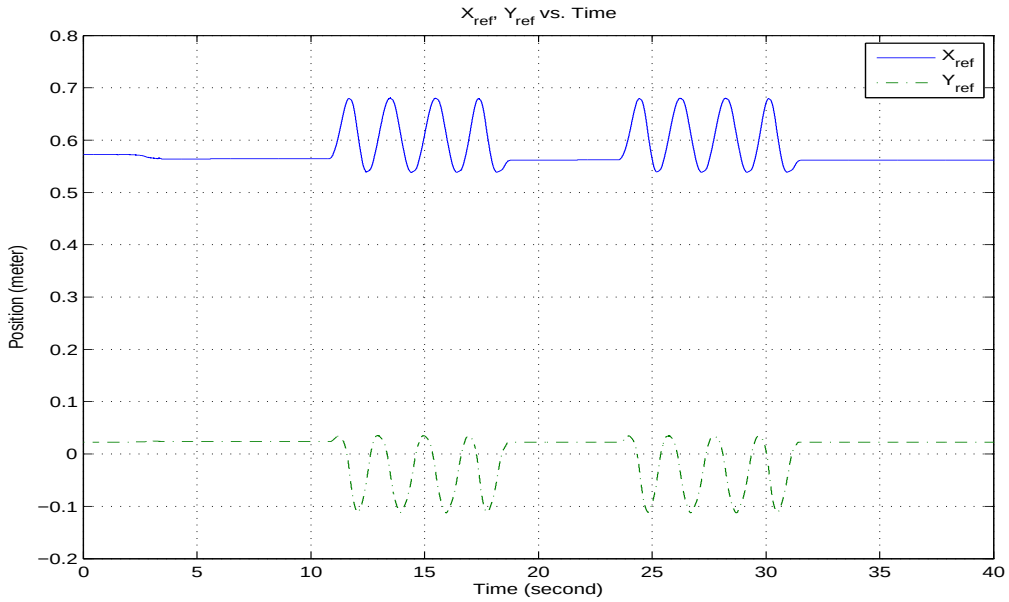

(a) Desired trajectories along $x_{\mathrm{E}}, y_{\mathrm{E}}$.

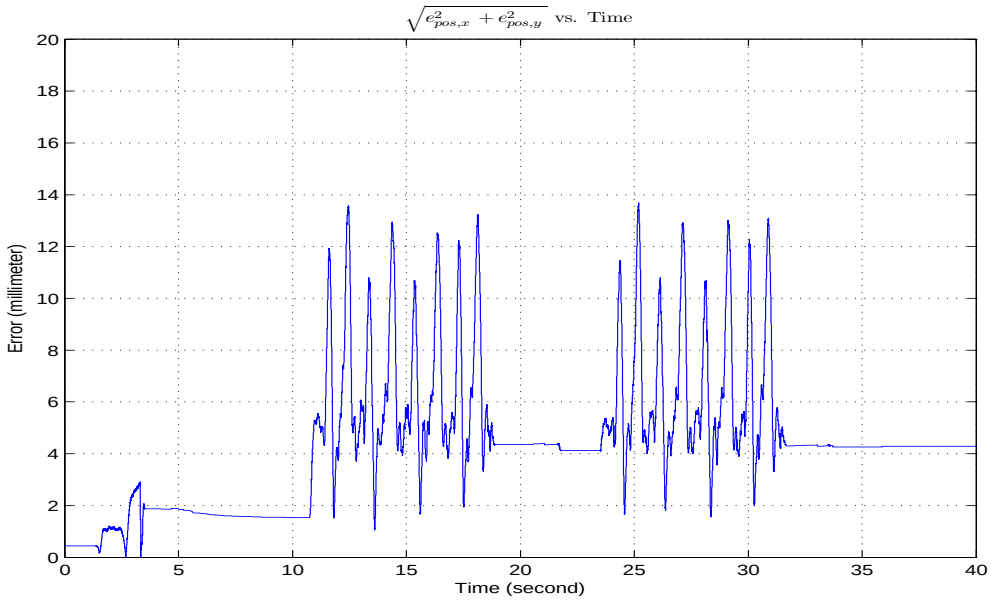

(b) The magnitude of $e_{\mathrm{pos},x}$ plus $e_{\mathrm{pos},y}$.

Figure 6.5: Motion control performance of the operational space Lagrangian dynamics force - motion control.

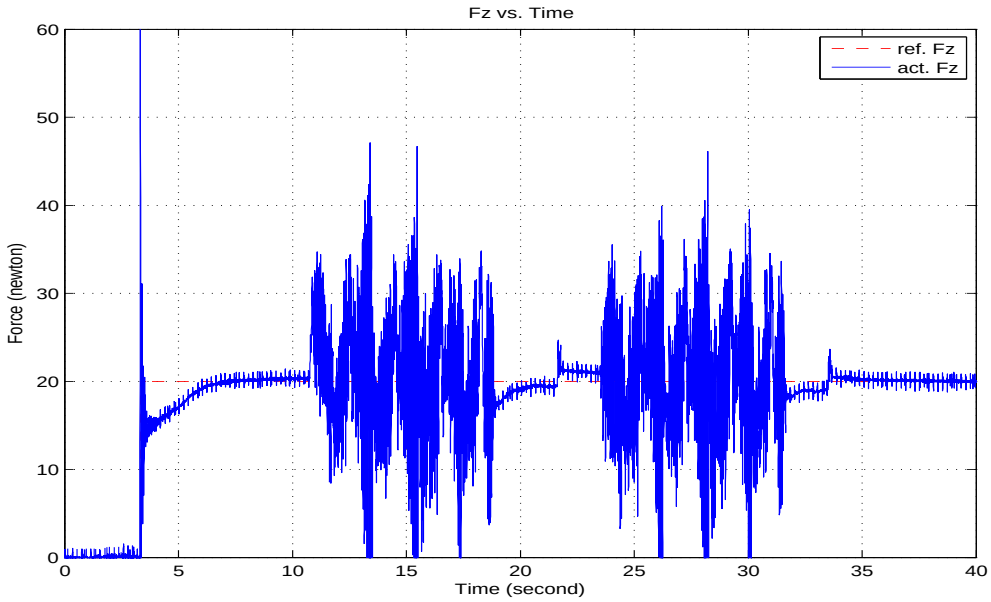

(a) Normal force reading along z_{E} axis (with 20N desired).

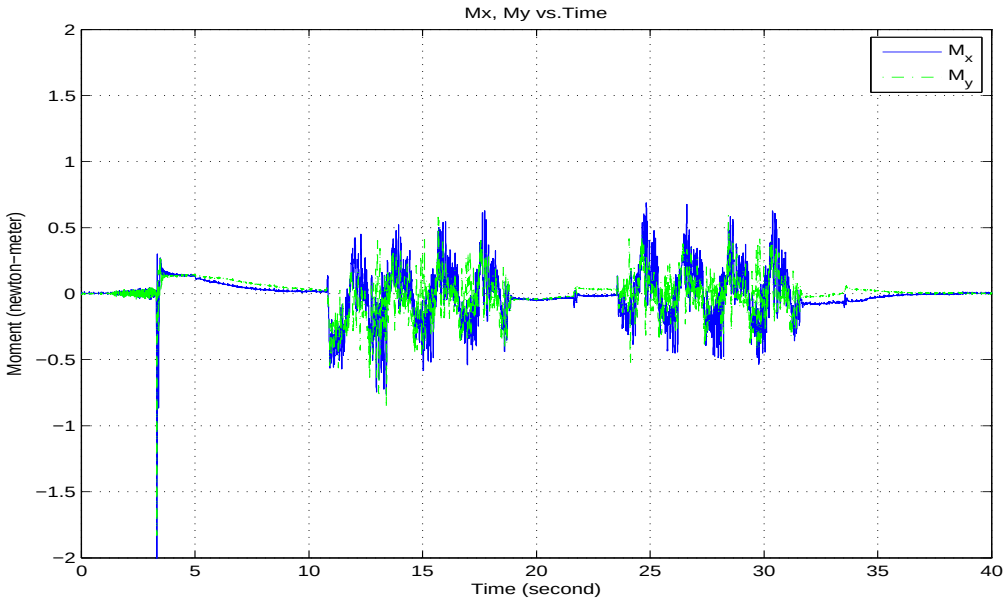

(b) Tangential moments reading along x_{E} and y_{E} axes.

Figure 6.6: Force/moment control performance using the operational space Lagrangian dynamics force - motion control.

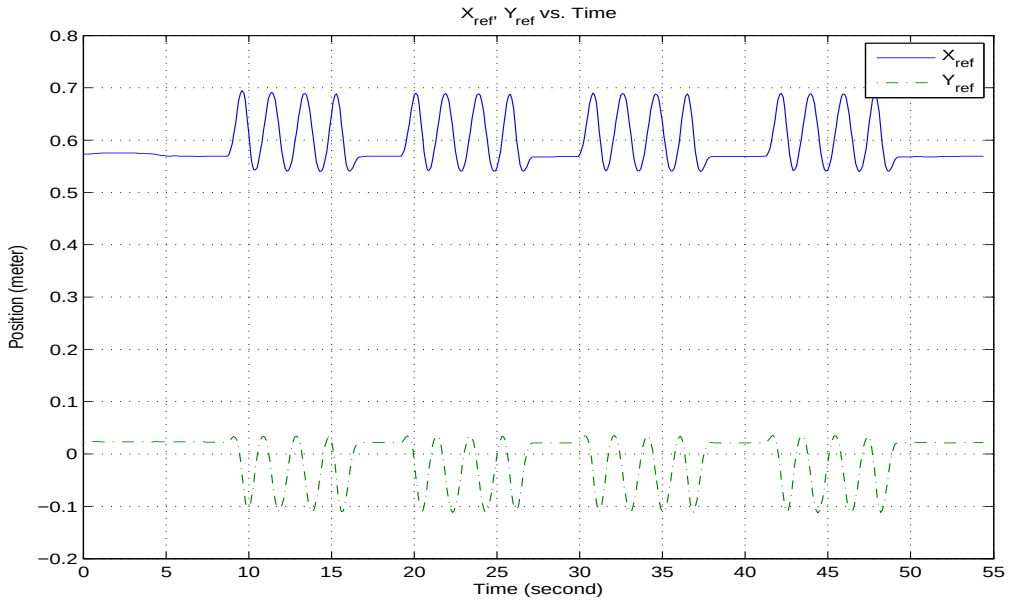

(a) Desired trajectories along $x_{\mathrm{E}}, y_{\mathrm{E}}$.

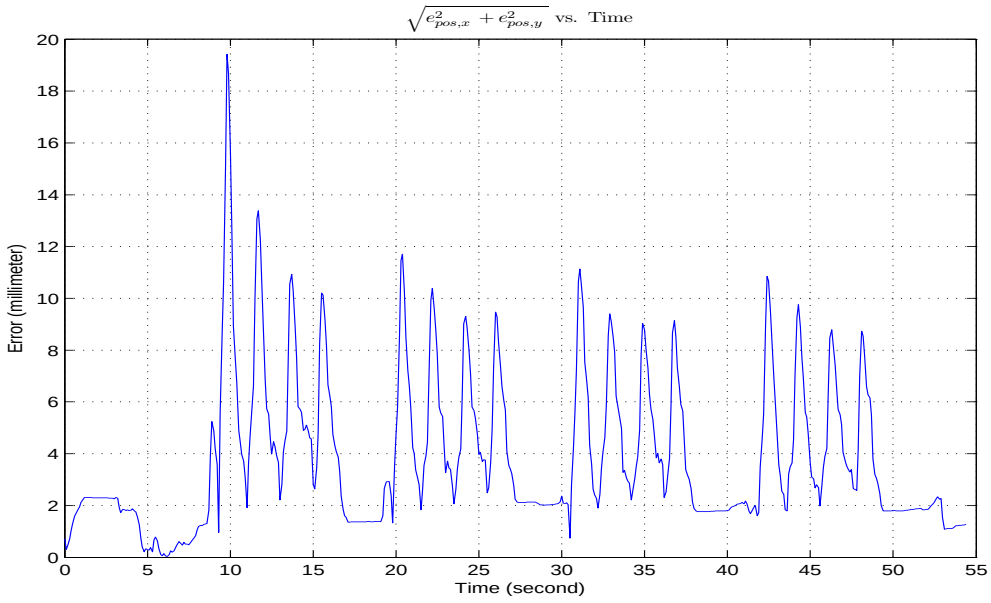

(b) The magnitude of $e_{\mathrm{pos},x}$ plus $e_{\mathrm{pos},y}$.

Figure 6.7: Motion control performance using the operational space NN adaptive force - motion control with velocity observer.

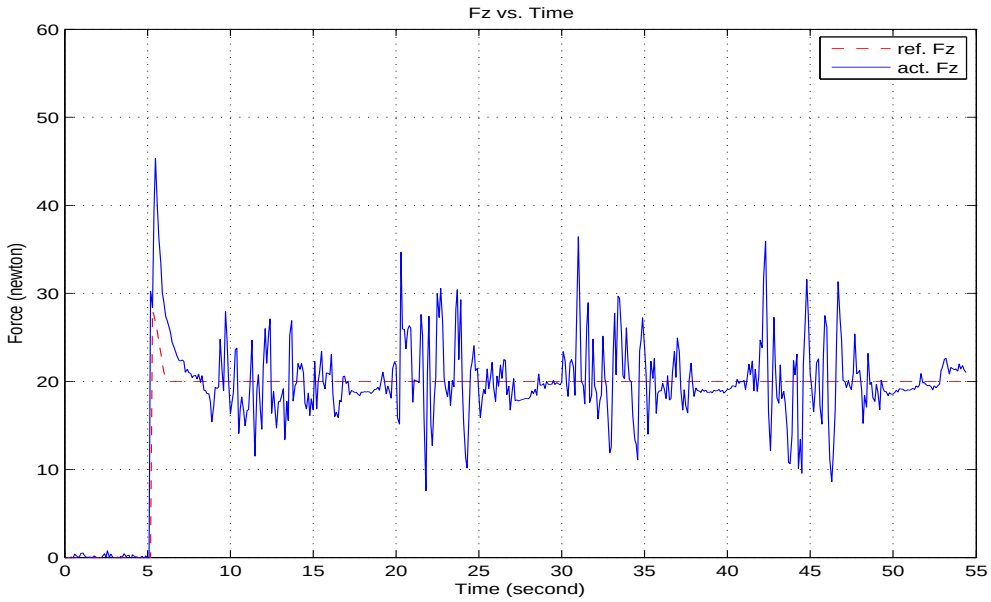

(a) Normal force reading along z_{E} axis.

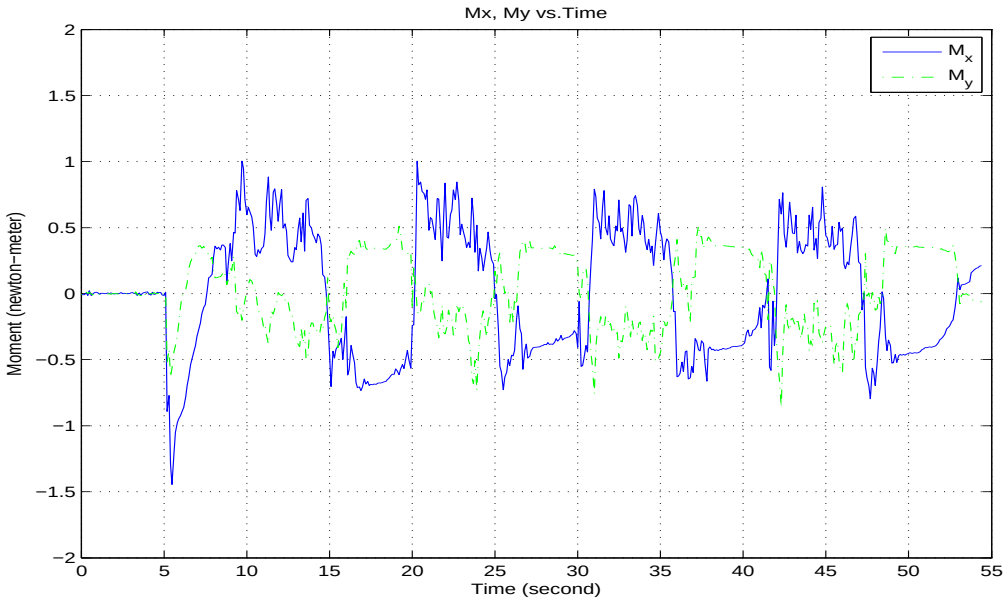

(b) Tangential moments reading along x_{E} and y_{E} axes.

Figure 6.8: Force/moment control performance using the operational space NN adaptive force - motion control with velocity observer.

The following gains are set for the proposed NN adaptive motion controller-observer (6.3): $\kappa = 0.1$, $\mathbf{\Lambda}_1 = \mathbf{\Lambda}_i = 30\mathbf{I} \in \Re^{m\times m}$, $\mathbf{F}_{M_{ij}}^{-1} = \mathbf{I} \in \Re^{N_2\times N_2}, \mathbf{F}_{B_{ij}}^{-1} = \mathbf{I} \in \Re^{N_2\times N_2}, \mathbf{F}_{g_i}^{-1} = 10\mathbf{I} \in \Re^{N_2\times N_2}, \mathbf{F}_{\tau_i}^{-1} = 10\mathbf{I} \in \Re^{N_2\times N_2}$, $\mathbf{\Lambda}_2 = 0.200\mathbf{I} \in \Re^{m\times m}$ and $\mathbf{l}_D = 400\mathbf{I} \in \Re^{m\times m}$. And $\mathbf{K}_e^{-1} = \text{diag}(1.0e^{-4}, 1.0e^{-4}, 1.0e^{-4}, 6.0e^{-3}, 6.0e^{-3}, 6.0e^{-3})$.

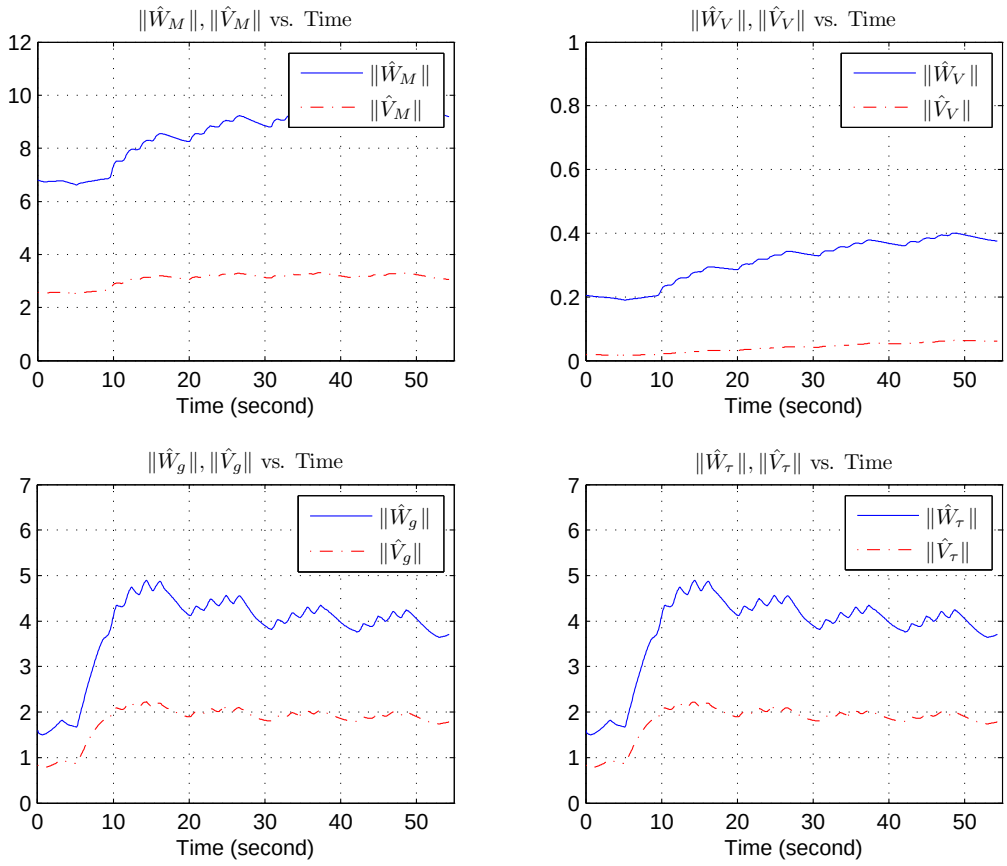

Figure 6.9: Real-time history of the estimated NN weights of the compliant motion NN adaptive strategy.

The real-time implementation videos of (i) the Lagrangian dynamics force-motion control and (ii) the proposed NN adaptive force-motion controller-observer (6.3) are provided in:

- http://guppy.mpe.nus.edu.sg/dandy/Videos/Dynamics-based/Compliant_motion_Dyn.MPG
- http://guppy.mpe.nus.edu.sg/dandy/Videos/NN-based/Compliant_motion_NN.MPG

6.6 Conclusion

In this chapter, the NN adaptive force-motion control with velocity observer in operational space was derived and validated through real-time experiment.

It can be concluded that the proposed NN adaptive compliant motion formulation is cost-effective and practical for real-time experiment, where the following characteristics can be shown:

1. no dynamic model is needed,
2. no environment geometry is needed,
3. no exciting trajectories are needed, and
4. the performance of the proposed NN adaptive force-motion strategy can be shown to be better than that of Lagrangian only dynamics strategy.

In the next chapter, we will present a consolidation view on how to combine overall algorithms for a multi-task operation i.e. compliant motion $\leftrightarrow$ free motion.

CHAPTER 7

CONSOLIDATED VIEW OF THE NN-BASED ALGORITHMS

7.1 Chapter Overview

In this chapter, we provide a consolidated view on how to combine overall algorithms for a multi-task operation. Without a right planning, a multi-task operation might not work properly, therefore, it is important to design carefully a proper plan for a multi-task operation. A case study is presented, where two main tasks are: (i) a circular compliant motion, followed by (ii) a circular free motion.

7.2 Planning Strategy

A planning strategy (presented in Fig. 7.1) for a sequential task, where two main tasks at concern are a circular compliant motion and a circular free motion, can be designed as follows: the robot starts from stationary, then the end-effector descends linearly into the working surface, impact control is then applied, and then the NN compliant motion control is executed, then the end-effector retracts linearly, then after it achieved stationary position, the NN free motion control can be executed, where afterward the end-effector becomes stationary again.

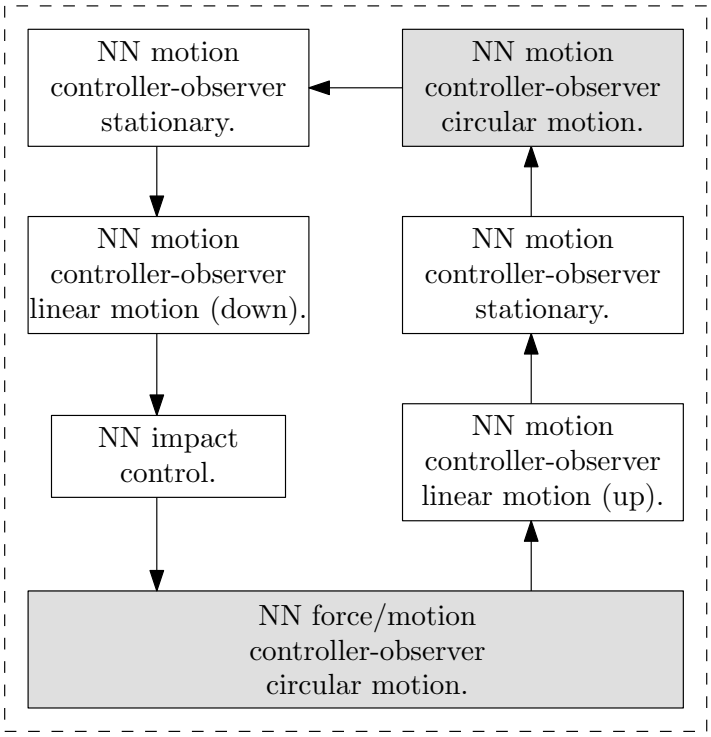

Figure 7.1: A sequential compliant motion and free motion planning.

The overall details can be described as follows:

- The NN motion controller-observer (5.2), which is initialized with the recorded weights of circular free motion, is used to provide a stationary position.

- The NN motion controller-observer (5.2) is then used to provide a descending linear motion.

- The NN impact control (6.88) is then applied to dissipate the impact energy.

- The NN compliant motion (6.3) is then used to provide a circular compliant motion. The initial desired normal force can be set equal to the actual force, $\mathbf{f}_d(0) = \mathbf{f}(0)$. After the compliant motion finished its task, then

the desired normal force is set to zero to prepare for the retracting of the end-effector.

- The NN motion controller-observer (5.2) is then used to provide a ascending linear motion.
- The NN motion controller-observer (5.2) is then used to provide a stationary position.
- The NN motion controller-observer (5.2) is then used to provide a circular free motion.
- The NN motion controller-observer (5.2) is then used to provide a stationary position, where either a free motion or compliant motion can be repeated.

The real-time implementation video of this two-task planning is provided in:

http://guppy.mpe.nus.edu.sg/dandy/Videos/NN-based/
Consolidated_2_tasks.MPG

7.3 Real-time Performance

The performance results of the two-task planning are shown as follows:

- For the compliant motion (task 1), the performances were recorded in Fig. 7.2 in term of: (i) normal force F_z with desired 20N normal force, and (ii) the zero-moment controls M_x and M_y.

Type of task	Performances
Task 1: Compliant motion control	$F_{z,\text{error}}$ = 15.0 (Newton) $M_{x,\text{error}}$ = 1.2 (Newton-meter) $M_{y,\text{error}}$ = 0.8 (Newton-meter)
Task 2: Free-motion control	$\max(\|\mathbf{e}_{\text{pos}}\|)$ = 5.45 (mm)

Table 7.1: Real-time performance of two-task planning.

- For the free-motion (task 2), performances were recorded in Fig. 7.3 in term of: (i) desired trajectories along x_{E} and y_{E} axes, and (ii) position errors along $x_{\text{E}}, y_{\text{E}}, z_{\text{E}}$.

The overall performance results are tabulated in Table 7.1: (i) for compliant motion the maximum normal force and tangential errors are: 15.0 (Newton), 1.2 (Newton-meter) and 0.8 (Newton-meter), respectively, and (ii) for free-motion, the maximum of the magnitude of the end-effector position tracking errors is 5.45 (mm).

The bounded stability of the norms of the estimated NN weights is shown in Fig. 7.4.

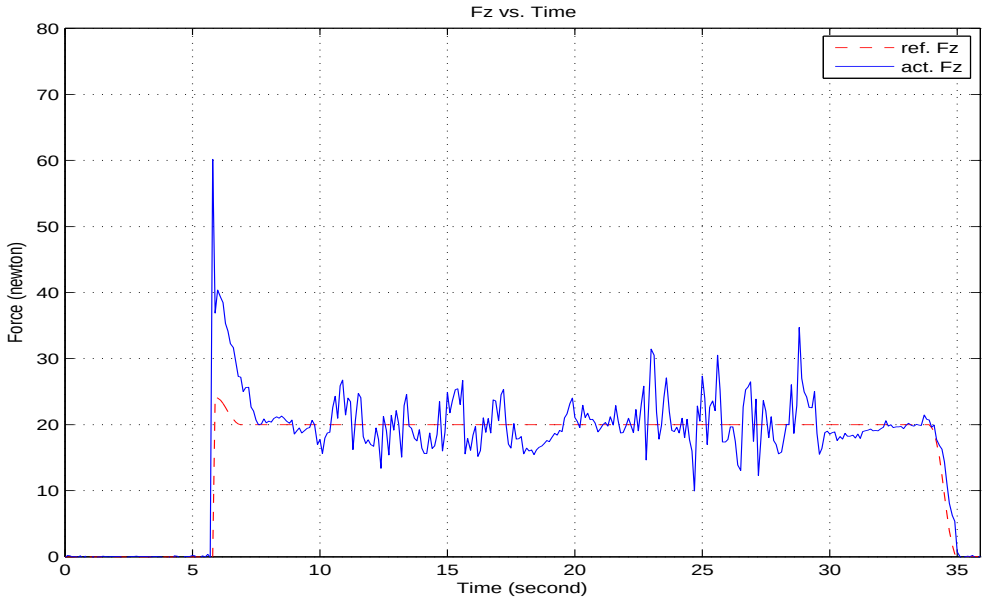

(a) Normal force reading along z_{E} axis (with 20N desired).

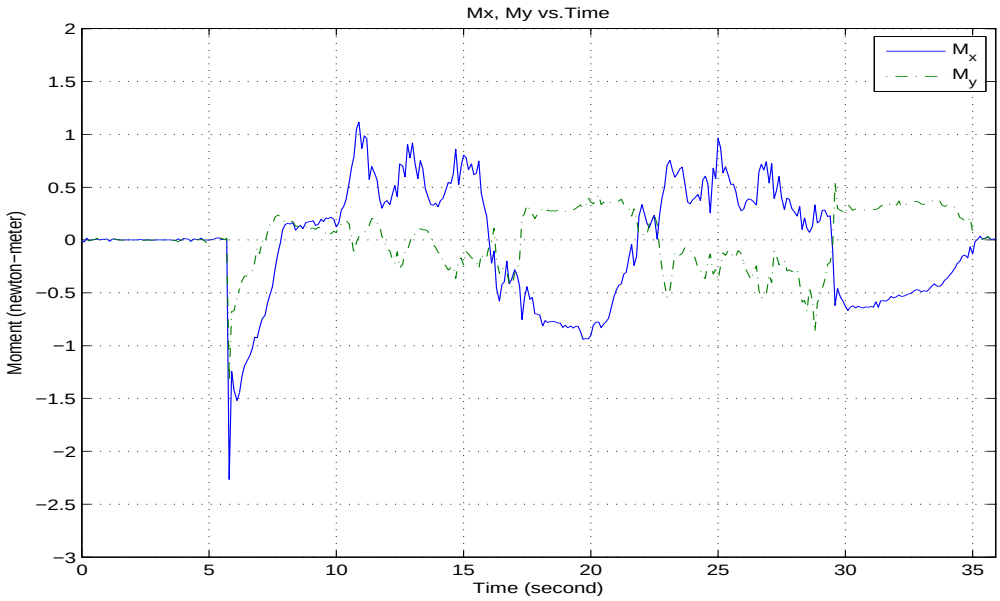

(b) Tangential moments reading along x_{E} and y_{E} axes.

Figure 7.2: Force/moment control performance (task 1).

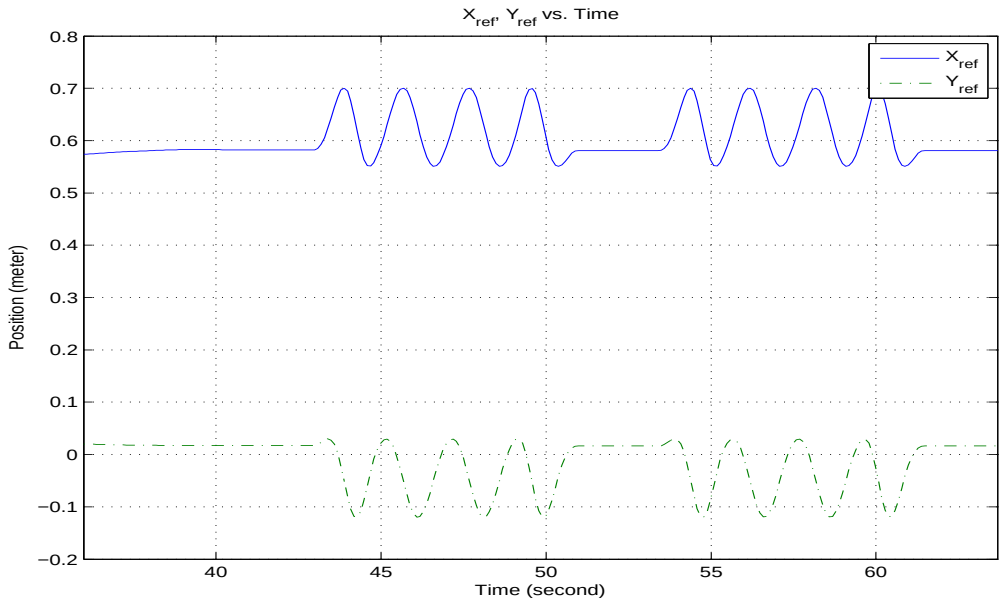

(a) Desired trajectories along $x_{\mathrm{E}}, y_{\mathrm{E}}$.

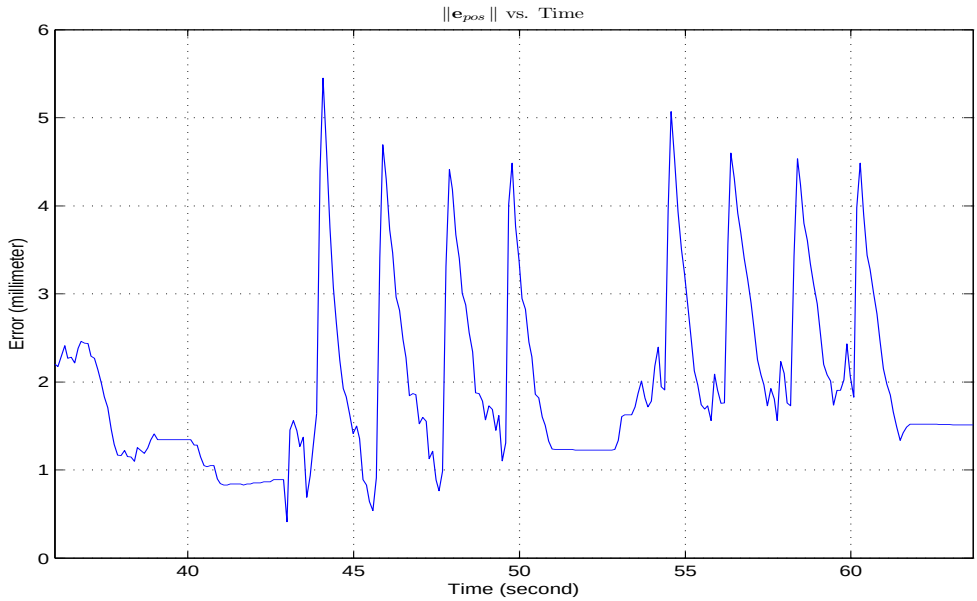

(b) The magnitude of the end-effector position tracking errors.

Figure 7.3: Free-motion control performance (task 2). Note: the time line is after task 1.

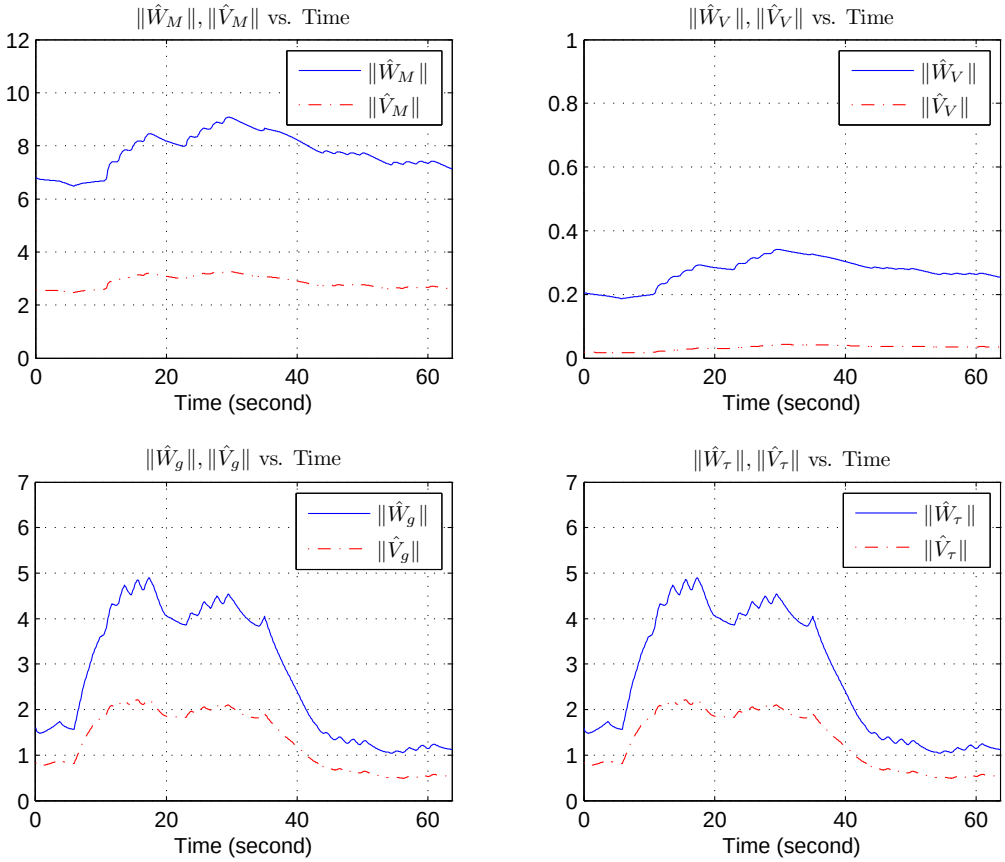

Figure 7.4: Real-time history of the estimated NN weights along the two-task planning.

CHAPTER 8

CONCLUSIONS

8.1 Summary of Contribution

In this thesis, we have developed several stable operational space NN adaptive formulations, where the ultimate focus is the compliant motion formulation.

It has been shown that the proposed NN adaptive compliant motion (force / motion) formulation has the following characteristics:

1. no dynamic model is needed,
2. no environment geometry is needed,
3. no exciting trajectories are needed, and
4. the performance of the proposed strategy is comparable with that of Lagrangian dynamics strategy.

Therefore, it can be concluded that the proposed NN adaptive compliant motion (force / motion) formulation can be considered to be cost-effective and practical, especially, when the Lagrangian dynamics for a particular robot is not available handily. Notice that the NN motion and force-motion control (with velocity observer) can be implemented directly into real-time implementation.

The detailed contributions of this Ph.D work are as follows:

- In the first step, the original NN adaptive approach in joint space [74, 75] was improved and extended into the operational space NN motion formulation. Several useful properties of the end effector dynamics were introduced to accommodate later developments.

  It was shown in simulation that a comparable performance, with that of the Lagrangian dynamics, was achieved, but has the advantage of no a priori knowledge of dynamics is required. However, it was shown that its performance on real-time experimentation was found to be inferior to the simulation equivalents.

- A separate Lyapunov analysis was presented to show that the filtered velocity signals, $\dot{\hat{\mathbf{q}}}$ and $\dot{\hat{\mathbf{x}}}$ (obtained by approximation through the filtered backward difference of the displacement feedback) are not suitable replacements to the non-existing actual velocity signals for the proposed adaptive motion strategy (previous point) in real-time implementation.

- In the second step, an NN adaptive motion control with velocity observer was proposed to overcome the absence of the actual velocity signal in the real-time experimentation.

  It can be shown in real-time implementation that the performance of the NN motion controller with velocity observer strategy is better than that of the NN motion control (where filtered velocity is used to replace the absence of the actual velocity). It also yielded, in real-time, a comparable performance to that of the Lagrangian dynamics strategy.

- In the third step, the NN adaptive force and motion control in

operational space (with velocity observer) was built upon the developed NN motion controller-observer in the second step.

Additionally, an NN adaptive impact strategy is also developed to complement the main strategy.

- The planning strategy to interactively use NN adaptive motion and force-motion formulation was also provided.

Note, Lyapunov stability proofs together with experimental verification for all formulations are provided. And all the real-time implementation videos are accessible in the following link:

http://guppy.mpe.nus.edu.sg/dandy/index.html

8.2 Future Work Possibilities

In this section we will discuss some possibilities for future works.

The works on this thesis cover mainly extending and improving the original NN adaptive control [74, 75] into ultimately the full force and motion control in operational space formulation in real-time implementation for a real robot.

It can be seen that, although, so far the proposed neuro-adaptive strategies showed comparable real-time performances with those of Lagrangian dynamics strategy, they cannot really outperform the inverse dynamics strategies. This is clearly because the stability for all the proposed strategy can be achieved only as bounded stability.

Technically speaking, the non-parametric structure of NN really forbids getting the convergence (asymptotic) stability, since there is always excess the whole error "ζ", which results from the difference between the system's structure and the NN structure. Coupled with the weight updates, it results bounded stability.

A more fundamental strategy to provide NN strategy with asymptotic stability (or maybe smaller bound), is not addressed in this thesis and is still an open problem for future research.

However, the proposed NN adaptive formulations in this thesis can be seen as a practical formulations for motion and compliant motion, respectively, when the Lagrangian dynamics for a particular robot is not available.

Based upon author's current knowledge, the most possible choice to remove completely the excess error "ζ" (and therefore to achieve asymptotic stability) is by using the linear-in-parameter (LIP) methodology as shown in the joint space direct LIP adaptive control in Chapter three, since the controller parameterized structure matches the robotic parameterized structure.

However the methodology requires the following developments:

- **The availability of an-easy-to-use simplification procedure to provide a simplified dynamic model.**

  To meet the requirement of the real-time deterministic sampling time the direct LIP adaptive control (Chapter three) requires the computation of the simplified dynamic models for the control and the parameter estimation.

  It is well established that for a real robot with more than three degrees of

freedom, the expressions of robot dynamic model are extremely complex. It makes the simplification procedure is not an easy task. Further, a systematic and easy-to-use simplification procedure based upon Lagrangian formalism is yet to be invented.

Therefore, the present challenge is the availability of a systematic and easy-to-use procedure based upon Lagrangian formalism, for the dynamic model simplification. This problem is presently the main bottleneck in this methodology.

Note that to achieve the first step, a symbolic software generator, based upon Lagrangian dynamics, is required to derive the un-simplified LIP model and the kinetic, coriolis/ Centrifugal matrices and gravity vector. A mathematical package such as Mathematica® can be used.

- **An easy-to-use excitation formulation to make the parameters to converge more rapidly.**

  At this current point, research on an easy-to-use and stable method for generating exciting trajectory is currently still in progress.

- Last but not least, it might be interesting to put everything together within the **optimal LIP adaptive framework** [105, 106]. Presently, selecting the controller gains and the parameter update gains is by trial-and-error.

Extended developments subsequently can be made as follows:

- the operational space free motion and to force / motion control , and

- another set of improved formulations of previous point, for both free motion and force/motion control with velocity observer, might be needed to confront the lack of actual velocity signal in real-time implementation.

Given time and resources, the author believes that this methodology can be developed and implemented in near future.

In scenarion, where the Lagrangian dynamics for a particular robot is not available (therefore simulation study cannot be performed), it is possible to make the proposed operational space NN adaptive formulation supporting the development of the direct LIP adaptive control in real-time robot implementation. Once the operational space NN adaptive formulation is ready, then we can add the direct LIP adaptive control in operational space.

Note that, the NN adaptive formulation or the direct LIP adaptive in operational space, mentioned so far, are only with respect to non-redundant manipulators. Further development for redundant manipulators (> 6 DOF) is highly possible.

We will present in brief (since it might require another one PhD. work) the possible development of the NN adaptive case for redundant manipulators, as follows:

The effector motion dynamics of a non-redundant manipulator can be expressed as the followings [47, 8, 91]:

$$\mathbf{\Gamma} = \mathbf{J}^{\mathrm{T}}(\mathbf{q})\mathbf{F} + (\mathbf{I} - \mathbf{J}^{\mathrm{T}}(\mathbf{q})\,\mathbf{J}^{\#^{\mathrm{T}}}(\mathbf{q}))\mathbf{\Gamma}_0 \tag{8.1}$$

where $\mathbf{\Gamma}$ is the joint space dynamics as in (2.25), $\mathbf{F} \in \Re^m$ is the operational space generalized forces (acting as control input), $\mathbf{\Gamma}_0 \in \Re^{n\times n}$ is the *null space*

torque vector (also control input) and $\mathbf{J}^{\#^{\mathrm{T}}}(\mathbf{q})$ is the *dynamically consistent inverse* Jacobian defined as

$$\mathbf{J}^{\#^{\mathrm{T}}} = \mathbf{M}_{\mathbf{x}}(\mathbf{q})\, \mathbf{J}(\mathbf{q})\, \mathbf{M}^{-1}(\mathbf{q}) \tag{8.2}$$

where $\mathbf{M}_{\mathbf{x}}(\mathbf{q})$ of a redundant manipulator is defined as [47, 8, 91]

$$\mathbf{M}_{\mathbf{x}}(\mathbf{q}) = (\mathbf{J}(\mathbf{q})\mathbf{M}^{-1}(\mathbf{q})\mathbf{J}^{\mathrm{T}}(\mathbf{q}))^{-1}. \tag{8.3}$$

The following steps are in order:

1. designing $\mathbf{F}$, $\mathbf{J}^{\#^{\mathrm{T}}}$ and $\mathbf{\Gamma}_0$, to obtain useful closed-loop dynamics for Lyapunov analysis.

2. designing the weight updates within Lyapunov analysis.

The development toward the NN adaptive compliant motion for a redundant manipulator then proceeds similarly as in this thesis as follows:

- NN motion control, assuming actual velocity is available,

- NN motion control, with velocity observer, to overcome the absence of the actual velocity signal in the real-time experimentation, and

- NN force-motion control with velocity observer.

Similarly, the direct LIP adaptive control in operational space for a redundant manipulator can be developed in similar fashion by taking into account the LIP model.

BIBLIOGRAPHY

[1] D. E. Whitney, “Resolved motion rate control of manipulators and human prostheses,” *IEEE Trans. Man-Machine Sys.*, vol. MMS-10, no. 2, pp. 47–53, 1969.

[2] ——, “Historical perspective and state of the art in robot force control,” in *Proc. IEEE Int. Conf. Robot. Autom.*, vol. 2, Mar. 1985, pp. 262 – 268.

[3] J. K. Salisbury, “Active stiffness control of a manipulator in cartesian coordinates,” in *Proc. 19th IEEE Conf. on Decision and Control including the Symposium on Adaptive Processes, 1980*, vol. 19, Dec. 1980, pp. 95 – 100.

[4] M. T. Mason, “Compliance and force control for computer controlled manipulators,” *IEEE Trans. Syst., Man, Cybern.*, vol. 11, no. 6, pp. 418 – 432, June 1981.

[5] S. Chiaverini and L. Sciavicco, “The parallel approach to force/position control of robotic manipulators,” *IEEE Trans. Robot. Autom.*, vol. 9, no. 4, pp. 361 – 373, Aug. 1993.

[6] S. Chiaverini, B. Siciliano, and L. Villani, "Force/position regulation of compliant robot manipulators," *IEEE Trans. Automat. Contr.*, vol. 39, no. 3, pp. 647 – 652, Mar. 1994.

[7] M. H. Raibert and J. J. Craig, "Hybrid position/force control of manipulators," *ASME J. Dynamic, Systems, Measurement and Control*, vol. 103, no. 2, pp. 126–133, June 1981.

[8] O. Khatib, "A unified approach for motion and force control of robot manipulators: The operational space formulation," *IEEE J. Robot. Autom.*, vol. RA-3, no. 1, pp. 43–53, Feb. 1987.

[9] N. H. McClamroch and D. Wang, "Feedback stabilization and tracking of constrained robots," *IEEE Trans. Automat. Contr.*, vol. AC-33, no. 5, pp. 419–426, May 1988.

[10] S. Chiaverini, B. Siciliano, and L. Villani, "A survey of robot interaction control schemes with experimental comparison," *IEEE/ASME Trans. Mechatron.*, vol. 4, no. 3, pp. 273 – 285, Sept. 1999.

[11] O. Khatib and J. Burdick, "Motion and force control of robot manipulators," in *Proc. IEEE Int. Conf. Robot. Autom.*, San Francisco, CA, USA, Apr.7 – 10, 1986, pp. 1381–1386.

[12] R. S. Jamisola, Jr., D. Oetomo, M. H. Ang, Jr., O. Khatib, T. M. Lim, and S. Y. Lim, "Compliant motion using mobile manipulator: An operational space formulation approach to aircraft canopy polishing," *Advanced Robotics*, vol. 19, no. 5, pp. 613–634, June 2005.

[13] J. Russakow, O. Khatib, and S. Rock, "Extended operational space formulation for serial-to-parallel chain (branching) manipulators," in *Proc. IEEE Int. Conf. Robot. Autom.*, vol. 1, Nagoya, Japan, May 21 – 27, 1995, pp. 1056–1061.

[14] J. J. Murray and C. P. Neuman, "Arm: An algebraic robot dynamic modeling program," in *Proc. IEEE Int. Conf. Robot. Autom.*, vol. 1, Mar. 1984, pp. 103 – 114.

[15] C. P. Neuman and J. J. Murray, "Computational robot dynamics: Foundations and applications," *J. of Robotic Syst.*, vol. 2, no. 4, pp. 425–452, winter 1985.

[16] ——, "The complete dynamic model and customized algorithms of the PUMA robot," *IEEE Tran. on Syst., Man and Cybernetics*, vol. SMC-17, no. 4, pp. 635 – 644, Jul./Aug. 1987.

[17] ——, "Customized computational robot dynamics," *J. of Robotic Syst.*, vol. 4, no. 4, pp. 503–526, Aug. 1987.

[18] ——, "Symbolically efficient formulations for computational robot dynamics," *J. of Robotic Syst.*, vol. 4, no. 6, pp. 743–769, Dec. 1987.

[19] B. Armstrong, O. Khatib, and J. Burdick, "The explicit dynamic model and inertial parameters of the PUMA 560 arm," in *Proc. IEEE Int. Conf. Robot. Autom.*, San Francisco, CA, USA, Apr.7–10, 1986, pp. 510–518.

[20] W. Khalil, "Modélisation et commande par calculateur du manipulateur MA23: extension à la conception par ordinateur des manipulateur," Ph.D. dissertation, Université des Sciences et Technologies de Lille (USTL), Montpellier, France, 1976.

[21] M. C. Leu and N. Hemati, "Automated symbolic derivation of dynamic equations of motion for robotic manipulators," *ASME J. Dynamic, Systems, Measurement and Control*, vol. 108, no. 3, pp. 172–179, Sept. 1986.

[22] J. J. Murray and C. P. Neuman, "Organizing customized robot dynamics algorithms for efficient numerical evaluation," *IEEE Tran. on Syst., Man and Cybernetics*, vol. 18, no. 1, pp. 115 – 125, Jan./Feb. 1988.

[23] J. Burdick, "An algorithm for generation of efficient manipulator dynamic equations," in *Proc. IEEE Int. Conf. Robot. Autom.*, vol. 1, 1986, pp. 212–218.

[24] R. S. Jamisola, Jr., "Full dynamics identification and control of PUMA 560 and mitsubishi PA-10 robots," Master's thesis, National University of Singapore, Singapore, 2001.

[25] W. Khalil, J.-F. Kleinfinger, and M. Gautier, "Reducing the computational burden of the dynamic models of robots," in *Proc. IEEE Int. Conf. Robot. Autom.*, vol. 3, Apr. 1986, pp. 525 – 531.

[26] W. Khalil and J.-F. Kleinfinger, "Minimum operations and minimum parameters of the dynamic models of tree structure robots," *IEEE J. Robot. Autom.*, vol. RA-3, no. 6, pp. 517 – 526, Dec. 1987.

[27] M. Gautier and W. Khalil, "A direct determination of minimum inertial parameters of robots," in *Proc. IEEE Int. Conf. Robot. Autom.*, vol. 3, Apr. 24 – 29, 1988, pp. 368 – 373.

[28] ——, "Direct calculation of minimum set of inertial parameters of serial robots," in *Proc. IEEE Int. Conf. Robot. Autom.*, vol. 6, no. 3, June 1990, pp. 368 – 373.

[29] W. Khalil and F. Bennis, "Symbolic calculation of the base inertial parameters of closed-loop robots," *Int. Journal of Robotics Research*, vol. 14, no. 2, pp. 112 – 128, Apr. 1995.

[30] W. Khalil and E. Dombre, *Modeling, identification and control of robots*, 3rd ed. London: Hermes Penton Science, 2002.

[31] F. Caccavale and P. Chiacchio, "Identification of dynamic parameters and feedforward control for a conventional industrial manipulator," *Control Engineering Practice*, vol. 2, no. 6, pp. 1039 – 1050, Dec. 1994.

[32] G. Antonelli, F. Caccavale, and P. Chiacchio, "A systematic procedure for the identification of dynamic parameters of robot manipulators," *Robotica*, vol. 17, no. 4, pp. 427 – 435, July – Aug. 1999.

[33] R. S. Jamisola, Jr., M. H. Ang, Jr., T. M. Lim, O. Khatib, and S. Y. Lim, "Dynamics identification and control of an industrial robot," in *Proc. 9th Int. Conf. Adv. Robot.*, Tokyo, Japan, Oct. 25–27, 1999, pp. 323–328.

[34] W. Khalil, M. Gautier, and P. Lemoine, "Identification of the payload inertial parameters of industrial manipulators," in *Proc. IEEE Int. Conf. Robot. Autom.*, Kobe, Japan, Apr. 10-14, 2007, pp. 4943 – 4948.

[35] B. Armstrong-Hélouvry, *Control of Machines with Friction*. Boston, MA: Kluwer Academic Press, 1991.

[36] A. Woźniak, W. Szynkiewicz, and C. Zieliński, "Robot cotroller with a self-measurement capability enabling the identification of friction," *Archives of Control Sciences*, vol. 13, no. 4, pp. 391–414, 2003.

[37] C. H. An, C. G. Atkeson, and J. M. Hollerbach, "Estimation of inertial parameters of rigid body links of manipulators," in *Proc. 24th IEEE Conf. on Decision and Control*, vol. 24, no. 1, Dec. 1985, pp. 990 – 995.

[38] M. Gautier, "Identification of robots dynamics," in *Proc. IFAC Symp. on Theory of Robots*, Vienne, 1986, pp. 351–356.

[39] P. K. Khosla and T. Kanade, "Parameter identification of robot dynamics," in *Int. IEEE Conf. on Decision and Control*, vol. 24, no. 1, Dec. 1985, pp. 1754 – 1760.

[40] P. K. Khosla, "Estimation of robot dynamics parameters: Theory and application," Robotics Institute, Pittsburgh, PA, Tech. Rep. CMU-RI-TR-87-08, March 1987.

[41] ——, "Categorization of parameters in the dynamic robot model," *IEEE Trans. Robot. Autom.*, vol. 5, no. 3, pp. 261 – 268, June 1989.

[42] J. J. Craig, P. Hsu, and S. S. Sastry, "Adaptive control of mechanical manipulators," in *Proc. IEEE Int. Conf. Robot. Autom.*, San Francisco, CA, Apr.7–10, 1986, pp. 190–195.

[43] R. H. Middleton and G. C. Goodwin, "Adaptive computed torque control for rigid link manipulators," *Syst. Contr. Lett.*, vol. 10, no. 1, pp. 9–16, Jan. 1988.

[44] R. Ortega and M. Spong, "Adaptive motion control of rigid robots: A tutorial," in *Proc. IEEE Conf. on Decision and Control*, vol. 2, Austin, TX, USA, Dec.7 – 9, 1988, pp. 1576–1584.

[45] J.-J. E. Slotine and W. Li, "On the adaptive control of robot manipulators," *Int. Journal of Robotics Research*, vol. 6, no. 3, pp. 49–59, Fall 1987.

[46] ——, "Adaptive robot control: A new perspective," in *Proc. of the 26th IEEE Conf. on Decision and Control*, vol. 26, no. 1, Dec. 1987, pp. 192 – 198.

[47] L. Sciavicco and B. Siciliano, *Modelling and Control of Robot Manipulators*, 2nd ed. London: Springer-Verlag, 2000.

[48] P. Hsu, M. Bodson, S. Sastry, and B. Paden, "Adaptive identification and control for manipulators without using joint accelerations," in *Proc. IEEE Int. Conf. Robot. Autom.*, vol. 4, Mar. 1987, pp. 1210 – 1215.

[49] Z. Lu, K. B. Shimoga, and A. A. Goldenberg, "Experimental determination of dynamic parameters of robotic arms," *J. of Robotic Syst.*, vol. 10, no. 8, pp. 1009–1029, Dec. 1993.

[50] M. Gautier and W. Khalil, "An efficient algorithm for the calculation of the filtered dynamic model of robots," in *Proc. IEEE Int. Conf. Robot. Autom.*, vol. 1, Apr. 22 – 28, 1996, pp. 323 – 328.

[51] M. Gautier, A. Janot, and P. O. Vandanjon, "Didim: A new method for the dynamic identification of robots from only torque data," in *Proc. IEEE Int. Conf. Robot. Autom.*, Kobe, Japan, May 19-23, 2008, pp. 2122 – 2127.

[52] A. Janot, P. O. Vandanjon, and M. Gautier, "Identification of robots dynamics with the instrumental variable method," in *Proc. IEEE Int. Conf. Robot. Autom.*, Kobe, Japan, May 12-17, 2009, pp. 1762–1767.

[53] M. Gautier and W. Khalil, "Exciting trajectories for the identification of base inertial parameters of robots," in *Proc. 30th IEEE Conf. on Decision and Control*, vol. 1, Dec. 11-13, 1991, pp. 494 – 499.

[54] M. Gautier, "Optimal motion planning for robot's inertial parameters identification," in *Proc. 31st IEEE Conf. on Decision and Control*, vol. 1, Dec. 16-18, 1992, pp. 70 – 73.

[55] C. Presse and M. Gautier, "New criteria of exciting trajectories for robot identification," in *Proc. IEEE Int. Conf. Robot. Autom.*, vol. 3, May 2-6, 1992, pp. 907 – 912.

[56] M. M. Olsen, J. Swevers, and W. Verdonck, "Maximum likelihood identification of a dynamic robot model: Implementation issues," *Int. Journal of Robotics Research*, vol. 21, no. 2, pp. 89 – 96, Feb. 2002.

[57] N. A. Bompos, P. K. Artemiadis, A. S. Oikonomopoulos, and K. J. Kyriakopoulos, "Modeling, full identification and control of the mitsubishi PA-10 robot arm," in *IEEE/ASME Int. Conf. on Adv. Intel. Mechatronics (AIM2007)*, Sept.4 - 7, 2007, pp. 1–6.

[58] J. Swevers, W. Verdonck, and J. De Schutter, "Dynamic model identification for industrial robots," *IEEE Control Systems Magazine*, vol. 27, no. 5, pp. 58 – 71, Oct. 2007.

[59] N. D. Vuong, M. H. Ang, Jr., and Y. Li, "Dynamic model identification for industrial manipulator subject to advanced model based control," in *Proc. 4th Conf. on HNICEM*, Manila, Philippines, Mar. 12 - 16, 2009.

[60] P. M. La Hera, U. Mettin, S. Westerberg, and A. S. Shiriaev, "Modeling and control of hydraulic rotary actuators used in forestry cranes," in *Proc. IEEE Int. Conf. Robot. Autom.*, Kobe, Japan, May 12-17, 2009, pp. 1315–1320.

[61] M. M. Polycarpou and P. A. Ioannou, "Neural networks as on-line approximators of nonlinear systems," in *Proc. of the 31st IEEE Conf. on Decision and Control*, vol. 1, 1992, pp. 7 – 12.

[62] A. N. Poo, M. H. Ang, Jr., C. L. Teo, and Q. Li, "Performance of a neuro-model-based robot controller: adaptability and noise rejection," *Intelligent Systems Engineering*, vol. 1, no. 1, pp. 50–62, Autumn 1992.

[63] X. Cui and K. Shin, "Direct control and coordination using neural networks," *IEEE Trans. Syst., Man, Cybern.*, vol. 23, no. 3, pp. 686 – 697, May – June 1993.

[64] K. Kiguchi and T. Fukuda, "Robot manipulator contact force control application of fuzzy-neural network," in *Proc. IEEE Int. Conf. Robot. Autom.*, vol. 1, Nagoya, Japan, May 21 – May 27, 1995, pp. 875 – 880.

[65] S. J. C. Marques, L. F. Baptista, and J. S. da Costa, "Force control of robot manipulators with neural networks compensation: a comparative study," in *Proc. of the IEEE Intl. Symp. on Ind. Electron. (ISIE) 1997*, vol. 3, Vigo, Spain, July 7 – July 11, 1997, pp. 872 – 877.

[66] S.-T. Lin and S.-J. Tzeng, "Neural network force control for industrial robots," *Journal of Intel. and Robotic Sys.: Theory and App.*, vol. 24, no. 3, pp. 253–268, Mar. 1999.

[67] S. Jung and T. C. Hsia, "Robust neural force control scheme under uncertainties in robot dynamics and unknown environment," *IEEE Trans. Ind. Electron.*, vol. 47, no. 2, pp. 403–412, Apr. 2000.

[68] K. S. Narendra and K. Parthasarathy, "Identification and control of dynamical systems using neural networks," *IEEE Trans. Neural Networks*, vol. 1, no. 1, pp. 4–27, Mar. 1990.

[69] T. Yabuta and T. Yamada, "Neural network controller characteristics with regard to adaptive control," *IEEE Trans. Syst., Man, Cybern.*, vol. 22, no. 1, pp. 170 – 177, Jan. – Feb. 1992.

[70] R. M. Sanner and J.-J. E. Slotine, "Stable adaptive control and recursive identification using radial gaussian networks," in *Proc. of the 30th IEEE Conf. on Decision and Control*, vol. 3, Dec. 11 – Dec. 13, 1991, pp. 2116 – 2123.

[71] G. A. Rovithakis and M. A. Christodoulou, "Neural network controller characteristics with regard to adaptive control," *IEEE Trans. Syst., Man, Cybern.*, vol. 24, no. 3, pp. 400 – 412, Mar. 1994.

[72] S. S. Ge, Z.-L. Wang, and Z.-J. Chen, "Adaptive static neural network control of robots," in *Proc. of the IEEE Conf. on Industrial Technology*, vol. 3, Dec. 5 – Dec. 9, 1994, pp. 240 – 244.

[73] F. L. Lewis, K. Liu, and A. Yeşildirek, "Neural net robot controller with guaranteed tracking performance," *IEEE Trans. Neural Networks*, vol. 6, no. 3, pp. 703–715, May 1995.

[74] F. L. Lewis, A. Yeşildirek, and K. Liu, "Multilayer neural-net robot controller with guaranteed tracking performance," *IEEE Trans. Neural Networks*, vol. 7, no. 2, pp. 388–399, Mar. 1996.

[75] F. L. Lewis, S. Jagannathan, and A. Yeşildirek, *Neural Network Control of Robot Manipulators and Nonlinear Systems*, 1st ed. Philadelphia, PA: Taylor and Francis, 1998.

[76] J.-J. E. Slotine and W. Li, "Adaptive manipulator control: A case study," *IEEE Trans. Automat. Contr.*, vol. AC-33, no. 11, pp. 995–1003, Nov. 1988.

[77] S. Hu, M. H. Ang, Jr, and H. Krishnan, "Neural network controller for constrained robot manipulators," in *Proc. IEEE Int. Conf. Robot. Autom.*, vol. 2, San Francisco, CA, May 2000, pp. 1906–1911.

[78] C. M. Kwan, A. Yeşildirek, and F. L. Lewis, "Robust force/motion control of constrained robots using neural network," in *Proc. 33rd IEEE Conf. on Decision and Control 1994*, vol. 2, Lake Buena Vista, Florida, USA, Dec. 14 – 16, 1994, pp. 1862–1867.

[79] C. C. Cheah, Y. Zhao, and J.-J. E. Slotine, "Adaptive jacobian motion and force tracking control for constrained robots with uncertainties," in *Proc. IEEE Int. Conf. Robot. Autom.*, Orlando, FL, USA, May 15 – May 19, 2006, pp. 2226–2231.

[80] S. Hu, M. H. Ang, Jr, and H. Krishnan, "NN controller of the constrained robot under unknown constraint," in *IEEE Intl. Proc. on Ind. Elec. Society (IECON) 2000*, vol. 3, Nagoya, Japan, Oct. 22 – Oct. 28 2000, pp. 2123–2128.

[81] T. Yoshikawa and A. Sudou, "Dynamic hybrid position/force control of robot manipulators-on-line estimation of unknown constraint," *IEEE Trans. Robot. Autom.*, vol. 9, no. 2, pp. 220 – 226, Apr. 1993.

[82] Z. Doulgeri and Y. Karayiannidis, "An adaptive force regulator for a robot in compliant contact with an unknown surface," in *Proc. IEEE Int. Conf. Robot. Autom.*, Barcelona, Spain, Apr. 18 – Apr. 22 2005, pp. 2685–2690.

[83] Y. Karayiannidis and Z. Doulgeri, "An adaptive law for slope identification and force position regulation using motion variables," in *Proc. IEEE*

Int. Conf. Robot. Autom., Orlando, FL, May 15 – May 19 2006, pp. 3538–3543.

[84] Y. Karayiannidis, G. Rovithakis, and Z. Doulgeri, "A neuro-adaptive controller for the force/position tracking of a robot manipulator under model uncertainties in compliance and friction," in *14th Mediterranean Conference on Control and Automation, 2006*, 2007, pp. 1–6.

[85] ——, "Force/position tracking for robotic manipulator in compliant contact with a surface using neuro-adaptive control," *Automatica*, vol. 43, no. 7, pp. 1281–1288, July 2007.

[86] Z. Doulgeri and Y. Karayiannidis, "Force/position tracking of a robot in compliant contact with unknown stiffness and surface kinematics," in *Proc. IEEE Int. Conf. Robot. Autom.*, Roma, Italy, Apr. 10 – Apr. 14 2007, pp. 4190–4195.

[87] C. Bechlioulis, Z. Doulgeri, and G. Rovithakis, "Robot force/position tracking with guaranteed prescribed performance," in *Proc. IEEE Int. Conf. Robot. Autom.*, Kobe, Japan, May 12-17, 2009, pp. 3688–3693.

[88] Y. Zhao, C. C. Cheah, and J.-J. E. Slotine, "Adaptive vision and force tracking control of constrained robots with structural uncertainties," in *Proc. IEEE Int. Conf. Robot. Autom.*, Roma, Italy, Apr. 10 – Apr. 14, 2007, pp. 2349–2354.

[89] J. J. Craig, *Introduction to Robotics, Mechanics, and Control*, 2nd ed. Reading, MA: Addison-Wesley, 1987.

[90] F. L. Lewis, C. T. Abdallah, and D. M. Dawson, *Control of Robot Manipulators*, 1st ed. NY: MacMillan, 1993.

[91] O. Khatib, "Lecture notes on advanced robotics," Stanford University, 1996.

[92] Q. H. Xia, S. Y. Lim, M. H. Ang, Jr, and T. M. Lim, "Adaptive joint friction compensation using a model-based operational space velocity observer," in *Proc. IEEE Int. Conf. Robot. Autom.*, vol. 3, New Orleans, LA, USA, Apr. 26 – May 1, 2004, pp. 3081–3086.

[93] J.-J. E. Slotine and W. Li, *Applied Nonlinear Control*, 1st ed. Englewood Cliffs, NJ: Prentice Hall, 1991.

[94] L. Sciavicco, B. Siciliano, and L. Villani, "Lagrange and newton-euler dynamic modeling of a gear-driven robot manipulator with inclusion of motor inertia effects," *Advanced Robotics*, vol. 10, no. 3, pp. 317–334, 1996.

[95] M. Gautier and W. Khalil, "On the identification of the inertial parameters of robots," in *Proc. 27th IEEE Conf. on Decision and Control*, vol. 3, Dec. 7 – 9, 1988, pp. 2264 – 2269.

[96] B. Anderson, "Exponential stability of linear equations arising in adaptive identification," *IEEE Trans. Automat. Contr.*, vol. 22, no. 1, pp. 83 – 88, Feb. 1977.

[97] A. P. Morgan and K. S. Narendra, "On the uniform asymptotic stability of certain linear nonautonomous differential equations," *SIAM J. on Control and Optimization*, vol. 15, no. 1, pp. 5–24, Jan. 1977.

[98] J.-J. E. Slotine and W. Li, "Adaptive manipulator control: Parameter convergence and task-space strategies," in *Proc. American Cont. Conf.*, June10 – 12, 1987, pp. 828 – 835.

[99] S. S. Ge, T. H. Lee, and C. J. Harris, *Adaptive neural network control of robotic manipulators*. River Edge, NJ: World Scientific, 1998.

[100] P. J. Werbos, "Backpropagation: Past and future," in *Proc. IEEE Int. Conf. Neural Networks*, vol. 1, San Diego, CA, USA, July 24 – July 27, 1988, pp. 343–353.

[101] G. V. Cybenko, "Approximation by superpositions of a sigmoidal function," *Mathematics of Control, Signals, and Systems*, vol. 2, no. 4, p. v, 1989.

[102] J. P. LaSalle, "Some extensions of liapunov's second method," *IRE Trans. Circuit Theory*, vol. 7, no. 4, pp. 520–527, Dec. 1960.

[103] D. B. Soewandito, D. N. Oetomo, and M. H. Ang, Jr., "The operational space formulation with neural-network adaptive motion control," in *Proc. Int. Fed. of Automat. Contr. (IFAC) World Congress 2008*, Seoul, Korea, July 6 – July 11, 2008, pp. 12 775–12 780.

[104] Q. H. Xia, S. Y. Lim, M. H. Ang, Jr., and T. M. Lim, "An operational space observer-controller for trajectory tracking, Tech. Rep. SIMTech AT/02/014/PM, 2002.

[105] D. Vrabie and F. L. Lewis, "Adaptive optimal control algorithm for continuous-time nonlinear systems based on policy iteration," in *Proc. 47th IEEE Conf. on Decision and Control*, Dec. 9-11, 2008, pp. 73 – 79.

[106] D. Vrabie, O. Pastravanu, M. Abu-Khalaf, and F. L. Lewis, "Adaptive optimal control for continuous-time linear systems based on policy iteration," *Automatica*, vol. 45, no. 2, pp. 477–484, Feb. 2009.

[107] R. S. Jamisola, Jr., M. H. Ang, Jr., D. Oetomo, O. Khatib, T. M. Lim, and S. Y. Lim, "The operational space formulation implementation to canopy polishing using a mobile manipulator," in *Proc. IEEE Int. Conf. Robot. Autom.*, Washington, DC, May11 – 15, 2002, pp. 400–405.

[108] Q. H. Xia, S. Y. Lim, M. H. Ang, Jr, and T. M. Lim, "Adaptive friction compensation for operational space tracking control with global asymptotic stability," in *3rd IFAC Symposium on Mechatronic Systems*, Sydney, Australia, Sept. 6 - 8, 2004, pp. 187–192.

[109] H. Berghuis and H. Nijmeijer, "A passivity approach to controller-observer design for robots," *IEEE Trans. Robot. Autom.*, vol. 9, no. 6, pp. 740–754, Dec. 1993.

[110] Y. H. Kim and F. L. Lewis, "Neural network output feedback control of robot manipulators," *IEEE Trans. Robot. Autom.*, vol. 15, no. 2, pp. 301–309, Apr. 1999.

[111] S. Nicosia and P. Tomei, "Robot control by using only joint position measurements," *IEEE Trans. Automat. Contr.*, vol. AC-35, no. 9, pp. 1058–1061, Sept. 1990.

[112] M. Tanaka, Y. Kaneda, S. Makino, and J. Kojima, "Fast projection algorithm and its step size control," in *Int. Conf. on Acoustics, Speech, and Signal Processing*, vol. 2, 1995, pp. 945 – 948.

[113] M. Rupp, "A family of adaptive filter algorithms with decorrelating properties," *IEEE Trans. on Signal Processing*, vol. 46, no. 3, pp. 771 – 775, 1998.

[114] S. Chen, S. McLaughlin, and B. Mulgrew, "Complex-valued radial basis function network. i. network architecture and learning algorithms," *ASME J. Dynamic, Systems, Measurement and Control*, vol. 35, no. 1, pp. 19–31, Jan. 1994.

[115] D. B. Soewandito, D. N. Oetomo, and M. H. Ang, Jr., "Neuro-adaptive motion controller with velocity observer for operational space formulation," in *Proc. Int. Fed. of Automat. Contr. (IFAC) World Congress 2008*, Seoul, Korea, July 6 – July 11, 2008, pp. 13 755–13 760.

[116] ——, "The operational space formulation using neuro-adaptive motion controller with velocity observer," 2010, to appear.

[117] ——, "Neuro-adaptive force-motion controller with velocity observer for operational space formulation," 2010, to appear.

[118] Q. H. Xia, M. H. Ang, Jr, S. Y. Lim, and T. M. Lim, “Parallel force and motion control using adaptive observer-controller,” in *IEEE Int. Conf. on Sys., Man and Cybernetics (SMC2008)*, Singapore, Oct.12 – 15, 2008, pp. 3143–3149.

APPENDIX A

PUMA 560 FRAMES AND JACOBIAN

A.1 Frame Assignment for PUMA 560

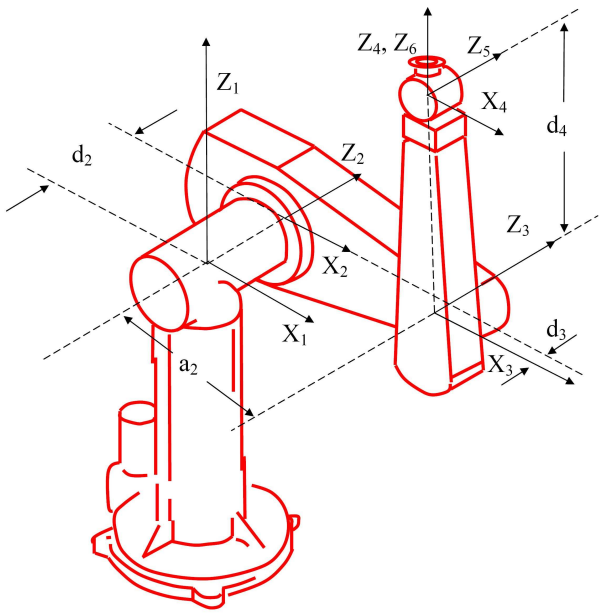

Figure A.1: Frame Assignment for PUMA 560 in the experiment.

Table A.1: The DH parameters for PUMA manipulator

i	α_{i-1}	a_{i-1}	d_i	θ_i
1	0	0	0	θ_1
2	-90	0	d_2	θ_2
3	0	a_2	d_3	θ_3
4	90	a_3	d_4	θ_4
5	-90	0	0	θ_5
6	90	0	0	θ_6

The numerical values for the Denavit-Hartenberg parameters of PUMA 560 are:

a_2=0.4318 m, a_3=-0.0203 m, d_2=0.2435 m, d_3=-0.0934, d_4=0.4331m [19].

APPENDIX B

COMPUTING $\mathbf{F}^*_{\text{motion}}$

B.1 Computing $\mathbf{F}^*_{\text{motion}}$

In the following, the computation of $\mathbf{F}^*_{\text{motion}}$ is presented. Further details can be found in [91]. In general, since the operational space coordinates consists of translational and rotational motions, therefore, $\mathbf{F}^*_{\text{motion}}$ consists of two types of control forces: one is force control to control translational motion and the other one is moment control to control rotational motion.

Let's assume that the desired positional and rotational representation trajectories, $\mathbf{x}_{p,d}, \dot{\mathbf{x}}_{p,d}, \ddot{\mathbf{x}}_{p,d} \in \Re^3$ and $\mathbf{x}_{r,d}, \dot{\mathbf{x}}_{r,d}, \ddot{\mathbf{x}}_{r,d} \in \Re^9$, respectively, are provided by trajectory generator. Note that, $\mathbf{x}_{r,d}, \dot{\mathbf{x}}_{r,d}, \ddot{\mathbf{x}}_{r,d}$ equals to

$$\mathbf{x}_{r,d} = \begin{pmatrix} (\mathbf{s}_1)_d^{\mathrm{T}} & (\mathbf{s}_2)_d^{\mathrm{T}} & (\mathbf{s}_3)_d^{\mathrm{T}} \end{pmatrix}^{\mathrm{T}} \tag{B.1}$$

$$\dot{\mathbf{x}}_{r,d} = \begin{pmatrix} (\dot{\mathbf{s}}_1)_d^{\mathrm{T}} & (\dot{\mathbf{s}}_2)_d^{\mathrm{T}} & (\dot{\mathbf{s}}_3)_d^{\mathrm{T}} \end{pmatrix}^{\mathrm{T}} \tag{B.2}$$

$$\ddot{\mathbf{x}}_{r,d} = \begin{pmatrix} (\ddot{\mathbf{s}}_1)_d^{\mathrm{T}} & (\ddot{\mathbf{s}}_2)_d^{\mathrm{T}} & (\ddot{\mathbf{s}}_3)_d^{\mathrm{T}} \end{pmatrix}^{\mathrm{T}} \tag{B.3}$$

Also, let's assume that we have a full 3D space translational and rotational motion i.e. $m_P, m_O = 3$. Then, $\mathbf{F}^*_{\text{motion}}$ can be computed as

$$\mathbf{F}^*_{\text{motion}} = \begin{cases} \mathcal{F}^*_{\text{motion}} = & \ddot{\mathbf{x}}_{p,d} + \mathbf{K}_{\mathbf{v}}(\dot{\mathbf{x}}_{p,d} - \dot{\mathbf{x}}_p) + \mathbf{K}_{\mathbf{p}}(\mathbf{x}_{p,d} - \mathbf{x}_p) \\ \mathcal{M}^*_{\text{motion}} = & \dot{\boldsymbol{\omega}}_d + \mathbf{K}_{\mathbf{v}}(\boldsymbol{\omega}_d - \boldsymbol{\omega}) + \mathbf{K}_{\mathbf{p}}\,\mathbf{e}_{\text{orient}} \end{cases} \tag{B.4}$$

where all necessary terms are computed as:

- $\mathbf{x}_p$ and $\mathbf{x}_r$ can be obtained from the direct kinematics.

- $\dot{\mathbf{x}}_p$ and $\boldsymbol{\omega}$ can be obtained from the basic differential kinematics

$$\begin{pmatrix} \dot{\mathbf{x}}_p \\ \boldsymbol{\omega} \end{pmatrix} = \mathbf{J}(\mathbf{q})\, \dot{\mathbf{q}}. \tag{B.5}$$

- $\mathbf{e}_{\text{orient}}$ is the *instantaneous angular error* which can be obtained from the following:

$$\mathbf{e}_{\text{orient}} = \frac{1}{2} \left([\mathbf{s}_1\times]\, (\mathbf{s}_1)_d \;+\; [\mathbf{s}_2\times]\, (\mathbf{s}_2)_d \;+\; [\mathbf{s}_3\times]\, (\mathbf{s}_3)_d \right) \tag{B.6}$$

where 3×3 skew-symmetric matrix operator $[\mathbf{s}\times]$ is defined as

$$\begin{pmatrix} 0 & -s_z & s_y \\ s_z & 0 & -s_x \\ -s_y & s_x & 0 \end{pmatrix}. \tag{B.7}$$

- The desired angular velocity, $\boldsymbol{\omega}_d$, can be obtained by

$$\boldsymbol{\omega}_d = \mathbf{E}_r^+(\mathbf{x}_{r,d})\, \dot{\mathbf{x}}_{r,d} \tag{B.8}$$

where

$$\mathbf{E}_r^+(\mathbf{x}_{r,d}) = \frac{1}{2} \begin{pmatrix} [(\mathbf{s}_1)_d\times] & [(\mathbf{s}_1)_d\times] & [(\mathbf{s}_3)_d\times] \end{pmatrix}. \tag{B.9}$$

- The desired angular acceleration, $\dot{\boldsymbol{\omega}}_d$, can be obtained by

$$\dot{\boldsymbol{\omega}}_d = \frac{1}{2}\mathbf{E}_r^+(\mathbf{x}_{r,d})\, \ddot{\mathbf{x}}_{r,d} + \mathbf{R}^{\mathrm{T}}(\mathbf{x}_{r,d}\,, \boldsymbol{\omega}_d)\, \dot{\mathbf{x}}_{r,d} \tag{B.10}$$

where

$$\mathbf{R}^{\mathrm{T}}(\mathbf{x}_{r,d}\,, \boldsymbol{\omega}_d) = \begin{pmatrix} ((\mathbf{s}_1)_d^{\mathrm{T}}\, \boldsymbol{\omega}_d)\, \mathbf{I}_{3\times3} \\ ((\mathbf{s}_2)_d^{\mathrm{T}}\, \boldsymbol{\omega}_d)\, \mathbf{I}_{3\times3} \\ ((\mathbf{s}_3)_d^{\mathrm{T}}\, \boldsymbol{\omega}_d)\, \mathbf{I}_{3\times3} \end{pmatrix}. \tag{B.11}$$

And clearly, $\ddot{\mathbf{x}}_d, \dot{\mathbf{e}}_{\mathbf{x}}, \mathbf{e}_{\mathbf{x}}$ (2.33) are defined as

$$\ddot{\mathbf{x}}_d = \begin{pmatrix} \ddot{\mathbf{x}}_{p,d} \\ \dot{\boldsymbol{\omega}}_d \end{pmatrix}, \qquad \dot{\mathbf{e}}_{\mathbf{x}} = \begin{pmatrix} \dot{\mathbf{x}}_{p,d} - \dot{\mathbf{x}}_p \\ \boldsymbol{\omega}_d - \boldsymbol{\omega} \end{pmatrix}, \qquad \mathbf{e}_{\mathbf{x}} = \begin{pmatrix} \mathbf{x}_{p,d} - \mathbf{x}_p \\ \mathbf{e}_{\text{orient}} \end{pmatrix}. \tag{B.12}$$